Maritime Autonomous Surface Ships (MASS) and Energy Management System

Harriet Laryea

A Thesis

In the Department of

Concordia Institute for Information Systems Engineering (CIISE)

Presented in Partial Fulfillment of the Requirements

For the Degree of

Doctor of Philosophy (Information and Systems Engineering)

at Concordia University

Montréal, Quebéc, Canada

August 2025

CONCORDIA UNIVERSITY

School of Graduate Studies

This is to certify that the thesis prepared

By: **Harriet Laryea**

Entitled: **Maritime Autonomous Surface Ships (Mass) and Energy Management System**

and submitted in partial fulfillment of the requirements for the degree of

Doctor of Philosophy (Information and Systems Engineering)

complies with the regulations of this University and meets the accepted standards with respect to originality and quality.

Signed by the Final Examining Committee:

_____ Chair
Dr. Emre Erkmen

_____ External Examiner
Dr. Rajeev Jaiman

_____ External Examiner to Program
Dr. Chunyan Lai

_____ Examiner
Dr. Arash Mohammadi

_____ Examiner
Dr. Jun Yan

_____ Supervisor
Dr. Andrea Schiffauerova

Approved by _____
Dr. Farnoosh Naderkhani, Graduate Program Director

August 18, 2025 _____
Dr. Mourad Debbabi, Dean of Gina Cody School of Engineering and Computer Science

Abstract

Maritime Autonomous Surface Ships (MASS) and Energy Management System

Harriet Laryea, Ph. D.

Concordia University, 2025

The research and development of Maritime Autonomous Surface Ships (MASS) is underway in several countries, with operations either remotely controlled from a Shore Control Center (SCC) or fully autonomous, without the need for Officer of the Watch (OOW) supervision. This study focuses on integrating renewable energy systems, alternative fuels, and energy management strategies (EMS) to enhance the efficiency and sustainability of both conventional and fully autonomous vessels. In response to rising fuel costs and stringent International Maritime Organization (IMO) regulations, the research aims to optimize vessel performance, reduce emissions, and improve energy efficiency across various ship types.

The study begins by assessing conventional vessels before transitioning to fully autonomous operations. The research then examines the optimization of a hybrid renewable energy system (HRES) that incorporates photovoltaic (PV) arrays, vertical axis wind turbines (VAWTs), and battery storage into the existing ship power system. A comparative analysis is conducted between conventional and fully autonomous vessels using an artificial bee colony (ABC) algorithm. The optimal configuration for both vessel types is identified as Genset/PV/VAWT/Battery, minimizing the annualized cost of the system (ACS), while maximizing the renewable energy fraction and reducing carbon emissions. Notably, autonomous vessels demonstrate superior performance in terms of cost and emissions when compared to conventional vessels.

Further, the study investigates optimal marine alternative fuels for short-sea shipping, including hydrogen, LNG, and traditional fuels. Mathematical modeling in Python is used to evaluate key performance indicators (KPIs), with LNG proving to deliver the highest Net Present Value (NPV), especially for autonomous vessels. This provides insights for optimizing fuel selection and ensuring compliance with environmental regulations.

Finally, a multi-objective predictive energy management system is developed using nonlinear model predictive control (NMPC) combined with grey wolf optimization (GWO) to optimize energy distribution in autonomous vessels under dynamic wave conditions. The NMPC-GWO

algorithm demonstrates robustness and adaptability, ensuring reliable performance in varying environmental and operational conditions.

In summary, this research offers a comprehensive framework for optimizing energy systems and fuel selection, driving improvements in operational efficiency and environmental sustainability in the maritime industry.

Acknowledgements

I would like to express my sincere gratitude to Dr. Anjali Awasthi for her invaluable guidance during the early stages of my Ph.D. journey, particularly in selecting my research and thesis topic. I also extend my thanks to my committee members for their constructive feedback, patience, and motivation, which were instrumental throughout the research and thesis writing process. Special thanks go to my supervisor, Dr. Andrea Schiffauerova, for providing essential support and guidance at a critical stage, even though my thesis topic was outside her primary research area.

I would also like to thank my colleagues at the Gina Cody School of Engineering and Computer Science, particularly Mrs. Charlene Wald the Graduate Program Coordinator from the Department of Mechanical, Industrial, and Aerospace Engineering (MIAE), for encouraging me to pursue a Ph.D. rather than an additional master's degree in Industrial Engineering. I clearly remember your candid conversation, where you said, "*Harriet, you do not require an additional master's degree. I have witnessed your progression from Bachelor's to Master's level in this department, and I believe you are fully capable of pursuing a Ph.D. Please seek a supervisor and return to proceed with your Ph.D.*" This conversation played a pivotal role in my decision to continue with the Ph.D. program. I am also grateful to Mrs. Silvie Pasquarelli and Mrs. Mireille Wahba the Graduate Program Coordinators from the Concordia Institute for Information Systems Engineering (CIISE) for their unwavering support and encouragement throughout my academic journey. I would also like to express my appreciation to Dr. Alex De Visscher, Chair of the Department of Chemical and Materials Engineering (CME), for supporting my decision to pursue a Ph.D.

Additionally, I am thankful to my colleagues in the Navy and the marine sector for their moral support and expert advice. Furthermore, I extend my heartfelt thanks to my nuclear and extended family, especially my husband and our wonderful children. I am also deeply grateful to my extended family—particularly my siblings, aunties, uncles, and cousins—for their constant support. Lastly, a special thanks goes to my mother (Gifty), Mr. Jacob Marmon, and Mr. Jonathan Addo, whose encouragement to pursue a Ph.D. immediately after my Master's was invaluable. Thank you all for being the wind beneath my wings.

Indeed "***in His time, He makes all things beautiful***" Ecclesiastes 3:11. Thank you Abba!

Dedication

I humbly dedicate this dissertation to God Almighty, whose guidance and Grace have made all things possible. "***With man this is impossible, but with God all things are possible***."

Secondly, I dedicate this work to my beloved husband (Ekow) and our lovely children and our wonderful children—Joel, Cherub, and Seraph—whose steadfast strength, support, patience, and encouragement have been a constant source of motivation throughout this journey. I am deeply grateful to have you as my family, and sharing this life experience with me.

Lastly, I dedicate this work to my respected high school teacher, Mr. Wilson Adzraku, whose mentorship instilled in me the values of prioritizing God and striving for excellence. I am profoundly grateful for the foundation of excellence you instilled in me at such an early stage of my life.

To Him be all the Glory. For the Great things He has done, and the Great things, He will do!

Contributions of authors

Chapter 3: This chapter is based on an article I co-authored with Dr. Andrea Schiffauerova. I conceptualized the project, collected the data, designed and executed the analysis, and wrote the manuscript, all under the guidance of Dr. Schiffauerova.

Chapter 4: This chapter is based on an article I co-authored with Dr. Andrea Schiffauerova. I conceptualized the project, designed and executed the simulation, and wrote the manuscript, with guidance and supervision from Dr. Schiffauerova.

Chapter 5: This chapter is based on an article I co-authored with Dr. Andrea Schiffauerova. I conceptualized the project, collected the data, designed and conducted the simulations, performed all data analyses, interpreted the results, and wrote the manuscript, all with the guidance of Dr. Schiffauerova.

TABLE OF CONTENTS

List of Figures

List of Tables

Appendix Tables

CHAPTER 1. INTRODUCTION

The evolution of ships has spanned over many years, driven by the commissioning and decommissioning of vessels that once relied on natural wind and tidal forces. However, the advent of steamships in the early 19th century revolutionized maritime navigation. The transportation of goods and passengers via sea became a significant force in global commerce and travel. Currently, there are over 7,000 conventional ships (CS) and more than 2,500 active seaports and inland ports worldwide [1].

During the Industrial Revolution, steam propulsion in marine vessels was gradually replaced by more efficient fuels such as diesel, fossil fuels, liquefied natural gas (LNG), and electric or battery power. Conventional ships are now predominantly powered by diesel engines, marine gas turbines, or Low-Pressure Dual Fuel (LPDF) engines. These vessels typically operate using heavy fuel oil, marine-grade diesel, or LNG. Unfortunately, the incomplete combustion of these fuels results in the emission of greenhouse gases (GHGs), including Sulphur Oxides (SOx), Nitrogen Oxides (NOx), and Carbon Dioxide (CO_2). A recent study indicates that air pollution from conventional ships accounts for more than 18% of global pollutants, with the maritime industry contributing 13% of the global sulfur oxide emissions [2]. These pollutants are primarily emitted during harbor maneuvering and operations at sea. In response, the International Maritime Organization (IMO) has implemented a regulation requiring a maximum sulfur content of 0.50% m/m (mass by mass) in fuel oil to mitigate sulfur emissions [3].

The growing concern over greenhouse gas emissions and fuel consumption in conventional ships has highlighted several contributing factors, including fuel composition, machinery (such as auxiliary engines), charter planning, vessel category, ship condition (for example, coating and servicing), and operational factors. As a result, the IMO's Maritime Environment Protection Committee (MEPC) has established mandatory guidelines for energy efficiency in ships, encapsulated in the Energy Efficiency Design Index (EEDI). The EEDI monitors greenhouse gas emissions and promotes improvements in "hull design and machinery operations." It serves as a critical technical measure governing new ships and the implementation of the Ship Energy Efficiency Management Plan (SEEMP) [4], [5]. Additionally, the SEEMP encourages the use of the Energy Efficiency Operational Indicator (EEOI) to assess the energy efficiency of existing

ships, considering environmental factors such as sea state, waves, currents, speed, draught, distance, and the condition of the hull and machinery [6], [7]. These regulations significantly impact both existing conventional ships and new vessels using the aforementioned fuels.

Technological advancements have also spurred interest in autonomous ships (AS), with research in this area drawing from unmanned vehicles in sectors such as space transportation, commercial rail, aerospace, and automotive industries [8]. The knowledge gained from these autonomous systems has led to the development of human-machine interfaces (HMIs) for fully unmanned and remotely controlled ships [9]. However, the implementation of autonomous ships presents challenges similar to those encountered in other autonomous transportation sectors, including cybersecurity, ship maintenance, grounding, environmental disasters, passenger safety, and system reliability and efficiency. While the full realization of autonomous ships may take years, the potential advantages outweigh the challenges [8]. Furthermore, with the integration of EEDI and SEEMP for autonomous ships, the IMO's goals can be more readily achieved, as these vessels are equipped with more environmentally friendly engines and technologies.

1.1 Research Problem Statement or Motivation

The International Maritime Organization (IMO) aims to decarbonize international shipping, actively supporting the integration of technology to help achieve the targets set by the Paris Agreement. As part of its commitment to addressing climate change, the IMO plays a key role in advancing the *United Nations' Sustainable Development Goal 13* [10], [11]. A notable advantage of Maritime Autonomous Surface Ships (MASS) is their potential to enhance energy efficiency and reduce emissions by utilizing renewable energy sources, electricity, or hybrid systems. The IMO has set ambitious goals to lower CO_2-equivalent emissions from international shipping, with the target for 2050 being a 50% reduction in CO_2 emissions compared to 2008 levels [10], [11]. These objectives have increased the demand for advanced technologies in ship design and construction to achieve automation that optimizes energy efficiency.

This ambitious target has posed significant challenges for naval architects worldwide in designing vessels that meet the required levels of energy efficiency. At the MEPC 76 [12] several measures to improve ship energy efficiency were identified, but implementing these solutions has proven

difficult. Therefore, further measures need to be explored to meet the IMO's long-term goals. This research is motivated by the need to examine the energy management systems of MASS, focusing on emissions and their associated environmental costs.

1.2 Research Justification

The automobile industry has brought significant changes to our roads with the induction of autonomous vehicles, and similar innovation are currently being implemented in the marine industry. The deployment of MASS on the open sea clearly indicates that they are likely to be more successful than self-driving cars navigating the congested streets of our cities [13]. Therefore, the increasing urgency to reduce carbon emissions and improve the sustainability of maritime operations underscores the importance of integrating renewable energy systems (RES) and alternative fuels into ship power systems. However, research on the application of these technologies, especially in the context of autonomous vessels, remains sparse. Autonomous ships introduce unique challenges due to their reliance on renewable energy sources like PV, wind turbines, and battery bank, their operational dynamics, which differ significantly from conventional manned vessels. This research is therefore justified by the necessity to fill the gap in knowledge regarding the integration of hybrid renewable energy systems (HRES) in autonomous ships. By developing advanced energy management strategies and optimization frameworks, this study aims to enhance the operational efficiency and environmental performance of both conventional and autonomous vessels. The findings will not only provide practical solutions for integrating renewable energy into maritime transport but also contribute to achieving operational strategies in marine transportation and offer valuable guidance for decision-making and investment in the marine sector, ensuring regulatory compliance and environmental sustainability.

1.3 Research Objectives

The objectives of this research work are as follows:

- To perform a comprehensive techno-economic analysis on both conventional and fully autonomous vessels, evaluating various HRES configurations in terms of cost, energy

efficiency, and environmental impact. This involves the application of metaheuristic optimization algorithms to identify the most cost-effective and efficient configurations.

- To identify optimal marine fuels for short-sea shipping vessels by employing a proposed global warming potential (GWP) approach in conjunction with bottom-up methodology to examine key performance indicators (KPIs) for marine alternative fuels.
- To employ advanced predictive-metaheuristic algorithms such as Nonlinear Model Predictive Control (NMPC) via Grey Wolf Optimization (GWO), and Genetic Algorithm (GA), to optimize power distribution and energy management. This study also assesses the impact of irregular wave disturbances on the propeller load torque while minimizing fuel consumption and emissions.

1.4 Research Scope

This study focuses on the energy management of fully autonomous short-sea shipping vessels, particularly tugboats, high speed passenger ferries operating along the California coast, with the Port of Los Angeles serving as the primary operational region. Additional navigational routes include surrounding terminals such as Dana Point, Long Beach, Avalon, and Two Harbors. The research encompasses three main components. First, it conducts a comparative analysis of metaheuristic optimization algorithms—namely artificial bee colony (ABC), genetic algorithm (GA), and particle swarm optimization (PSO)—to determine the optimal HRES configurations for both conventional and autonomous tugboats. Furthermore, it presents a detailed environmental and cost evaluation of various marine alternative fuels for autonomous short-sea shipping vessels using a global warming potential (GWP) methodology integrated with a bottom-up emissions approach. In addition, the study develops a comprehensive nonlinear model predictive control (NMPC) framework for the energy management system (EMS) of autonomous vessels, utilizing optimization techniques such as the grey wolf optimizer (GWO) and GA**.** The model incorporates vessel dynamics**,** including the impact of irregular sea states and environmental interactions. The study utilizes automatic identification System (AIS) data collected over a one-year period, vessel logbooks, equipment technical datasheets, renewable energy technical datasheets, and regional meteorological profiles, with simulations conducted within MATLAB**,** Python, and hybrid optimization of multiple energy resources (HOMER) Pro environments. Lastly, the key analytical

tools include sensitivity analysis, Monte Carlo simulation, and rule-based strategies to evaluate optimal energy dispatch, emission reduction, fuel consumption, operational cost, and emission-associated costs.

1.5 Dissertation Outline

This dissertation is organized into six chapters. The structure of this dissertation is as follows: Chapter 2 provides an overview on marine autonomous surface ships, marine propulsion systems, and relevant metaheuristic and control algorithms. This is followed by Chapter 3, an article that discusses and performs a techno-economic assessment on standalone hybrid renewable energy system onboard conventional and autonomous tugboats. Chapter 4 presents an article proposing environmental and cost assessments of marine alternative fuels for fully autonomous short-sea shipping vessels, based on the global warming potential approach. Additionally, Chapter 5 develops a predictive model and performs mathematical simulations on an energy management system for fully autonomous vessels with hybrid renewable energy systems, using NMPC via the GWO algorithm. Finally, Chapter 6 concludes the dissertation and outlines directions for future work.

CHAPTER 2. OVERVIEW OF MARINE HYBRID SYSTEM AND CONTROL APPROACHES

This chapter provides a comprehensive review of existing research and developments related to marine autonomous systems, energy sources for ship propulsion, hybrid power systems, and control strategies. It begins with an exploration of MASS, discussing their operational modes, levels of autonomy, and the classification of MASS. Additionally, the chapter concludes with a literature review of case studies on unmanned and autonomous surface vessels utilizing hybrid and renewable power sources.

2.1 Marine Autonomous Surface Ship (MASS)

The autonomous vessel operates with its autopilot set to tracking mode, enabling the ship to follow a pre-determined route without intervention from the Officer of the Watch (OOW). The autopilot system is integrated with HMI, allowing the MASS to navigate and detect both stationary and moving obstacles, even in uncharted waters. The operation of the vessel can be either remote or fully autonomous, with different levels of autonomy defined by various maritime regulations under the IMO. Figure 1 is an illustration of the communication structure for the MASS.

Additionally, remote control and watchkeeping are managed from the shore control center (SCC) through the vessel's sensors and communication systems. The SCC can control the vessel remotely, but only when access to the autopilot is granted by the Officer of the Watch (OOW). The MASS automation is pre-programmed to facilitate communication and interaction with other vessels. However, the MASS may still have crew members onboard for maintenance purposes [5], [9]. Furthermore, the management of the MASS involves supervision and control from fleet management, as well as coordination and implementation from the port and fleet forwarding services. The operational zones are illustrated in Figure 2.

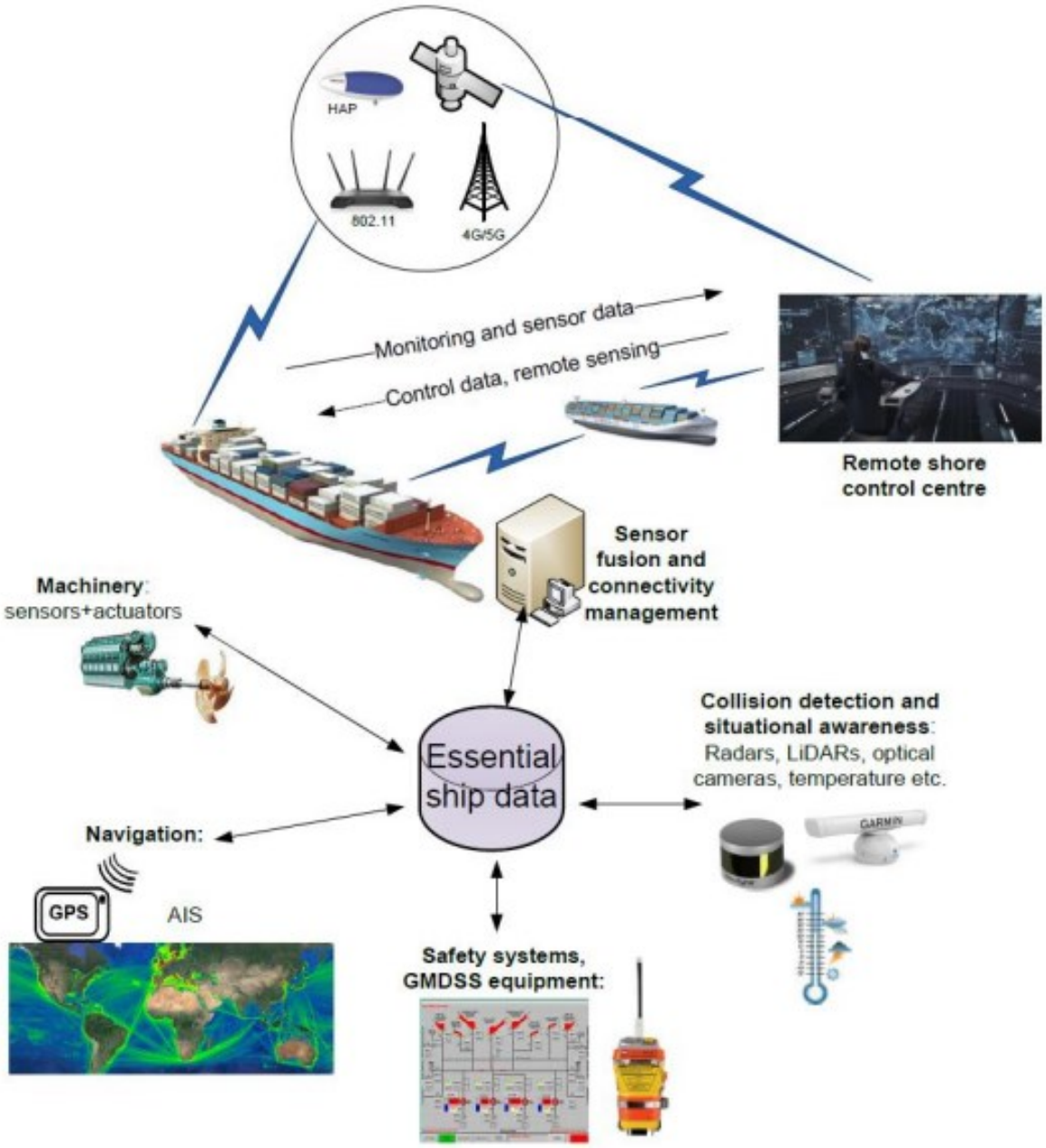

Figure 1: Communication structure for the autonomous ship [8].

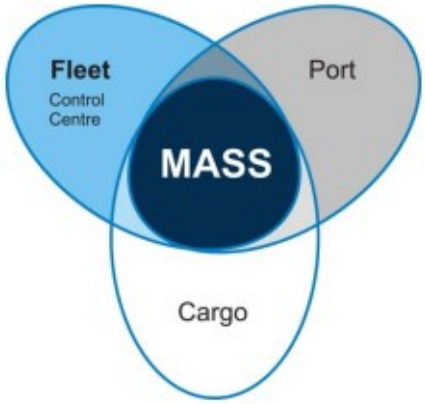

Figure 2: Fleet Management for autonomous maritime systems [9].

2.1.1 Degree of Autonomy for MASS

The levels of autonomy are determined by the extent to which a MASS operates with or without human intervention. Additionally, the variation in autonomy levels is influenced by the operating environment of the vessel. During the 100th Session of the Regulatory Scoping Exercise on MASS, the International Maritime Organization's (IMO) Maritime Safety Committee (MSC) defined four levels of autonomy [9], each representing a different degree of human involvement in ship operations. These four levels of manning are briefly described as follows [2], [10], [11]:

i. **Degree one (On board decision support):** The ship is equipped with automated processes and decision support systems. While many operations are automated, all actions are still controlled by the onboard crew.
ii. **Degree two (On and off board):** Decisions and support actions are performed at both onboard and remote locations by qualified seafarers.
iii. **Degree three (Fully Remotely)**: All decisions and actions are executed remotely from different location (SCC), with no crew onboard the vessel.
iv. **Degree four (Fully Autonomous)**: The ship's operating system autonomously makes decisions for the entire mission, without human supervision, and the vessel remains unmanned.

Furthermore, the *MSC 2018 Regulatory Scoping Exercise for Maritime autonomous Surface Ship*, distinguishes between technical autonomy and operational control. Technical autonomy, as defined by the MSC working group, refers to a closed concept that includes two states with a manned crew and two states without a crew onboard. Operational control provides flexibility and additional options for MASS execution. The technical autonomy and operational control levels are outlined as follows [2]:

a. Technical Levels:

- ***A0 (Manual)****:* The ship's operations are entirely controlled manually by the crew.
- ***A1 (Delegated)***: The operator requires permission from a qualified operator before executing functions, decisions, or actions, although the operator can abort the operation at any stage.
- ***A2 (Supervised)****:* The system makes decisions without the qualified operator's permission, but the operator can intervene and override the system at any time.
- **A3 (Autonomous)**: The system executes functions, decisions, and actions without requiring the qualified operator's approval. The operator is only informed if the ship operates outside predefined parameters, at which point they can override the system if necessary.

b. Operational Control:

- ***B0*****:** There are no qualified operators on the ship but there are qualified operations at the SCC (remote location).
- ***B1:*** Qualified operators manned the ship.

According to the Norwegian Forum of Autonomous Ship (NFAS), the autonomous ships (AS) are classified based on the area of operation, mode of controls, and the levels of manning as illustrated in Figure 3 [7]. Furthermore, the combination of any technical autonomy and operational control levels offers both strengths and challenges. However, the integration of these two concepts is expected to result in improved economic benefits, particularly through enhanced safety and reliability. Therefore, the interaction between these levels is governed by existing international maritime regulations, including the *Safety of Life at Sea (*SOLAS) and the *Standards of Training, Certification, and Watchkeeping for Seafarers (STCW)***.**

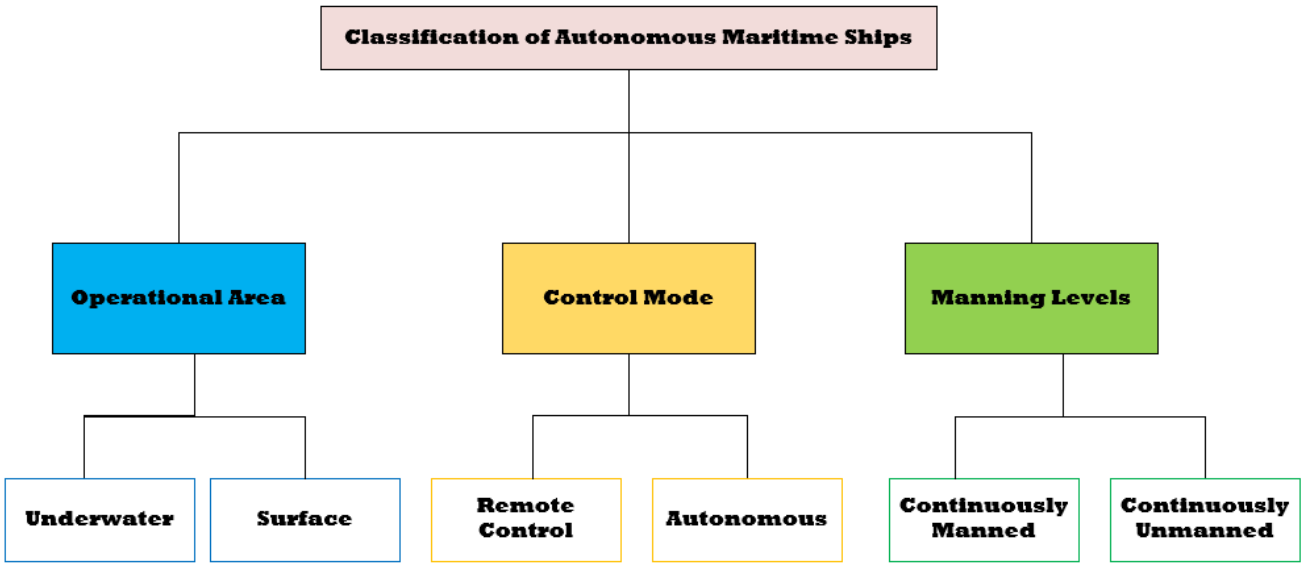

Figure 3: Classification of MASS [14].

2.1.2 Benefits and Challenges of MASS in the Marine Sector

The implementation of MASS offers significant potential to not only improve environmental conditions but also positively impact the social, economic, and political aspects of the maritime industry. Below are the advantages associated with the adoption of MASS [9]:

a. **Benefits for Stakeholders**: The introduction of MASS would provide various benefits to key stakeholders in the maritime industry, including maritime administrations, industry players, research and development organizations, ship owners, classification societies, and insurance companies [2]. For instance, the incorporation of new technologies would enhance profitability within the marine industry. Additionally, as illustrated in Figure 4, ship owners would achieve reductions personnel and equipment costs. The research and development sector would see increased job opportunities due to the growing demand for cognitive advancements. Insurance companies would benefit from reduced risks and fewer incidents, leading to lower premiums and higher economic returns. Moreover, maritime administrations would find it easier to supervise and manage the various entities involved,

facilitating the transition to an "as low as reasonably practicable" (ALARP) approach to risk management [2].

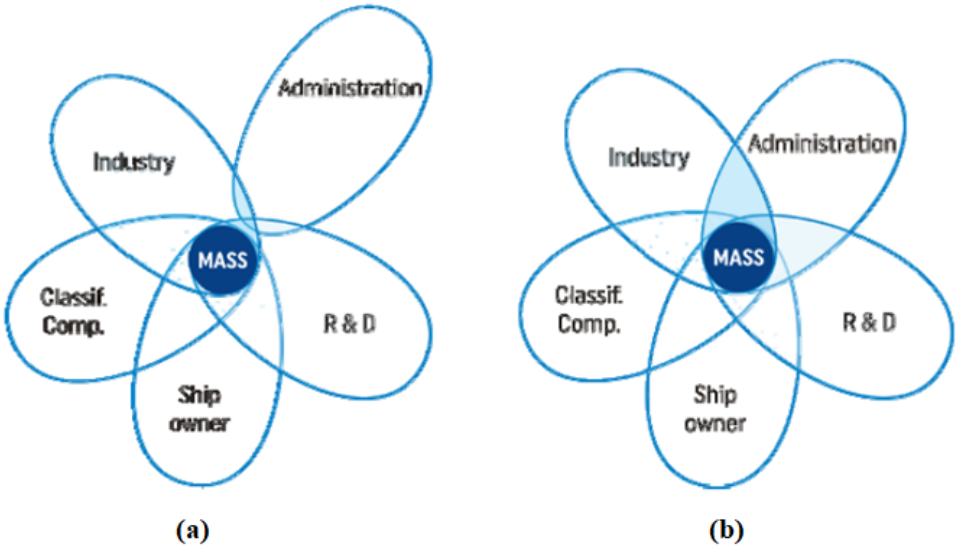

Figure 4: Five group of entities involved in the life cycle of MASS: (a) present (b) expected [9].

b. **Reduction of Human Error and Risk**: Human error, which is a leading cause of accidents in conventional ships (CS), often arises from crew workload and fatigue. The integration of autonomy in the maritime industry would significantly reduce human error, lowering the costs associated with accidents and insurance premiums [6]. According to the 2017 Global Claims Review report by Allianz Global Corporate & Specialty, between 75% and 96% of maritime accidents are attributed to human error as shown in Figure 5 [12]. High-profile examples, such as the Costa Concordia and MV Rena disasters, demonstrate the catastrophic consequences of human error. These types of collisions could be prevented on MASS, as their human-machine interfaces (HMIs) are integrated with the International Regulations for Preventing Collisions at Sea (COLREGs), enabling autonomous vessels to detect and avoid collisions without human intervention [2].

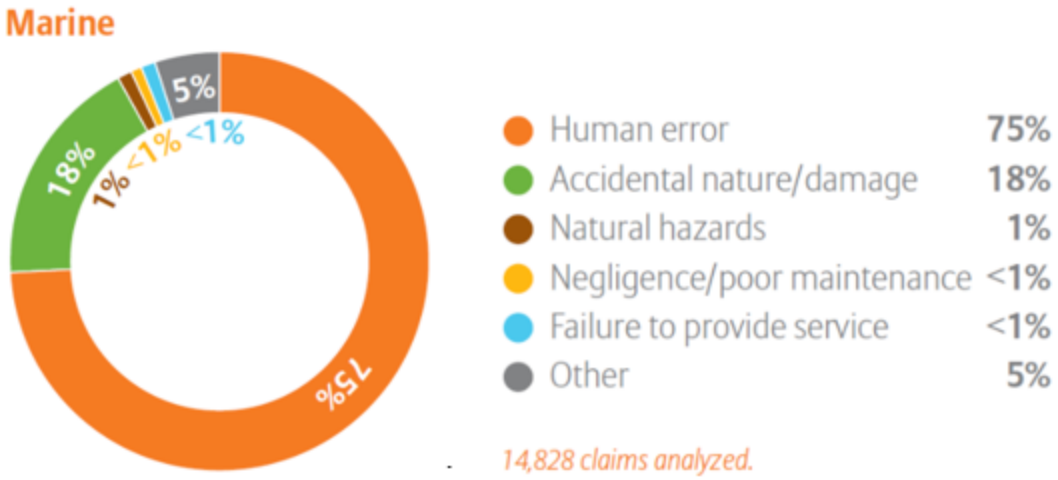

Figure 5: Main causes of liability in the marine sector [13].

c. **Cost reduction or Elimination:** Operating an AS would be more cost-effective than a conventional ship. The reduction or elimination of crew members onboard would lead to lower salary and employee benefit costs. Additionally, operating costs would decrease due to reduced maintenance needs and more efficient operation [2], [6], [9]. For example, unmanned autonomous cargo vessels operating at 12 knots would consume 22% less fuel compared to conventional cargo vessels as shown in Figure 6 [13].

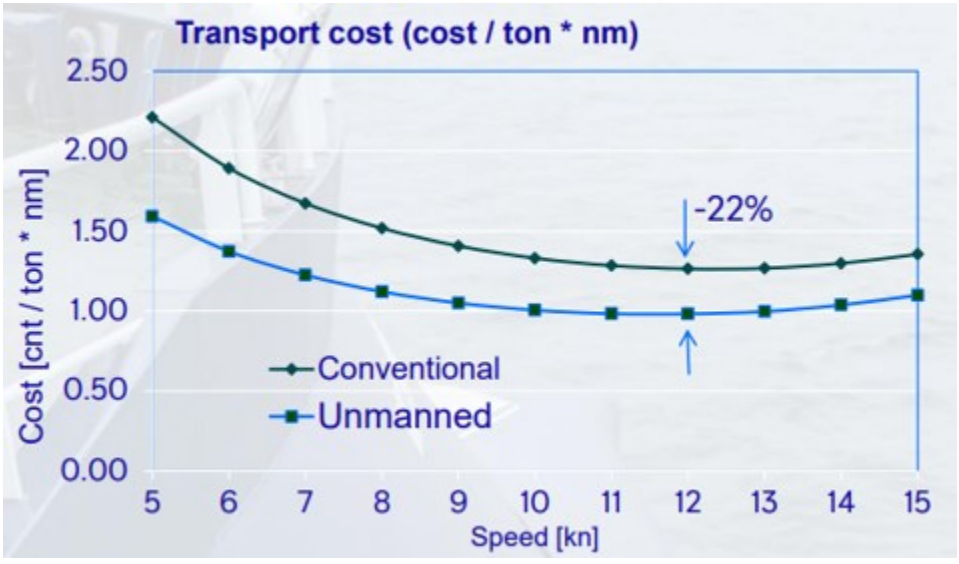

Figure 6: Rolls Royce internal study for 20, 000 dwt general cargo vessel for oil consumption [15]

d. **Increased Ship Efficiency**: The removal of crew accommodations, such as cabins and bridges, would optimize the design and structural integrity of the ship. This redesign would create additional space for cargo, making the loading process more efficient and enhancing overall vessel capacity [6].
e. **Promotion of Greenhouse Gas Emission Reduction:** Autonomous ships powered by fully electric or hybrid systems would reduce overall energy consumption. The elimination of onboard facilities such as galleys, heads, and messes would further reduce energy demand, resulting in up to a 60% reduction in greenhouse gas emissions [16], [17].

The implementation of MASS presents certain safety concerns, similar to the challenges faced by any emerging technology. These concerns could potentially lead to legal complications or accidents. Below are some of the disadvantages associated with MASS [9], [16], [18]:

a. **Underdeveloped Technology:** As a relatively new innovation, AS technology is still evolving, with several uncertainties and aspects that have not yet been fully developed or reviewed by the IMO.
b. **Susceptibility to Cyber Attack**: Fully autonomous vessels are connected through land and satellite networks, which exposes the ship's control systems to potential cyberattacks, jeopardizing the security and integrity of the vessel.
c. **Job Losses:** The transition from CS to AS could result in significant job displacement. This shift may impact individuals in the workforce, particularly those without higher education qualifications, both on board and at the shipyard.
d. **Limited Capability to Perform Diverse Transport Tasks:** Concerns exist regarding the ability of AS to perform the range of tasks typically carried out by crew members during various stages of transportation. These tasks often require human intervention before and after loading and unloading goods or passengers, which may not be fully automated.

Despite these challenges, the widespread implementation of MASS could offer numerous societal benefits, as there are several technological solutions available to convert conventional ships into autonomous ones or to design new autonomous vessels from the ground up. As a result, many shipping companies are embracing this innovation. For example, the Norwegian Shipowners' Association and 50% of global shipping companies are expected to incorporate autonomous operations into their fleets by 2050 [14]. For example, Table 1 presents a snapshot of some of the

notable autonomous ships that have been tested or are currently in operation, developed by various sectors within the maritime industry. The findings from these sea trials are being incorporated into the company's Advanced Autonomous Waterborne Applications (AAWA) research project for further study [19], [20].

Table 1: List of tested and operational autonomous ships.

Vessel Name	Type of Ship	Powered by	Reference(s)
MF Folgefonn	Cargo Ferry	Hybrid	[21]
Ferry Falco	Car Ferry	Hybrid	[22]
Suomenlinna II	Ice-breaking Passenger Ferry	Fully- electric	[23]
Zhi Fei	Container Vessel	Fully- electric	[24]
ReVolt	Container Vessel	Fully- electric	[25]
NTNU Autoferry	Passenger Ferry	Fully- electric	[26], [27]
Soleil	High- Ro-Pax Ferry	Fully electric	[28], [29]
Mayflower 400	Research vessel	Hybrid	[24]
Yara Birkeland	Cargo Ship	Fully- electric	[24], [30]
ASKO Seadrones	Cargo Vessel	Fully- electric	[31]

2.2 Literature Review

The integration of advanced energy systems in autonomous surface vessels (ASVs) and unmanned surface vehicles (USVs) has been a focal point for improving endurance, power efficiency, and operational autonomy. Multiple studies have explored hybrid and renewable-based propulsion systems. Tu et al.[32] addressed the inherent limitations of lithium batteries for long-endurance missions by incorporating a proton exchange membrane fuel cell (PEMFC) system augmented with a supercapacitor on USV. This configuration substantially increased cruising range from 8 km to 38 km and enhanced hydrogen utilization, suggesting a robust solution for prolonged deployments. Similarly, Renau et al. [33] investigated PEMFC-battery hybrid systems, comparing active and passive power plant configurations. The results show that the active configuration with DC-DC converters significantly enhances energy management, extending the USV's autonomy to over 12 hours in calm waters, while maintaining constant fuel cell power and improving overall performance. Complementarily, advanced energy management algorithms also played a pivotal role. Li et al. [34] implemented a rule-based fuzzy control and equivalent consumption minimization strategy (ECMS) on a hybrid power system of battery-capacitor-PEMFC for a traditional vessel within MATLAB/Simulink. The results show that, the EMCS with frequency decoupling effectively reduces hydrogen consumption, while stabilizing output power, and enhancing the system's robustness, economy, and endurance. Similarly, Fu et al. [35] designed a hybrid electric USV powered by hydrogen, integrating a fuel cell and energy storage cell. The proposed power distribution algorithm, based on Pontriagin's minimum principle, effectively reduced fuel cell output fluctuations, enhancing fuel cell longevity and demonstrating the feasibility of a lightweight and high-endurance hybrid power system for small power USVs. Equally, Zaman et al. [36] developed a comprehensive EMS integrating photovoltaics (PV), PEMFC, battery, and hydro generators for an eco-robotic ASV via MATLAB/ Simulink. The system maintained zero-emission operation under extreme environmental conditions, while meeting vessel's power demands for sensors, navigation, control, and propulsion.

Subsequently, research into vessel architecture, control systems, and mission capability continues to define the operational boundaries of ASVs. To illustrate, Rynne et al. [37] pioneered the design of a wind and solar powered autonomous surface vehicle (WASP-ASV), focusing on aerodynamic, hydrodynamic, and systems integration aspects. The results demonstrated that the rigid wing sail

outperforms conventional cloth sails, with the control approach allowing for efficient speed and heading control, while initial field trials confirm the accuracy of predicted performance and vessel behavior. Furthermore, Kristensen et al. [38] examined the research vessel (*AutoNaut)*—a PV-battery powered and wave-propelled USV—highlighting the importance of assessing safety and security risks in green-powered autonomous systems. The findings emphasized that environmental factors and autonomous functionalities can impact mission performance; and the study provides insights for integrating alternative energy sources into MASS, with implications for risk management and operational safety. Similarly, Eide et al. [39] reported the successful deployment and testing of the fully electric autonomous urban passenger ferry (*milliAmpere2*), which demonstrated feasibility of using ASVs for passenger transport, while identifying key challenges related to human-autonomy interaction, fleet management, and integration with urban traffic. Likewise, Wolfe et al. [40] study addressed the challenge of real-time, extended-duration water quality monitoring using ASVs, specifically solar-battery powered ASVs like the *SeaTrac SP-48*, which serve as mobile monitoring stations. The results show that while the *SP-48's* energy production and consumption were balanced over a 29-days mission, energy consumption slightly exceeded production due to varying solar energy availability, highlighting the need for effective energy budget management and optimization for future extended-duration missions. In another case, Riccobono et al. [41] proposed a multi-source hybrid energy system—combining PV modules, PEMFCs, and batteries for a research vessel (*SWAMP Vehicle*). The results demonstrated that the proposed energy system, validated by MATLAB/Simulink simulations, significantly improves *SWAMP Vehicle* endurance, doubling it to 12 hours on the most favorable day, while adhering to the *SWAMP Vehicle* 's weight, size, and payload constraints. Similarly, Zhang et al. [42] analyzed wind-assisted propulsion systems, employing wind sails and rotor sails on ASVs . The results show that an autonomous control strategy based on a nonlinear mathematical model and backstepping technique achieves a 13% energy optimization ratio in a rotor sail-assisted vessel, demonstrating significant potential for energy savings and lower emissions in real-world maritime operations. Equally, Chen et al. [43] introduced a distributed MPC algorithm for *Eco-Vessel Train Formations (VTF)* using diesel-electric hybrid propulsion in MATLAB environment. The results showed that the *Eco-VTF* algorithm leads to significantly lower fuel consumption compared to standard *VTF* control, particularly for vessels with higher engine power. Although

Eco-VTF results in longer travel times due to lower consensus speeds, and the reduction in fuel usage is substantial.

Thereafter, addressing the environmental footprint of maritime operations is a central theme in autonomous vessel research. To exemplify, Makhsoos et al. [44] addressed the environmental challenges posed by fossil fuel reliance and explores the integration of solar power in the energy system of an unmanned surface vehicle (USV) designed for autonomous bathymetry tasks. The results showed that the proposed hybrid power system, with PV-battery, optimizes energy usage, enabling the USV to operate for up to 7 hours daily on cloudy days without charging, demonstrating the feasibility and efficiency of solar-powered autonomous marine vehicles. Additionally, Sornek et al. [45] explored similar research where a solar-powered ASV research boat used for water quality monitoring, highlighting the vehicle's capability to measure various water parameters. The results show that the vessel's optimized design, including a high-efficiency PV panel, significantly improves power generation, and simulations indicate that its operation can lead to substantial primary energy savings, with potential to replace existing water quality monitoring systems. Furthermore, in larger-scale applications, Ait Allal et al. [46] assessed autonomous container and cargo ships powered by liquefied natural gas (LNG) and fuel oil, in improving the sustainability of the maritime industry by reducing energy consumption and environmental pollution. The study affirmed that the elimination of crew and associated facilities on AS leads to significant energy savings, lower greenhouse gas emissions, and enhanced environmental protection, with case studies on container and general cargo ships demonstrating substantial fuel savings compared to conventional ships (CS). Similarly, Laryea and Schiffauerova [47] explored various alternative fuel options, including hydrogen and fully electric configurations, for fully autonomous short-sea shipping vessels, focusing on energy efficiency and regulatory compliance. The results show that hydrogen and electric fuels offer zero emissions, while LNG provides the highest net present value (NPV) for autonomous vessels, demonstrating both economic and environmental advantages compared to traditional fuels like heavy fuel oil (HFO) and marine diesel oil (MDO). Also, the same authors [48] proposed an optimized HRES using solar panels, wind turbines, batteries, and diesel gensets for autonomous tugboats. Employing metaheuristic algorithms (Artificial Bee Colony Algorithm (ABC), Particle Swarm Optimization (PSO), Genetic Algorithm (GA)) and Hybrid Optimization of Multiple Energy Resources (HOMER) Pro, the study demonstrated that ABC outperformed others in minimizing costs and

emissions, reinforcing the model's robustness for marine applications under variable operating conditions. Lastly, in a broader framework, Dantas and Theotokatos [49] addressed the lack of decision-support systems for MASS. Through a case study using a short-sea cargo vessel operating in Norwegian waters, both retrofitting of existing vessels into *Transition Autonomous Ship (TAS)* and the design of *Next Generation of Autonomous Ship (NGAS)* were evaluated. The results suggested that TAS could reduce lifetime costs by 1–12% and CO_2 emissions by 4%, while NGAS can achieve additional reductions of 3 –4% in cost and 4 –7% in emissions. Furthermore, additional cost savings of 6 –7% could be realized by minimizing idle port time, made possible through reduced crew requirements.

In brief, the reviewed literature underscores the growing capability and environmental potential of autonomous surface vessels in the marine engineering domain. Innovations in renewable energy integration**,** hybrid system optimization, and advanced control strategies not only enhance operational endurance but also significantly contribute to the decarbonization of the maritime sector. The convergence of system-level simulation**,** experimental validation, and control engineering lays a robust foundation for the deployment of next-generation autonomous vessels across a broad range of applications—from scientific surveying to commercial transport.

Despite extensive studies on hybrid energy systems in microgrids and land-based applications, current literature lacks holistic, techno-economic, and operational frameworks specifically tailored for maritime applications—particularly for the integration of hybrid renewable energy systems (HRES) into conventional and fully autonomous ships. Existing models often neglect the spatiotemporal variability in shipboard power demands, constrained onboard space, dynamic sea-state conditions, and real-time operational uncertainties. Furthermore, energy management strategies for autonomous ships frequently omit ship dynamics, emissions beyond CO_2 and NO_x, and predictive control under uncertain environmental conditions. There is also a critical gap in comparative assessments of alternative marine fuels based on real operational profiles, emission dispersion, and environmental-economic trade-offs. Most notably, limited attention has been paid to developing predictive, multi-objective EMS frameworks capable of optimizing power flows under variable marine conditions while adhering to IMO regulations and addressing performance indicators such as fuel consumption, emission cost, mass emission rate (MER), and EEOI. This

calls for a new class of marine-specific energy systems modeling that integrates weather-dependent RES performance, ship dynamics, regulatory constraints, and cost-environmental trade-offs into a unified decision-support framework for autonomous and short-sea shipping vessels.

In this dissertation, we seek to fill that gap by systematically addressing the techno-economic, environmental, and operational challenges associated with hybrid renewable energy systems and alternative fuels in autonomous and conventional maritime applications.

To begin with, Chapter 3, we present a detailed techno-economic analysis of standalone hybrid renewable energy systems onboard both conventional and autonomous tugboats. The analysis applies advanced metaheuristic algorithms to determine optimal system configurations that minimize cost and environmental impact, thereby providing a baseline for comparative performance assessment.

Subsequently, Chapter 4, we evaluate the environmental and cost implications of integrating marine alternative fuels into the propulsion systems of fully autonomous short-sea vessels. Using a bottom-up emissions framework and global warming potential (GWP) methodology, we quantify the trade-offs in fuel selection across various operational scenarios, with particular attention to emission factors, fuel pricing, and propulsion loads.

Following this, Chapter 5, we develop and validate a predictive energy management model for autonomous vessels employing nonlinear model predictive control (NMPC) optimized via Grey Wolf Optimization (GWO). For the first time, we incorporate real-world environmental disturbances—including irregular wave impacts—into the propeller load torque model, and show that predictive-metaheuristic strategies can significantly reduce fuel consumption, emissions, and battery degradation while maintaining optimal energy dispatch.

Finally, Chapter 6 synthesizes the findings and outlines future research directions, particularly the development of onboard real-time adaptive control frameworks and further investigation into maritime regulatory compliance under autonomous operational conditions.

CHAPTER 3. A NOVEL STANDALONE HYBRID RENEWABLE ENERGY SYSTEMS ONBOARD COVENTIONAL AND AUTONOMOUS TUGBOATS

In this chapter, we focus on the computation, simulation, and optimization of a hybrid renewable energy system (HRES) to ensure continuous power supply for auxiliary loads and critical systems on both conventional and fully autonomous tugboats. The primary aim is to design an optimal HRES with minimal annualized cost of system (ACS) and a higher proportion of renewable energy while using an artificial bee colony (ABC) algorithm. Validation of optimization outcomes is conducted using particle swarm optimization (PSO), genetic algorithm (GA), and Hybrid Optimization of Multiple Energy Resources (HOMER) Pro. The HRES incorporates diesel generators (Gensets), photovoltaic (PV) arrays, vertical axis wind turbines (VAWT), and battery banks. The optimal HRES configuration for both conventional and fully autonomous tugboats is found to be Genset/PV/VAWT/Battery. We observe that the ABC algorithm exhibits superior convergence, reliability, cost-effectiveness, renewable energy fraction, and reduced carbon emissions compared to alternative algorithms. Results of robustness tests suggest that the shipload variation, fuel prices, temperature fluctuations, wind speed and solar irradiance along the navigation route have significant impact on the optimal HRES configuration. Ultimately, we conclude that the fully autonomous tugboat demonstrates superior performance in terms of costs, carbon dioxide emissions, and renewable energy fraction compared to its conventional counterpart.

This chapter is based on the following publication: *H. Laryea and A. Schiffauerova, "A novel standalone hybrid renewable energy systems onboard conventional and autonomous tugboats," Energy, vol. 303, p. 131948, 2024. [Online]. Available :https://doi.org/10.1016/j.energy.2024.131948*

3.1 Introduction

Maritime transport is considered pivotal in global trade, with nearly 80% of global commerce conducted through seaborne trade [50]. It relies heavily on conventional ships and ports worldwide, with over 50,000 conventional ships (CS) [51], and more than 835 active seaports and inland ports in the world [52]. The generation of power on ships plays a crucial role in the maritime industry, as it provides the necessary electrical energy for propelling vessels between ports. Over time, marine engines have transitioned from using coal to utilizing marine diesel oil (MDO) and heavy fuel oil (HFO). According to the International Maritime Organization (IMO), global fuel consumption in the maritime sector ranges from 250 to 350 million tons annually, contributing to approximately 2.8% of global greenhouse gas (GHG) emissions and resulting in a yearly carbon dioxide (CO_2) emission rate of 3.1%. It has been suggested [53], [54] that the emissions rate could triple by 2050 if left unchecked. As a result, the International Convention for the Prevention of Pollution from Ships (MARPOL) has established four mandatory requirements for both new and existing vessels to mitigate air pollution. These requirements include the utilization of cleaner fuel with reduced carbon content, adoption of renewable energies, implementation of emission reduction technologies, and enhancement of energy efficiency [54], [55]. Utilizing an emerging type of vessel known as maritime autonomous surface ships (MASS) offers a means to mitigate environmental impact. MASS operates autonomously, employing artificial intelligence (AI) for steering and decision-making without intervention from seafarers. In fully autonomous fleets, the absence of onboard ship crews contributes to energy conservation and pollution reduction [56], [57]. For instance, a fully autonomous container vessel achieves a 74.5% reduction in energy consumption compared to a conventional counterpart, primarily due to the elimination of crew facilities and equipment [46]. Thus, integrating autonomous MASS with renewable energy sources presents an effective strategy for reducing greenhouse gas (GHG) emissions within the maritime sector.

The primary challenges associated with integrating renewable resources into power systems include their initially high costs and the variability of wind and solar energy generation. Nevertheless, there has been a decrease in the cost of renewable energy sources [58], and numerous studies have investigated the integration of renewable energy systems into existing energy infrastructures. For example, Ma et al. [59] employed a commercially available microgrid

software, Hybrid Optimization of Multiple Energy Resources (HOMER Pro), to identify an optimal PV/Wind/Battery hybrid system to replace the existing diesel generator on a remote island while minimizing costs. They conducted sensitivity analyses to assess the impact of various inputs on their proposed models. Additionally, several researchers utilized a genetic algorithm (GA) to construct models integrating wind turbines and photovoltaic (PV) systems with Genset/battery configurations for stand-alone HRES in remote communities. For example, Ogunjuyigbe et al. [60] devised a model replacing a large Genset with a smaller split Genset in HRES, capable of adapting to varying inputs with low emissions, dump energy, and lifecycle costs. In another study, Farahmand et al. [61] examined the optimal configuration of an HRES aiming for minimal electricity expenses for consumers, considering PV efficiency and the quantity of PV modules. Similarly, in order to reduce both lifecycle costs and greenhouse gas emissions in an island microgrid, Zhao et al. [62] investigated a novel operational approach and sizing strategy.

The existing literature primarily focuses on optimizing the distribution of electrical power from hybrid generation systems aboard ships, particularly emphasizing capacity optimization for small systems, predominantly involving photovoltaic power production systems and energy storage systems. While some studies have delved into transient assessments of power systems [63], [64], multi-energy integration for energy management [65]-[67], and hybrid energy storage solutions [68], [69] in conjunction with actual ship navigation, research on the utilization of renewable energy sources on ships remains scarce compared to land-based microgrid systems [70], [71]. Some of these discoveries from land-based HRES contribute to advancing research in the maritime industry [72]. There is limited literature on the integration of PV and wind turbines for shipboard power systems [73]-[76]. For example, Wen et al. [73] assessed an optimal energy storage system for PV/Genset on an oil tanker ship. To minimize the net present cost of the power system and greenhouse gas (GHG) emissions, the authors utilized discrete Fourier transform (DFT) along with the particle swarm optimization (PSO) algorithm, while considering the sea states and rolling effect of the vessel. Similarly, Yang et al. [74] employed the PSO algorithm in a similar model, albeit aboard a RoRo ship, demonstrating an improvement in the ship's energy management strategy under varying electrical loads. Additionally, several researchers have explored the implementation of PV/Genset/Wind/Battery hybrid power systems on ships. For instance, Bouhouta et al. [75] utilized HOMER Pro to optimize PV and wind turbine integration with the harbor tugboat's emergency power system, aiming to minimize its annualized cost of system and

CO_2 emissions particularly during blackout. Also, Wen et al. [76] employed a multi-objective PSO (MOPSO) algorithm to conduct techno-economic analysis for a large oil tanker. The results of the simulations indicate that the optimized hybrid system effectively reduces CO_2 emissions and the system cost of HRES, considering both vessel speed and course as inputs.

However, while the existing literature makes valuable contributions to the optimization of HRES, there are several areas that require further enhancement. For instance, there has been no comprehensive study comparing optimization methodologies for both conventional and autonomous ships. For example, Bouhouta et al. [75] conducted an optimization methodology on HRES during standby, focusing solely on nighttime operations rather than encompassing the entire day. Additionally, sensitivity analysis was not conducted on the proposed model, potentially limiting its robustness and practical applicability. Furthermore, while several authors [73], [77] utilized multiple algorithms to optimize HRES for shipboard power systems, neither robustness tests on the optimal HRES concerning variable inputs nor post-hoc tests on the metaheuristic algorithms were performed [73], [74], [76]. Table 2 offers a comparison among various studies implementing HRES.

Even though existing literatures offer optimal configurations for integrating renewable energy sources (RES) and battery energy storage (BES) in microgrid systems, there are numerous opportunities for improvements and further research. For example, techno-economic evaluation of incorporating hybrid renewable energy systems (HRES) into the power systems of both conventional and autonomous ships is missing in the literature. Furthermore, a comprehensive decision-making model for energy management strategy integrated into HRES for both existing conventional ships and fully autonomous ships has also not been much explored, especially in recent literature, to the best of the authors' knowledge. Additionally, unlike land-based HRES for buildings, ships' HRES are standalone and mobile, thus weather profiles are influenced by both environmental conditions and ship dynamics. As a result, power generation from RES is sporadic, necessitating rapid and continuous decision-making by the energy management system. Moreover, the quantity of PV modules, wind turbines, and batteries to be installed onboard is constrained by space availability (on the weather deck, pilotage area, and in battery compartments), weight limits, and the structural integrity of the ship. This underscores the necessity for further research in order to develop appropriate models facilitating the integration of HRES into the power systems of both

autonomous and existing ships. This study introduces a novel integrated multi-energy supply system designed for ships, incorporating PV, wind, battery, and genset technologies, with a specific focus on providing uninterrupted clean electrical power. The uniqueness of this approach lies in its adaptation from land to both conventional and fully autonomous ships, while simultaneously addressing to the distinct requirements of energy management systems onboard ships.

Table 2 : A tabulated comparison of HRES implementation in both building and transportation sectors.

Ref	Objective	Country	Application	Algorithm	Remarks
[59]	Design, optimize hybrid system, to replace current diesel.	China	Remote Island	HOMER Pro	Sensitivity analysis is done base on variation of load demand and rated power of components.
[60]	Minimize life cycle costs, reduce pollutants, and minimize dump energy.	Nigeria	Remote Building	GA	The reliability of the system is not considered.
[61]	Optimize HRES for building to minimize the overall system cost.	Iran	Urban Building	GA	Emission analysis, system reliability, and sensitivity analysis not considered.
[62]	Optimize HRES for remote microgrids.	China	Remote Island	GA	The reliability of the system is not considered.
[65]	minimize economic costs while considering energy balance and constraints	China	Cruise Ship*	Unspecified	The variability of energy storage based on specific load profile is not considered.
[67]	Emission reduction and ensuring continuous, reliable power for ships	Unspecified	Ships*	MPC, GA, MOPSO	Comprehensive review on configuration and characteristics of HRES for ships.
[68]	Examine hybrid energy storage system (HESS) to improve shipboard power systems	Unspecified	Ships*	Unspecified	Examine multiple energy storage integration on ships.
[69]	Reduce ship hybrid power plant fuel consumption, considering battery constraints.	Unspecified	Naval Vessel*	MPC	Study lacks ship particulars, emission and sensitivity analyses.
[72]	Enhancing shipboard microgrid efficiency, reliability, and cost-effectiveness for safe operation.	Unspecified	Ships*	PSO, GA	Metaheuristic algorithms are effective for multi-objective optimization.
[73]	Utilize diverse HESS to stabilize solar energy fluctuations.	China - Yemen	Oil Tanker Ship*	PSO, DFT	Battery degradation and energy management strategy overlooked.
[74]	Create multi-objective model for ship fuel consumption and Genset efficiency.	Unspecified	RoRo Ship*	PSO	Irradiance variability not addressed
[75]	Utilize renewables for tug safety during blackout.	Algeria	Tugboat*	HOMER Pro	Optimized HRES for short-term emergency use lacks sensitivity analysis.
[76]	Optimize HRES to minimize cost and emissions.	From China to Yemen	Oil Tanker Ship*	MOPSO	Sole reliance on load variation sensitivity; no system reliability consideration.
[77]	Optimize clean energy for load, while minimizing costs.	From China to Yemen	Bulk Carrier Ship*	ABC, QABC, PSO, QPSO, SQP	Sensitivity analysis and post hoc tests omitted.

MPC: Model predictive control, ***SQP***: Sequential Quadratic Programming, ***QABC***: Quantum Artificial bee colony, ***QPSO***: Quantum Particle Swarm Optimization.

***** The marine vessels utilized by the authors are conventional ships.

To address these challenges emphasis is placed on prioritizing a standalone HRES system, while employing objective function alongside three metaheuristic algorithms to size and optimize multiple HRES configurations. These configurations encompass economic analysis, carbon emissions, loss of power supply probability, energy management strategy, and weather data along navigation routes. The goal is to identify the optimal HRES that enhances energy efficiency while simultaneously minimizing ACS and carbon emissions, all within the confines of predefined constraints.

This research brings notable contributions to the existing literature. Firstly, To the best of our knowledge, this study marks the inaugural exploration of HRES optimization tailored specifically for autonomous ships. Moreover, the method outlined in this study simultaneously explores and compares diverse HRES configurations for both conventional and fully autonomous ships, enabling a comprehensive assessment. Secondly, in our HRES optimization, we employ a predetermined set of scenarios, each characterized by its specific level of uncertainty. This approach enables us to account for fluctuations in ship loads and other input parameters, including temperature and wind speed variations, while also depicting scenarios incorporating VAWT and PV systems along the navigation route. Notably, prior literature lacks consideration of scenario analysis for the variability of input factors. Thirdly, in our pursuit of optimal HRES configurations, we utilize and compare three algorithms—PSO, ABC, and GA. Additionally, we introduce integrated energy management strategies that encompass economic and renewable considerations. While prior studies have typically employed one or two of these algorithms for ship optimization, our simultaneous application and comparative analysis of all three algorithms represent a novel approach. Lastly, this study underscores the advancement of two optimization strategies—design and energy management—while proposing multi-objective algorithms that factor in component costs, project duration, lifespan, weather conditions, and power system reliability. This comprehensive framework represents a unique contribution to the field.

The remaining sections of the paper are structured as follows: Section 3.2 details the modeling and simulation process of a standalone hybrid renewable energy system onboard a tugboat. Section 3.3 provides an analysis of the results and discussions, and Section 3.4 offers concluding remarks along with insights into potential future research directions.

3.2 Modeling of Hybrid Renewable Energy Models Onboard Tugboat

This section outlines the modeling of components within the HRES installed on both existing conventional and proposed fully autonomous tugboats. The schematic representation of the proposed hybrid model is depicted in Figure 7. The marine HRES operates by harnessing power generated from PV panels, vertical axis wind turbines (VAWT), and a diesel generators (Genset). Excess energy is stored in a battery bank, and the generated power is managed through bidirectional converters to transfer power to and from the buses. Subsection 3.2.6 provides a detailed description of the HRES models, including the number of components, cost metrics, loss of power supply probability (LPSP), and renewable fraction, all of which are utilized to define the objective function for determining an optimal HRES configuration for each ship type. Additionally, discussions on ship particulars, weather data, and simulation analysis are included.

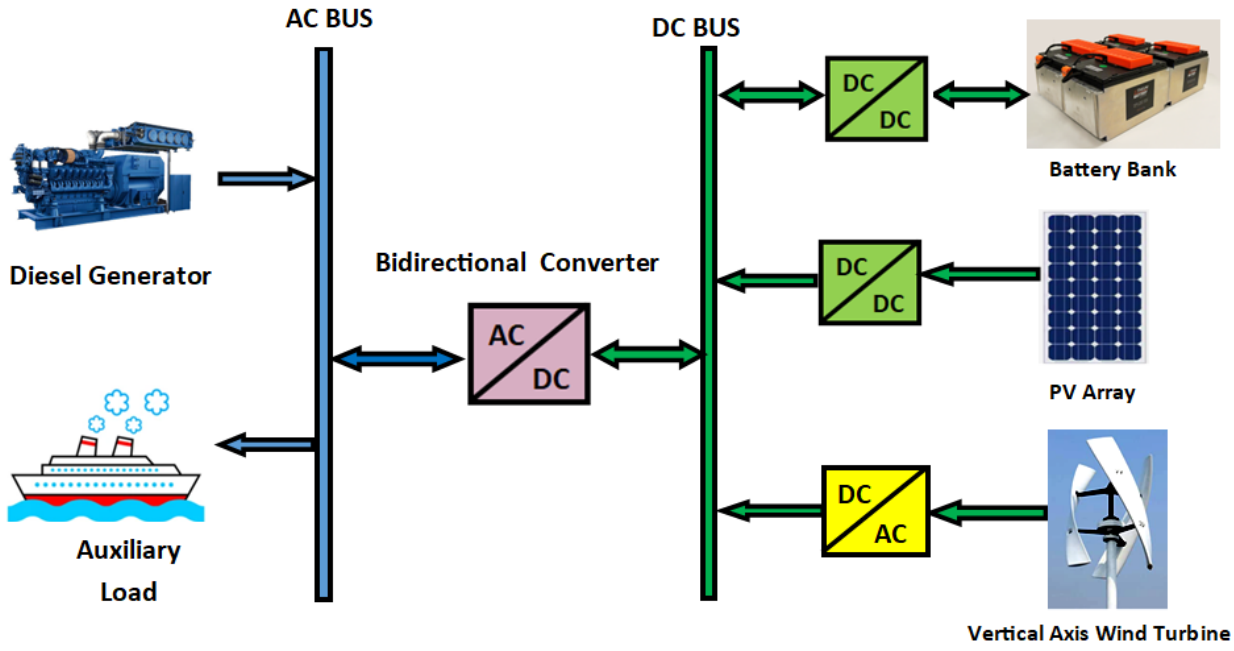

Figure 7: Proposed standalone hybrid renewable energy system (HRES) configuration onboard conventional and autonomous tugboat

3.2.1. Modelling of Marine Diesel Generator (Genset)

The marine diesel generator commonly serves as a backup power source on ships, supplying electrical power for the ship's propulsion and other electrical systems onboard. However, in this study, Gensets serve as the primary energy sources in the HRES to meet the ship's load requirements for both conventional and fully autonomous tugboats. The Genset operates by converting the chemical energy in diesel fuel into mechanical energy through the combustion process, which drives the rotating shaft. This mechanical energy is subsequently converted into electrical energy by the rotation of the alternator's main rotor. Thus, the generation of electrical energy by the diesel generator is described as follows [78]:

$$P_{genset,total}(t) = P_{genset,nom} * \eta_{bt,eff} * \eta_{genset,eff} * N_{genset} \quad (1)$$

where $P_{Genset,total}(t)$ is the total output power by Genset at time t (kWh), $P_{Genset,nom}$ is the nominal power for the diesel generator (kW), $\eta_{bt,eff}$ denotes the brake thermal efficiency which is in the range of 35% - 40% [79], $\eta_{Genset,eff}$ is the diesel Genset efficiency (%) and N_{Genset} is the number of diesel generators fitted on the tugboat (unitless). In this paper, the rated power of the genset aboard the traditional tugboat is 125 kW. The amount of fuel consumed by the Genset depends on its overall output power, which is expressed as [80], [81]:

$$F_{consum,total}(t) = a_{Genset} * P_{Genset,total}(t) + b_{Genset} * P_{Genset,nom} \quad (2)$$

where $F_{consum,total}(t)$ is total amount of diesel fuel consumption at time t (L/h), a_{Genset} is the coefficient of the consumption curve (0.0845 L/kWh) and b_{Genset} denotes the coefficient of the consumption curve (0.246 L/kWh). Lastly, the tonnage of CO_2 emitted by the diesel generator during the ship's operation is estimated as [82] :

$$CO_{2,emission}(t) = \frac{F_{consum,total}(t) * E_{factor} * EC_{factor}}{1000} \quad (3)$$

where $CO_{2,emission}(t)$ is the amount of CO_2 emission by the diesel Genset at time t (tons), E_{factor} is the emission factor for the diesel fuel (69.5 kg /GJ), EC_{factor} denotes the energy content factor

of the diesel fuel (38.6 GJ/kL), and $F_{consum,total}(t)$ is the total amount of diesel fuel consumption at time t (kL/h).

3.2.2. Modelling of Photovoltaic (PV) Panel

The daily solar energy generated by the absorption of solar radiation through PV cells within the PV panel under standard testing conditions (STC) is articulated as follows [83]-[86]:

$$P_{PV,total}(t) = P_{PV,nom} * N_{PV,modules} * \eta_{wire,eff} * \eta_{PV-cell,eff} * \frac{I_{amb}(t)}{I_{STC}} * \left[1 - \lambda_{PV,temp} * \left\{T_{amb}(t) + I_{amb}(t) * \left(\frac{NOCT - 20}{I_{PV,cell}}\right) - T_{PV,STC}\right\}\right] \quad (4)$$

where $P_{PV,total}(t)$ is the total power generated by the PV panels at time t [kWh], $P_{PV,nom}$ is the nominal or rating power of the PV cells (kW), $N_{PV,modules}$ is the number of PV panels, $\eta_{PV-cell,eff}$ is the efficiency of the PV panel (%), $\eta_{wire,eff}$ denotes the efficiency of the wire (%), $I_{amb}(t)$ is the ambient radiation intensity at time t (kW/m^2), I_{STC} is the radiation intensity at the standard test conditions (1 kW/m^2), $\lambda_{PV,temp}$ is the temperature coefficient of the PV modules and it falls in the range of (% / °C), T_{amb} is the ambient temperature at the study area (°C), $NOCT$ is the nominal operating cell temperature (°C), $I_{PV,cell}$ is the radiation intensity on cell surface (0.8 kW/m^2), and $T_{PV,STC}$ is the PV cell nominal temperature at the standard test conditions (25°C). The technical specifications for the selected PV panels used in this research are shown in Table 3. Similarly as in the study of Bouhouta et al. [75], the PV modules are to be mounted on the starboard and port side of the vessel.

Table 3: Technical specifications for the PV modules.

Component	Nominal Power (kW)	Temp Coefficient (% / °C)	Efficiency (%)	NOCT (°C)
PV Module	0.370	−0.29	22.7	41.5

3.2.3. Modelling of Vertical Axis Wind Turbines (VAWT)

The vertical axis wind turbines (VAWT) are proposed for this research due to their quieter operation, simpler maintenance [87], ability to generate wind energy at low cut-in speed, and the potential for clustering turbines closely together [88]. In addition, the energy generation is primarily affected by the hub height of the VAWT and the wind speed in the study region. Thus, in using the wind profile power law, the speed of the VAWT at the turbine height can be expressed as [86]:

$$V_{VAWT,hub} = V_{anemo} * \left[\frac{H_{VAWT,hub}}{H_{VAWT,anemo}}\right]^{\alpha} \quad (5)$$

where $V_{VAWT,hub}$ is the wind speed at the hub height $H_{VAWT,hub}$ [m/s], V_{anemo} is the known wind speed (or anemometer speed) at a reference height $H_{VAWT,anemo}$ (m/s) , $H_{VAWT,hub}$ is the hub height of the VAWT (m), $H_{VAWT,anemo}$ is the height of the anemometer or reference height (m), and α is the friction coefficient for the wind turbine which equals 0.143.

As stated above, the output power of the VAWT is related to the wind speed and this can be expressed as [86]:

$$P_{VAWT}(t) = \begin{cases} n_{VAWT} * \eta_{VAWT} * P_{VAWT,nom} * \frac{V^2(t) - {V_{ci}}^2}{{V_r}^2 - {V_{ci}}^2} & V_{ci} < V(t) < V_r \\ n_{VAWT} * \eta_{VAWT} * P_{VAWT,nom} & V_r < V(t) < V_{co} \\ 0 & V(t) < V_{ci} \ or \ V(t) < V_{co} \end{cases} \quad (6)$$

where $P_{VAWT}(t)$ is the power generated by the fitted VAWT onboard ship (kW), n_{VAWT} is the number of VAWTs [unitless], η_{VAWT} denotes the efficiency of the VAWT [%], $P_{VAWT,nom}$ is the nominal power of the VAWT [kW], $V(t)$ is the wind speed at time t (m/s), V_{ci} is the VAWT cut-in wind speed (m/s), V_{co} is the VAWT cut-off speed (m/s), and V_r is the rated wind speed for

VAWT (m/s). Table 4 shows the technical specifications for the proposed VAWT. For this research, the use of two VAWT is proposed, thus one turbine mounted on starboard mast and the other on the port mast. Furthermore, each VAWT is equipped with a permanent magnet synchronous generator tasked with converting the mechanical energy generated by the rotating blades into electrical energy.

Table 4: Technical specifications for the vertical axis wind turbine (VAWT)

Nominal Power (kW)	Hub Height (m)	Efficiency (%)	Rate Wind Speed (m/s)	Survival Wind Speed (m/s)	Cut-in Wind Speed (m/s)	Cut-out Wind Speed (m/s)
5	4.8	29.8	11	52.2	1.5	15

3.2.4. Modelling of Battery Energy Storage System (BESS)

The battery bank serves to store surplus energy produced by the diesel generator and/or renewable sources during periods of low demand. Consequently, when the demand for power is lower than the combined output from the Genset, PV, and VAWT, the excess energy is used to charge the battery bank. The capacity of the battery bank during charging is determined by [78], [81]:

$$E_{batt}(t) = E_{batt}(t-1) * (1-\sigma) + [\sum E_i(t) - \left(\frac{E_{AC,load\,(t)}}{\eta_{\,inveter}}\right)] * \eta_{\,batt,ch} \qquad (7)$$

During the high peak demand, the total generated power from PV and/or VAWT is insufficient to meet the ship's load requirement. Therefore, power from the battery bank is discharged to fulfill the load demand. The available capacity of the battery bank during discharge is determined as follows [78], [81]:

$$E_{batt}(t) = E_{batt}(t-1) * (1-\sigma) - [-\sum E_i(t) + \left(\frac{E_{AC,load\,(t)}}{\eta_{\,inveter}}\right)] * \eta_{\,batt,disch} \qquad (8)$$

where $E_{batt}(t)$ is the available battery bank capacity during charging and discharging at time t (kWh), $E_{batt}(t-1)$ is the available battery bank capacity at time (t-1) (kWh), σ is the self-discharge rate of the battery bank, $E_i(t)$ is total energy generated by the PV and VAWT (kWh), $E_{AC,load\,(t)}$ denotes the AC load demand at time t (kWh), $\eta_{\,inveter}$ is AC-DC inverter efficiency

(90%), $\eta_{batt,ch}$ is battery efficiency during charging process, and $\eta_{batt,disch}$ is battery efficiency during discharging process. Consequently, the minimum energy of the charged battery bank at time t is estimated as follows [80], [89], [90]:

$$E_{batt,min}(t) = E_{batt,max}(t) * (1 - DOD) \quad (9)$$

where $E_{batt,max}(t)$ is the maximum energy of the charged battery bank (kWh), and DOD is the battery depth of discharge which is equal to 0.80.

In addition, lithium-ion (Li-ion) battery is considered for this research over the lead acid battery [91], nickel metal hybrid battery [92], silver–zinc battery, and open water-powered battery [93], due to its optimal chemical composition or battery chemistry [93]-[95]. Table 5 shows the technical specifications of the Li-ion battery used in this study.

Table 5: Technical specifications for the Lithium-ion battery

Nominal Voltage (V)	Maximum Charging Current (A)	Maximum State of charge (%)	Minimum State of Charge (%)	Charging Efficiency (%)	Discharge Efficiency (%)
12	100	100	20	80	100

3.2.5. Modelling of the Bidirectional Converter

The DC power generated by the VAWT and PV modules, along with the stored power from the battery bank, is converted into AC energy by the DC/AC inverter to meet the AC load demand. Hence, the expression for the output power from the inverter is as follows [86]:

$$P_{DC-AC,convert} = \eta_{DC-AC,eff} * \left(P_{batt,total} * P_{VAWT,total} * P_{PV,total}\right) \quad (10)$$

where $P_{DC-AC,convert}$ is the generated power for the DC-AC converter (kW), $\eta_{DC-AC,eff}$ is the DC-AC converter which is equal to 90%, $P_{batt,total}$ is the total power from the battery bank (kW), and $P_{PV,total}$ is the total power from the PV modules (kW).

3.2.6. Proposed HRES Model and Energy Management Strategy (EMS)

The proposed HRES for this research consists of Genset(s), batteries, PV, and VAWTs. In order to meet the objectives of the onboard power system, the following HRES models are proposed:

- ***Case 1 (Genset/PV/VAWT/Battery):*** This configuration utilizes Gensets, PV panels, and VAWTs as primary power sources, with excess energy stored in the battery bank.
- ***Case 2 (Genset/PV/Battery):*** This setup relies on Gensets and PV panels for power generation, with surplus energy stored in batteries.
- ***Case 3 (Genset/VAWT/Battery):*** This configuration utilizes Gensets and VAWTs as main power sources, with excess power stored in the battery bank.
- **Case 4 (Genset*/Battery)***: This basic setup comprises Gensets and a battery bank for storing extra power.
- **Case 5 (Genset*)***: This case represents the fundamental model with Gensets as the sole power source.

In addition, the power balance ($P_{balance}$) for the proposed HRES setup on both conventional and fully autonomous tugboat is the difference between the power generated by the renewable energy sources (PV and VAWT) and the required ship power, $P_{load,ship}$ [kW]. This is expressed as follows:

$$P_{PV}(t) + P_{VAWT}(t) - P_{load,ship}(t) = \begin{cases} P_{balance} < 0 \ : Unmet \\ P_{balance} = 0 \ : Balance \\ P_{balance} > 0 \ : Excess \end{cases} \quad (11)$$

Moreover, the energy management strategy entails a controlled and systematic monitoring procedure employed to guarantee the economic feasibility and reliability of the proposed HRES in meeting the shipload. The research employs three operational scenarios for the energy management strategy, as illustrated in Figure 8, with detailed descriptions provided below:

- $\boldsymbol{P_{balance} = 0}$ **(*Meet*):** This indicates that the power generated by the onboard energy components matches the shipload precisely. Consequently, neither the batteries nor the Gensets are utilized by the power system.

- $\boldsymbol{P_{balance} > 0}$ $\boldsymbol{(Excess)}$**:** During periods of low ship demand or favorable weather conditions, the total power generated by renewable energy exceeds the shipload and battery requirements. In such cases, the surplus power is either diverted to deferred loads or dumped.
- $\boldsymbol{P_{balance} < 0}$ $\boldsymbol{(Unmet)}$: This occurs during peak loading times or high seasons when the power generated by renewable energy is insufficient to meet the shipload. In such scenarios, one of the following strategies is implemented:

  a*. *Battery bank at maximum utilization: In this scenario, energy stored in the battery bank is combined with renewable energy to meet the shipload.

  b. *Battery bank at minimum utilization*: Here, the Gensets are activated alongside renewable energy to fulfill the shipload demand and recharge the battery bank.

3.2.7. Loss of Power Supply Probability (LPSP)

The loss of power supply probability (LPSP) is a statistical metric indicating the likelihood of the generated power from the onboard HRES to meet the ship's load. The LPSP for the hybrid power system is calculated as follows [90], [96], [97]:

$$LPSP(t) = \frac{\sum_{t=1}^{t=8760} P_{load,ship}(t) - P_{Generation}(t)}{\sum_{t=1}^{t=8760} P_{load,ship}(t)} \quad (12)$$

where $P_{Generation}(t)$ is the total power generated by the components in the hybrid power (kW) at time t. The LPSP ranges from 0 to 1, where a value of 1 designates unmet load demand, and 0 signifies fulfilled load demand [90]. Thus, the reliability of the HRES is determined as 1 - $LPSP(t)$.

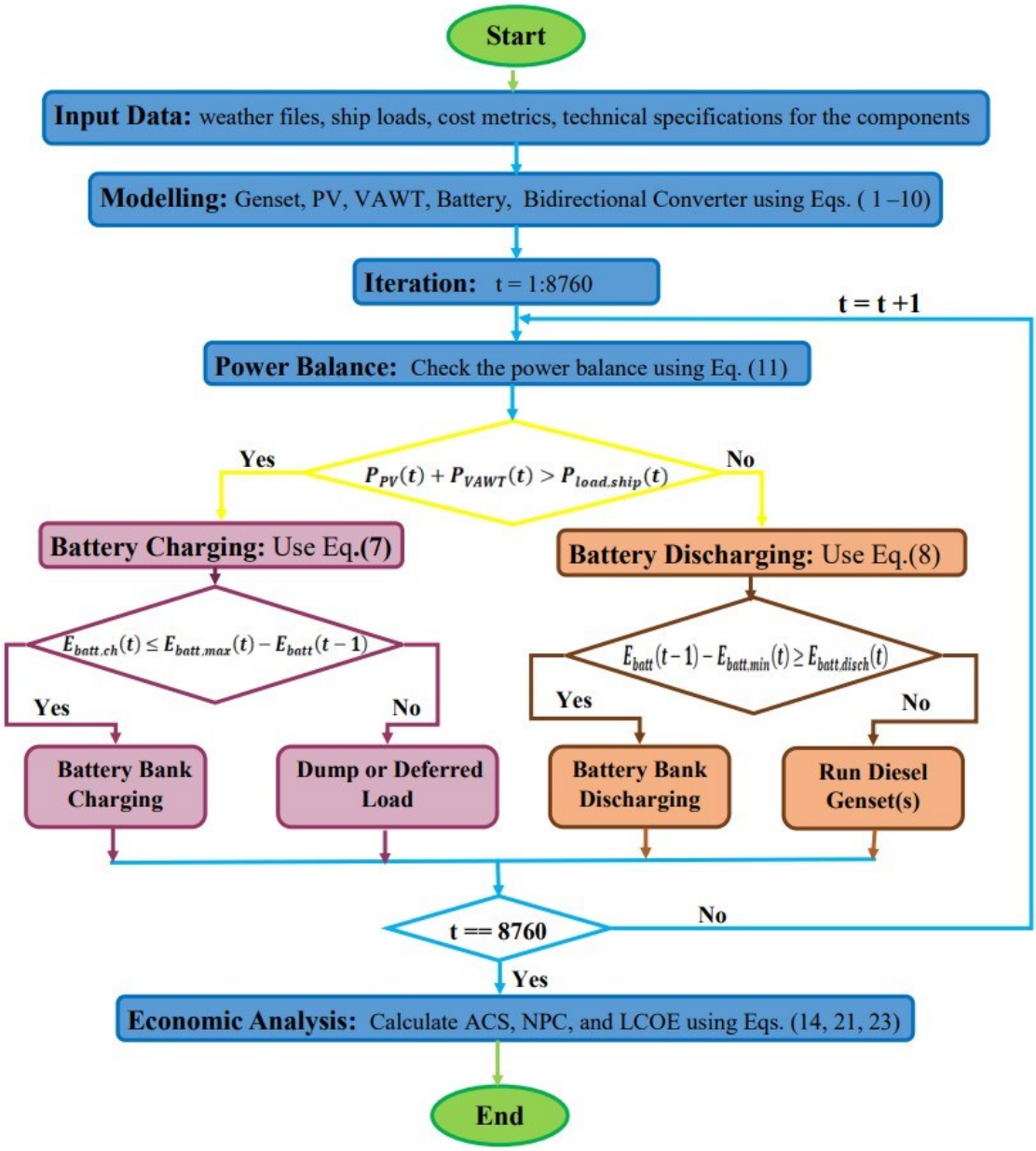

Figure 8: Energy management strategy (EMS) for the proposed HRES configuration.

3.2.8. Economic Analysis for the Proposed Hybrid Power Systems

The economic analysis is employed to analyze the proposed models and derive the objective function. The cost metrics utilized in the computation are capital cost (C_{CC}), operating & maintenance cost ($C_{O\&M}$) replacement cost (C_{RC}), salvage cost (C_{SC}), cost of fuel (F_C), annualized cost of system (ACS), net present cost, and levelized cost of energy (LCOE) during the project life. These calculations encompass the following components: Genset, diesel fuel, PV panels, VAWTs, bidirectional converter, and battery bank. The costs associated with the components are delineated in Table 6.

3.2.8.1. Objective Function

The goal of the objective function in the proposed HRES models is to minimize the annualized cost of the system (ACS) while ensuring that all constraints are met. The ACS is expressed as follows:

$$min\, ACS = min\{C_{ann}^{Genset} + C_{ann}^{PV} + C_{ann}^{VAWT} + C_{ann}^{BAT} + C_{ann}^{BICON} + C_{ann}^{FUEL}\} \quad (13)$$

where C_{ann}^{Genset}, C_{ann}^{PV} , C_{ann}^{VAWT} , C_{ann}^{BAT} , C_{ann}^{BICON}, and C_{ann}^{FUEL} are the annualized cost of the diesel generator, PV, VAWT, batteries, bidirectional converter, and fuel cost for the hybrid model. Thus the annualized costs for the components are expressed as [89]:

$$C_{ann}^{Genset} = N_{Genset} * \left(C_{CC}^{Genset} + C_{O\&M}^{Genset} + C_{RC}^{Genset} - C_{SC}^{Genset}\right) \quad (14)$$

$$C_{ann}^{PV} = N_{PV} * (C_{CC}^{PV} + C_{O\&M}^{PV} + C_{RC}^{PV} - C_{SC}^{PV}) \quad (15)$$

$$C_{ann}^{VAWT} = N_{VAWT} * \left(C_{CC}^{VAWT} + C_{O\&M}^{VAWT} + C_{RC}^{VAWT} - C_{SC}^{VAWT}\right) \quad (16)$$

$$C_{ann}^{BAT} = N_{BAT} * (C_{CC}^{BAT} + C_{O\&M}^{BAT} + C_{RC}^{BAT} - C_{SC}^{BAT}) \quad (17)$$

$$C_{ann}^{BICON} = N_{BICON} * \left(C_{CC}^{BICON} + C_{O\&M}^{BICON} + C_{RC}^{BICON} - C_{SC}^{BICON}\right) \quad (18)$$

$$C_{ann}^{FUEL} = \sum_{t=1}^{8760} F_C * F_{consum,total}(t) \quad (19)$$

Table 6: Costs for the hybrid power components.

Component	Capacity	Capital Cost (US$)	Replacement Cost (US$)	O &M Cost (US$ per Year)	Lifetime (Year)
Diesel Genset	125 kW	24,500.00	24,500.00	20.00[2]	15,000[3]
PV Module	0.370 kW	0.45[4]	0.30[4]	25.00	15
VAWT	5 kW	3,400.00	1,000.00	50.00	15
Battery	12V, 290Ah	1,695.95	1,000.00	100.00	15
AC/DC Converter	105 kW	1,600.00	1,000.00	100.00	20
Inflation rate (%)	1.75				
Discount rate (%)	4.3				
Project Life (yrs.)	25				

1. Fuel price is USD per liter
2. O&M cost is US$ per operation hour(s)
3. Lifetime is based on hours of operation
4. PV price is $US per Watt

3.2.8.2. Net Present Cost (NPC)

The net present cost encompasses all expenses associated with the installation and operation of the hybrid components over their lifespan, and it is represented as follows:

$$NPC_{total} = \frac{ACS}{CRF(r, n_{proj})} \tag{20}$$

where recovery cost $\mathrm{CRF}(\mathrm{i}, \mathrm{n}_{\mathrm{proj}})$ for the project over the project lifecycle ($\mathrm{n}_{\mathrm{proj}}$) at rate r, is expressed as:

$$CRF_i(r, n_{proj}) = \frac{r * (1+r)^{n_{proj}}}{(1+r)^{n_{proj}-1}} \tag{21}$$

3.2.8.3. Levelized cost of energy (LCOE)

The levelized cost of energy represents the total present cost of electricity production for the HRES throughout its project lifecycle. It calculates the average cost per kWh of the total electrical energy generated by each model as follows [83]:

$$LCOE = \frac{ACS}{\sum_{t=1}^{8760} P_{ship,load}\,(t)} \tag{22}$$

3.2.9. Constraints

The constraints governing the proposed onboard hybrid power system pertain to the power generation sources, backup power sources, and the cost of each component. The constraints for the power components are expressed as:

$$0 \leq N_{genset} \leq N_{genset,max} \tag{23}$$

$$0 \leq N_{PV} \leq N_{PV,max} \tag{24}$$

$$0 \leq N_{VAWT} \leq N_{VAWT,max} \tag{25}$$

$$0 \leq N_{batt} \leq N_{batt,max} \tag{26}$$

$$E_{batt,min} \leq E_{batt} \leq E_{batt,max} \tag{27}$$

$$R_f \geq R_{f\,min} \tag{28}$$

$$LPSP \leq LPSP_{max} \tag{29}$$

where $N_{PV,max}$is the maximum number of PV modules that can be installed onboard based on available space [unitless], $N_{VAWT,max}$ is the maximum number of VAWTs that can be installed onboard based on available space [unitless], $N_{batt,max}$ is the maximum number of batteries [unitless], $R_{f_{min}}$is the lower bound or minimum energy produced by renewable sources [98] as compared to energy produced by Genset which is set to 10%, and $LPSP_{max}$ is the maximum or upper bound for the LPSP and is equal to 5%. These values are set low to effectively minimize the financial redundancy for proposed HRES [99].

3.2.10. Artificial Bee Colony (ABC) Algorithm

The artificial bee colony (ABC) algorithm draws inspiration from the foraging behavior of honey bees. Introduced by Karaboga [100], this metaheuristic has proven effective in solving various engineering problems and optimization tasks. It employs three types of bee agents: employee bees, onlooker (follower) bees, and scout bees. Employee bees search for nectar and communicate their findings to onlooker bees through a waggle dance, allowing the onlookers to exploit the food source. Meanwhile, scout bees seek out new food sources. The number of food sources corresponds to the number of employee bees. ABC offers several advantages over other evolutionary algorithms, including efficiency, minimal reliance on preset parameters, and fast convergence in solving optimization problems within reasonable time frames [101]-[106]. The main steps of the ABC algorithm are depicted in Figure 9 and elaborated below [107]:

i. ***Initialization Phase***: During this phase, parameters such as problem dimension, colony size, number of food sources, maximum number of iterations, and limits are established. Furthermore, the initial population of food sources (SN) is randomly generated as follows:

$$X_{ij} = X_{j_{min}} + rand[0,1](X_{j_{max}} - X_{j_{min}}) \qquad (30)$$

where i= 1, 2… SN, j= 1, 2, …D, D is the number of optimization parameters, $X_{j_{max}}$ and $X_{j_{min}}$ are the upper and lower limits of the jth component. Similarly, the fitness value of each agent in the population is determined using the following equation:

$$fitness_i = \begin{Bmatrix} \frac{1}{1+f_i} & f_i \geq 0 \\ 1+|f_i| & otherwise \end{Bmatrix} \qquad (31)$$

where f_i is the cost function of the solution X_{ij}.

ii. Employee Bee Phase: During this phase, each employee bee forages around the allocated nectar (X_i) to find the food sources within the neighborhood (X_i^{new}) in Equation (32). The newly discovered food source is then compared to the previous one using a greedy selection approach to identify the nectar source with the highest fitness value. Additionally, information about the location, fitness value, and distance of the new food source is communicated to the onlooker bees through the waggle dance.

$$X_{ij}^{new} = X_{ij}^{old} + \emptyset_{ij}(X_{ij}^{old} - X_{kj}) \quad (32)$$

where $\emptyset_{ij}$ is a random number in the range of -1 to 1, k = 1,2 ... SN , and k ≠ i.

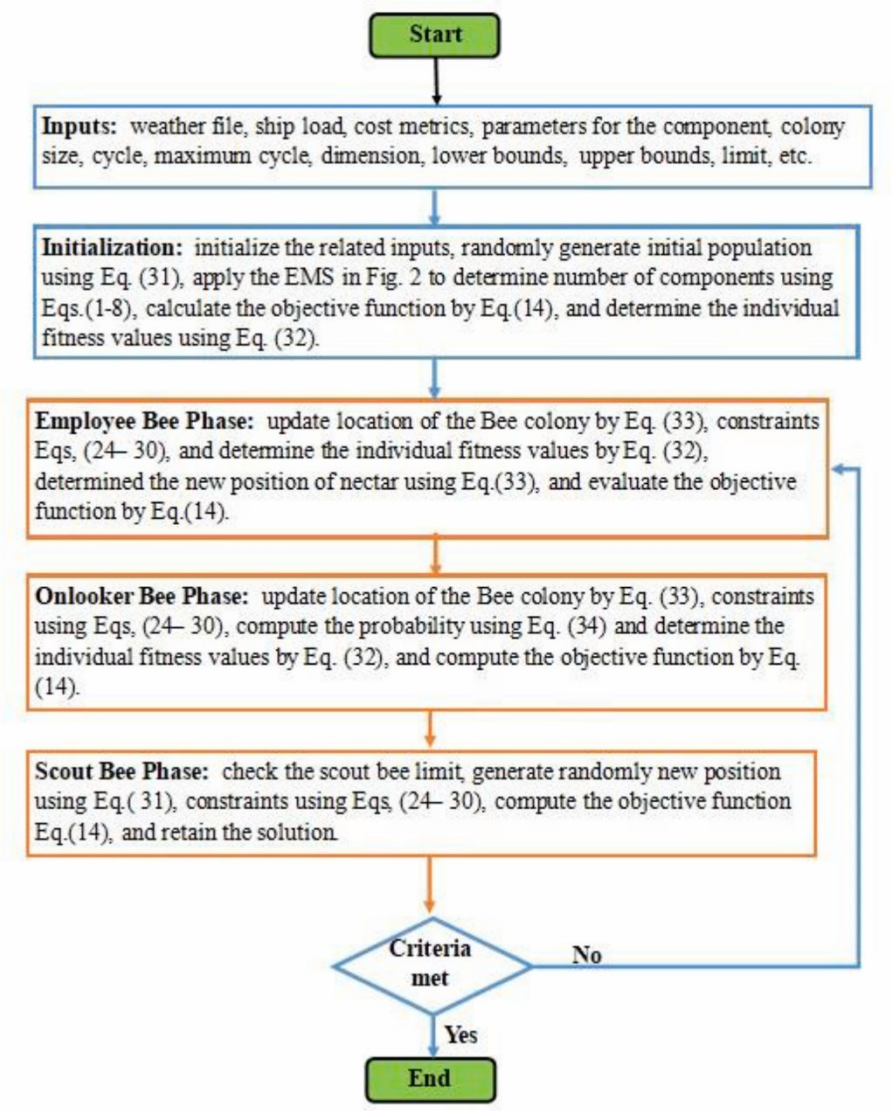

Figure 9: Flowchart of the ABC algorithm for the HRES onboard conventional and fully autonomous tugboat.

iii. ***Onlooker Bee Phase***: The onlooker bees select their nectar based on the fitness values provided by the employee bees. They choose the nectar with the highest fitness value according to the probability equation below.

$$p_i = \frac{fit_i}{\sum_{j=1}^{SN} fit_j} \quad (33)$$

where p_i is the probability value of the onlooker bee's choice of nectar, and fit_i is the fitness value of i^{th} solution. Using the probability value obtained and the roulette wheel selection method, the onlooker bees produce a new solution using Equation (32). They decide and select nectar from neighboring food sources based on greedy selection criteria, aiming to choose the optimal solution with the highest fitness. However, if the nectar source does not show improvement, the solution is discarded, and the bees transition into scout bees at this stage.

iv. Scout Bee Phase: During the scout bee phase, the bees randomly generate new food source locations using Equation (30). The best solution is remembered, and this process continues until the cycle reaches the maximum number of cycles.

3.2.11. Ship Characteristics

For the purpose of this study, we have chosen a tugboat as our focus, aiming to enhance its energy efficiency and management at a minimal cost. The conventional tugboat measures 25 meters in overall length, 10 meters in extreme breadth, with a maximum draught of 5 meters, and a gross tonnage of 298 tons. It boasts a top speed of 12 knots and is equipped with two diesel engines primarily for propulsion, along with two diesel Gensets totaling 250 kW in power. These Gensets serve various auxiliary loads onboard, including lighting, navigation equipment, communication systems, hoteling amenities, and the operation of winch motors, pumps, and compressors. Operational data retrieved from the ship log and the Automatic Identification System (AIS) via MarineTraffic [108] indicate that the tugboat operates year-round, completing approximately two to five assignments daily along the West Coast of the United States.

The dynamic load profile illustrating the power demand of auxiliary systems essential for the safe operation of the tugboat is depicted in Figure 10. Additionally, the energy consumption of the tugboat is calculated based on the electrical load factor and the duration of each operation, provided by the tugboat operator. For the fully autonomous tugboat, we assume a similar operational profile to that of the conventional tugboat. However, load profiles for the autonomous vessel are estimated

by excluding power consumption from fitted equipment and personnel [109]. Consequently, the average daily energy consumption of onboard auxiliary equipment for the conventional tugboat and proposed fully autonomous tugboats are 260.28 kWh/day and 153.48 kWh/day, respectively.

3.2.12. Weather Data

Data regarding environmental conditions along the navigation route were sourced from the NASA Prediction of Worldwide Energy Resource (POWER) database. Figure 11 illustrates the monthly average solar radiation, wind speed, and temperature within the operational zone, which are recorded as 5.14 kWh/m2 /day, 4.12 m/s, and 16.96°C, respectively.

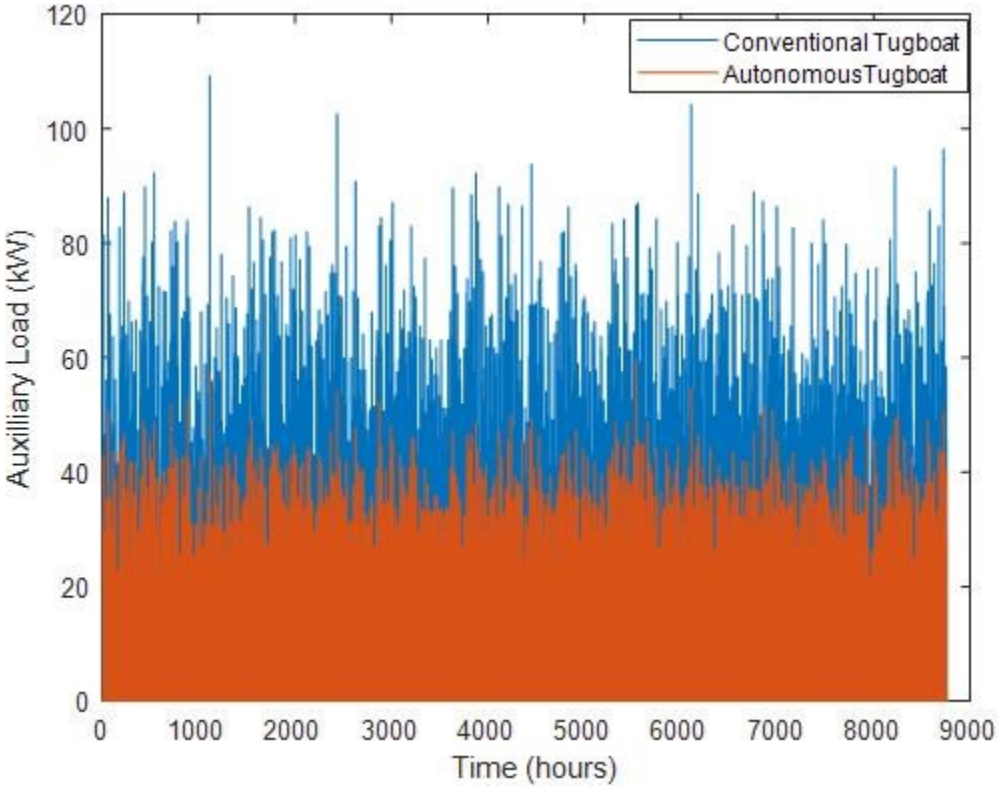

Figure 10: Auxiliary loads for the conventional and the proposed fully autonomous tugboat.

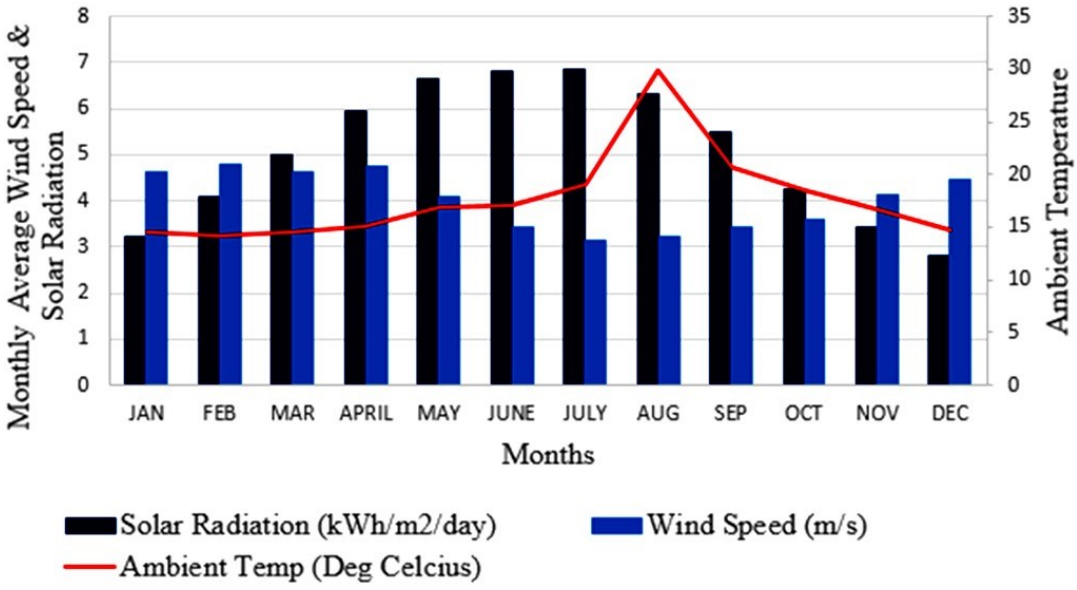

Figure 11: Monthly average wind speed, solar radiation, and ambient temperature along the navigation routes.

3.2.13. Simulation Analysis

For this study, the tugboat is simulated with renewable energy sources and a battery bank to store surplus energy for critical loads as necessary. It is assumed that the available space for installing PV modules and batteries on the autonomous tugboat is larger compared to the conventional tugboat, owing to the absence of sailors and certain equipment. Ship and weather data were imported into both HOMER Pro and MATLAB software. The nominal ratings, maximum component numbers, and cost metrics were selected based on industry expert assessments and recommendations. Subsequently these parameters were entered into the aforementioned computational software. The optimized results obtained from the three metaheuristic optimization algorithms were compared with those from HOMER Pro to assess efficiency and best fitness values. Finally, robustness tests were conducted on the optimal HRES model and the three metaheuristic algorithms.

3.3 Results and Discussions

This section presents the simulated outcomes for the HRES models. Table 7 displays the feasible results of the optimal sizing of the proposed HRES models for the conventional tugboat, as determined by the metaheuristic algorithms and HOMER Pro. It is evident that the three metaheuristic algorithms outperform HOMER Pro, achieving better results. Particularly, the ABC algorithm yields the lowest ACS with the least TNPC and LCOE across all proposed cases compared to PSO, GA, and HOMER Pro. Notably, the optimal model for the conventional tugboat is the Genset/PV/VAWT/Battery (Case 1), exhibiting the lowest cost metrics. This is attributed to the high penetration rate of renewable energy along the ship route. It can be inferred that the next successive optimal models with minimum cost are Genset/PV/Battery (Case 2), Genset/VAWT/Battery (Case 3), Genset/Battery (Case 4), and Genset (Case 5) respectively; suggesting that integrating renewable sources reduces HRES operating costs. Additionally, the ABC algorithm generates the lowest ACS for Cases 1 to 4 due to its superior fitness values compared to other algorithms. The optimized results for the metaheuristic algorithms are nearly identical, except for Case 5 (Genset alone), where their cost values (that is ACS, TNPC and LCOE) match those of HOMER Pro. The rationale behind this assertion lies in the foundational nature of the model, which lacks both renewable energy sources and storage components, a premise also corroborated by the findings of Maleki and Pourfayaz [81] . Moreover, the optimized results from HOMER Pro are higher than those from the metaheuristics in Cases 1 to 4 due to the generation of higher dump energy, as observed in previous study by Singh et al [89].

Figure 12 illustrates the convergence graph of the three metaheuristic algorithms for the conventional tugboat. It is clear that the optimization results achieved by the ABC algorithm for Case 1 surpass those of the other algorithms due to its remarkable convergence speed and optimization performance. The computational time for the proposed cases using HOMER Pro software is longer, whereas that of the metaheuristic algorithms takes only a few minutes. Table 8 provides a comprehensive summary of the techno-economic outcomes of the proposed HRES for the conventional tugboat utilizing the ABC Algorithm. It can be deduced that Case 1 exhibits the highest renewable fraction (R_f) due to the incorporation of both PV and VAWTS, resulting in the lowest CO_2 emissions compared to the other cases. Similarly, Case 2 follows as the next HRES

model with lower CO_2 emissions, succeeded by Case 3. As anticipated, the base model (Case 5) emits the highest CO_2 emissions compared to Case 4.

Table 7: Results of the optimization methods of the proposed HRES for the conventional tugboat

Cases	Algorithms	Genset (kW)	PV (kW)	VAWT (kW)	Battery (units)	ACS (US$/yr.)	TNPC (US$/yr.)	LCOE (US$/kWh)
1	PSO	125	4.44	10	4	53,599.03	1,077,580.68	0.513
	ABC	125	4.44	10	4	53,592.33	1,077,446.31	0.513
	GA	125	4.44	10	4	53,599.03	1,077,580.68	0.513
	HOMER Pro	125	4.44	10	12	73,818.03	1,488,741.25	0.706
2	PSO	125	4.44	N/A	4	58,601.35	1,178,171.14	0.560
	ABC	125	4.44	N/A	4	58,585.85	1,177,859.36	0.506
	GA	125	4.44	N/A	4	58,586.03	1,177,863.10	0.506
	HOMER Pro	125	4.44	N/A	8	63,377.76	2,921,696.00	0.606
3	PSO	125	N/A	10	8	58,922.12	1,184,333.69	0.563
	ABC	125	N/A	10	8	58,920.17	1,184,294.45	0.563
	GA	125	N/A	10	8	58,922.12	1,184,333.69	0.563
	HOMER Pro	125	N/A	10	12	74,485.98	1,497,167.03	0.713
4	PSO	125	N/A	N/A	4	61,503.70	1,236,245.95	0.588
	ABC	125	N/A	N/A	4	61,491.73	1,236,005.43	0.588
	GA	125	N/A	N/A	4	61,503.70	1,236,245.95	0.588
	HOMER Pro	125	N/A	N/A	4	61,536.25	1,236,900.22	0.589
5	PSO	125	N/A	N/A	N/A	83,700.81	1,682,761.86	0.801
	ABC	125	N/A	N/A	N/A	83,700.81	1,682,761.86	0.801
	GA	125	N/A	N/A	N/A	83,700.81	1,682,761.86	0.801
	HOMER Pro	125	N/A	N/A	N/A	83,700.81	1,682,761.86	0.801

Figure 13 depicts the monthly energy analysis for the optimal HRES (Case 1). It is evident that the highest solar energy generation occurs during the summer months, with the majority of this energy utilized to meet the shipload. Conversely, the maximum wind energy generation is observed in the winter season. However, the usage of the Genset and battery bank remains consistent every month throughout the year to fulfill the stable auxiliary load demand. Furthermore, it is observed that there is either no surplus energy or minimal surplus energy, as the HRES is designed to minimize dump energy.

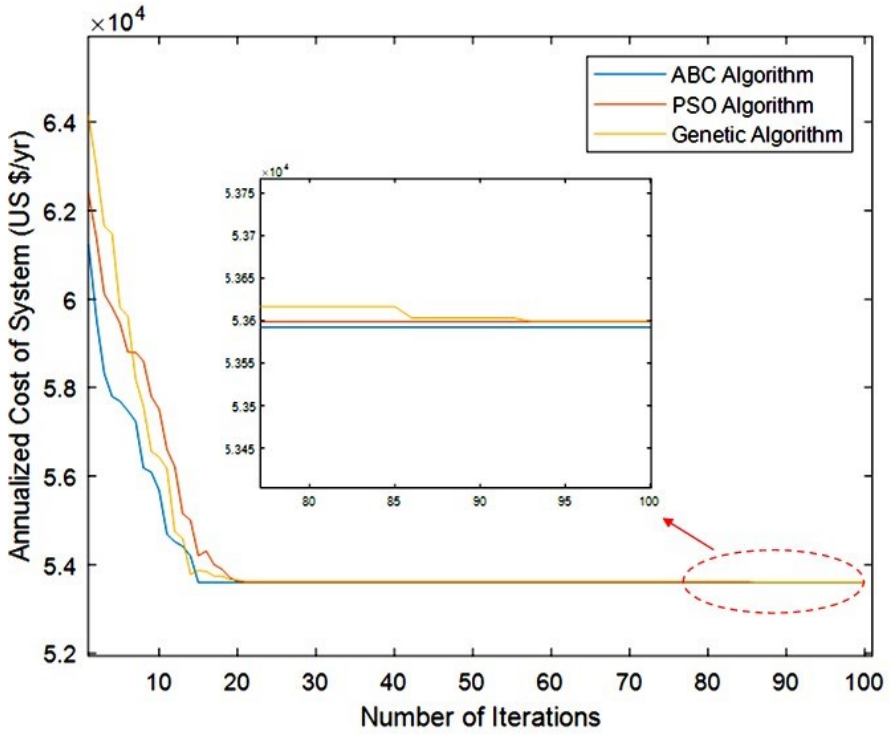

Figure 12: Comparison of convergence of the three metaheuristic algorithms for the Case 1 (Genset/PV/VAWT/Battery) HRES model for conventional tugboat.

Table 8: Detailed techno-economic results of proposed HRES for conventional tugboat using ABC algorithm.

System Component	Parameters	Case 1	Case 2	Case 3	Case 4	Case 5
Mono PV	Solar Energy (kWh)	32,309.62	32247.47	-	-	-
Wind	Wind Energy (kWh)	17,765.14	-	17,786.64	-	-
Battery	Battery Charge (kWh)	27,876.24	16,420.65	11,486.34	1,185.53	-
	Battery Discharge (kWh)	25,623.96	15,220.38	10,724.03	965.20	-
Genset	Diesel Energy (kWh)	62,485.11	78,955.34	93,285.06	109,715.93	110,002.55
Annualized Cost for components	PV ($)	437.05	436.21	-	-	-
	VAWT ($)	471.96	-	472.53	-	-
	Battery ($)	847.93	851.57	861.10	848.59	-
	Genset ($)	51,659.31	57,121.99	57,410.46	60,467.06	83,700.81
	Inverter ($)	176.08	176.08	176.08	176.08	-
Other factors	Load Demand (kWh)	104,502.42	104,502.42	104,502.42	104,502.42	104,502.42
	CO_2 Emission(tons)	73,741.05	93,178.20	110,89.25	129,479.94	129,818.19
	Dump Energy(kWh.)	103.79	43.37	13.19	-	-
	Ren Fraction (%)	40.21	24.45	10.73	-	-

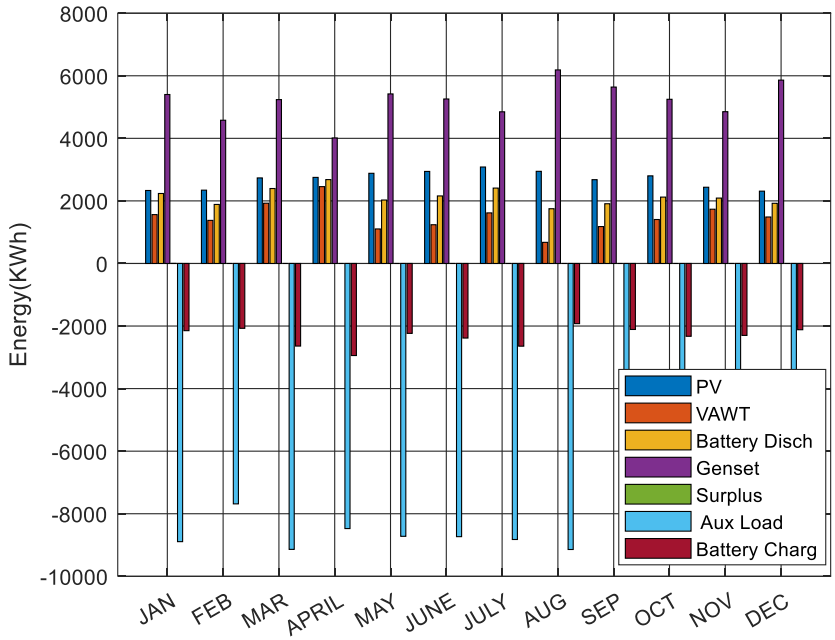

Figure 13: Monthly energy analysis (kWh) for optimal Genset/PV/VAWT/Battery (Case 1) HRES using ABC algorithm for Conventional tugboat.

Table 9 displays the optimized outcomes of the proposed hybrid power systems for the fully autonomous tugboat. It is evident that Case 1 yields the lowest ACS, followed by Case 2, Case 3, Case 4, and Case 5. The sequence of models with the lowest ACS mirrors that of the conventional tugboat, attributed to the assumption that the autonomous tugboat shares the same navigation routes and ship particulars as its conventional counterpart. However, the costs of the optimized HRES models for the autonomous tugboat are lower than those of the conventional tugboat due to reduced shipload.

The optimization results obtained from the ABC algorithm are favored for achieving optimal HRES configurations compared to other algorithms and HOMER Pro. For instance, Figure 14 illustrates the convergence rate comparison between the ABC algorithm and the other two algorithms for the Case 1 model of the fully autonomous tugboat. Notably, the ABC algorithm demonstrates superior convergence speed compared to PSO and GA algorithms.

Table 9: Results of the optimization methods of the proposed HRES for the fully autonomous tugboat

Case	Algorithm	Genset (kW)	PV (kW)	VAWT (kW)	Battery (units)	ACS (US$/yr.)	TNPC (US$/yr.)	LCOE (US$/kWh)
1	PSO	125	5.92	10	8	17,355.53	348,863.73	0.282
	ABC	125	5.92	10	8	17,345.82	348,670.03	0.282
	GA	125	5.92	10	8	17,357.14	348,896.25	0.281
	HOMER Pro	125	5.92	10	10	29,297.97	589,020.06	0.476
2	PSO	125	5.92	N/A	4	41.254.76	829,448.11	0.670
	ABC	125	5.92	N/A	4	41,254.75	829,262.63	0.670
	GA	125	5.92	N/A	4	41,288.43	830,125.11	0.670
	HOMER Pro	125	5.92	N/A	8	61,196.43	1,230,322.84	0.994
3	PSO	125	N/A	2	4	50,022.32	1,005,369.52	0.812
	ABC	125	N/A	10	4	50,021.78	1,005,358.69	0.812
	GA	125	N/A	10	4	50,022.32	1,005,369.52	0.812
	HOMER Pro	125	N/A	10	8	53,077.76	1,067,101.15	0.862
4	PSO	125	N/A	N/A	4	55,643.89	1,118,412.47	0.903
	ABC	125	N/A	N/A	4	55,631.93	1,118,171.96	0.903
	GA	125	N/A	N/A	4	55,643.89	1,118,412.47	0.903
	HOMER Pro	125	N/A	N/A	4	59,205.36	1,190,293.40	0.962
5	PSO	125	N/A	N/A	N/A	77,218.91	1,552,446.59	1.255
	ABC	125	N/A	N/A	N/A	77,218.91	1,552,446.59	1.255
	GA	125	N/A	N/A	N/A	77,218.91	1,552,446.59	1.255
	HOMER Pro	125	N/A	N/A	N/A	77,218.91	1,552,446.59	1.255

Table 10 provides a comprehensive breakdown of the proposed HRES outcomes for the fully autonomous tugboat utilizing the ABC Algorithm. It is evident that Case 1, featuring Genset/PV/VAWT/Battery configuration, exhibits the lowest diesel energy consumption and highest $R_{f,}$ leading to minimal CO_2 emissions compared to other models. This is attributed to the significant contribution of energy generated by PV and VAWT. Sequentially, the subsequent optimal HRES models in terms of techno-economic results for the fully autonomous tugboat are as follows: Genset/PV/Battery (Case 2), Genset/VAWT/Battery (Case 3), Genset/Battery (Case 4), and Gensets (Case 5). These results mirror the trends observed in optimized HRES models for the conventional tugboat. Consequently, models with limited or no integration of renewable energy sources exhibit higher CO_2 emissions and ACS due to increased fuel consumption. Figure 15 illustrates the monthly energy balance of the optimal HRES (Genset/PV/VAWT/Battery) for the fully autonomous tugboat. Similarly, the PV modules exhibit the highest monthly

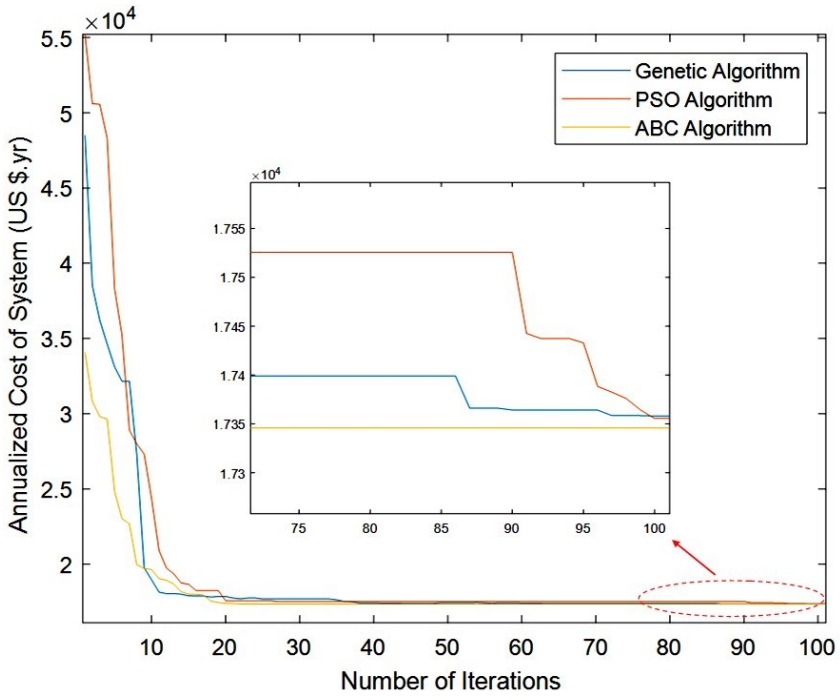

Figure 14: Comparison of convergence of the three metaheuristic algorithms for Genset/PV/VAWT/Battery (Case 1) HRES Model on fully autonomous tugboat.

renewable energy generation compared to the VAWT. However, minimal energy from the Gensets is required to supplement the renewable energy sources to meet the shipload. Additionally, the battery bank is consistently utilized throughout the year, with surplus energy available in each month, mirroring the scenario observed in a conventional tugboat. Nonetheless, the proposed models for the fully autonomous tugboat show the highest generated renewable energy and R_f, alongside minimal ACS, fuel consumption, and CO_2 emissions compared to models for the conventional tugboat.

Finally, robustness tests are conducted on the optimal HRES onboard both the conventional and fully autonomous tugboats. Since the primary power generation sources for this system (Case 1) are Genset, PV, and VAWT, the test is performed on their respective key parameters.

Table 10: Detailed techno-economic results of proposed HRES for fully autonomous tugboat using ABC algorithm.

System Component	Parameters	Case 1	Case 2	Case 3	Case 4	Case 5
Mono PV	Solar Energy (kWh)	42,996.63	42,996.63	-	-	-
Wind	Wind Energy (kWh)	17,765.26	-	17,765.26	-	-
Battery	Battery Charge (kWh)	33,514.60	21,950.31	11,472.54	1,203.22	-
	Battery Discharge (kWh)	31,088.12	20,245.73	10,711.29	689.61	-
Genset	Diesel Energy (kWh)	7,013.76	23,569.21	48,163.72	64,574.65	64,861.27
Annualized Cost for components	PV ($)	581.61	581.61	-	-	-
	VAWT ($)	471.96	-	471.96	-	-
	Battery ($)	1,834.23	845.79	860.54	849.29	-
	Genset ($)	14,291.65	39,651.27	48,513.20	54,606.56	77,218.91
	Inverter ($)	176.08	176.08	176.08	176.08	-
Other Factors	Load Demand (kWh)	61,618.21	61,618.21	61,618.21	61,618.21	61,618.21
	CO_2 Emission(tons)	8,277.21	27,814.93	56,839.84	76,207.00	76,545.25
	Dump Energy(kWh.)	319.73	113.37	123.06	-	-
	Ren Fraction (%)	88.61	61.75	21.84	-	-

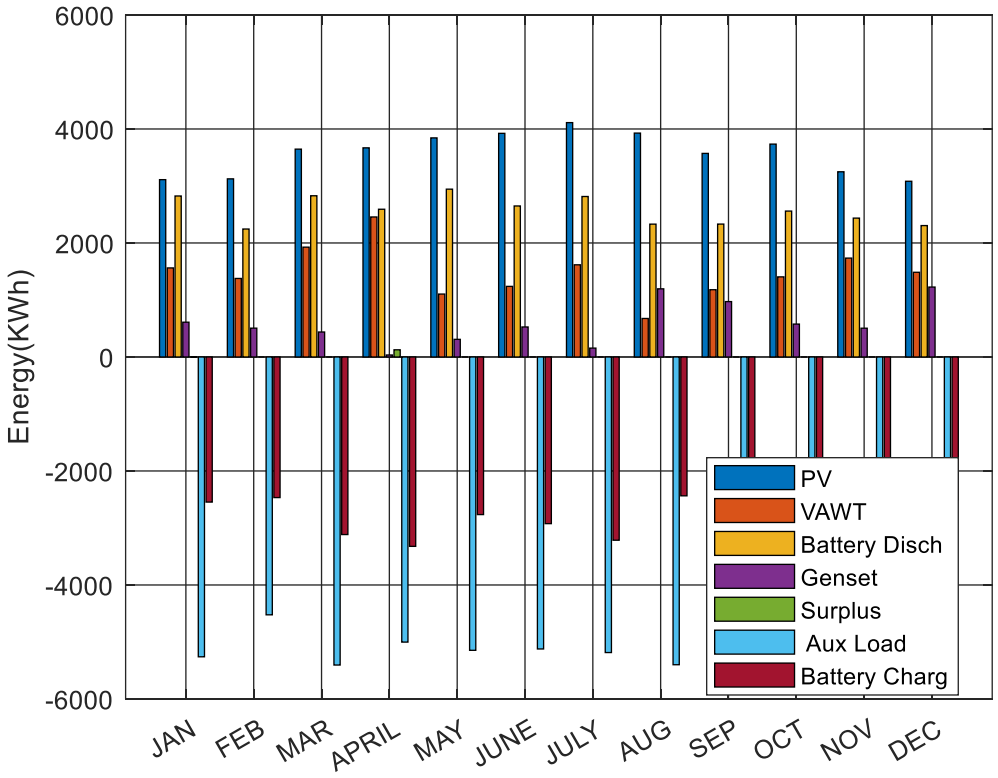

Figure 15: Monthly energy analysis (kWh) for optimal Genset/PV/VAWT/Battery (Case 1) HRES using ABC algorithm for fully autonomous tugboat.

3.3.1. Robustness Test

The aim of conducting the robustness test is to confirm the efficacy of the optimal model (Case 1) acquired using the ABC algorithm for both conventional and autonomous tugboats. This validation is achieved by manipulating fundamental input data, including shipload, fuel price, solar irradiance, wind speed, and ambient temperature along the navigation routes. Furthermore, statistical analysis is carried out on the ACS results obtained by the three metaheuristic algorithms for the optimal Case 1 model specifically for the fully autonomous tugboat. The findings of this critical analysis are outlined in the subsequent subsections.

3.3.1.1. Robustness Test on the Optimal Hybrid Model by Variable Load Fuel Price, Solar Irradiance, Wind Speed, and Ambient Temperature

Tables 11 and12 present the robustness test results for both conventional and fully autonomous tugboats across various variable parameters including loads, fuel prices, solar irradiance, wind speeds, and temperature for the optimal model (Case 1). The findings indicate that a decrease in shipload results in the lowest values of ACS, NPC, and CO_2 emissions, but in a higher R_f. Conversely, an increase in shipload leads to contrary outcome. Furthermore, the fluctuation in fuel prices affected the objective function and related costs but had no influence on the CO_2 emissions and R_f, given that the HRES relied predominantly on generated renewable energy during both high and low energy demand periods by the tugboat. Therefore, an increase in fuel prices generated high system costs, while a decrease in fuel prices led to the opposite outcome. Likewise, it can be confirmed that the reduction in solar irradiance resulted in higher ACS, TNPC, and CO_2 emissions, but a lower R_f, whereas an increase in solar irradiance yielded the converse outcome. Similarly, the reduction in wind speed led to high ACS, TNPC, and CO_2 emissions, and lower R_f, while an increase in wind speed had the converse result. Lastly, decreasing ambient temperature resulted in high ACS, TNPC, and CO_2 emissions, but low R_f, whereas increasing ambient temperature generated the opposite outcomes.

In summary, the change in fuel price, shipload, solar irradiance, ambient temperature, and wind speed had significant impact on the proposed optimal HRES onboard both conventional and fully autonomous tugboats. Nonetheless, the results obtained for the autonomous tugboat surpass those obtained for the conventional tugboat.

Table 11: Robustness test results based on varying load, fuel price and solar irradiance on the optimal Genset/PV/VAWT/Battery (Case 1) for conventional tugboat using ABC algorithm.

Parameters	Variation	ACS (US$/yr.)	TNPC (US$/yr.)	LCOE ($US/kWh)	CO_2 Emission (kg/yr.)	Renewal Fraction (%)
Load (kW)	-35%	38,041.93	764,813.69	0.560	28,388.22	64.59
	+35%	60,546.42	1,217,254.79	0.429	119,182.14	28.41
Fuel Price (USD/L)	-35%	50,763.23	1020568.80	0.486	73,741.05	40.21
	+35%	56,405.28	1,133,999.29	0.540	73,741.05	40.21
Solar irradiance ($kWh/m^2/day$)	-1.06	58,793.58	1,182,014.78	0.563	105,761.61	14.24
	+1.06	53,328.32	1,072,138.58	0.510	72,967.93	40.83
Wind Speed (m/s)	-2.12	58,428.81	1,174,681.26	0.559	91,222.31	26.03
	+2.12	37,095.14	745,778.43	0.355	42,142.73	65.82
Temperature (°C)	-6	52,897.98	1,063,486.68	0.506	71,621.40	41.93
	+6	54,212.14	1,089,907.28	0.519	76,170.83	38.23

Table 12: Robustness test results based on varying load, fuel price and solar irradiance on the optimal Genset/PV/VAWT/Battery (Case 1) for fully autonomous tugboat using ABC algorithm.

Parameters	Variation	ACS (US$/yr.)	TNPC (US$/yr.)	LCOE ($US/kWh)	CO_2 Emission (kg/yr.)	Renewal Fraction (%)
Load (kW)	-35%	4,517.39	90,819.82	0.113	0.00	100
	+35%	39,087.12	785,826.56	0.470	35,249.54	64.09
Fuel Price (USD/L)	-35%	17,001.13	341,799.08	0.276	8,277.21	88.56
	+35%	17,677.15	355,390.06	0.287	8,277.21	88.56
Solar irradiance ($kWh/m^2/day$)	-0.94	49,057.56	986,277.26	0.796	51,036.25	29.81
	+1.06	53,328.32	1,072,138.58	0.258	7,208.52	90.08
Wind Speed (m/s)	-2.12	38,952.64	783,122.83	0.632	25,086.19	65.50
	+2.12	4,775.54	96,009.86	0.078	0.00	100
Temperature (°C)	-6	13,421.39	269,820.17	0.2178	4,829.24	93.36
	+6	20,947.88	421,146.30	0.340	11,512.95	84.16

3.3.1.2. Statistical Analysis on Metaheuristic Algorithms of ACS for Optimal Fully Autonomous Tugboat

We conducted an ANOVA test to evaluate potential statistically significant differences among the means of multiple populations. Specifically, we applied the one-way ANOVA test to the optimization ACS results generated by the ABC, PSO, and GA algorithms for the Case 1 model of the fully autonomous tugboat to assess their effectiveness. This analysis was conducted using Minitab software. Table 13 presents the sources of variance between groups (algorithms) and within groups (error), along with their respective degrees of freedom (DF), adjustment sum of squares (Adj SS), adjusted mean squares (Adj MS), F-statistic (or F-value), and associated P-value. The adjusted mean square error (Adj MS) representing the variance within all groups was found to be 45560163, indicating the variability of data points around the fitted values. Additionally, the P-value was determined to be zero, which is less than the significance level (α) of 5%, signifying the presence of statistically significant differences in the data groups. Consequently, the null hypothesis is rejected, confirming the statistical significance of the results. It was concluded that all three algorithms have distinct means, as indicated in Table 14. Moreover, the PSO algorithm exhibited the highest mean, standard deviation, and confidence interval compared to the ABC and GA algorithms, suggesting that the PSO algorithm produces higher ACS values than the other two algorithms. Given the differences in means observed among the three metaheuristic algorithms in Table 14, further analysis beyond ANOVA is warranted.

.

Table 13: Analysis of variance (significance level α =0.05) result for one-way ANOVA

Source	DF	Adj SS	Adj MS	F-Value	P-Value
Algorithm	2	10,116,204,280	5,058,102,140	111.02	0
Error	297	13,531,368,309	45,560,163		
Total	299	23,647,572,589			

Table 14: Mean and standard deviation result for one-way ANOVA

Algorithms	Number	Mean	Standard Deviation	95% CI
ABC	100	17,755	2,167	(16426, 19083)
GA	100	19,646	5,080	(18317, 20974)
PSO	100	30,909	10,304	(29581, 32238)

Hence, the post-hoc test (or multiple comparison) is conducted to determine whether differences between pairs of groups hold statistical significance. Accordingly, the Tukey pairwise comparisons test is applied to the three algorithms while maintaining a simultaneous confidence level of 95%. In Figure 16, the confidence interval plot illustrates the disparity between the pairings. Notably, the GA-ABC pairing exhibits the most favorable outcome, as the confidence interval encompasses zero, indicating no significant difference between the compared groups. Conversely, the confidence intervals for PSO-ABC and PSO-GA include entirely positive numbers, indicating statistically significant differences between them. Table 15 delineates that *Grouping A* exclusively comprises the PSO algorithm, while *Grouping B* encompasses both GA and ABC algorithms. This suggests that the means for the ABC and GA algorithms do not differ significantly. However, the PSO algorithm does not share a grouping letter, signifying its notable difference attributed to its higher mean. Lastly, the optimal algorithm is identified based on the grouping with the smallest mean; thus, the ABC algorithm emerges as the best choice, offering a significantly lowest mean than both the PSO and GA algorithms. Subsequently, the GA algorithm follows as the next successive optimal choice, exhibiting a lower mean than the PSO algorithm.

Table 15: Grouping information using the Tukey method and 95% confidence.

Algorithms	**Number**	**Mean**	**Grouping**	
PSO	100	30,909	A	
GA	100	19,646		B
ABC	100	17,755		B

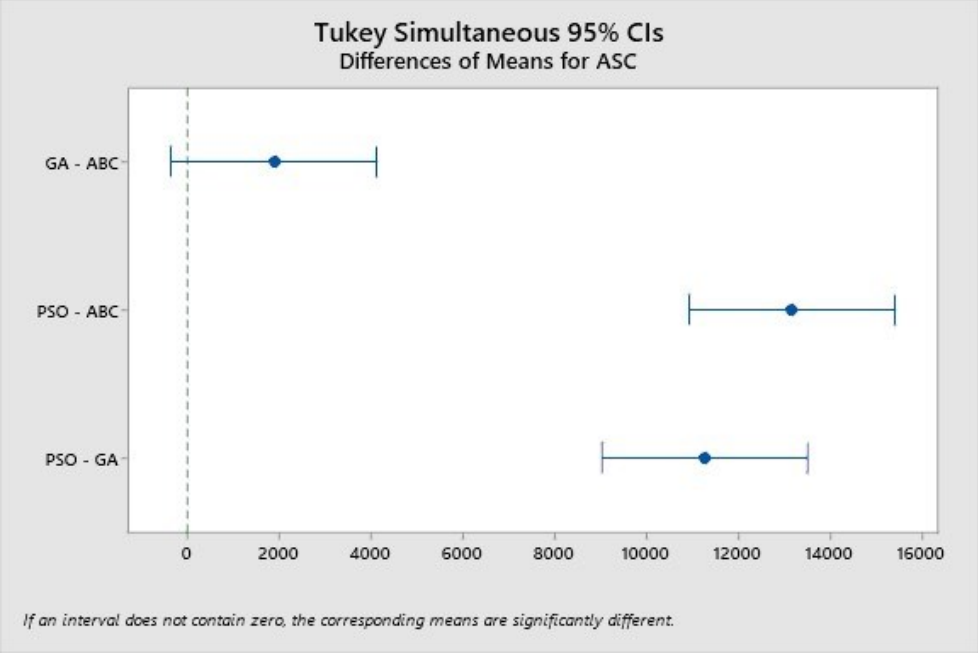

Figure 16: Tukey simultaneous tests for difference of means for the metaheuristic algorithms.

3.4 Conclusion

This research paper introduces a standalone hybrid renewable energy system designed for an existing tugboat operating along the West Coast of the United States. Techno-economic analyses are conducted for both conventional and fully autonomous tugboats using mathematical models. The developed HRES models consist of PV, VAWT, batteries, and Gensets. In addition, the simulation and optimization processes are carried out using the ABC algorithm. The aim of the modeling is to find the optimal HRES with a minimum ACS and emissions while adhering to specified constraints.

We observe that the ABC algorithm outperforms PSO, GA, and HOMER Pro. Also, among the five proposed reliable and sustainable configurations, Genset/PV/VAWT/Battery (Case 1) emerges as the optimal standalone HRES for both conventional and fully autonomous tugboats. Notably, the fully autonomous tugboat demonstrates superior outcomes in terms of cost, CO_2 emissions, and renewable fraction compared to its conventional counterpart. In addition, the robustness test reveals that variations in shipload, fuel price, solar irradiance, wind speed, and ambient temperature significantly affect the proposed optimal HRES for both conventional and fully autonomous tugboats. Consequently, comparing the results of the optimal HRES (Genset/PV/VAWT/Battery) onboard the conventional tugboat with those of the fully autonomous tugboat, we find that the latter records minimum ACS, TNPC, LCOE, CO_2 emissions, and maximum percentage of renewable fraction. Moreover, the fully autonomous tugboat generates a higher percentage of excess energy compared to the conventional tugboat, which generates less excess energy. Additionally, a one-way ANOVA is applied to the ACS results of the Case 1 model for the fully autonomous ship, confirming the statistical significance of the ACS results and indicating that the ABC algorithm produces optimal outcomes. Furthermore, the application of the Tukey pairing reveals that the GA-ABC pair is statistically similar, suggesting that there is no difference between their means unlike the other pairings.

This study encountered significant constraints primarily stemming from the absence of reliable data regarding the energy demands of autonomous tugboats. Consequently, the paper resorts to mathematical simulation based on the energy requirements of conventional tugboats.

In conclusion, future research endeavors should delve into implementing the proposed HRES across a range of fully autonomous surface ships, encompassing diverse navigation routes, variable ship speeds, and a variety of energy storage options. This is prompted by the scarcity of pertinent research literature that could serve as comparative benchmark and by the need to broaden the knowledge of HRES applications onboard fully autonomous ships. Furthermore, there is a suggestion to explore alternative fuels as a means to reduce emissions and improve ship energy systems.

CHAPTER 4. ENVIRONMENTAL AND COST ASSESSMENTS OF MARINE ALTERNATIVE FUELS FOR FULLY AUTONOMOUS SHORT-SEA SHIPPING BASED ON THE GLOBAL WARMING POTENTIAL APPROACH

In this chapter, we explore an effective approach to reducing marine pollution and costs by determining the optimal marine alternative fuels framework for short-sea shipping vessels, with a focus on energy efficiency. Employing mathematical models in a Python environment, the analyses are tailored specifically for conventional and fully autonomous high-speed passenger ferries (HSPFs) and tugboats, utilizing bottom-up methodologies, ship operating phases, and the global warming potential approach. The study aims to identify the optimal marine fuel that offers the highest Net Present Value (NPV) and minimal emissions, aligning with International Maritime Organization (IMO) regulations and environmental objectives. Data from the ship's Automatic Identification System (AIS), along with specifications and port information, were integrated to assess power, energy, and fuel consumption, incorporating parameters of proposed marine alternative fuels. This study examines key performance indicators (KPIs) for marine alternative fuels used in both conventional and autonomous vessels, specifically analyzing total mass emission rate (TMER), total global warming potential (TGWP), total environmental impact (TEI), total environmental damage cost (TEDC), and NPV. The results show that hydrogen (H2-Ren, H2-F) fuels and electric options produce zero emissions, while traditional fuels like HFO and MDO exhibit the highest TMER. Sensitivity and stochastic analyses identify critical input variables affecting NPV, such as fuel costs, emission costs, and vessel speed. Findings indicate that LNG consistently yields the highest NPV, particularly for autonomous vessels, suggesting economic advantages and reduced emissions. These insights are crucial for optimizing fuel selection and operational strategies in marine transportation and offer valuable guidance for decision-making and investment in the marine sector, ensuring regulatory compliance and environmental sustainability.

This chapter is based on the following publication: *H. Laryea and A. Schiffauerova, "Environmental and cost assessments of marine alternative fuels for fully autonomous short-sea shipping vessels based on the global warming potential approach," J. Mar. Sci. Eng., vol. 12, no. 11, p. 2026, 2024. [Online]. Available: https://doi.org/10.3390/jmse12112026*

4.1. Introduction

The shipping industry, responsible for transporting over 80% of international trade, is the most energy-efficient mode of goods transport. However, despite the relatively low total carbon dioxide (CO_2) emissions from shipping, the industry cannot ignore its role in addressing global warming. The fourth International Maritime Organization (IMO) GHG report indicates that shipping emitted approximately 1,056 million tonnes of CO_2 in 2018, accounting for 2.89% of global CO_2 emissions [110]. Ship energy management significantly influences both cost efficiency and environmental impact, primarily due to the considerable CO_2 emissions stemming from ship operations. Decreasing energy consumption not only directly mitigates emissions, but also reduces the environmental footprint and operational expenditures [111]. Therefore, the IMO has endorsed a proposed amendment requiring the adoption of a Ship Energy Efficiency Management Plan (SEEMP) and an Energy Efficiency Design Index (EEDI) for newly constructed vessels. This regulatory measure aims to curtail greenhouse gas (GHG) emissions within the maritime domain [112]. The proposed net zero target for 2050 by the IMO [113] can be achieved through the changes of ship design, including weight reduction, the use of advanced coatings on the hull [114], the optimization of the ship's hull dimensions and bow thrusters, just to mention a few [115]. Similarly, energy efficiency and sustainability can be achieved by using alternative fuels with minimal or zero emissions onboard vessels. The best marine alternative fuels are biofuels (biodiesel, biomethane, bioethanol), E-fuels (green hydrogen, E-diesel, green ammonia, E-methane), blue fuels (blue hydrogen, blue ammonia), electricity (grid, renewable energy sources), and fossil fuels (mixture of fossil fuel and advanced biofuels) [116]. However, the application of some of the aforementioned alternative fuels is not mature in terms of production processes and bunkering infrastructure [115], [117]. The choice of energy source or fuel type for a vessel [53] is contingent upon both the vessel's classification and the specific route it navigates on [118], [119].

Short-sea shipping vessels [120] facilitate the transportation of goods and passengers over relatively short distances [119], within port waters and between deep sea terminals [121]. As evidenced in Europe and other North American regions [122], [123], short-sea shipping presents opportunities to improve efficiency and address environmental impacts associated with goods and passenger transport [124]. Moreover, short-sea shipping vessels operating in inland waterways play a pivotal role in regional and national transportation networks, offering benefits such as

reduced energy consumption, lower emissions, and maintaining a high safety standard compared to road transport [125]-[127].

International Convention for the Prevention of Pollution from Ships (MARPOL) mandates four key requirements for both new and existing vessels to address air pollution, emphasizing cleaner fuels, renewable energies, emission reduction technologies, and enhanced energy efficiency [53], [54]. The utilization of maritime autonomous surface ships (MASS) offers a promising approach to mitigate environmental impact within the maritime sector, operating independently with artificial intelligence (AI) driven navigation. Fully autonomous fleets, without onboard crews, demonstrate significant conservation of energy and reduction of pollution [128], with a notable decrease of 74.5% [46] in energy consumption in autonomous container vessels compared to traditional counterparts [129]. Integrating MASS with marine alternative fuels emerges as a robust strategy for reducing GHG emissions in maritime operations [130], [131].

In the quest to identify the most suitable alternative fuel for vessels, two principal methodologies are used to measure ship fuel consumption and predict emissions: the top-down and bottom-up approaches [132]. The top-down approach, used in several existing studies, focuses on the utilization and analysis of marine fuel sales data [133], [134]. Conversely, an increasing number of studies is adopting the bottom-up approach [132], [133], [135], which involves analyzing fuel consumption in relation to specific shipping activities [136]. The latter method offers a more accurate representation of actual emission levels. To predict fuel usage in maritime vessels, the bottom-up methodology uses a cubic correlation between fuel consumption and vessel speed [133]. Table 16 presents comparative analyses conducted by previous researchers that were aimed at identifying the optimal marine fuel.

A recent review by Chen and Yang [137] explored the application of automatic identification system (AIS)-based methods for estimating ship emissions. This study encompassed data acquisition via AIS, analysis of ship characteristics, calculation of engine loads, and determination of emission factors. In contrast, Aarskog et al. [138] evaluated the economic feasibility of fuel cell (FC) propulsion for high-speed crafts (HSC) using an energy analysis method, juxtaposing it with traditional diesel and biodiesel alternatives. Their findings indicate potential cost competitiveness of FC-equipped HSCs compared to diesel propulsion by 2025 –2030. Similarly, Jafarzadeh and Schjølberg [139] used cubic law of design and operational speed to examine optimal propulsion

power utilization for enhancing electric or hybrid propulsion in suitable ship types. Ocean-going reefers achieve peak efficiency at 0.6–0.7 of their capacity loads, whereas other vessels peak at lower loads, limiting hybrid or electric integration benefits. Additionally, various studies [140]-[145] have investigated the economic and emissions impacts of alternative marine fuels based on ship-specific considerations. These studies hinge on intricate technical specifications and operational data that are distinct to individual vessels. For instance, Kouzelis et al. [140] applied simple multi-attribute rating technique (SMART) decision-making models to assess optimal alternative fuel technologies for large container vessels, highlighting upgraded bio-oil (UBO), Fischer-Tropsch diesel (FTD), and liquefied bio-methane (LBM) as promising future fuels. Meanwhile, conventional fuels like heavy fuel oil (HFO) and liquefied natural gas (LNG) are likely to maintain dominance without regulatory changes. Additionally, Kosmas and Acciaro [141] used Cobweb Theorem to analyze the economic and environmental effects of bunker levies on shipping fuels for cargo ships, showing potential reductions in speed and fuel consumption, akin to sector energy efficiency improvements through regulatory measures. Similarly, Ammar and Seddiek [142] explored selective catalytic reduction (SCR), seawater scrubbers (SWS), marine gas oil (MGO), and LNG using eco-environmental analysis methods for reducing RoRo exhaust emissions, with LNG emerging as the most effective option both economically and environmentally. Furthermore, Helgason et al. [143] compared conventional methanol from natural gas (NG), and renewable methanol (RN) with HFO using impact pathway analysis (IPA) in Iceland's maritime sector, highlighting fossil methanol's current cost competitiveness and projecting renewable methanol's future cost-effectiveness. On the contrary, there is limited literature addressing simultaneous economic and emission analyses for both conventional and autonomous MASS [144], [145]. For example, Jovanović et al. [144] used cubic law of design to conduct environmental and economic evaluations of RoRo passenger ferries, identifying methanol and electric propulsion as optimal choices across all routes. Autonomous shipping shows substantial ecological and economic benefits across various propulsion options and vessel types, except for renewable hydrogen-powered vessels on longer shipping routes. Similarly, Kretschmann et al. [145] used cost-benefit analysis to perform a comprehensive cost analysis comparing conventional and autonomous bulkers, emphasizing the economic advantages of autonomous vessels, particularly with MDO despite higher voyage expenses.

The complexities inherent in integrating alternative fuels into maritime operations underscore the necessity for tailored solutions that consider vessel type and operational context. However, further advancements are required in several key areas. Notably, there remains a gap in comprehensive studies that compare the environmental and economic impacts of marine alternative fuels across both conventional and autonomous vessels using AIS data and employing a global warming potential approach. Previous studies conducted by previous authors by [138] [139] focused solely on conventional vessels using AIS data. The sensitivity analysis performed by Aarskog et al. [138] was restricted to fuel cells without consideration of other fuel types and lacked a stochastic analysis. Additionally, Jafarzadeh and Schjølberg [139] exclusively calculated power consumption for main engines, neglecting the significant contributions of auxiliary engines. Furthermore, analyses conducted by some authors [144], [145] utilized ship-specific particulars rather than AIS-based methods, limiting their ability to capture real-time operational dynamics effectively. Moreover, previous assessments often omitted critical factors such as carbon monoxide emissions, port costs, and hydrogen storage tank costs [144], [145]. Furthermore, the environmental impacts, environmental cost assessments, and stochastic analysis were frequently overlooked across studies. Neglecting these aspects can lead to inaccurate estimations of a fuel's ecological footprint and economic implications, thereby hindering informed decision-making regarding sustainable fuel selection. Incorporating comprehensive environmental and economic analyses, including stochastic considerations, is essential for ensuring robust evaluations of marine alternative fuels. Such an approach facilitates more informed decisions that balance environmental sustainability with economic viability, crucial for advancing the adoption of sustainable marine fuels. For instance, Table 16 provides a comparative analysis of research utilizing a bottom-up methodology, which integrates AIS data and ship-particulars to evaluate the environmental and economic impacts of alternative fuels in marine applications.

Table 16: Comparative analysis of environmental and economic assessments for marine alternative fuels.

Objective	Study Area	Type of Ship	Type of Fuel Analysis	Data Source	Comments	Reference
Perform economic assessments contrasting fuel cell with diesel and biodiesel.	Norway	HSC	Hydrogen, diesel, and biodiesel	AIS Data	No stochastic analysis was performed, only sensitivity analysis on hydrogen FC	[138]
Analyze operational profiles to select suitable ships for electric/hybrid propulsion.	Norway	Tankers, bulk carriers, general cargo ships, container ships, roll-on/roll-off (Ro-Ro) ships, reefers (refrigerator/freezer), offshore ships and passenger ships.	FC, batteries, MGO	AIS Data	No sensitivity or stochastic analysis was performed.	[139]
Optimize fuel technology for efficient freight across technical and environmental standards.	Denmark to Greece from Denmark, China, Norway, Greece	Large container vessel	HFO, FTD, UBO & LBM	Ship particulars	Conduct sensitivity analysis on SFOC[2], fuel cost, vessel speed relative to required freight rate (RFR).	[140]
MBMs[3] proposals improve shipping sector efficiency and reduce emissions	N/A	Cargo ships	N/A	Ship particulars	No sensitivity, environmental, or stochastic analysis was conducted.	[141]

1. Both conventional and autonomous vessels are considered. 2. **SFOC**: specific fuel oil consumption 3. **MBMs**: Market-based measures

Objective	Study Area	Type of Ship	Type of Fuel Analysis	Data Source	Comments	Reference
Analyze environmental, economic impacts of diverse ship fuel options for IMO compliance	Hurghada port (Egypt) and Duba port (Saudi Arabia)	Medium RoRo cargo ship	SCR, SWS, MGO, LNG,	Ship particulars	Sensitivity analysis is conducted based on variable emission reduction percent & interest rate.	[142]
Conducts comprehensive cost-competitive analysis of three marine fuels.	Iceland	N/A	NG, RN, & HFO	N/A	Performed sensitivity analysis on years, price trajectories, and total costs; no stochastic analysis conducted.	[143]
Optimizing power for autonomous ro-ro ships considering environmental and economic factors.	Croatian	RoRo passenger ship[1]	MDO, HFO, LNG, methanol, electricity, and hydrogen	Ship particulars	Sensitivity analysis focused on autonomous vessels' economic input variations only; stochastic analysis excluded for optimal fuel.	[144]
Examines autonomous bulker costs vis-à-vis conventional vessel	Australia to Europe	Bulk Carrier[1]	MDO, HFO	Ship particulars	Sensitivity analysis on RFR impact, emphasizing fuel consumption and vessel costs; no stochastic analysis.	[145]

1. Both conventional and autonomous vessels are considered. 2. **SFOC**: specific fuel oil consumption 3. **MBMs**: Market-based measures

Despite considerable existing literature on alternative marine fuels, consensus remains elusive regarding the optimal choice for future maritime operations. Moreover, few studies have comprehensively addressed the environmental impacts and simultaneous variations in input parameters, particularly concerning the application of marine alternative fuels across diverse short-sea vessels with varying speeds and routes. Incorporating dynamic methodologies within bottom-up calculations of ship pollutant emissions using geospatial inputs provides a precise depiction of real-time fuel consumption and emission dispersion during vessel operations. Such insights are crucial for stakeholders aiming to integrate alternative fuels effectively within the marine sector. Therefore, this research aims to investigate how these alternative fuels could potentially influence the design and operation of both conventional and autonomous surface ships

This study seeks to forecast fuel consumption for conventional and fully autonomous high-speed short-sea shipping vessels based on their operational profiles using AIS data, employing a bottom-up approach. Furthermore, it evaluates the environmental impact and associated costs of these alternative marine fuels. The modeling considers key performance indicators (KPIs) and utilizes annual AIS data alongside ship specifications and port data. Predictions of fuel consumption are made using different marine fuels, employing a global warming potential approach in conjunction with design specifications and operational speeds. Additionally, the study assesses emission factors to determine environmental impacts and cost implications, integrating cost metrics for a comprehensive economic analysis. Sensitivity analyses are performed to evaluate the impact of variable inputs on the models, aiming to identify optimal marine alternative fuels that not only comply with environmental policies but also offer high profitability.

This research makes significant contributions to the existing literature by introducing a novel application of the global warming potential approach tailored specifically for conventional and autonomous ships. This approach facilitates the assessment of mass emission rates, global warming potential, environmental impact, real-time fuel consumption, and associated costs for proposed alternative fuels. Moreover, the study introduces sensitivity and stochastic analyses that explore the effects of varying load factors, vessel speeds, emissions, and nautical miles on the selection of optimal marine alternative fuels. Prior literature has typically overlooked such detailed sensitivity analyses. Additionally, this research leverages port data from Los Angeles and Long Beach to develop a comprehensive mathematical model for environmental-economic assessments

specific to the chosen vessels. This model serves as a valuable tool for marine stakeholders to evaluate emission policies and identify feasible marine fuels that offer both environmental benefits and economic viability for short-sea shipping operations.

The rest of the paper is organized as follows: Section 4.2 introduces the materials and methods, which include data collection and the features for evaluating fuel consumption; environmental and cost analyses for the proposed marine alternative fuels are detailed. The results and discussion are presented in Section 4.3 and Section 4.4 respectively. Section 4.5 provides concluding remarks as well as perspectives on potential future research directions.

4.2. Materials and Methods

The ship's AIS data, specifications, and port information are employed to determine power, energy, and fuel consumption. Additionally, parameters of the proposed marine alternative fuels are integrated with this data for environmental and cost analyses using the global warming potential approach, with the aim of identifying KPIs. Sensitivity analyses are conducted for each alternative fuel across both conventional and autonomous vessels to validate their test results. Furthermore, a stochastic analysis is specifically conducted on the optimal alternative marine fuel for the chosen vessel. All computations take place within a Python environment, and detailed explanations, along with relevant equations used in the mathematical model, are provided in the subsequent sections. Figure 17 depicts the analysis flowchart. All computations are performed in a Python 3.11.6 environment, with comprehensive explanations and relevant equations presented in subsequent sections. This framework is specifically designed to evaluate fuel consumption and emissions based on ship AIS data and particulars.

The program begins by importing essential libraries, including Pandas for data manipulation, NumPy for numerical calculations, Matplotlib and Seaborn for visualizing fuel consumption, emissions, KPIs, and NPV, as well as Statsmodels for advanced statistical modeling and SciPy for statistical analysis and distributions.

Initially, the AIS dataset is loaded, and critical parameters such as ship particulars, engine power, fuel properties, and emission factors (as outlined in tables in section 4.2.4), along with financial data, are defined. The data undergoes preprocessing to ensure it is clean and properly formatted, addressing any missing values and converting units as required.

The core of the code includes functions that calculate fuel consumption based on ship speed and engine power, estimate emissions based on the fuel consumed, and compute key performance indicators to offer insights into fuel efficiency and operational costs. Additionally, NPV is calculated to assess the financial viability of the vessel's operations over its service life.

Furthermore, the code incorporates sensitivity and stochastic analyses to evaluate how variability in key parameters—such as fuel cost, distance, speed, emission cost, load factor, and rate—affects the NPV results for fully autonomous vessels. The stochastic analyses model uncertainty in these key parameters concerning the NPV. The findings are visualized through various plots, illustrating trends in fuel consumption, emissions, NPV, and KPIs over the vessel's service life.

4.2.1. Ship Main Particulars and Navigation Route

For this research, we have selected a high-speed passenger ferry (HSPF) and a tugboat as the vessels under study. Ship specifications for these two vessels are sourced from various entities including the MarineTraffic [146], shipbuilders, fleet operators, port, and they are presented in Table 17. Similarly, details regarding operating modes and coverage are extracted from Automatic Identification System (AIS) data obtained from MarineTraffic. According to the AIS data and ship data, the high-speed passenger ferry (HSPF) shuttles passengers and goods between the mainland (specifically the Port of Los Angeles and the Port of Long Beach) and Santa Catalina Island (Avalon). Additionally, the tugboat operates within the ports of Los Angeles and towing vessels from the Port of Los Angeles to either the Port of Long Beach or Seal Beach. A segment of the navigation routes is illustrated in Figure 18.

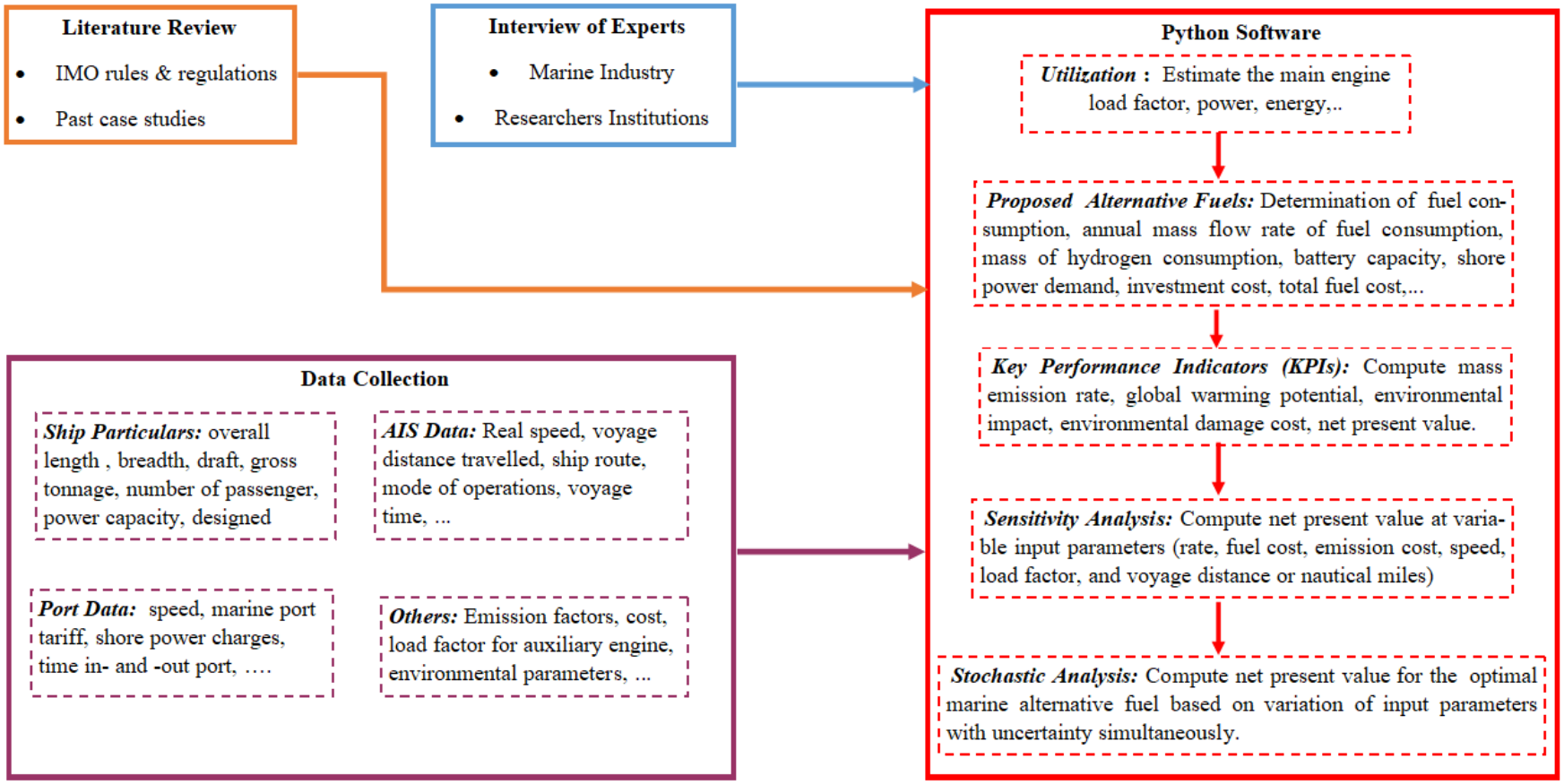

Figure 17: Flowchart of the data analysis process for marine alternative fuels in conventional and fully autonomous vessels

Table 17 : Main particulars for the conventional vessels adapted from [146].

Parameters	Vessel 1	Vessel 2
Ship Type	HSPF	Tugboat
Overall Length (m)	44.20	25
Breadth (m)	10.45	10
Draft (m)	3.96	5
Gross Tonnage (ton)	462	298
Design Speed (knots)	37	12.5
Number of Passenger,	381	2 - 6
Main Engine Power(kW)	6,869.56	3,840.35
Aux Engine Power (kW)	198	250
Navigation Route(s)	Avalon – Long Beach Avalon –Los Angeles	Los Angeles - Long beach Los Angeles – Seal Beach

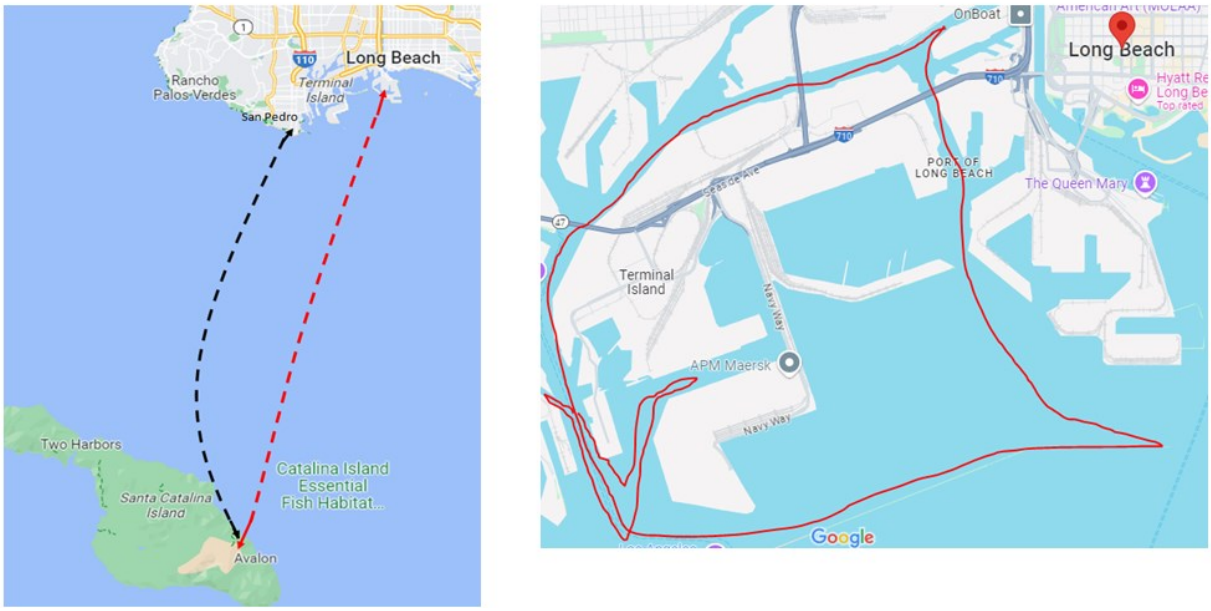

Figure 18: A segment of navigation routes depicted on a map sourced from Google maps [147]: (a) HSPF, (b) tugboat.

4.2.2. Estimation of Fuel Consumption

Fuel consumption in vessels occurs during propulsion and while powering auxiliary systems onboard. Therefore, to accurately assess total fuel consumption per voyage, it is essential to consider factors such as ship speed, load factor, and power demand along navigation routes must be considered.

4.2.2.1. Ship Speed

The speed of a vessel is directly correlated with its fuel consumption. As a result, the operational pattern of the vessel along navigation routes is segmented into three distinct phases based on speed and engine load: cruising mode, maneuvering mode, and idling (or hoteling) mode. In cruise mode, operational activities are governed by the inputs of cruise distance and speed. Typically, for conventional vessels, the cruising speed ($V_{crus,conv}$) exceeds 12 knots for normal cruising and falls within the range of 8 knots to 12 knots for low cruising speed. In maneuvering mode, the vessel's speed is determined based on the nautical distance from land or to the port (that is, from the port entrance to the berth, pier, wharf, or dock). For instance, at ports like the Port of Los Angeles (San Pedro) and Port of Long Beach, maneuvering operations occur within the precautionary area, limiting the maneuvering speed for conventional vessels ($V_{man,conv}$) to less than 12 knots [148], [149].

In the case of idle mode, when the ship is at berth or anchorage, the main engines are shut off, resulting in a speed of zero ($V_{idle,conv}$), while the auxiliary engines continue to operate. Table 18 presents the estimated average speeds for the vessels using real-time data for the three operational modes based on AIS data.

Table 18: Average daily estimates for marine vessels across two operational modes.

Type of Vessels	Average Cruising (knots)	Average Maneuvering (knots)
HSPF	23.70	10.25
Tugboat	9.50	6.70

4.2.2.2. Load Factor (LF)

The load factor represents the percentage of the vessel's total power. Utilizing AIS data for the vessels, the estimation of the load factor for the main engines ($LF_{ME,i}$) is derived. Hence, by employing the Propeller Law, the $LF_{ME,i}$ is determined as follows [150], [151]:

$$LF_{ME,i} = \left(\frac{V_{avg,conv,i}}{V_{max}}\right)^3 = \left(\frac{V_{avg,conv,i}}{\left(\frac{V_{design}}{0.937}\right)}\right)^3 \quad (34)$$

where $LF_{ME,i}$ is the load factor for the main engine, i represents the vessel operating modes (that is, cruising, maneuvering, and idling), $V_{avg,conv,i}$ is the average speed for the operational modes in Table 18 (knots), V_{max} is the maximum speed (knots), and V_{design} is the design speed (knots), and 0.937 represents a safety margin that offers a conservative estimate for maximum speed, ensuring that the vessel can operate effectively under various conditions while minimizing the risk of damage or excessive strain on the propulsion system. In addition, if the determined $LF_{ME,i}$ is less than 2%, it is adjusted to a minimum of 2% [150] this is to ensure a baseline level of efficiency and to maintain consistency in performance metrics.

The same activity-based calculation formula was applied to the auxiliary engine. However, since these engines are primarily used for providing electricity rather than propulsion, their loads are independent from the vessel speed. In addition, given the limited data available regarding onboard auxiliary engines, the load factors ($LF_{Aux,i}$) were derived from a technical report conducted by the US Environmental Protection Agency for the ports of Los Angeles and Long Beach [150], [152]. Table 19 presents the estimated load factors for both main engines and auxiliary engines.

Table 19: Estimated load factors of the main engines and auxiliary engines for the vessels.

Engine Type	Type of Ships	Cruising	Maneuvering	Idling
Main Engines	HSPF	21.82%	2.00%[1]	-
	Tugboat	26.10%	3.87%	-
Aux Engines	HSPF	17%	45%	22%
	Tugboat	17%	45%	22%

1.The determined value is 1.76%, but it has been adjusted to 2% for the purpose of this research.

4.2.2.3. Ship Power Demand and Energy Consumption

The load demand varies for each mode of operation and is specific to each vessel. Consequently, the power requirements for the vessel and its integrated auxiliary systems are met by the onboard main engines and auxiliary engines. To illustrate, the effective power generated by the main engines for propelling the conventional ship ($P_{eff,ME-conv}$) is calculated as follows:

$$P_{eff,ME-conv} = P_{nom-ME,conv} * \eta_{ME} * LF_{ME,i} \quad (35)$$

where $P_{nom-ME,conv}$ is the total nominal power of the main engine (kW), and η_{ME} denotes the efficiency of the main engines which falls within the range of 70% - 90% [153].

Likewise, while the vessel is in port during idling mode, the auxiliary engines are operational, and the resultant effective power generated by the installed auxiliary engines on the conventional vessel ($P_{eff,Aux-conv}$) at an efficiency (η_{Aux}) of 95% [154] is represented as follows:

$$P_{eff,Aux-conv} = P_{nom-Aux,conv} * \eta_{Aux} * LF_{Aux,i} \quad (36)$$

Hence, the total power required ($P_{total-conv}$) for the conventional ship, considering all three modes of operation, is calculated as follows:

$$P_{cru-conv} = P_{nom-ME,conv} * \eta_{ME} * LF_{ME,cru} + P_{nom-Aux,conv} * \eta_{Aux} * LF_{Aux,cru} \quad (37)$$

$$P_{man-conv} = P_{nom-ME,conv} * \eta_{ME} * LF_{ME,man} + P_{nom-Aux,conv} * \eta_{Aux} * LF_{Aux,man} \quad (38)$$

$$P_{idle-conv} = P_{nom-Aux,conv} * \eta_{Aux} * LF_{Aux,idle} \quad (39)$$

$$P_{total-conv} = P_{cru-conv} + P_{man-conv} + P_{idle-conv} \quad (40)$$

where $P_{cru-conv}$ is the cruising power for the conventional ship (kW), $LF_{ME,cru}$ and $LF_{Aux,cru}$ are the load factors for main and auxiliary engine at cruising state (%), $P_{man-conv}$ is the maneuvering power for the conventional ship (kW), $LF_{ME,man}$ and $LF_{Aux,man}$ are the load factor for the main

and auxiliary engines at maneuvering state (%), $P_{idle-conv}$ is the idle power for conventional ship (kW), and $LF_{Aux,idle}$ is the load factor of auxiliary engine at idle state.

Similarly, the total energy consumption by the conventional vessel ($E_{total-conv}$) in kilowatt-hours (kWh) is estimated based on the ship's load and speed. Thus, the relationship between loads and the three states of operation in real-time is expressed as follows:

$$E_{total-conv} = \left(P_{idle-conv} * T_{idle,conv}\right) + P_{man-conv} * \left(\frac{ND_{man,conv}}{V_{man,conv}}\right) + P_{cru-conv} * \left(\frac{ND_{crus,conv}}{V_{crus,conv}}\right) \quad (41)$$

where $V_{crus,conv}$ denotes the instantaneous cruising speed for the conventional ferry (knots), $ND_{man,conv}$ is the nautical distance from berth during maneuvering phase (NM), $ND_{crus,conv}$ denotes the length of navigation route per one-way trip during cruising (NM), and $V_{man,conv}$ represents the instantaneous maneuvering speed for the conventional vessel (knots).

In the case of fully autonomous ships, we assume that they share the same dimensions and navigation routes as conventional ships to prevent excessive fuel consumption. Moreover, the absence of a ship crew results in a reduction in the required auxiliary power [155], as well as the elimination of crew living quarters and certain applicable auxiliary systems, which affects the vessel's displacement, decreases the space consumption [156] and required propulsion power [46]. For instance, studies have shown that a fully autonomous container vessel can achieve energy savings of up to 74.5% compared to a conventional one, primarily due to the elimination of facilities and equipment used by sailors [46]. The vessels utilized in our research are short-sea vessels, which return to port after each trip, as opposed to container ships that undertake long voyages. However, the assumptions in this study are derived from findings concerning fully autonomous container vessels, owing to the limited data available on energy consumption for fully autonomous tugboats and high-speed ferries. However, in our research, although there is no ship crew, passengers are still onboard. Therefore, we assume that the total power required by autonomous vessels is 40% lower than their respective conventional ships [145]. By substituting these assumptions into Equation (40) and Equation (41), it follows that the total power

($P_{total-auto}$) and energy consumption ($E_{total-auto}$) for fully autonomous vessels are 40% lower than $P_{total-conv}$ and $E_{total-conv}$, respectively. Additionally, we anticipate a 30% increase in energy and power requirements to accommodate potential expansions and uncertainties in loads in the near future. Consequently, we have substituted these values into the subsequent equations in subsections 4.2.3 – 4.2.5 for fully autonomous vessels.

4.2.3. Proposed Alternative Fuels for the Marine Vessels

The use of fuel by marine engines is vital in the propulsion of ships and for providing power to other fitted systems on board. To reduce the rate of GHG emissions, the IMO has proposed enforcing stringent rules and regulations on ships' emissions. As a result, the IMO has teamed up with the Global Industry Alliance in support of low-carbon shipping in the marine industry [132], [157] via the use of alternative low- and zero-carbon fuels [158]. The alternative marine fuels include conventional fuels (marine diesel oil (MDO), heavy fuel oil (HFO), marine gas oil (MGO), biofuel (B20), methane (or liquefied natural gas (LNG)), hydrogen, methanol, battery-electric, ethanol, dimethyl ether (DME), liquefied petroleum gas (LPG), ethane, and ammonia) [94], [159]. The applications of the aforementioned fuels are not limited to environmental impacts but also economic criteria, fuel properties, effects on the propulsion system, and safety handling criteria [160], just to mention a few. However, for this research, only the first six alternative marine fuels will be considered due to their maturity regarding regulatory readiness levels.

4.2.3.1. Diesel - Propelled Marine Vessel

Formally, marine diesel fuel encompasses any type of diesel used in seagoing vessels. The three primary marine fuels are Marine Diesel Oil (MDO), Heavy Fuel Oil (HFO), and Marine Gas Oil (MGO) distinguished by their sulfur contents. For instance, MDO, readily available, is composed of various distillate blends with a minor inclusion of HFO. In addition, it possesses a slightly greater density and exhibits a lower cetane value as compared to MGO [152]. Similarly, HFO, with a higher sulfur content, requires the use of approved exhaust gas cleaning systems (or scrubbers) [161] when used onboard vessels. Likewise, MGO, comprising a blend of distillates, features a lower sulfur content compared to HFO and MDO [161]-[163].

Additionally, most existing marine engines and fuel-burning equipment are specifically engineered for the use of HFO, MDO, or MGO [161]. The total fuel consumption of the marine engine is determined by its overall energy usage, which is expressed as follows:

$$FC_{diesel-conv} = E_{total-conv} * SFC_{diesel} \tag{42}$$

where $FC_{total-conv}$ denotes the fuel consumption per trip (kg), and SFC_{diesel} is the specific fuel consumption (kg/kWh). The SFC_{diesel} for slow-speed diesel vessels and high -speed diesel vessels are 0.165 kg/kWh and 0.210 kg/kWh respectively [164], [165]. Likewise, the annual mass flow rate of the total fuel consumption ($\dot{m}_{conv}$) (kg/h) is estimated as follows:

$$\dot{m}_{diesel-conv} = \sum_{n=1}^{n=N} \frac{FC_{diesel-conv}}{(T_{crus,conv} + T_{man,conv} + T_{idle,conv})} = \sum_{n=1}^{n=N} \frac{FC_{diesel-conv}}{T_{total,conv}} \tag{43}$$

where N is the total number of trips in a year (unitless), $T_{crus,conv}$ is the cruising time (hrs.), and T_{total} denotes the total hours in the context of the ships' operational profiles for the entire year (hrs.).

These fuels use the preexisting propulsions and fuel systems, therefore, the total investment costs ($IC_{\mathrm{i},conv}$) and the total operating cost of fuel ($CF_{\mathrm{total-i},conv}$) for the MDO, HFO, and MGO are determined as follows:

$$IC_{diesel-conv} = C_{in} * P_{total-conv} \tag{44}$$

$$CF_{\mathrm{total-i},conv} = C_{\mathrm{i}-fuel} * FC_{diesel-conv} \tag{45}$$

where C_i denotes the investment cost which ranges from 240 - 460 USD/kW [166], $C_{\mathrm{i}-fuel}$ is the cost of fuel (USD/kg), and i denotes the type of fuel. The cost of MDO, HFO, and MGO are 3.09 USD/kg [167], 0.511 USD/kg [168] and 0.956 USD/kg [169] respectively. In addition, the maintenance cost of the diesel-propelled conventional marine vessel is 50 USD/kW [170]. Nevertheless, the maintenance cost for the fully autonomous vessel exhibits a 15% increment, attributed to the elevated necessity of skilled ship crew members required for the maintenance of

the ship while at berth [145]. This percentage increase is applied to the fully autonomous ship powered by the other alternative fuels.

4.2.3.2. Hydrogen- Propelled Marine Vessel

In terms of propulsion, the use of the above fuels in the preceding engines are feasible, with the exception of hydrogen, which can only be applied to four-stroke engines (shorter voyage) due to ample hydrogen storage space requirements and safe handling of the generated hydrogen [116]. The vessel's propulsion system is motor-driven via electrical power [110]. We proposed proton exchange membrane fuel cells (PEMFC) over the solid oxide fuel cells (SOFC) due to their quicker start-up time, strong dynamic responsiveness, operation at low temperature, and excellent power density [171].

The hydrogen fuel use in the PEMFC is produced through two different methods. The first option is via electrolysis of water using renewable energy sources (H_2 - Ren) [172], as a result the generated hydrogen is considered low or net-zero emission [94]. In addition, the second method is from fossil fuels (H_2 - F). This approach generates a significant amount of CO_2 as a byproduct during its production. In contrast, the utilization of hydrogen in combustion or fuel cells does not result in CO_2 emissions [173]. Thus, the required mass of hydrogen consumption by the PEMFC ($FC_{hyd-conv}$) (kg) in both options is determined as follows [174]:

$$FC_{hyd-conv} = \frac{E_{total-conv}}{\eta_{FC} * LHV} \tag{46}$$

where η_{FC} is the fuel cell efficiency during beginning of life (51%), and LHV denotes the lower heating value of hydrogen (120,000 KJ/kg). In addition, the annual mass flow rate of the total hydrogen fuel consumption ($\dot{m}_{hyd-conv}$) (kg/h), is estimated by substituting $FC_{hyd-conv}$ into Equation (43). We presume that the PEMFC power system will engage in cold-ironing while at berth. This is to aid in the warming of the system until it reaches its designated operating temperature and for the production of electric power. The power demand by fuel cell components from shore power ($P_{\text{hyd,shore}-conv}$) (kW) is determined as follows:

$$P_{\text{hyd,shore}-conv} = \ 1.30 * \text{P}_{\text{idle}-\text{conv}} \tag{47}$$

Therefore, the annual cost of cold-ironing is $P_{\text{hyd,shore}-conv}$ times the idling time and the shore power charging fees (SC_{cost}) of 0.20USD/kWh [175]. In addition, the total investment cost ($IC_{\text{hyd}-conv}$) of PEMFC and its accessories is determined as follows:

$$IC_{\text{hyd}-conv} = C_{in-FC} * P_{\text{hyd}-conv} + C_{acc} * P_{\text{hyd,shore}-conv} \quad (48)$$

where C_{in-FC} is the initial investment cost for PEMFC, which is in the range of 730 – 2,860 USD/kW [166], and C_{acc} represents the cost of accessories, which consist of gas supply system and type IV 700 bar hydrogen storage tanks - and ranges from 576-868 USD/kW [166]. Likewise the replacement cost is 40% of the total component cost [176], and annual maintenance cost is 6% of the total capital cost per lifetime [177]. The cost of green hydrogen fuel (option 1) and blue hydrogen fuel are 4.5-12 USD/kg and 1.8 – 4.7 USD/kg respectively [178]. Thus, total cost for the hydrogen fuel ($CF_{\text{hyd},conv}$) is determined as similar by substituting the cost of fuel and $FC_{hyd-conv}$ into Equation (45).

4.2.3.3. Battery or Electric - Propelled Marine Vessel

The battery electric systems onboard vessels are operated in three different ways: as hybrid, plug-in hybrid, and fully electric [94]. For this research, we focus on fully electric systems, where the battery bank stores the necessary energy for propulsion and to satisfy the auxiliary loads. The advantage of electrifying ships is the elimination of GHG emissions [94]. Additionally, lithium-ion (Li-ion) batteries are considered for this research over the lead- acid batteries [91], nickel metal hybrid batteries [92], silver–zinc batteries, and open water-powered batteries due to their optimal chemical composition or battery chemistry [94], [179].

To avoid excessive battery weight onboard, the battery capacity ($B_{cap-conv}$) (kWh) required by the fully battery-electric vessel is determined based on round trips using Equation (45). In addition, to prevent power failure, the battery capacity is increased by a power factor (P_f) of 20 % for the conventional vessel and 40% for the fully autonomous vessel to provide onboard power supply for a round trip.

$$B_{cap-conv} = \frac{P_f * E_{total-conv} * 2}{\eta_{Li-ion} * \eta_{motor} * DOD * \eta_{inverter}} \quad (49)$$

where η_{Li-ion} is the efficiency of the Lithium-ion battery (100%) [180], η_{motor} is the efficiency of the DC motor (80%) [181], DOD denotes the battery depth of discharge (80%) [181], and $\eta_{inverter}$ is the inverter efficiency (90%) [182]. Thus Equation (41) is substituted into Equation (50), but the average speeds, average nautical distances, and average duration are used. The investment cost ($B_{invest-conv}$) and cost for the shore power connection ($BC_{cost-conv}$) for the battery bank are determined as follows:

$$B_{invest-conv} = N_{inst} * (B_{cap-conv} * B_{cost} + P_{total-conv} * EM_{cost}) \quad (50)$$

$$BC_{cost-conv} = B_{cap-conv} * SC_{cost} \quad (51)$$

where N_{inst} is the number of times to install the battery bank during its lifetime (unitless), B_{cost} is the initial cost of the Li-ion marine battery which ranges from 500 – 1000 USD/kWh [166], and EM_{cost} is the cost of the electric motor which we assumed it to be equal to 250 USD/ kW. Also, we assumed that the battery bank needs replacement every 4–5 years. In addition, the annual cost of shore power connection is estimated by multiplying Equation (51) by the total number of voyages in a year.

4.2.3.4. B20 - Propelled Marine Vessel

Biodiesel is a renewable and non-toxic fuel- that offers a cleaner combustion option, serving as a noteworthy alternative to conventional diesel. Its combustion results in diminished air emissions, encompassing reductions in soot, smoke, carbon monoxide, and GHG emissions [183], rendering it highly environmentally friendly.

In this research, we explore a biodiesel diesel blend, denoted as B20. This composite fuel consists of 20% biodiesel and 80% conventional diesel [184]. The adoption of B20 in lieu of traditional diesel enables ships - to achieve a potential reduction of up to 20% in GHG emissions [183].

The total B20 fuel consumption ($FC_{B20-conv}$) by the conventional vessel is determined as follows:

$$FC_{B20-conv} = E_{total-conv} * (0.20 * SFC_{biodiesel} + 0.80 * SFC_{diesel}) \quad (52)$$

where specific fuel consumption for biodiesel ($SFC_{biodiesel}$) is 0.74 kg/kWh [185], [186]. Similarly, the mass flow rate of the total fuel consumption for B20 ($\dot{m}_{B20-conv}$) is estimated by dividing the annual $FC_{B20-conv}$ by $T_{total,conv}$.

The total investment cost of replacing the existing diesel power system with B20 power system is calculated by multiplying the initial investment cost of B20 system which ranges from 240 to 460 USD/kW [166], by the total power ($P_{total-conv}$). Similarly, the total cost of operating the B20 fuel is estimated by multiplying the cost of B20 fuel, which is 3.980 USD/ kg [187], by the total fuel consumption ($FC_{diesel-conv}$). The maintenance cost for a ship powered by B20 is comparable to that of a vessel powered by diesel.

4.2.3.5. Liquefied Natural Gas (LNG) - Propelled Marine Vessel

Liquefied Natural Gas (LNG) is regarded as a feasible substitute fuel for diverse classes of ships, encompassing those involved in deep-sea, short-sea, and inland navigation. The evaluation of various technologies has raised significant apprehensions regarding the potential shift of ships to LNG as the primary fuel source in recent times [188]. Furthermore, the current bunkering strategies implemented by shipping companies have a pivotal influence on the decision-making process between LNG and low-sulfur fuel [189].

The fuel consumption of the LNG marine engine encompasses not just the direct utilization of LNG but also incorporates the consumption of pilot fuel [188]. The purpose of the pilot fuel is to initiate the combustion process and to ensure a dependable source of ignition [190]. This dual-fuel

approach enables the vessel to curb the emission of pollutants. The mixing proportion of LNG and pilot fuel in a dual-fuel system is 98% and 2%, respectively [191] .

The total fuel consumption by LNG-propelled ship is calculated as follows:

$$FC_{LNG-conv} = E_{total-conv} * (0.98 * SFC_{LNG} + 0.02 * SFC_{pilot\ fuel}) \quad (53)$$

where the SFC_{LNG} and $SFC_{pilot\ fuel}$ represent specific fuel consumption for LNG (0.15 kg/kWh) and pilot fuel (0.02 kg/kWh) [188] respectively.

The overall investment cost for the replacing the existing diesel power system with an LNG power system is determined by multiplying the initial investment cost of 400USD/kW [166] by $P_{total-conv}$. Likewise, the total operating cost of LNG fuel is estimated by multiplying the cost of LNG fuel, which is 1.560 USD/kg [168], by the total fuel consumption ($FC_{LNG-conv}$). The maintenance cost for the LNG-propelled ship is 0.005 USD/kWh [192] .

4.2.3.6. Methanol - Propelled Marine Vessel

Currently, methanol (MeOH) stands out as a prospective alternative to traditional fuels in maritime transport. Notably, methanol exhibits a heat of vaporization nearly four times higher than that of diesel fuel. This characteristic implies that methanol requires more heat energy for vaporization, leading to a charge cooling effect and a subsequent reduction in in cylinder temperature. Furthermore, the charge cooling effect contributes to a reduction in NO_X emissions, attributable to its lower combustion temperature compared to diesel fuel [193], [194].

In this study, a combustion strategy involving the use of methanol–diesel is employed for ships powered by methanol. The primary fuel comprises 98% methanol, supplemented by 2% pilot fuel added to the methanol–air mixture within the cylinder to initiate ignition [54].

The calculation of fuel consumption for the ship powered by methanol ($FC_{meth-conv}$) is as follows:

$$FC_{meth-conv} = E_{total-conv} * (0.98 * SFC_{meth} + 0.02 * SFC_{pilot\ fuel}) \quad (54)$$

where SFC_{meth} is the specific fuel consumption of methanol which is equal to 0.48964 kg/kWh [195].

The total investment cost for replacing the current diesel power system with a new methanol power system is computed by multiplying the initial investment cost of 265-505 USD/kW [166], by the total converted power ($P_{total-conv}$). Similarly, the total operational cost of methanol is estimated by multiplying the cost, set at 0.520 USD/kg [168], by the total fuel consumption ($FC_{meth-conv}$). The maintenance cost for the ship propelled by methanol is equivalent to that of the ship powered by diesel.

4.2.4. Environmental Impact and Environmental Cost Assessments

The marine vessels used for this case study are HSPF and a tugboat, which are known to cause a very high rate of emissions due to their speed and variable modes of transportation [138] Additionally, the internal combustion of marine fuels emits numerous of pollutants into the atmosphere. Therefore, this section presents a detailed discussion on the mass emission rate, global warming potential, environmental impact and damage cost.

4.2.4.1. Mass Emission Rate

The mass emission rate is defined as the discharge rate of a pollutant, denoted by its weight per unit of time [196]. Similarly, the emissions factor refers to the quantity of pollutants emitted into the atmosphere relative to a specific activity [197]-[199]. The main pollutants associated with marine alternative fuels include carbon monoxide (CO), CO_2, sulfur oxides (SO_X), nitrogen oxide (NO_X), nitrous oxide (N_2O), particulate matter (PM) or black carbon, and unburned hydrocarbons (UHC) or methane (CH_4) [200], [201]. The mass emission rate by each pollutant for the alternative fuels is expressed as follows:

$$\dot{m}_{ij,conv} = \dot{m}_{conv} * EF_j \quad (55)$$

where $\dot{m}_{ij,conv}$ is the mass emission rate of each pollutant (kg/h), i is the type of alternative marine fuel, j denotes the type of pollutant from marine fuel (unitless), and EF_j denotes the emission

factor (g/kg-fuel), which is tabulated in Table 20. In addition, the Total Mass Emission Rate (TMER) of pollutants from a particular alternative fuel is calculated by aggregating the individual mass emission rates of the pollutants emitted by that specific alternative fuel.

Table 20: Emission factors (EF) for marine alternative fuels (g/kg fuel)

Alternative Fuels	**CO_2**	**CO**	**N_2O**	**NOx**	**SOx**	**PM**	**CH4**
B20 (Biofuel)	- [202]	2.52 [184]	0.15 [202]	61.21 [202]	2.64 [202]	1.02 [202]	0.06 [202]
HFO	3114 [201]	2.87 [201]	0.18 [201]	78.61 [201]	50.83 [201]	7.53 [201]	0.05 [201]
Hydrogen	- [202]	- [202]	- [203]	- [202]	- [202]	- [202]	- [203]
LNG	2753 [201]	3.57 [201]	0.10 [201]	10.95 [201]	0.03 [201]	0.18 [201]	51.6 [202]
Methanol	1375 [202]	- [201]	- [202]	8 [202]	- [201]	- [202]	- [202]
MGO	3206 [204]	0.70 [204]	0.18[1] [201]	51.23 [204]	2.74[1] [201]	0.97[1] [201]	0.05[1] [201]
MDO	3206 [201]	2.54 [201]	0.18 [201]	57.62 [201]	2.74 [201]	0.97 [201]	0.05 [201]

1. *The designation "MDO" in the 4th IMO GHG study refers to the emission factors (EFs) for both MGO and MDO. Consequently, some of the EFs assigned to MDO are also attributed to MGO.*

The table mentioned above presents the emission factors (EFs) for all alternative fuels under investigation, excluding electricity. Additionally, the EFs for B20 are sourced from references [184], [202] while hydrogen is considered to have zero emissions according to references [202] [203]. The EFs for HFO and MDO are derived exclusively from the Fourth IMO GHG report [201], whereas the EFs for LNG and methanol are obtained from both [201] [202] . Furthermore, the values for MGO are sourced from [201] [204] . In addition, the total mass emission rate (TMER) of pollutants from a particular alternative fuel is calculated by aggregating the individual mass emission rates of the pollutants emitted by that specific alternative fuel.

4.2.4.2. Global Warming Potential (GWP)

The global warming potential a measure of the amount of energy a single ton of gas will consume over a specific period compared to one ton of CO_2. The greater the GWP, the more a particular gas contributes to heating the earth in comparison to CO_2 over that period [205]. Additionally, the typical time horizon used for regulatory the GWP assessments is 100 years [206], [207]. Although NOx and SOx are not classified as greenhouse gases (GHGs), they can exert indirect effects on the climate. Their primary impacts are localized, influencing air quality and human health; however, they may also have broader environmental repercussions. Consequently, they were included in the GWP calculations; thus, the total GWP of emissions ($GWP_{ij,conv}$) indicated by the GWP index ($\frac{kg}{h}$ CO_2 eqv.) is expressed as follows [208]:

$$TGWP_{ij,conv} = \sum_{n=1}^{n=i} \dot{m}_{ij,conv} * GWP_j \quad (56)$$

where GWP_j denotes the GWP value for each pollutant (unitless) as shown in Table 21.

Table 21 Global warming potentials values for greenhouse gases, environmental impact factor, and environmental costs of emissions.

Pollutants	Global warning Potential (GWP) Value (unitless)	Environmental Impact factor, b (mPts/kg)	Environmental Cost of Emission, C (USD/kg) [2]
CO_2	1[205]-[209]	5.45 [208], [210], [211]	0.128 [208], [210]
CO	1 [208]	8.36 [208], [210], [211]	0.201 [208], [210]
N_2O	273 [205]	163.8[1] [212]	2.66 [211]
NOx	310 [208]	2,749.36 [208] [213]	5.912 [208]
SOx	23,900 [208]	1,499.37 [208]	9.670 [208]
PM	460 [214]	240.00 [215]	40.40 [216]
CH_4	28 [209]-[217]	114.62 [208]	2.78 [208], [210]

1 Converted from KG/TJ to mPts/kg. 2. These values have been converted to USD.

The values for global warming potential (GWP), environmental impact factor (b), and environmental cost of each emission (C) are presented in Table 21. However, the cost values (C)

are originally reported in GBP/kg, and we have converted them to USD/kg to ensure consistency with the context of our research conducted in North America.

4.2.4.3. Environmental Impact and Damage Cost

The environmental impact (EI) is defined as the change to the environment resulting from a direct activity, which can have either adverse or beneficial consequences for the inhabitants of an ecosystem [218]. The total EI (TEI) for the marine engine emissions can be expressed as:

$$TEI_{ij,conv} = \sum_{n=1}^{n=i} \dot{m}_{ij,conv} * b_j \tag{57}$$

where $TEI_{ij,conv}$ signifies the total environmental impact (mPts/h) and b_j denotes the environmental impact factor (mPts/kg) in Table 21.

In addition, the environmental damage cost (EDC) is defined as the cost of emissions released into the atmosphere by the combustion of the marine alternative fuels [219]. Thus, the total EDC can be determined as follows:

$$TEDC_{ij,conv} = \sum_{n=1}^{n=1} \dot{m}_{ij,conv} * C_j \tag{58}$$

where $TEDC_{ij,conv}$ denotes the total environmental damage cost (US$/h) and C_j denotes the environmental cost of emission (US$/kg) in Table 21.

4.2.5. Total Cost Assessment

The total cost assessment is the process of incorporating environmental cost into the cost analysis for a long term [220]. The cost analysis comprises of the capital cost, operating cost, voyage cost, and net present value, which are discussed in detail in the subsections.

4.2.5.1. Capital Cost

Capital cost refers to the expense associated with the ship. Additionally, the capital cost for the conventional ferry varies based on the marine vessel's specific particular and conditions. The elimination of onboard ship crew, hoteling systems, and certain deckhouses for the fully autonomous ship directly affects the capital cost. Nevertheless, the implementation of the advanced sensors and control systems for onboard navigation and lookout systems at the shore

control center (SCC) leads to an increase in capital costs due to redundancy in these systems, resulting in an overall increase of 10% [170].

4.2.5.2. Voyage Cost

The voyage cost consists of the fuel cost for the engines, the environmental damage cost, and the port call costs. However, the port call cost is assumed to be 20% higher for the fully autonomous marine vessels due to the implementation of new framework and assistance from the SCC crew. Therefore, the annual voyage cost ($VC_{\text{annual},conv}$) for the ship's lifetime is determined as follows:

$$VC_{\text{annual},conv} = \left(\text{TEDC}_{\text{ij,conv}} * T_{total,conv} + D_{total-days,conv} * PC_{\text{total-i},conv} + CF_{\text{total-i},conv}\right) \quad (59)$$

where $T_{total,conv}$ is the total hours of operation per year (hrs.), $D_{total-days,conv}$ is the total days of voyage in a year (days), $PC_{\text{total-i},conv}$ is the port cost (124 USD/day)[221], and $FC_{\text{total-i},conv}$ is the annual fuel cost.

4.2.5.3. Net Present Value (NPV)

The net present value is the difference between the present cash inflows and outflows over a given period, at a discount rate of today's value. The cashflow comprises the investment cost, operating cost, voyage cost, and cost of revenue. Although the vessels chosen for this research have been in operation for more than a decade, we assume their respective engines will be replaced after 25 years, as a well-maintained marine engines can last for approximately 40 years [222]. Thus, the NPV for conventional vessels with a lifetime (t) of 25 years at a discount rate (r) of 5.50% [223] is determined as follows:

$$NPV_{conv} = \left(\sum_{t=1}^{25}\left(\frac{[cashflow]_t}{[1+r]^t}\right)\right) - IC_{\text{i},conv} \quad (60)$$

where $IC_{\mathrm{i},conv}$ represents the investment cost of the conventional vessel for the different marine fuels as specified in subsections 4.2.3.1 to 4.2.3.3. However, the investment cost for the fully autonomous ships ($IC_{\mathrm{i},auto}$) is expected to be 30% higher than $IC_{\mathrm{i},conv}$ due to the newly fitted advanced sensors and control systems [170].

4.3. Results

This study investigates KPIs for marine alternative fuels across both conventional and autonomous vessels, including total mass emission rate (TMER), total global warming potential (TGWP), total environmental impact (TEI), total environmental damage cost (TEDC), and net present value (NPV), as illustrated in Figure 19. The findings reveal that alternative fuels, such as H2-Ren, H2-F, and Elec, exhibit zero environmental emissions and costs during ship operations. In contrast, traditional fuels like HFO, MDO, MGO, and MeOH demonstrate the highest TMER due to their pollutant constituents and mass flow rates, with B20 and LNG showing comparatively lower emissions. To illustrate, the TMER associated with traditional fuels is significantly impacted by their constituent pollutants and mass flow rates, whereas B20 and LNG exhibit a contrasting trend across different vessel types. Additionally, HFO ranks highest in TGWP, indicating substantial contributions to global warming, while LNG and MeOH have the lowest potential, suggesting a more favorable environmental profile. Regarding TEI, B20 has the highest TEI value, primarily due to incomplete combustion and increased NOx emissions, whereas LNG shows the lowest TEI value, indicating a lesser overall environmental impact. In terms of TEDC, HFO exhibits the highest TEDC, attributable to the environmental damage caused by SOx emissions, while LNG presents the lowest TEDC, showcasing its advantages in terms of environmental costs. All proposed marine fuels demonstrate viable economic values (NPVs), with LNG achieving the highest NPV owing to its fuel efficiency, lower capital costs, and significant environmental benefits, including reduced emissions of SOx, PM, NOx, and TGWP.

Moreover, the analysis indicates that alternative marine fuels for autonomous vessels yield better environmental and economic outcomes compared to conventional vessels. This improvement is primarily due to reductions in fuel consumption, energy usage, operating costs, and the overall environmental footprint. A comparative analysis based on vessel types reveals that alternative

marine fuels for high-speed passenger ferries (HSPF) achieve lower emissions, benefiting from high operational speeds and engine efficiency. In contrast, tugboats emit more pollutants despite shorter navigation routes due to their lower operating speeds, continuous operation, and port activities. However, alternative fuels for tugboats exhibit higher NPV values than those for HSPF, a trend attributed to greater utilization rates, stable revenue streams, lower operating costs per unit of time or distance traveled and reduced initial capital investments.

In summary, the data presented in Figure 19 underscores the significant differences in environmental impact and economic viability among various marine fuels. By illustrating these KPIs, the figure serves to enhance understanding of the advantages and challenges associated with alternative fuels in the marine sector, particularly in relation to both conventional and autonomous vessels.

4.3.1. Sensitivity Analysis

In this study, a sensitivity analysis is conducted to examine the critical technical and economic input variables with respect to the NPV of alternative marine fuels for both conventional and fully autonomous vessels. The input parameters considered for the analysis include rate, fuel costs, emission costs, vessel speed, load factor, and nautical miles (or navigation distance). These input parameters are systematically adjusted within a range from −50% to +50% with increments of 10%. The outcomes of the sensitivity analyses for each vessel are depicted in Figure 20 through Figure 23. Specifically, Figure 20 illustrates the sensitivity analysis for the conventional high-speed passenger ferry (HSPF), while Figure 21 focuses on the sensitivity analysis for the fully autonomous HSPF. Figure 22 depicts the sensitivity analysis for the conventional tugboat, and finally, Figure 23 presents the sensitivity analysis for the fully autonomous tugboat. It can be inferred that the figures from the sensitivity analyses demonstrate a consistent trend.

The findings reveal that interest rate variation has the most significant impact on NPV values compared to the other five input parameters. Lowering the rate increases NPV by raising the present value of future cash flows, whereas increasing the rate decreases NPV. LNG consistently achieves the highest NPV across all vessel types while Elec and B20 exhibit the lowest NPV for conventional and fully autonomous HSPFs, respectively. Similarly, B20 has the lowest NPV for both conventional and fully autonomous tugboats.

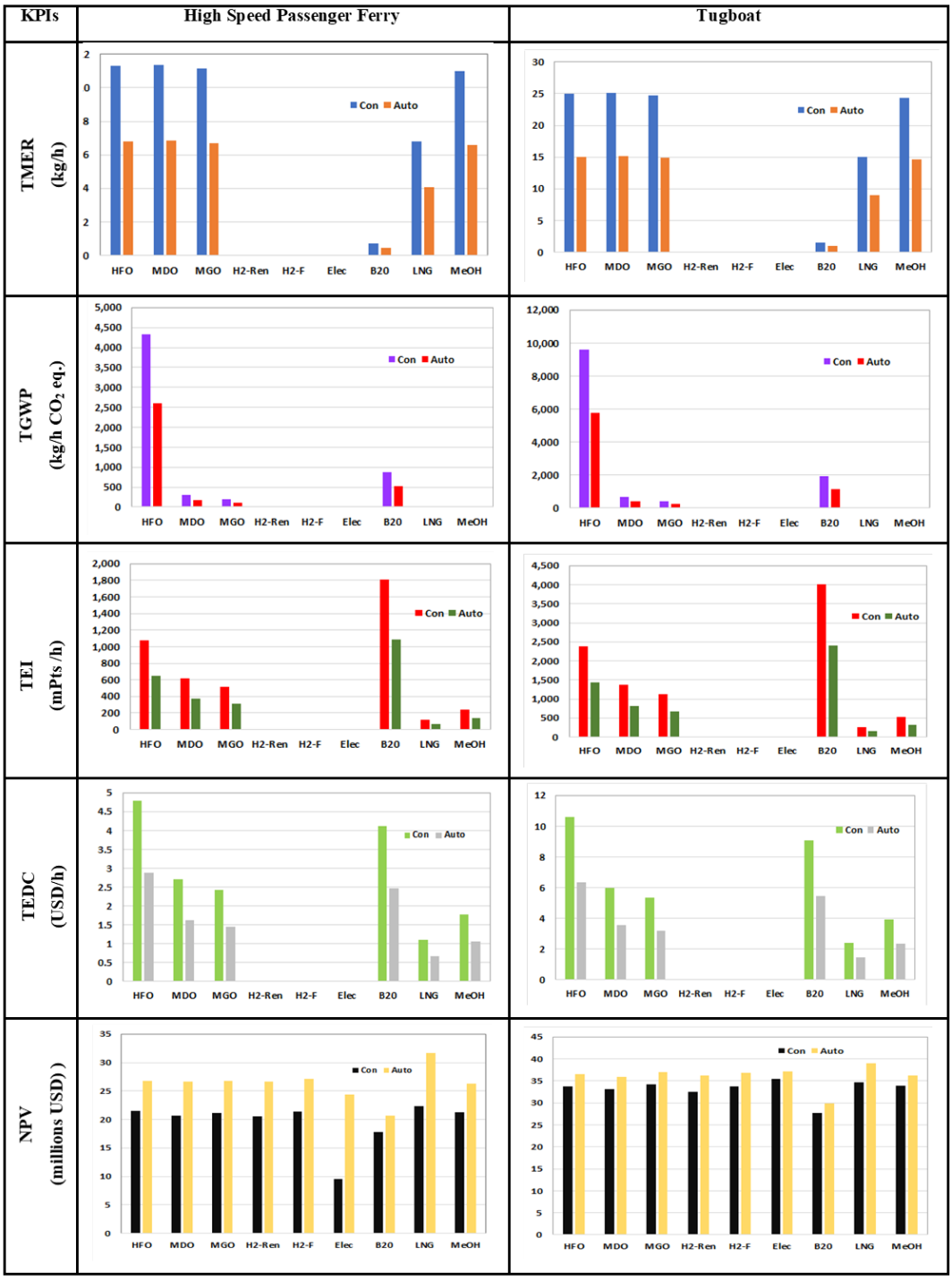

Figure 19: Results of the KPIs for the conventional and fully autonomous ships: HSPFs and tugboats

Following interest rates, load factor variation emerges as the second most critical parameter. A lower load factor results in higher NPV due to reduced operational and environmental costs per unit of distance traveled; while a higher load factor decreases NPV. Again, LNG records the highest NPV for all vessels, while Elec and B20 have the lowest NPV for conventional and fully autonomous HSPFs, respectively. Also, it shows the lowest NPV for both conventional and fully autonomous tugboats.

Fuel cost variation is the third most significant input parameter with lower NPV values. Lower fuel costs lead to higher NPV due to reduced operational expenses per unit of distance traveled, while higher fuel costs have the opposite effect. LNG maintains the highest NPV for all ships, while Elec and B20 present the lowest NPV for conventional and fully autonomous HSPFs respectively. Similarly, B20 records the lowest NPV for both conventional and fully autonomous tugboats.

Emission cost variation is the fourth most significant input parameter with low NPV values. Lower emission costs increase profitability due to reduced operational and environmental expenses, while higher emission costs have the opposite effect. LNG attains the highest NPV for all ships, while B20 records the lowest NPV.

Nautical miles variation is ranked fifth, with shorter distances leading to reduced fuel consumption, emissions, and associated costs, resulting in higher NPV values. However, longer distances have the opposite effect. LNG records the highest NPV for all ships. Elec and B20 have the lowest NPV for conventional and fully autonomous HSPFs, respectively. B20 also records the lowest NPV for both conventional and fully autonomous tugboats.

Lastly, speed variation is identified as the least significant parameter, recording the lowest NPV values among all parameters. Reducing ship speed leads to extended operational times, increased emissions, higher fuel and emission costs per unit of distance traveled, which impacts profitability and reduces NPV. Conversely, increasing ship speed results in the opposite outcome. LNG achieves the highest NPV for all ships. Elec has the lowest NPV for both conventional and fully autonomous HSPFs. Similarly, B20 records the lowest NPV for both conventional and fully autonomous tugboats.

In summary, LNG is determined to be the optimal choice for the four proposed vessels in this study. Autonomous vessels consistently achieved the best results in all scenarios, supporting the argument that implementing fully autonomous vessels would not only reduce pollutant emissions but also increase both profitability and potential revenue. Consequently, the subsequent section focuses exclusively on LNG-fueled vessels for the proposed fully autonomous HSPF and tugboat, using the same input parameters simultaneously to examine their respective impacts on NPV.

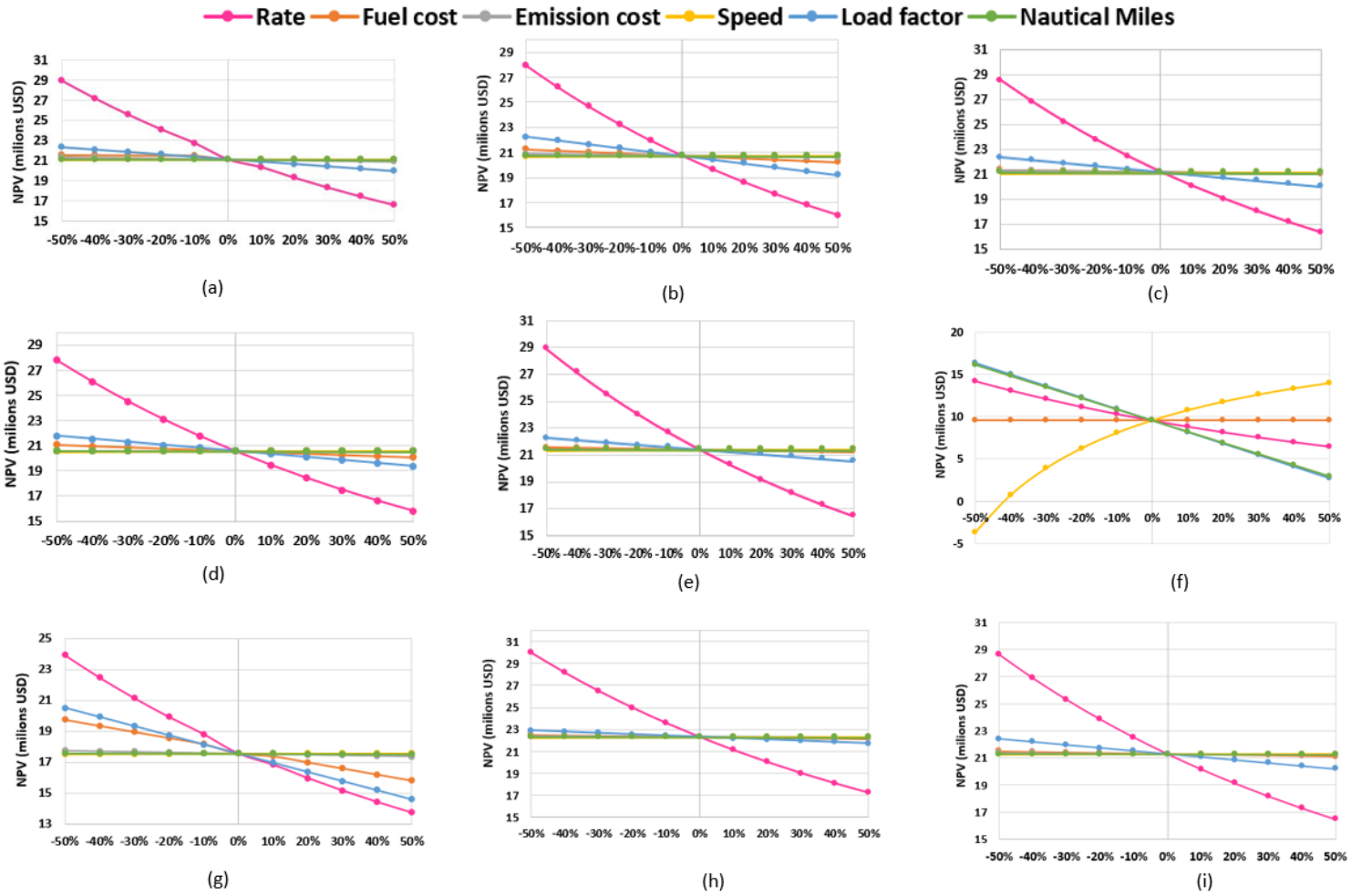

Figure 20: Sensitivity analysis for conventional HSPF: (a). HFO, (b). MDO, (c). MGO, (d). H_2 Ren, (e). H_2-F, (f). Elec (g). B20 (h). LNG (i). MeOH.

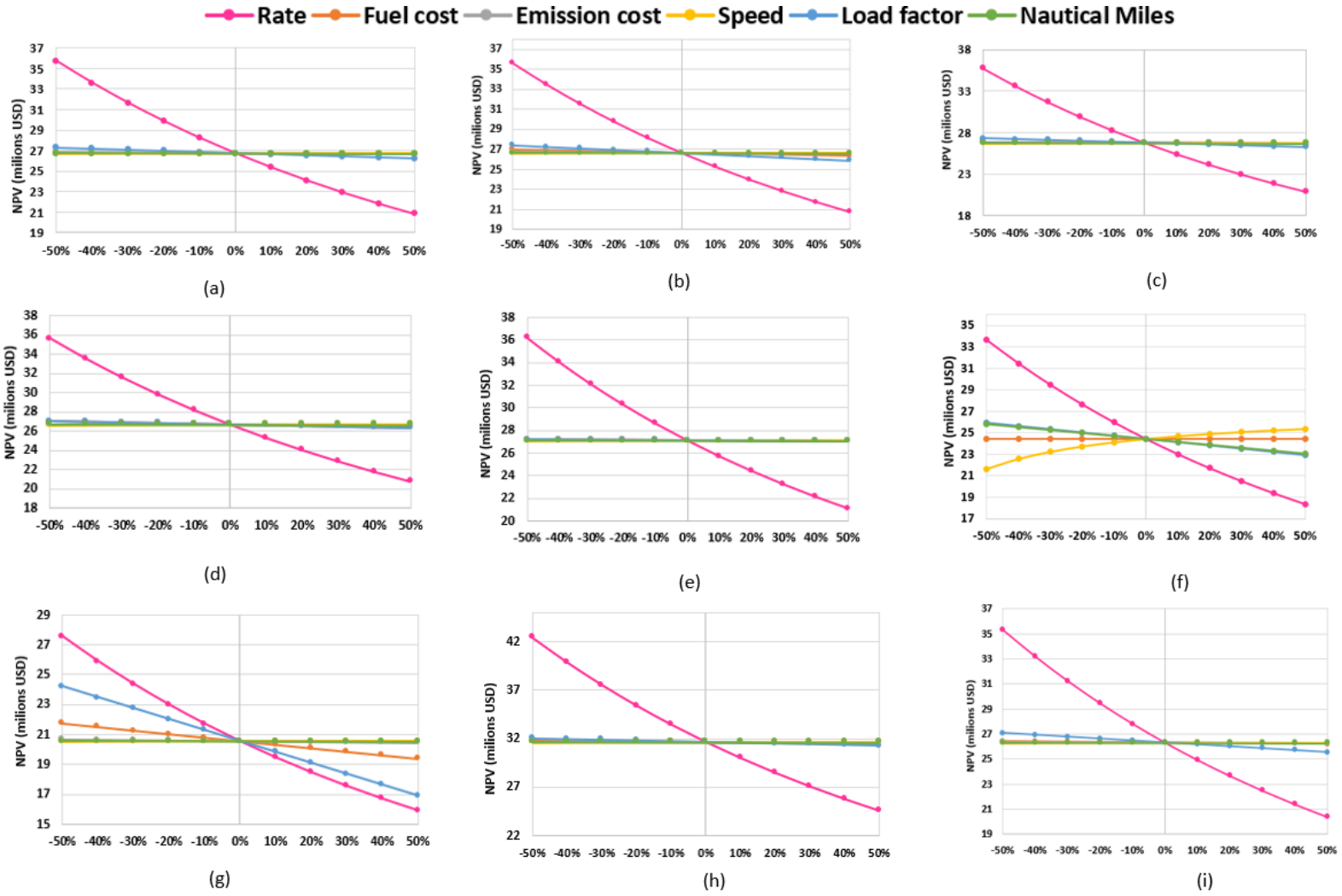

Figure 21: Sensitivity analysis for fully autonomous HSPF: (a) HFO, (b) MDO, (c) MGO, (d) H_2 Ren, (e) H_2-F, (f) Elec, (g) B20, (h) LNG, and (i) MeOH

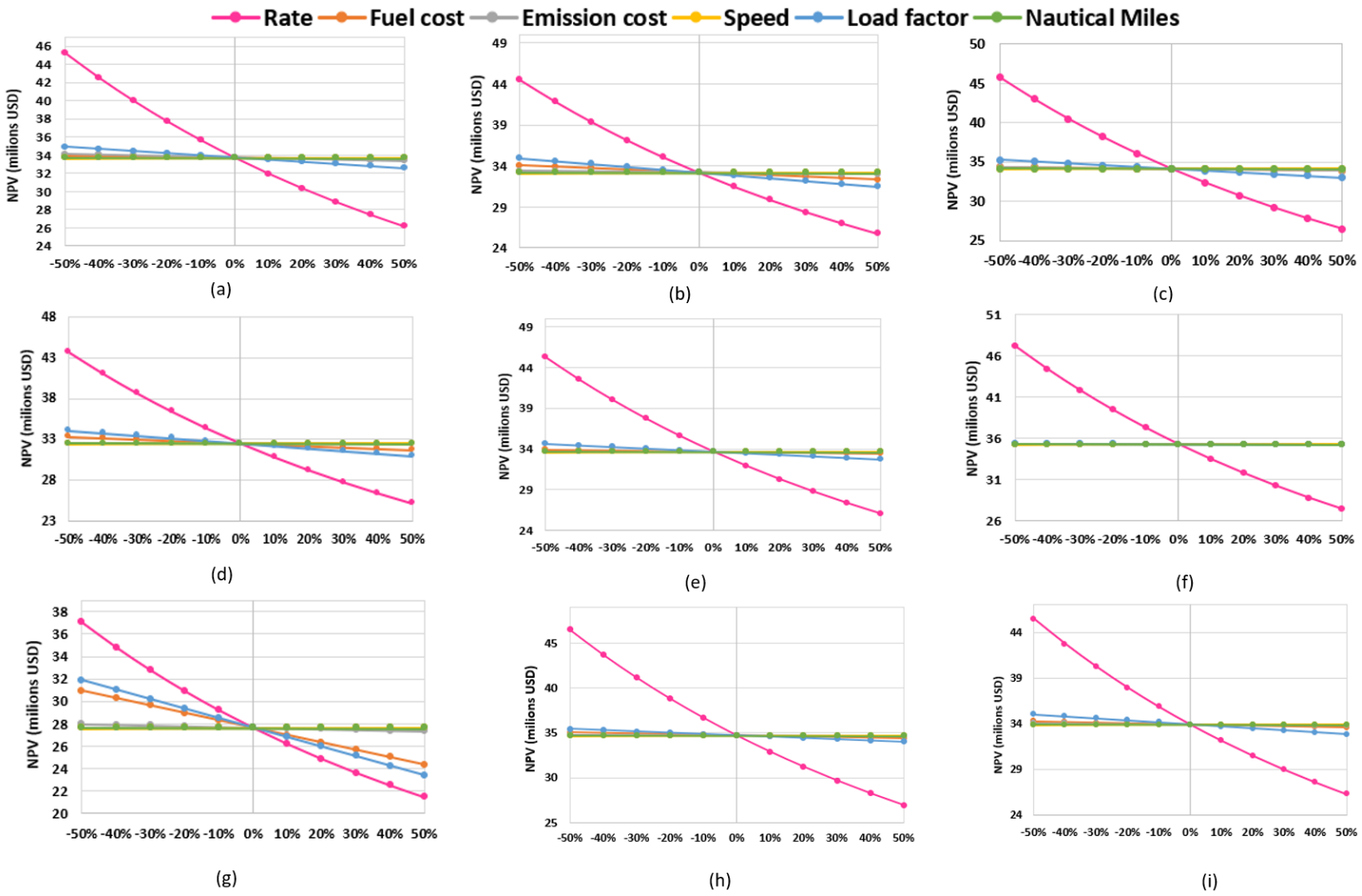

Figure 22: Sensitivity analysis for conventional tugboat: (a) HFO, (b) MDO, (c) MGO, (d) H_2 Ren, (e) H_2-F, (f) Elec, (g) B20, (h) LNG, and (i) MeOH

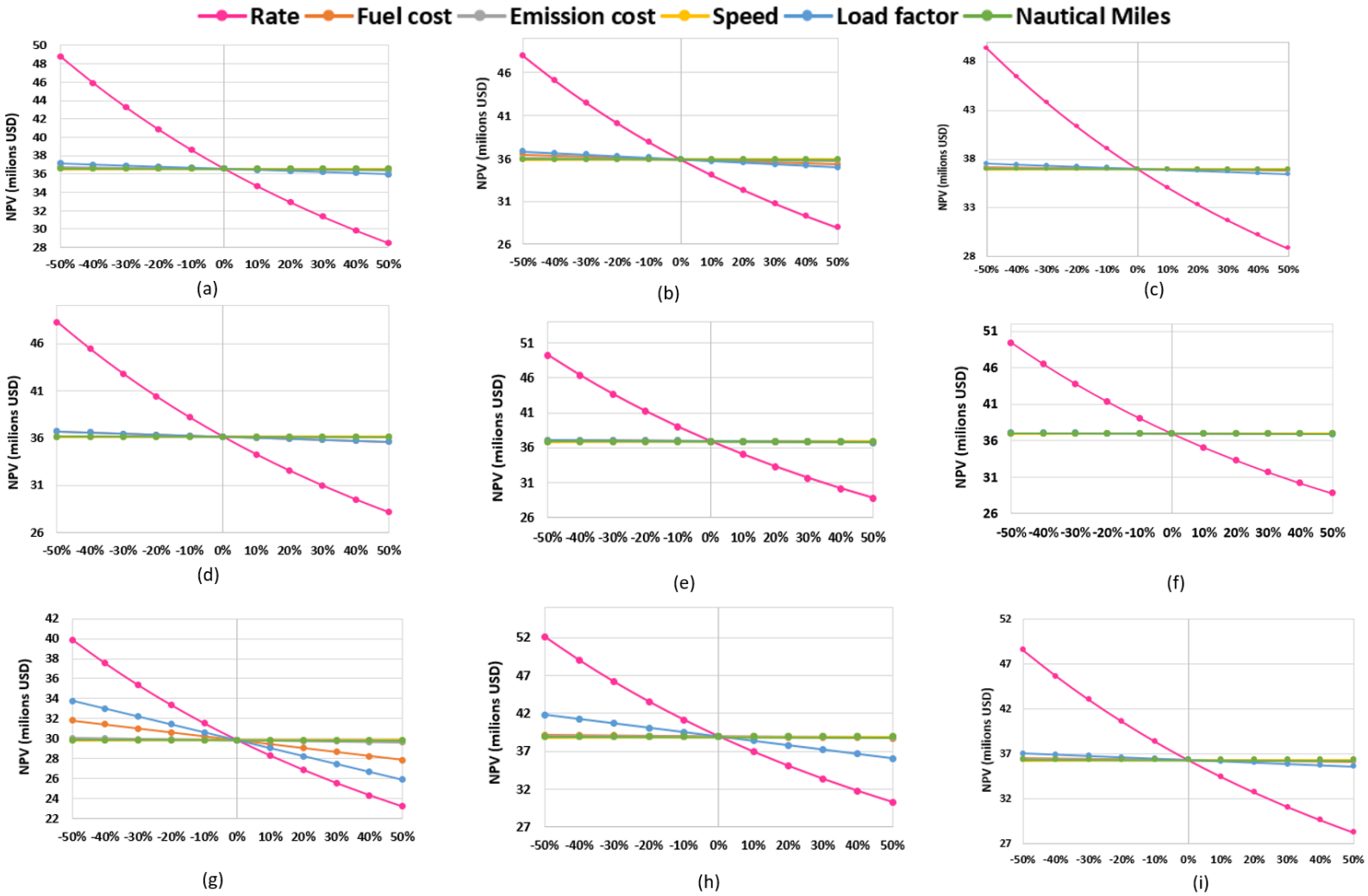

Figure 23: Sensitivity analysis for fully autonomous tugboat: (a) HFO, (b) MDO, (c) MGO, (d) H_2 Ren, (e) H_2-F, (f) Elec, (g) B20, (h) LNG, and (i) MeOH

4.3.2. Stochastic Analysis

This study employs stochastic analysis to ascertain the NPV of LNG-powered fully autonomous vessels, utilizing probability and random sampling techniques to assess performance and economic outcomes amidst uncertainty. Each input parameter is varied between a lower bound of -50% and an upper bound of +50% of its base value, with these variations applied simultaneously and uniformly across 1,000 model runs.

Figure 24 presents the results of the tornado analysis and cumulative distribution function (CDF) for both the fully autonomous HSPF and tugboat. In the tornado analysis, which ranks uncertain input parameters by their impact, the rate emerges as the most critical factor affecting NPV estimates, suggesting that improving economic rate accuracy and reducing uncertainty could enhance these estimates. The load factor follows as the next crucial parameter, highlighting the significance of efficient load factor management in controlling operational costs. Therefore, enhancing energy efficiency through optimized hull designs and advanced propulsion systems is crucial for enhancing economic performance. The emission cost ranks third, indicating significant costs associated with regulatory compliance, which can fluctuate based on changes in regulations and fuel quality, underscoring the necessity for emission reduction technologies. For the fully autonomous HSPF, speed and nautical distance are significant factors, while fuel cost has the least impact on NPV variability. In contrast, for the fully autonomous tugboat, fuel cost is significant, followed by speed and nautical distance. These findings stress the importance of strategic rate setting, energy-efficient technologies, compliance with IMO regulations, and optimized operational planning for financial success.

The stochastic analysis illustrates the range of potential financial outcomes for LNG-powered fully autonomous vessels through the CDF of the NPV. At the 5th percentile, NPV values for both vessels are zero, suggesting the possibility of no financial gain or a potential loss in worst-case scenarios, emphasizing the need for effective risk management. At the 95th percentile, NPV for the fully autonomous HSPF and tugboat is approximately 35 billion USD and 4 billion USD, respectively, indicating substantial profitability under favorable conditions. This extensive range illustrates the considerable uncertainty and variation associated with critical input parameters. These observations emphasize the necessity for meticulous management and optimization of these factors to enhance economic feasibility and address risks. The outcomes provide valuable

perspectives for guiding strategic decisions, validating investments, and ensuring compliance with regulatory and environmental objectives in the marine sector.

In brief, this stochastic analysis reveals critical insights into the net present value (NPV) of LNG-powered fully autonomous vessels, identifying interest rate, load factor, and emission costs as key determinants. The analysis underscores the potential for zero NPVs in adverse scenarios, highlighting the importance of effective risk management. Conversely, favorable conditions could yield substantial profitability, with NPVs reaching approximately 35 billion USD for high-speed passenger ferries and 4 billion USD for tugboats. These findings emphasize the need for strategic decision-making and operational optimization to ensure economic viability in the marine sector.

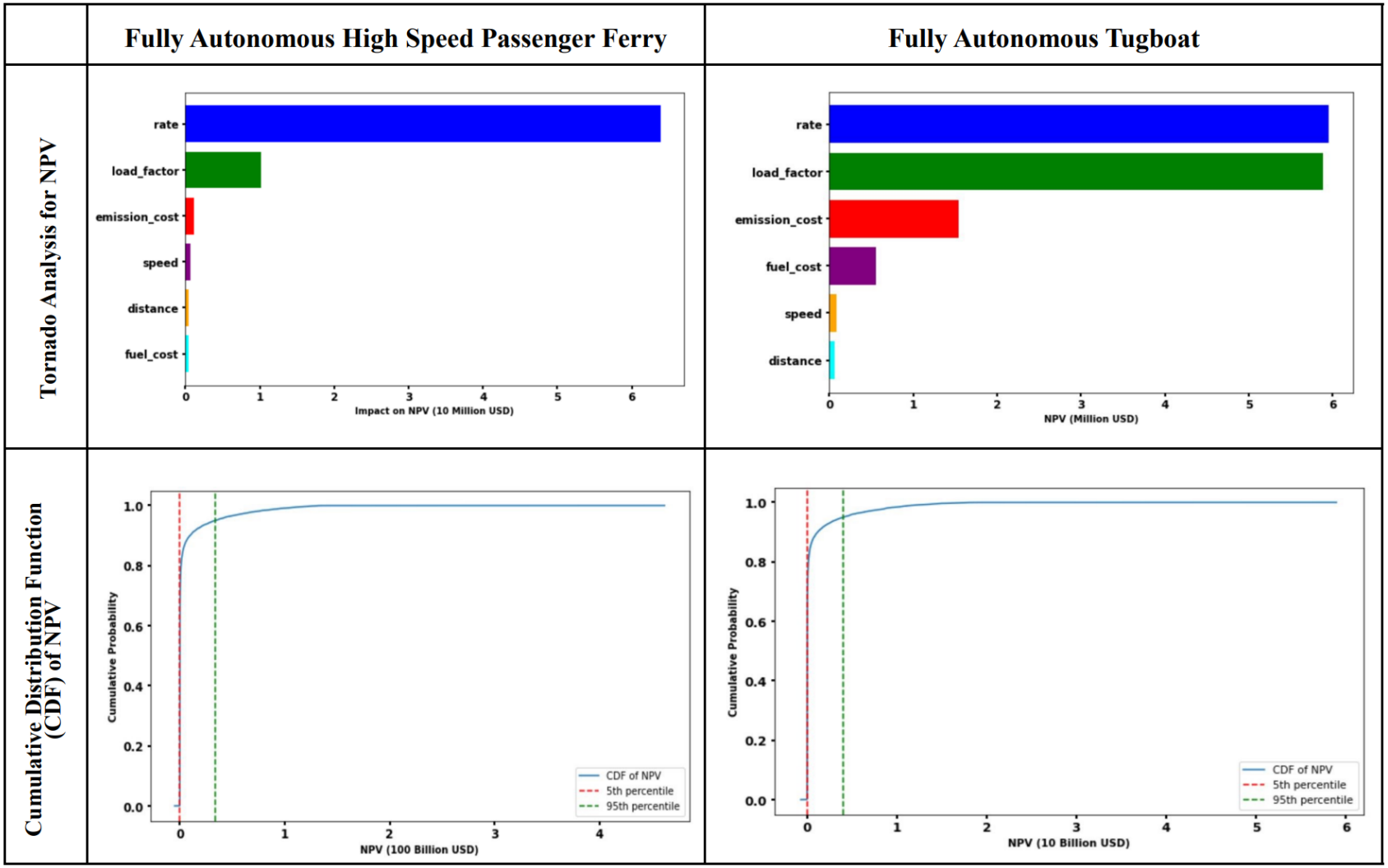

Figure 24: Result of stochastic analysis for fully autonomous HSPF and tugboat powered by LNG fuel

4.4. Discussion

The pursuit of improved energy efficiency and reduced emissions in maritime operations is increasingly vital as the industry grapples with sustainability challenges. This study enhances the understanding of alternative marine fuels by conducting a comprehensive analysis using key performance indicators (KPIs), such as total mass emission rate (TMER) and net present value (NPV). This discussion contextualizes our findings within the existing literature, highlighting the contributions and unique insights of our research.

The findings align with previous studies, such as those by Chen and Yang [137], which utilized automatic identification system (AIS) data for emission estimations. Our approach extends this methodology by integrating AIS data to evaluate both environmental and economic impacts across conventional and autonomous vessels, offering a more nuanced understanding of real-time operational dynamics. This integration addresses a noted gap in prior research that often relied on vessel-specific data, potentially limiting the applicability of findings.

Furthermore, our results corroborate the work of Aarskog et al. [138] , which highlighted the economic feasibility of fuel cell (FC) propulsion. Our study builds on this by showcasing the zero emissions of hydrogen and electric options, contrasting starkly with traditional fuels like HFO and MDO, which exhibited the highest TMER. This reinforces the necessity for adopting cleaner fuels and aligns with calls for transitioning towards sustainable maritime practices.

The analysis conducted by Jafarzadeh and Schjølberg [139] regarding optimal propulsion power utilization supports our findings on the operational efficiency of alternative fuels. Our results indicate that high-speed passenger ferries benefit significantly from alternative fuels, achieving lower emissions due to enhanced engine efficiency at operational speeds. This observation diverges from previous study that identified limited benefits in hybrid or electric integration for certain vessel types, such as ocean-going reefers, suggesting that our findings may indicate broader applicability of alternative fuels for high-speed vessels.

Moreover, our research contributes a comprehensive mathematical model for assessing environmental and economic impacts, a feature underexplored in existing literature. This model, designed specifically for selected ships, offers stakeholders a practical tool for evaluating fuel options in line with environmental policies. Our stochastic analysis further distinguishes our study,

allowing for sensitivity assessments that have not been extensively covered in prior research. This analysis reveals how variations in load factors and operating conditions significantly affect NPVs, an aspect that previous studies often overlooked.

While many studies, including those by Kouzelis et al.[140] and Kosmas and Acciaro [141], have focused on specific alternative fuels, our holistic approach enables a direct comparison of multiple fuels across various vessel types and operational profiles. This comparative analysis not only highlights the economic viability of LNG and biofuels but also underscores the necessity for adaptive regulatory measures to promote sustainable fuel use.

In conclusion, this study provides valuable insights into the environmental and economic assessments of alternative marine fuels, building on previous research while introducing innovative methodologies. By addressing the simultaneous analysis of economic feasibility and emissions for both conventional and autonomous vessels, our findings advance the discourse on sustainable shipping solutions. The comprehensive mathematical model and stochastic analysis presented here serve as critical tools for industry stakeholders, guiding decisions that align with both ecological sustainability and economic performance. As the maritime sector evolves, the adoption of alternative fuels will be essential in achieving the dual goals of reducing emissions and enhancing energy efficiency, ultimately contributing to the global commitment to sustainable development.

4.5. Conclusion

This research paper presents an effective approach aimed at reducing marine pollution and costs by determining the optimal marine alternative fuel for short-sea operating shipping vessels while maximizing energy efficiency. Utilizing mathematical models in a Python environment, analyses are conducted on both conventional and fully autonomous HSPFs and tugboats, employing bottom-up approaches, analyzing ship operating phases, and utilizing the global warming potential approach.

The study's objective is to identify the optimal marine fuel with the highest NPV and minimal emissions that aligns with IMO regulatory standards, environmental objectives, and economic uncertainties. The analysis integrates ships' AIS data, specifications, and port information to determine power, energy, and fuel consumption while incorporating parameters of proposed marine alternative fuels for environmental and cost analyses. In addition, the key performance indicators (KPIs) are investigated for marine alternative fuels across both conventional and autonomous vessels, including TMER, TGWP, TEI, TEDC, and NPV. Sensitivity analyses are conducted for each alternative fuel to validate results, and a stochastic analysis is performed on the optimal marine fuel.

The study identifies LNG fuel as the optimal choice for the proposed vessels, with autonomous vessels consistently yielding favorable results. Sensitivity analyses reveal the critical technical and economic input variables that affect NPV for both conventional and autonomous vessels. Additionally, stochastic analysis demonstrates the range of potential financial outcomes for LNG-powered fully autonomous vessels.

Despite significant constraints due to data limitations, the study underscores the importance of conducting further research to assess the techno-economic impacts and emissions effects of fully autonomous vessels across different navigation routes. Overall, the findings emphasize the need for meticulous management and optimization of critical input parameters to enhance economic feasibility and address risks, providing valuable insights for decision-making, justifying investments, and ensuring regulatory compliance in the marine sector.

CHAPTER 5. MODELING OF ENERGY MANAGEMENT SYSTEM FOR FULLY AUTONOMOUS VESSELS WITH HYBRID RENEWABLE ENERGY SYSTEMS USING NONLINEAR MODEL PREDICTIVE CONTROL VIA GREY WOLF OPTIMIZATION ALGORITHM

In this chapter, we present a multi-objective predictive energy management system (EMS) for optimizing hybrid renewable energy systems (HRES) in autonomous marine vessels. The objective is to minimize fuel consumption and emissions while maximizing renewable energy usage and pure-electric sailing durations. The EMS combines nonlinear model predictive control (NMPC) with metaheuristic optimizers—Grey Wolf Optimization (GWO) and Genetic Algorithm (GA)—and is benchmarked against a conventional rule-based (RB) method. The HRES architecture comprises photovoltaic arrays, vertical-axis wind turbines (VAWTs), diesel engines, generators, and a battery storage system. A ship dynamics model was used to represent propulsion power under realistic sea conditions. Simulations were conducted using real-world operational and environmental datasets, with state prediction enhanced by an Extended Kalman Filter (EKF). Performance is evaluated using marine-relevant indicators—fuel consumption, emissions, battery state of charge (SOC), and emission cost—and validated using standard regression metrics. The NMPC-GWO algorithm consistently outperformed both NMPC-GA and RB approaches, achieving high prediction accuracy and greater energy efficiency. These results confirm the reliability and optimization capability of predictive EMS frameworks in reducing emissions and operational cost in autonomous maritime operations

This chapter is based on the following publication*: H. Laryea and A. Schiffauerova, "Modeling of energy management system for fully autonomous vessels with hybrid renewable energy systems using nonlinear model predictive control via grey wolf optimization algorithm,"* J. Mar. Sci. Eng.*, vol. 13, no. 7, p. 1293, 2025. [Online]. Available: https://doi.org/10.3390/jmse13071293*

5.1. Introduction

Marine shipping represents the most energy-efficient mode of freight transportation, serving as the backbone of global trade. It is responsible for transporting 80 % of the world's goods by volume and over 70% by value. Although not the largest consumer, the maritime sector remains heavily dependent on fossil fuels [224], [225].The maritime industry—including container ships, bulk carriers, cruise liners, ferries, tankers and tugboats—has an estimated annual fuel consumption of approximately 330 million metric tons (87 billion gallons), surpassing the world's annual jet fuel consumption of 220 million metric tons (1.4 billion barrels). With the anticipated growth in global trade, the overall demand for marine fuels is projected to double by 2030 [226]. While the shipping industry is one of the lowest contributors to carbon dioxide (CO_2) emissions relative to other transportation modes, it accounts for approximately 3% of global greenhouse gas (GHG) emissions, with CO_2 comprising the vast majority of these emissions [227]. According to recent IRENA projections, under a Business-As-Usual' scenario, if current trends continue, marine CO_2 emissions could reach approximately 0.92 Gt per year by 2050—representing a nearly 65% increase from 2018 levels [228].

The International Maritime Organization (IMO) is actively implementing a global cap on marine fuels to mitigate emissions from the shipping sector. Thus the 2023 IMO strategy aims for zero or near-zero greenhouse gas (GHG) emission technologies and fuels to constitute at least 5%, with a target of 10%, of the energy used in international shipping by 2030 [11].This has led to increased interest in enhancing fuel efficiency and reducing the environmental impact of marine vessels. Utilizing high-efficiency power sources, such as fuel cells, along with renewable energy sources (RES) like wind and solar energy, offers promising solutions [76], [77], [229]. Moreover, the advent of maritime autonomous surface ships (MASS) positively influences environmental performance. In fully autonomous fleets the absence of onboard crew reduces energy consumption and pollution. [230], [231]. For instance, a fully autonomous container vessel can achieve a 74.5% reduction in energy usage compared to conventional vessels, primarily due to the removal of crew facilities. While such savings are specific to container ships, the example illustrates the broader potential of autonomous operation to improve energy efficiency in marine applications. Consequently, integrating autonomous MASS with renewable energy sources represents a viable strategy for decreasing GHG emissions in the maritime sector [48], [232]. Furthermore, the IMO's

Interim MASS Code represents a goal-based, non-mandatory regulatory framework developed to support the safe design and operation of Maritime Autonomous Surface Ships (MASS). At MSC 105–108, IMO Member States advanced its development and approved a roadmap to finalize and adopt the non-mandatory MASS Code by mid-2025 [233], transitioning to a mandatory code by 2030 with expected entry into force by 1 January 2032 [234], [235]. In parallel, the Facilitation Committee (FAL 48) scheduled an assessment of the finalized Code in Spring 2025, including considerations for updating the FAL Convention [236]. The inclusion of the MASS Code in this study aligns the energy and propulsion strategy with internationally recognized standards for autonomous vessel operation.

The optimal operation of hybrid renewable energy sources (HRES) within the shipboard power system (SPS) of fully autonomous vessels can enhance efficiency and reduce emissions during operations. For instance, the *Mayflower Autonomous Ship*—a fully autonomous, unmanned research vessel—features a state-of-the-art hybrid propulsion system integrating solar photovoltaic panels, wind-assist technology, and auxiliary diesel generators, demonstrating reduced reliance on fossil fuels and lower emissions during transatlantic trials [237], [238]. While specific performance data remain limited, such configurations illustrate the growing potential of HRES integration in reducing the environmental footprint of autonomous marine operations. However, challenges arise when integrating diverse energy sources, including complex power flow conditions, environmental conditions, and the need for coordination among multiple energy resources. A reliable integrated energy system is essential for improving fuel efficiency, reducing overall costs, and ensuring environmental sustainability, which underscores the necessity of an effective power management system (PMS) [229]. Measures to enhance energy efficiency on vessels include power and energy management, vessel performance optimization [239], [240], and power system reconfiguration [241]. The current strategies for the PMS and energy management systems (EMS) are generally categorized into rule-based (RB) and optimization-based approaches [242]-[244].These classifications have been widely adopted in the automotive industry, particularly for hybrid electric vehicles [244], or in land-based applications. A comprehensive comparison of the advantages and disadvantages of these strategies is provided by Inal et al. [70] and Peng et al. [245]. Rule-based (RB) methods, on one hand, depend on human expertise, predefined strategies, and established priorities [246]-[248]. These methods are easier to implement, exhibit lower computational complexity, and are well-suited for real-time applications. In contrast, optimization-based

approaches, such as model predictive control (MPC) [7], [249]-[252], Pontryagin's minimum principle, equivalent consumption minimization strategy (ECMS) [253]-[255], dynamic programming (DP) [256], [257], optimal control theory, and mixed-integer optimization [258], focus on real-time optimization. Additionally, various machine learning (ML) techniques [244], [259]-[261] have been employed in energy management systems. However, ML algorithms require extensive validation and training to ensure their real-time performance can be reliably maintained.

The existing literature predominantly focuses on optimizing energy management systems for standalone hybrid generation systems aboard ships, primarily involving marine diesel engines, diesel generators, and energy storage. RB and ECMS have been extensively studied as effective methods for online implementation in hybrid propulsion and ship power distribution [248], [255]. To illustrate, Roslan et al. [248] applied the RB method to analyze an LNG hybrid tugboat system across four configurations: fixed speed, variable speed, and with or without a battery bank. The results indicate that the LNG-battery hybrid configuration is optimal, offering significant reductions in CO_2 emissions, daily fuel costs, and improved energy efficiency compared to the other configurations. Similarly, Chan et al. [255] implemented an intelligent power management strategy to optimize real-time power distribution between the generator sets and batteries, aiming to reduce fuel consumption and emissions while meeting load requirements for the tugboat. The results demonstrated that the ECMS method achieved up to 18% fuel savings over the RB approach, assuming constant battery efficiency. Nevertheless, most recent and advanced works use predictive control for the power-split problem, and power plant performance. The MPC is a more effective method for EMS strategies due to its ability to simultaneously handle multivariable control and state with apparent real-time optimization effects [7], [239], [262]-[264]. For example, Haseltalab et. al. [239] proposed a multi-level model predictive control approach for DC-PPS, enabling effective power generation and stability control in constant power-loaded microgrids. Also, Haseltalab et. al. [7], applied an MPC-based predictive energy management (PEM) system for a hybrid autonomous tugboat, optimizing the energy split between onboard sources to enhance fuel efficiency and performance. This approach accounts for environmental disturbances during missions, improving the operation of all-electric autonomous vessels. Similarly, Haseltalab et. al [262], used MPC for the control of a diesel-generator-rectifier set and voltage stabilization in a DC Power and Propulsion Systems (DC-PPS). The control strategy is capable of handling sudden changes in load conditions as well as adverse effects of constant power loads (CPL). Furthermore,

some authors propose joint optimization algorithms [263], [264], to analyze EMS for the ships. To illustrate, Wang et al. [263], implemented MPC-PSO for dynamic optimization of ship energy efficiency, using a rolling optimization strategy to determine optimal sailing speeds based on real-time environmental factors. The method effectively enhances energy efficiency and reduces CO_2 emissions for the cruise ship under varying weather conditions. Similarly, Xie et al. [264], designed a power management system (PMS) for Shipboard Power Systems (SPS) using MPC - ECMS to handle high-frequency propulsion loads from sea wave conditions, efficiently distributing power between diesel generators and hybrid energy storage systems (HESSs) to minimize fuel consumption for an electrical ship. Whereas the MPC is widely recognized and demonstrates predictable performance, adaptive model predictive control (AMPC) offers greater flexibility and adaptability to real-time changes in system dynamics, resulting in improved performance in uncertain or time-varying conditions [265], [266]. For example, Hou et al. [265] used integrated power generation, electric motors, and hybrid energy storage control using AMPC to estimate and predict propulsion load torque across various sea states, improving system efficiency, enhancing reliability, and reducing mechanical wear. Similarly, Hou et al. [266] applied AMPC on both simulations and experiments to optimize power distribution between the battery and ultra capacitor (UC), aiming to mitigate load fluctuations and enhance system efficiency and reliability. Although, both MPC and AMPC algorithms are suitable for HRES, nonlinear MPC (NMPC) is considered optimal for standalone HRES under variable load and environmental conditions [250], [258], [267]. This is due to its ability to provide more accurate control without relying on linear approximations or model adjustments, in contrast to traditional MPC and AMPC. For example, Chen et al. [250], developed an energy management strategy to optimize ship energy use and torque distribution between the internal combustion engine and motor in random waves for a tugboat, while balancing fuel consumption and carbon emissions under reference operating conditions. The NMPC strategy outperforms the genetic algorithm (GA) and DP, effectively achieving energy conservation and emission reduction goals. Similarly, Planakis et al. [258] implemented an NMPC-based predictive energy management system to optimize fuel consumption and nitrogen oxides (NOx) emissions for parallel hybrid diesel-electric propulsion plants onboard a tugboat. The system calculates power-split, estimates propeller load, and predicts operator input, achieving reductions in both fuel consumption and NOx emissions. Whereas NMPC can address the complex challenges associated with hybrid ship power systems, it is often

hindered by limited solution accuracy and low computational efficiency. As result, Chen et al. [267] design an NMPC energy management strategy for a tugboat using a hybrid algorithm combining chaotic and grey wolf optimization (GWO) to optimize energy distribution. The results demonstrate that the chaotic grey wolf optimization (CGWO)-based NMPC outperforms other algorithms in real-time performance, fuel consumption, carbon emissions, and engine load path.

Although the existing literature offers valuable insights into optimizing power splits for EMS, there are areas requiring further improvement, particularly in fuel consumption and emissions analysis. Several studies [248], [255], [265], [268] overlook ship dynamics, which may result in inaccurate and inefficient outcomes, undermining both operational efficiency and sustainability. Additionally, while some authors [248], [250], [255], [267], [269] analyze emissions from proposed EMS, they focus only on CO_2 or NOx, neglecting other pollutants such as carbon monoxides (CO), nitrous oxide (N_2O), sulfur oxides (SOx), methane (CH_4), and particulate matter (PM). This narrow focus leads to incomplete environmental assessments, missed opportunities for emission reductions, and potential regulatory non-compliance. Furthermore, only a few studies [248], [263] incorporate the energy efficiency operational indicator (EEOI) into their models. Notably, Haseltalab et al. [7] did not determine the EEOI for the autonomous tugboat, which is required by IMO regulations to ensure energy efficiency and reduce CO_2 emissions for a new ship. Lastly, while several authors [263], [264], [267] use joint algorithms to optimize EMS for HRES, only two authors [263] [264] performed sensitivity analysis. Without this, the predictive energy management system may suffer from inaccurate predictions, poor risk assessment, and failure to handle uncertainty, thereby limiting its reliability and effectiveness. Table 22 presents a synthesis of relevant EMS studies for hybrid-powered vessels, emphasizing key methodological omissions such as the exclusion of real-time environmental factors, non-CO_2 emissions, and sensitivity analysis—regardless of ship type or application.

Although substantial research has been conducted on the optimal configurations of hybrid energy storage systems (HESS) and hybrid energy sources (HES) in microgrid systems, significant gaps remain in the literature. While significant research has been conducted on EMS optimization for conventional and hybrid ships, studies focused specifically on fully autonomous vessels—particularly autonomous tugboats—remain scarce. Although the number of operational autonomous tugboats has surpassed 200 globally [270], indicating growing technological uptake,

many are still in developmental or trial stages. Consequently, this review draws on related work from both conventional and semi-autonomous vessels to inform the development of predictive EMS frameworks tailored to the unique operational and design challenges of fully autonomous ships. In particular, the integration of hybrid renewable energy systems (HRES) into the power systems of autonomous ships has not been thoroughly investigated. Furthermore, there is a lack of comprehensive decision-making models for energy management systems (EMS) in HRES, whether applied to conventional or autonomous vessels. This study introduces a novel integrated multi-energy supply system for autonomous ships, leveraging the combined potential of photovoltaic (PV) arrays, vertical axis wind turbines (VAWT), battery banks, diesel engines, and diesel generators to ensure reliable electrical power, meeting both propulsion and onboard shipload demands. Specifically, the paper develops a mathematical model for VAWT power generation, accounting for the relative wind velocity along the ship's navigation route. Additionally, a more accurate method is proposed for calculating power generation from onboard PV arrays, considering the vessel's sailing path. This approach incorporates reliable technologies from land-based and other transportation sectors to address the unique energy management needs of autonomous ships. Moreover, the study factors in ship dynamics, including frictional resistance, form resistance, wave resistance, wind resistance, and current resistance. Wind resistance, for example, takes into account the relative wind velocity to the vessel speed, wind direction, and ship course, while current resistance considers the current velocity relative to the vessel speed, sideslip angle, and course angle. To overcome these challenges, the study prioritizes standalone HRES and utilizes objective functions, predictive models, and metaheuristic algorithms to optimize the EMS for the HRES model. For a hybrid renewable fully autonomous tugboat's EMS with nonlinear dynamics and varying environmental conditions along navigation routes, the extended Kalman filter (EKF) is employed for predictive offline control, ensuring accuracy in nonlinear state estimation with high computational efficiency, ideal for real-time applications. The primary objective is to identify the optimal EMS, ensuring efficient power-splitting across the HRES while meeting load demands with minimal fuel consumption, mass emission rate (MER), emission cost and energy efficiency operational indicator (EEOI) within predefined operational constraints.

This study addresses a clear gap in the current literature on energy management systems (EMS) for shipboard hybrid renewable energy systems (HRES), especially in the context of autonomous tugboats. As summarized in Table 1, while several studies have investigated EMS optimization

for various vessel types—including tugboats [248], [250], [251], [255], [261], and autonomous vessels [7]—the majority either neglect ship hydrodynamics, environmental variability, or full-spectrum emission profiling. For instance, studies such as [248], [250], [255], [261] focus narrowly on CO_2 or NO_x emissions, omitting other regulated pollutants like SO_x, CH_4, PM, and N_2O. Ship dynamics—such as wave, wind, and current resistance—are either excluded or oversimplified, as seen in [239], [251], [255], [262], [263], despite their significance in propulsion load estimation. Furthermore, only a few works [49], [264] conduct sensitivity analyses, and even these are limited to a narrow set of parameters (for example, sailing speed or load). Notably, even the only study explicitly involving an autonomous tugboat [7] excludes wind and sea current effects and lacks emission or sensitivity analysis. These critical omissions hinder the robustness, adaptability, and compliance potential of proposed EMS frameworks.

This research makes a significant contribution to the existing body of literature by introducing the first known predictive, multi-objective EMS tailored to HRES-equipped autonomous vessels. To the best of our knowledge, no prior study has implemented a predictive, tri-objective EMS that integrates real-time environmental inputs, nonlinear ship dynamics, and regulatory constraints specifically for HRES-powered autonomous vessels. This study seeks to bridge that gap.

Unlike previous studies that primarily focus on minimizing fuel consumption, this approach aims to balance fuel consumption, renewable energy generation, and pure-electric sail time per day trip. The study also incorporates ship dynamics and scenarios characterized by uncertainty, considering factors such as total load fluctuations, ship speed, towing force, ambient temperature, wind speed, and solar irradiance along sailing routes—aspects often overlooked in prior research. Furthermore, the study advances energy management and design optimization strategies by introducing multi-objective algorithms that account for power distribution, fuel consumption, and environmental impact. In contrast to previous work, which typically relies on one or two algorithms for HES, this study employs HRES predictive-metaheuristic algorithms (NMPC- GWO, and NMPC- GA) and the RB method for optimizing energy management strategies, assuming a prior knowledge of the operating profile. Additionally, the rule-based approach integrates port regulatory requirements for operations. Finally, the performance of the tri-objective optimal design is validated through sensitivity analysis offering a comprehensive and innovative contribution to the field.

The remaining sections of the paper are structured as follows: Section 5.2 outlines the materials and methods for simulating and optimizing the HRES on an autonomous tugboat, Section 5.3 presents the results and discussion, and Section 5.4 concludes with remarks and suggestions for future research.

Table 22: Overview of energy management system (EMS) approaches in ship applications.

Ref.	Objective	Vessel type	Energy sources	Algorithms	Remarks
[239]	To ensure system stability by maintaining the DC voltage and diesel-generator shaft speed at their nominal values.	Unspecified	Diesel engine, battery	MPC	Emission analysis and sensitivity analysis were not conducted, and ship dynamics were not considered.
[248]	Evaluate the performance of an LNG-hybrid system under four distinct configurations.	Tugboat	LNG, Battery	RB	Only CO_2 emissions were calculated in the study. Ship dynamics were excluded, live data were not used, and sensitivity analysis was not performed.
[249]	To achieve comprehensive performance in mitigating load effects under varying sea states.	Cargo ship	Ultra Capacitor - battery, battery-flywheel.	AMPC	Performance comparisons were conducted for different cases across the two sea states, without sensitivity analysis.
[250]	To design an optimal energy management system for parallel hybrid power ships.	Tugboat	Diesel engine-battery	NMPC, DP, GA.	The algorithms' RMSE and computing time were compared, excluding sensitivity analysis, other pollutants, and sea currents
[251]	To minimized energy consumption and carbon emissions from ships.	Tugboat	Diesel engine-battery	NMPC-CGWO, NMPC-SQP NMPC-GA NMPC-GA-SQP	The model excludes sea currents, other pollutants, and robustness analyses.

Ref.	Objective	Vessel type	Energy sources	Algorithms	Remarks

[7]	To ensure efficient power availability, reduce trajectory tracking error, and improve fuel efficiency	Autonomous Tugboat	Diesel engine, battery	MPC, RB, PEM.	3D ship dynamics were considered, though wind and sea currents were excluded. Additionally, emission analysis and sensitivity analysis were not performed on the model.
[255]	To develop an intelligent power management strategy to ensure optimal power allocation in the system	Tugboat	Diesel engine, battery	RB, ECMS	Emission analysis was limited to CO_2, with ship dynamics and sensitivity analysis excluded from the study.
[261]	To design an optimal EMS for a hybrid ship propulsion plant.	Tugboat	Diesel engine, battery	NMPC, DP	Mathematical modeling and experiments are conducted, excluding sea currents, with only NOx emissions considered.
[262]	To control of a diesel-generator-rectifier set and achieve voltage stabilization in a DC-PPS.	Unspecified	Diesel engine, battery	MPC	A tube-based technique is used to enhance the algorithm's robustness. Ship dynamics, emission analysis, and sensitivity analysis were not considered in the simulation.
[263]	To optimize ship energy efficiency, accounting for time-varying environmental factors.	Cruise Ship	Diesel engine	MPC- PSO, DO, QSO, SO.	Sea currents were excluded, with only CO_2 emissions assessed and other pollutants not considered. Sensitivity analysis focused on variable sailing time and route.
[264]	To optimize real-time power-split between hybrid energy sources while minimizing fuel consumption.	Electrical Ship	Diesel engine, Ultra Capacitor, battery	MPC-ECMS	Sensitivity analysis was conducted based on variable ship speed, with sea currents not considered and emission analysis not performed.
[266]	To optimally split power, address constraints, and achieve the desired dynamic responses.	Cargo ship	Ultra Capacitor-battery	AMPC	Analysis was conducted at sea states 2 and 4, with sensitivity analysis on load power, voltages, and module numbers; emission analysis and sea currents were not considered.

***DO**: Dynamic optimization, **QSO**: Quasi-static optimization, **SO**: Static optimization*

5.2. Materials and Methods

The propulsion system of a fully autonomous tugboat comprises key components such as the main diesel engines, propellers, propeller shaft, motor, and gearbox, while the power supply for the vessel is sourced from a combination of renewable energy systems, batteries, diesel engines, and diesel generators. The primary focus is to develop mathematical models that accurately capture the physical characteristics of each of these components.

The HRES model for the vessel integrates various factors, including the vessel's specific characteristics, ship logs, port data, Automatic Identification System (AIS) data, technical specifications of the energy sources, and environmental conditions encountered along the navigation route.

The analysis flowchart is presented in Figure 25. All computational tasks are performed using Python 3.11.6, with the code incorporating simulation and optimization, as well as sensitivity to the variability of key input parameters. These key input variables—such as ship speed, wind speed, ambient temperature, solar irradiance, towing force, and ship load—were selected based on both engineering relevance and statistical analysis. The full dataset was collected over a 12 months period from a single tugboat operating in the Port of Los Angeles and its environs, encompassing approximately 520 voyages. However, due to variability in data quality and the need for temporal alignment across multiple sources, a representative subset was extracted for modeling. Specifically, a typical round-trip daily profile was selected for simulation, based on operational consistency and completeness of both environmental and vessel-specific parameters. Prior to modeling, the full dataset was preprocessed to remove outliers and synchronize the time series. Pearson correlation analysis was applied to assess the statistical significance of each input variable relative to model outputs such as propulsion load, fuel consumption, and emissions. Multicollinearity was further evaluated using the Variance Inflation Factor (VIF). Variables with a VIF exceeding a standard threshold were flagged for removal or transformation to reduce redundancy. Based on the combined statistical findings and engineering relevance, only variables that demonstrated both high correlation with output variables and low multicollinearity were retained for the simulation model and sensitivity analysis.

The energy management system (EMS) for the hybrid renewable energy system (HRES) employs a hybrid optimization framework that integrates Nonlinear Model Predictive Control (NMPC) with both GWO and GA, while also benchmarking their performance against a conventional RB method. This hybrid strategy is designed to predict and optimize the offline power distribution, fuel consumption, and environmental impact of the vessel under varying mission conditions. The NMPC framework operates over a finite prediction horizon to compute optimal energy allocation strategies across four independent power sources: marine diesel engines, Gensets, photovoltaic (PV) arrays, and vertical-axis wind turbines (VAWTs) —as well as a battery energy storage system (BESS), which operates bidirectionally to store excess energy or supply power during peak demands. Each energy source is mathematically modeled in a Python-based simulation environment, incorporating its dynamic behavior, efficiency, and operational constraints.

The optimization problem minimizes a multi-objective cost function that includes fuel consumption, emission cost, energy efficiency operational indicator (EEOI), and power tracking error, subject to practical constraints such as engine RPM, battery state-of-charge (SOC) bounds, VAWT operating power limits, and other system constraints. The ultimate objective is to enhance overall energy efficiency, reduce pollutant emissions, minimize emission-related costs, increase renewable energy utilization, and ensure compliance with physical and regulatory constraints as defined by IMO and MARPOL standards.

In addition, the energy management system for the HRES utilizes a hybrid optimization strategy combining NMPC with GA, and GWO while also benchmarking their performance against the RB method. This approach aims to predict and optimize the offline power distribution, fuel consumption, and environmental impact under different conditions. The goal is to enhance energy efficiency, minimize emissions and their cost, improve EEOI, maximize the use of renewable energy, and ensure compliance with both physical and operational constraints. The analysis flowchart is presented in Figure 25. All computational tasks are performed using Python 3.11.6, with the code incorporating simulation and optimization, as well as sensitivity to assess how variability in key input parameters—such as ship speed, wind speed, ambient temperature, solar irradiance, towing force, and ship load—affects the power distribution, fuel consumption, mass emission rate (MER), emission cost and energy efficiency operational indicator (EEOI). In addition, the dynamic equations governing the vessel and its HRES, along with the algorithms and

the overall mathematical model for the fully autonomous tugboat, are comprehensively explained in the following subsections.

5.2.1. Ship Dynamics

Marine vessels exhibit six degrees of freedom in their motion, encompassing translational movements in the horizontal plane (surge, sway, yaw) and rotational motions (roll, pitch, heave), as illustrated in Figure 26. For the purposes of this study, a one- degree-of-freedom (1-DOF) ship dynamic model is sufficient to analyze the hybrid renewable energy system (HRES) within the integrated energy and propulsion system framework of marine engineering.

Therefore, the 1-DOF ship dynamic equation governing the forward surge motion of the vessel incorporates external and based on Newton's second law can be expressed as follows [271]:

$$M_R * \dot{v_s}(t) = F_{hyd}(t) - R_{env}(t) + F_{tow}(t) \tag{61}$$

$$\Longrightarrow \frac{dV_s(t)}{dt} = \frac{1}{M_R}\left[\left(F_{prop}(t) - R_{resistance}(t)\right) - R_{env}(t) + F_{tow}(t)\right]$$

$$= \frac{1}{M_R}\left[F_{prop}(t) - R_{total}(t) + F_{tow}(t)\right]$$

where M_R denotes the mass of the rigid body which contains the mass of tugboat and added mass (kg), $V_s(t)$ is the surge velocity of the ship or vessel speed (knots or m/s), $\dot{v}_s(t)$ is the acceleration of the ship (m/s^2), $F_{hyd}(t)$ is the hydrodynamic force acting along surge direction (N), and $R_{env}(t)$is the environmental forces (N), $F_{prop}(t)$ is the propulsive force (N), $R_{resistance}(t)$ is the resistance force (N), $R_{total}(t)$ is the sum of the R_{env} and $R_{resistance}$(N), $F_{tow}(t)$ is the towing force (N) exerted by tugboat or bollard pull during tug operations (N) . In addition, the sub-section 5.2.2 elucidates the external forces depicted on the left-hand side of Equation (61).

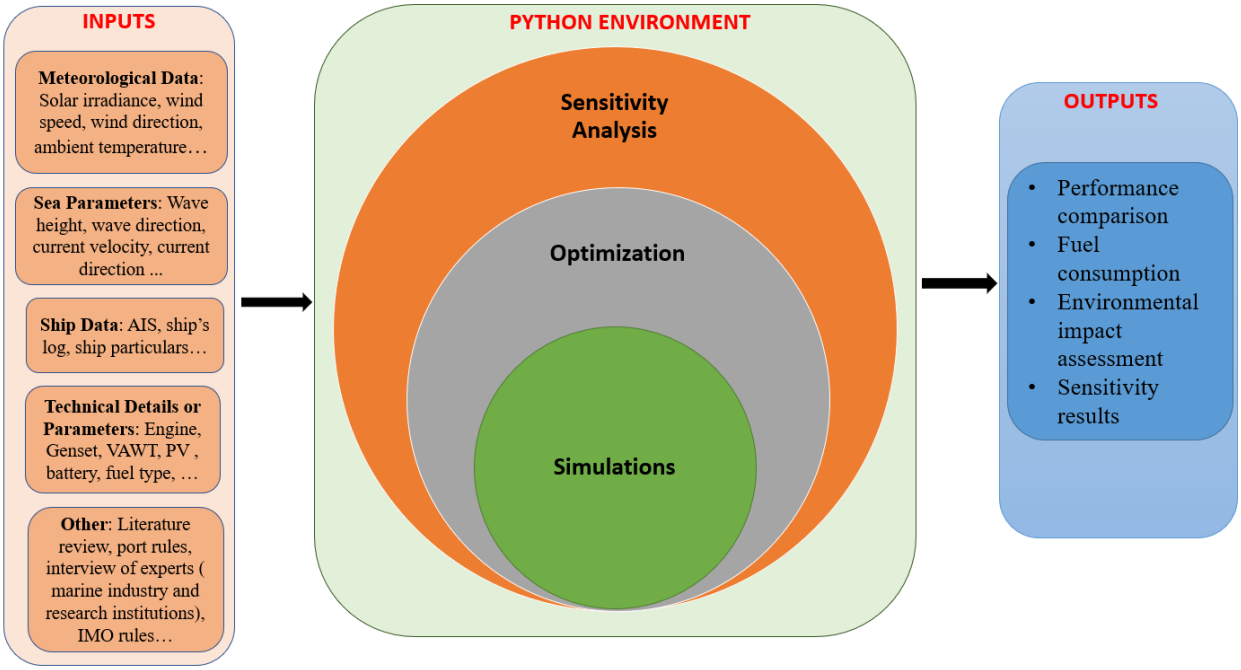

Figure 25: Schematic diagram of methodology for HRES assessment in a fully autonomous ship

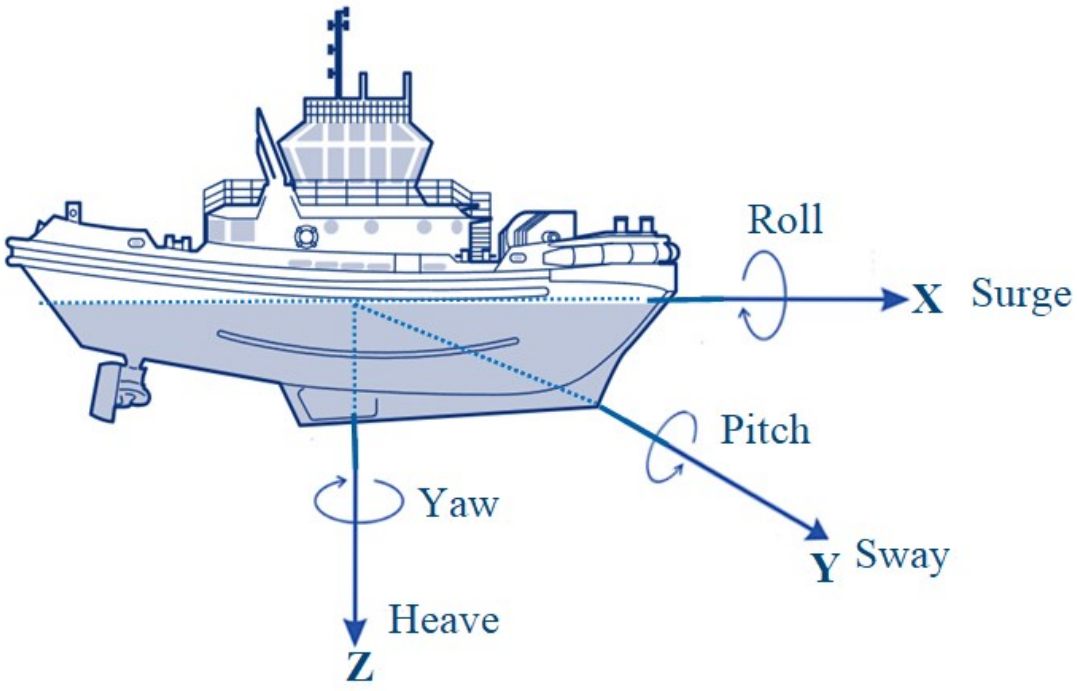

Figure 26: Ship dynamic motion and degrees of freedom (DOF).

5.2.2. Ship Resistances

The hydrodynamic resistance forces ($R_{resistance}$), which act in opposition to the vessel's forward motion, encompass various elements: frictional resistance force (R_{fric}), originating from the drag between the tugboat's hull surface and the water; and form resistance force (R_{form}) , which arises from the interaction of the tugboat's hull shape and profile with the water [272], [273]. The equation for the $R_{resistance}$ can be expressed as:

$$R_{resistance}(t) = R_{fric}(t) + R_{form}(t) = 0.5\,\rho_w V_s(t)^2\,(C_f\ A_{ws} + C_{form}\,A_{cs}) \quad (62)$$

where ρ_w is the density sea water (kg/m^3), C_f is frictional coefficient which ranges from 0.002 to 0.004 (smooth-hulled vessels) and from 0.004 to 0.006 (moderate surface roughness) [273], [274], A_{ws} is the wetted surface area of the vessel (m^2), C_{form} is form resistance coefficient, typical for vessel designed primarily for maneuverability at lower speeds rather than high speed, generally falls within the range of 0.8 to 1.2 [273], [274], A_{cs} is the cross-sectional or frontal area of the vessel (m^2).

This necessitates that the fully autonomous tugboat must produce adequate towing force to counteract the hydrodynamic resistance of both itself and the towed vessel, ensuring optimal towing performance.

Lastly, the environmental forces (R_{env}), which encompass external forces acting on the vessel from its surrounding natural environment contribute to the total resistance. These forces include random wave forces (R_{wave}) affecting the hull, current forces ($R_{current}$) influencing the vessel's hull and appendages due to water currents, and wind forces (R_{wind}) involving the interaction between the ship and external sea waves, thereby impacting the superstructure components above the waterline [272], [273]. The exerted environmental forces ($R_{env}(t)$) is expressed as follows [53], [275]:

$$R_{env}(t) = R_{wave}(t) + R_{wind}(t) + R_{current}(t)$$

$$R_{wave}(t) = \frac{1}{2}\,\rho_w g H(t)_{sw}^2 \left(\frac{2\pi}{T_m(t)}\right)^2 S(f_m(t))$$

(63)

$$R_{wind}(t) = \frac{1}{2}\,\rho_a V(t)_{rw}^2\, C_{wi} A_{wi}$$
$$= \frac{1}{2}\,\rho_a [V_s(t) - V_{wi}(t) cos(\beta_{wi}(t) - \psi(t))]^2 C_{wi} A_{wi}$$

$$R_{current}(t) = \frac{1}{2}\,\rho_w\, V(t)_{c,ship}^2 C_{d,curr} A_c$$
$$= \frac{1}{2}\,\rho_w\, (V_c(t)\, cos(\beta_c(t) - \psi(t)) - V_s(t))^2 C_{d,curr} A_c$$

where g is the acceleration due to gravity(m/s2), $H_{sw}(t)$ is the significant wave height (m), $T_m(t)$ is the mean wave period between the successive wave crest in a wave train (s), $S(f_m(t))$ is the spectral density of wave energy at frequency $f_m(t)$ in the JONSWAP spectrum [271], [276] , ρ_a is the density of air (kg/m^3), $V_{rw}(t)$ is the velocity of the wind relative to the vessel speed (m/s), C_{wi} is the drag coefficient of wind, and Awi is the reference area of the tugboat exposed to the wind (m^2), V_{wi} (t) is the wind velocity (m/s), $\beta_{wi}(t)$ is the wind direction (degrees), ψ(t) is the ship's course (degrees), $V_{c,ship}$ (t) is the velocity of sea or water current relative to the vessel (m/s), $Cd,curr$ is the drag coefficient of the vessel with respect to currents, Ac is the reference or cross section area of the tugboat exposed to the current force (m^2), V_c (t) is the current velocity along x-axis (m/s), and β_c (t) is the sea current direction (degrees).

5.2.3. Modeling of Propeller

The propeller hydrodynamic forces (F_{prop}) produced by the propeller's interaction with the water contributes to the propulsive force. The propeller hydrodynamic forces can be expressed as [277], [278]:

$$F_{prop}(t) = T_{prop}(t)(1 - T_{dc}) * N_{prop}(t) \quad (64)$$

where $T_{prop}(t)$denotes the propeller thrust (N), $N_{prop}(t)$ denotes the number of propellers (unitless), and T_{dc} is the thrust deduction coefficient (unitless) which is estimated using empirical relation, and this is expressed as follows [279]:

$$T_{dc} = 0.21593 + 0.099768 * C_b - \frac{D_{prop}}{\sqrt{B_{ship} * d_{ship}}} \quad (65)$$

where C_b is the block coefficient which is approximately 0.53 [280], D_{prop} is the propeller diameter (m), B_{ship} is the breadth of the ship (m), and d_{ship} denotes the draft of the ship (m). For ships equipped with a single propeller, the T_{dc} typically ranges from 0.12 to 0.30 [281].

The propeller component takes as input the rotational speed of the propeller ($n_{prop}(t)$) and the ship's speed ($V_s(t)$), which are provided by the engine shaft and ship components, respectively. Thus, the propeller inflow velocity in the presence of wake $V_{wp}(t)$ and propeller inflow velocity without interference $V_{hy}(t)$ are expressed as:

$$V_{wp}(t) = V_s(t)[1 - \omega(t)]] \quad (66)$$

$$V_{hy}(t) = \sqrt{V_{wp}(t)^2 + (0.7\pi D_{prop} n_{prop}(t))^2}$$

where $\omega(t)$ is the wake fraction coefficient (unitless) which can be determined from an empirical formula based on Taylor's model as $\omega(t) = -0.05 + 0.5 * C_b$. However, for ships equipped with a single propeller, the $\omega(t)$ typically ranges from 0.20 to 0.45 [281], [282].

The output of the propeller includes the torque ($T_{prop}(t)$), which is transmitted to the engine shaft component, and the propeller thrust ($Q_{prop}(t)$), which is delivered to the ship component. The propeller thrust and torque when considering open-water can be expressed as [277], [278]:

$$
\begin{aligned}
T_{prop}(t) &= K_T(J)\,\rho_w {D_{prop}}^4 {n_{prop}(t)}^2 \\
Q_{prop}(t) &= K_Q(J)\,\rho_w {D_{prop}}^5 {n_{prop}(t)}^2 \\
K_T(J) &= \beta_1 - \beta_2 J(t) \\
K_Q(J) &= \gamma_1 - \gamma_2 J(t) \\
J(t) &= \frac{V_{wp}(t)}{n_{prop}(t) D_{prop}} = \frac{V_s(t)[1-\omega(t)]]}{n_{prop}(t) D_{prop}} \\
\eta_o(t) &= \frac{J(t) K_T(J)}{2\pi K_Q(J)}
\end{aligned}
\tag{67}
$$

where $K_T(J)$ is thrust coefficient, J(t) is the advance coefficient, ρ_w is the density of sea or water (kg/m^3) D_{prop} is the propeller diameter (m), $K_Q(J)$ is the torque coefficient, $V_{wp}(t)$ is the water speed at the propeller or speed of advance (m/s) , $\omega(t)$ is the wake fraction, and n_{prop} is the propeller rotational velocity (rad/s), and $\eta_o(t)$ is the open-water propeller efficiency. The four coefficients $(\beta_1, \beta_1, \gamma_1, \gamma_2)$ for the propeller thrust and torque are illustrated in Figure 27, and likewise, the power consumed by the propeller,$P_{prop}(t)$) is given by $\frac{2\pi n_{prop}(t) Q_{prop}(t)}{\eta_o(t)}$.

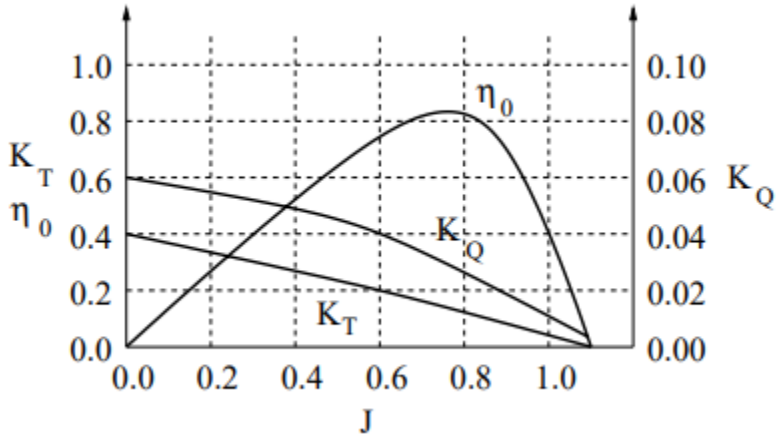

Figure 27: Thrust and torque coefficient for open-water propeller [278].

5.2.4. Modeling of Gearbox

The gearbox, which is connected between the motor and propeller, optimizes the power transmission from the motor to the propeller by balancing both the torque and rotational speed for effective and efficient ship movement at a certain gearbox reduction ratio λ_{gear}. The equation of gearbox in relation to the motor and propulsion torque is expressed as follows:

$$Q_{motor}(t) = \frac{Q_{prop}(t)}{\left(\frac{\eta_{gear}}{\lambda_{gear}}\right)} = Q_{prop}(t) * \left(\frac{\eta_{gear}}{\lambda_{gear}}\right) \tag{68}$$

$$\omega_{motor}(t) = 2 * \pi * \lambda_{gear} * n_{prop}(t)$$

where $\mathrm{Q_{motor}(t)}$ is the motor torque (Nm), η_{gear} denotes the gear efficiency, and $\omega_{motor}(\mathrm{t})$ is the angular velocity of the motor (rad/s). Furthermore, the gearbox, propeller shaft, and propeller are subjected to the load side torque (or resistance torque) $Q_{load}(t)$, which must be overcome by the engine to propel the ship. The governing equations for the propulsion system's shafting components are given as follows [261]:

$$Q_{load}(t) = \frac{Q_{prop,act}(t)}{\lambda_{gear}\,\eta_{shaft}}$$

$$Q_{prop,act}(t) = \frac{Q_{prop}(t)}{\eta_R} \tag{69}$$

$$\omega_{engine}(t) = \lambda_{gear} * \omega_{\mathrm{prop}}(\mathrm{t})$$

where $Q_{prop,act}(t)$ is the actual propeller torque, η_{shaft} is the mechanical efficiency of the shaft, η_R is the relative rotative efficiency (on ships with a single propeller it typically ranges from 1.0 to 1.07, while for two propellers it is approximately 0.98 [281]), and $\omega_{\mathrm{engine}}(\mathrm{t})$, $\omega_{\mathrm{prop}}(\mathrm{t})$, are the angular velocities of the engine and propeller (rad/s) respectively.

5.2.5. Modeling of Motor

The motor forms the core of the propulsion system in converting energy into mechanical power to drive the propeller shaft. The motor is modeled in relation to the engine's angular velocity using the simple Willian's equation as follows:

$$\begin{aligned} \omega_{engine}(t) * Q_{motor}(t) &= e * P_{motor}(t) - P_0 \\ Q_{motor}(t) &= \mathrm{f_{motor}} * \mathrm{C_{motor}} \end{aligned} \tag{70}$$

where $P_{motor}(t)$ is the motor electrical power (kW), the coefficients e and P_0 are the Willan's constants associated with power conversion efficiency and are valued at 0.9598 kW/Nm and 358.18 kW, respectively [261], C_{motor} is the torque command as a percentage of the maximum torque fed to the drive or torque distribution ratio of the motor , and f_{motor} is the unit conversion factor or torque coefficient constant for the motor.

5.2.6. Rotational Dynamic Interaction with Propeller, Motor and Engine

During tugboat operations, the hull, propeller, and engine interact along the surge direction. Also, the wave-induced forces drive the hull's surge motion, impacting the propeller's efficiency and thrust, while the engine adjusts its power output to compensate. This rotational dynamic interaction, essential for maintaining consistent propulsion and stability in a fluctuating wave environment, is modeled using the following equation:

$$J_{total} \frac{d\omega_{engine}(t)}{dt} = Q_{engine}(t) + Q_{motor}(t) - Q_{load}(t) \tag{71}$$

where $\mathrm{J_{total}}$ is the total moment of inertia of the system, which consists of the moment of the propeller, gear, added mass, engine, motor, and propeller shaft (kg·m²), $\frac{\mathrm{d}\omega_{engine}(t)}{\mathrm{dt}}$ is the engine angular acceleration (rad/s²), and $\mathrm{Q_{engine}(t)}$ is the engine delivered torque at the shaft or engine brake torque output (Nm).

5.2.7. Modeling of the Power Distribution System

The power distribution system is illustrated in Figure 28. On the DC bus's left side, power generation components include two diesel engines, two synchronous generators (SGs), additional diesel generators (Gensets), photovoltaic (PV) arrays, two vertical axis wind turbines (VAWTs), a battery bank, and shore power. On the right side of the DC bus, the energy consumption includes the propulsion system (motor, propeller shaft, thrusters, and propeller) and the ship's electrical loads (auxiliary systems and hotel services). To ensure optimal efficiency of the vessel, the fully autonomous tugboat dynamically alternates between renewable energy sources, the battery bank, and Gensets to supply the ship load, while the propulsion load demands are fulfilled by the marine diesel engines and the battery bank. Additionally, the battery bank is recharged through the utilization of the Gensets and surplus green energy.

Furthermore, the SGs are connected to rectifiers for AC/DC conversion to the DC link, while diesel generators use AC/DC converters to stabilize the DC output. In addition, the PV arrays and VAWTs connect to dedicated DC/DC converters for efficient power delivery. Similarly, the battery bank employs a bidirectional converter for charging, discharging, shore power connection, and to support the integration with renewable energy sources. The DC power distribution system, or the DC hub, is preferred for its stability, reduced weight of components, cost-effectiveness, and environmental benefits compared to AC systems [283], [284], [285]. This paper focuses on the primary power generation sources and energy consumption within the power generation system, omitting other electrical connectors.

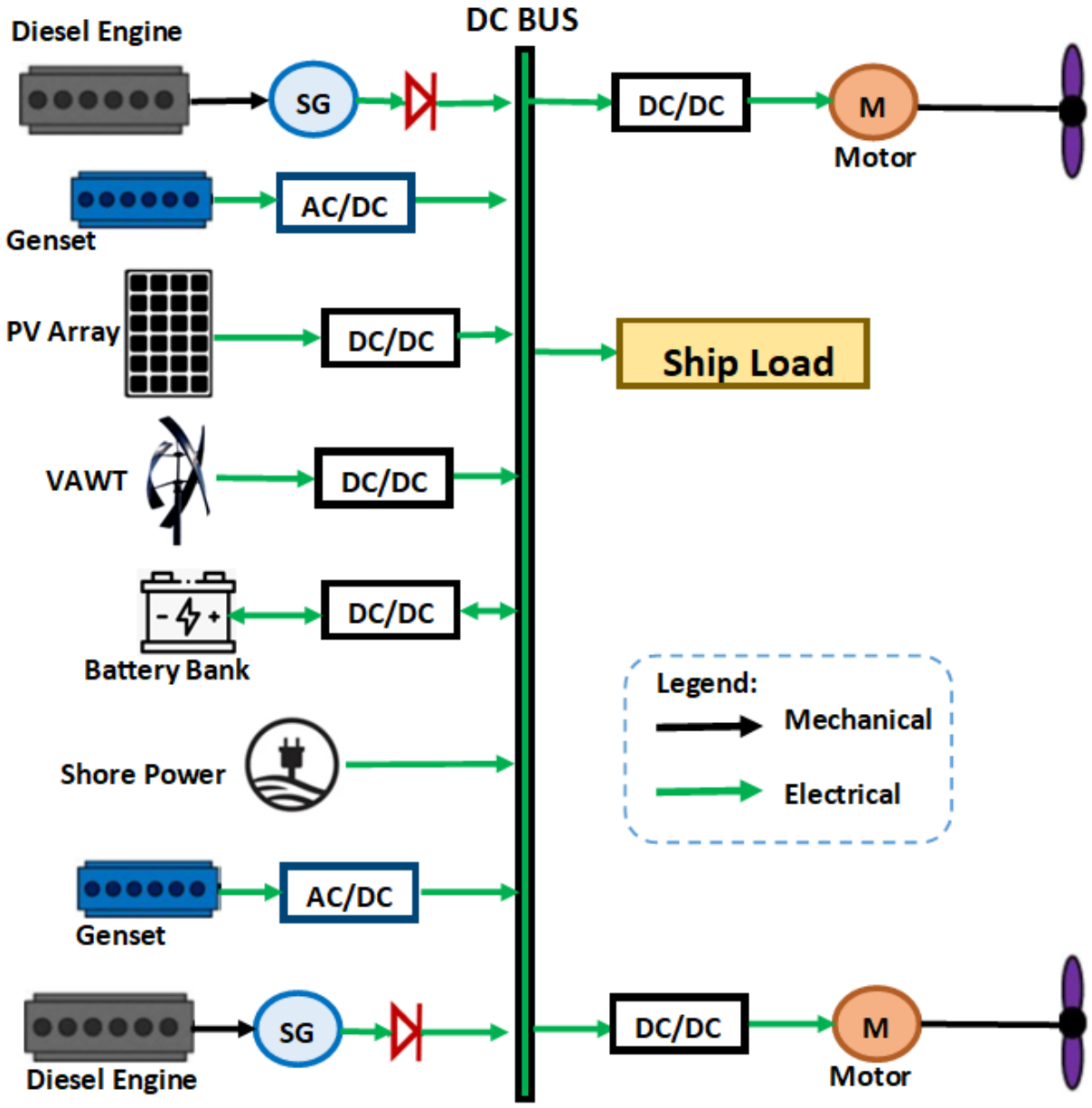

Figure 28: Simplified schematic of the hybrid renewable energy power distribution system for the fully autonomous tugboat.

5.2.7.1. Diesel Engine Model

The diesel engine acts as the primary source of mechanical power for propulsion. The rotational motion produced by the diesel engine is transferred to the propeller shaft, which then drives the propeller, enabling the vessel to move through the water. The diesel engine model is derived based on the engine's operating points along the lug curve and its power rating from the technical operating profile. Therefore, the mechanical output power of the engine $\mathrm{P_{engine}(t)}$ in conjunction with engine torque can be expressed as follows:

$$P_{engine,mech}(t) = s_{engine}(t) * N_{engine}(t) * Q_{engine}(t) * \omega_{engine}(t)$$
$$Q_{engine}(t) = C_1 * C_{engine} + C_2 * RPM_{engine}^2 + C_3 * RPM_{engine} + C_4 \quad (72)$$

where $s_{engine}(\mathrm{t})$ is the binary number for engine switch status using 1 (ON) and 0 (OFF), and $\mathrm{N_{engine}}$ is the number of engines in operation, $\mathrm{RPM_{engine}}$ is the engine rotational shaft speed (rpm), which equal to $\frac{60*\omega_{engine}(t)}{2\pi}$, C_{engine} is the engine torque command (%), and $\mathrm{C_1}$, $\mathrm{C_2}$, $\mathrm{C_3}$, and $\mathrm{C_4}$ are the coefficients determined from a dynamometer test or engine simulation.

Likewise, the quadratic relation between the diesel engine mass flow rate of the total fuel consumption $\mathrm{\dot{m}_{engine}}$ (kg/min) and the mechanical power output under variable speed operations can be approximated as follows:

$$\dot{m}_{engine}\ (t) = 4 * 10^{-4} P_{engine}^2(t) - 0.3502 P_{engine}(t) + 111.92 \quad (73)$$

In addition, the synchronous generator transforms mechanical energy derived from the diesel engine into electrical energy. The interconnection between the generator and the diesel engine occurs via the propeller shaft, where the torque produced by the diesel engine $Q_{engine}(t)$ serves as an input to the synchronous generator. Therefore, electrical output power for engine $\mathrm{P_{engine,mech}(t)}$and synchronous generator efficiency $\eta_{SG}(t)$ based on empirical data are expressed as follows:

$$P_{engine,elec}(t) = P_{engine,mech}(t) * \eta_{SG}(t) \quad (74)$$

5.2.7.2. Marine Diesel Generator Model

The marine diesel generator (or Genset) is used to supply the ship's onboard electrical load. In addition, the Genest is used to charge batteries and provide power as an emergency back up during power failures. The total diesel Genest output power $\mathrm{P_{genset}(t)}$ [48] can be expressed as follows:

$$P_{genset,mech}(t) = P_{genset,nom} * \eta_{brake} * N_{Genset} * \eta_{genset} \quad (75)$$

where $P_{genset,\mathrm{nom}}$ denotes the nominal power (kW), η_{brake} is the brake thermal efficiency, while $\mathrm{N_{Genset}}$, and $\mathrm{\eta_{genset}}$ are number of Gensets (unitless), and Gensets efficiency (%). In addition, the mass flow rate of the total fuel consumption $\mathrm{\dot{m}_{Genset}}$ is determined using the linear least-squares method, ensuring optimal alignment with the Gensets data by minimizing the overall deviation between the observed and predicted values. This approach guarantees accurate fuel consumption predictions across a range of Genset power outputs. The equation to determine the $\dot{m}_{genset}(t)$, (kg/min) is as follows:

$$\dot{m}_{genset}(t) = 0.005\, P_{genset,mech}(t) + 0.1095 \quad (76)$$

where $P_{genset,\mathrm{nom}}$ denotes the nominal power (kW), η_{brake} is the brake thermal efficiency, $\mathrm{N_{Genset}}$, and $\mathrm{\eta_{genset}}$ is the Gensets efficiency (%). In addition, and mass flow rate of the total fuel consumption $\mathrm{\dot{m}_{Genset}}$ is determined using the linear least-squares method, ensuring optimal alignment with the Gensets data by minimizing the overall deviation between the observed and predicted values. This approach guarantees accurate fuel consumption predictions across a range of Genset power outputs. The equation to determine the $\dot{m}_{genset}(t)$, kg/min. is as follows:

5.2.7.3. Photovoltaic Modules (PV) Model

The photovoltaic modules are to be installed on the starboard and port sides of the vessel. The daily solar energy output from the PV cells under standard testing conditions (STC) is described as follows [48]:

$$P_{PV}(t) = P_{PV,nom} * N_{PV,modules} * \eta_{wire,eff} * \eta_{PV-cell,eff} * \frac{I_{amb}(t)}{I_{STC}} * \left[1 - \lambda_{PV,temp} * \left\{T_{amb}(t) + I_{amb}(t) * \left(\frac{NOCT - 20}{I_{PV,cell}}\right) - T_{PV,STC}\right\}\right] \quad (77)$$

where $P_{PV}(t)$ is the total power generated by the PV panels at time t [kWh], $P_{PV,nom}$ is the nominal or rating power of the PV cells (kW), $N_{PV,modules}$ is the number of PV panels (unitless), $\eta_{PV-cell,eff}$ is the efficiency of the PV panel (%), $\eta_{wire,eff}$ denotes the efficiency of the wire [%], $I_{amb}(t)$ is the ambient radiation intensity at time t (kW/m^2), I_{STC} is the radiation intensity at the standard test conditions [1 kW/m^2], $\lambda_{PV,temp}$ is the temperature coefficient of the PV modules (% / °C), T_{amb} is the ambient temperature at the study area (°C), $NOCT$ is the nominal operating cell temperature (°C), $I_{PV,cell}$ is the radiation intensity on cell surface (0.8 kW/m^2), and $T_{PV,STC}$ is the PV cell nominal temperature at the standard test conditions (25°C).

5.2.7.4. Vertical Axis Wind Turbines (VAWT) Model

Vertical Axis Wind Turbines (VAWTs) are selected for this study due to their quieter operation, ease of maintenance, capability to generate power at low cut-in speeds, and suitability for close clustering. Energy output is influenced by the VAWT's hub height, local wind speed, and ship speed. This research proposes the installation of two VAWTs: one on the starboard mast and the other on the port mast. Each VAWT is fitted with a permanent magnet synchronous generator that converts the mechanical energy from the rotating blades into electrical power. Using the wind power law profile, the VAWT speed at the turbine height $V_{VAWT,hub}$ can be expressed as [48]:

$$V_{VAWT,hub} = V_{anemo} * \left[\frac{H_{VAWT,hub}}{H_{anemo}}\right]^{\alpha} \quad (78)$$

where V_{anemo} is the wind speed at the anemometer height (m/s), $H_{VAWT,hub}$ is the hub height of the VAWT above waterline (m), H_{anemo} is the height of the anemometer (m), and α power law exponent for the United State of America is equal to 0.216 [286] .

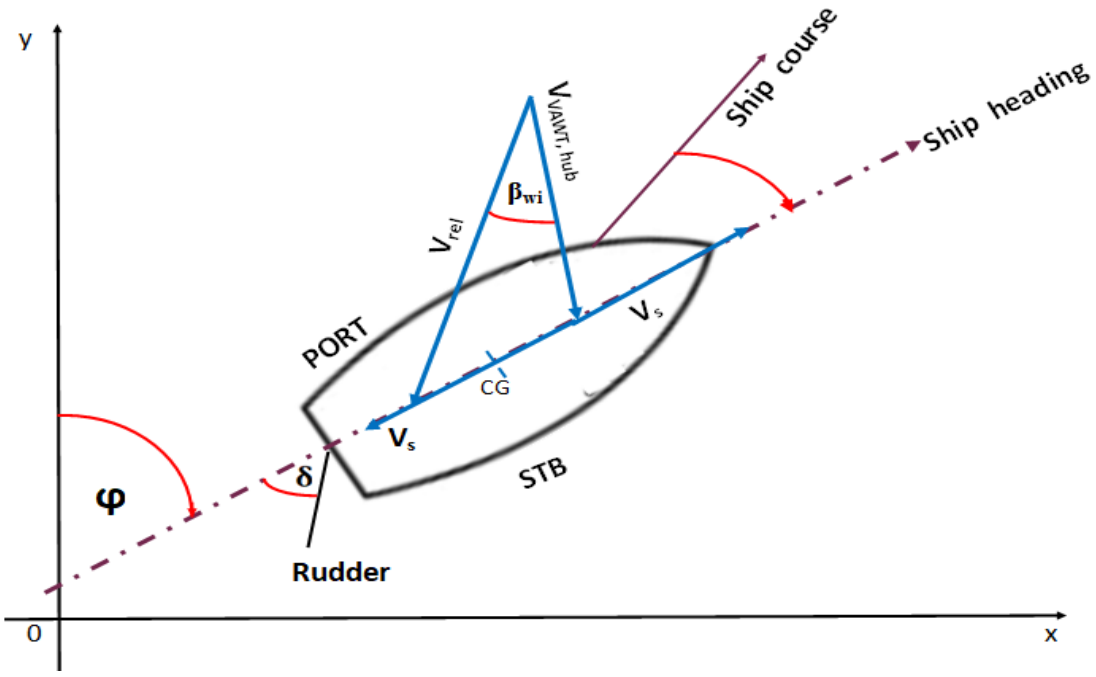

Figure 29: Schematic of ship's heading, course, speed, and wind direction.

Given that the tugboat is in motion, the relative speed $V_{rel}(t)$ is determined by the wind speed at the hub, $V_{wi}(t)$, ship speed $V_s(t)$, wind direction $\beta_{wi}(t)$, and ship heading $\varphi(t)$. This relationship is illustrated in Figure 29 and it can be expressed as follows:

$$V_{rel}(t) = \{V_s(t)^2 + V_{VAWT,hub}(t)^2 - 2V_s(t) * V_{VAWT,hub}(t)cos(\varphi(t) - \beta_{wi}(t))\}^{0.5} \quad (79)$$

Similarly, the output mechanical power extracted from the wind by the VAWT $P_{VAWT,mech}(t)$ can be modeled using the three distinct regions based on wind speed and these are expressed as follows:

$$P_{VAWT,mech}(t) = \begin{cases} \frac{1}{2}\rho_a A_{VAWT} C_{p,VAWT}(\lambda,\beta) * V_{rel}(t)^3 & V_{ci} < V_{rel}(t) < V_r \\ P_{VAWT,nom} & V_r < V_{rel}(t) < V_{co} \\ 0 & V_{rel}(t) < V_{ci} \ or \ V_{rel}(t) < V_{co} \end{cases} \quad (80)$$

$$\lambda = \frac{R_{VAWT} * \omega_{VAWT}}{V_{rel}(t)}$$

where V_{ci} is the VAWT cut-in wind speed (m/s), V_{co} is the VAWT cut-off speed (m/s), V_r is the rated wind speed for VAWT (m/s), A_{VAWT} is the swept area of the wind turbine (m^2), $C_{p,VAWT}(\lambda, \beta)$ is the power coefficient, which is function of tip speed λ and the pitch angle β of the VAWT, R_{VAWT} is the radius of turbine blade (m), ω_{VAWT} is the VAWT rotor speed (rad/s), and $P_{VAWT,nom}$ is the nominal power of the VAWT. In addition, $C_{p,VAWT}(\lambda, \beta)$ can be expressed as the mechanical parameters of the VAWT model as follows [287]:

$$C_{p,VAWT}(\lambda, \beta) = 0.5\left(\frac{116}{\xi} - 0.4\beta - 5\right) exp\left(\frac{-16.5}{\xi}\right) + 0.006\lambda$$

$$\xi = \left(\frac{1}{0.089\beta + \lambda} - \frac{0.035}{1 + \beta^3}\right)^{-1} \quad (81)$$

Furthermore, the output electrical power VAWT $P_{VAWT,elec}(t)$ based on Equation (81) can be expressed as follows:

$$P_{VAWT,elec}(t) = P_{VAWT,mech}(t) * N_{VAWT} * \eta_{total,VAWT} \quad (82)$$

where N_{VAWT} is the number of VAWTs (unitless), and $\eta_{total,VAWT}$ denotes the overall efficiency of the VAWT, which consists of the losses in mechanical conversion and electrical generation [%].

5.2.7.5. Battery Model

The battery bank stores excess energy from the prime mover, Gensets, and/or renewable sources during low-demand periods. This research favors lithium-ion (Li-ion) batteries over lead-acid, nickel-metal-hydride, silver-zinc, and open water-powered batteries due to their superior chemistry [48]. When the combined power from the renewable energy sources and Gensets exceeds the load or when the state of charge SOC(t) is less than the minimum $SOC_{min}(t)$ the battery bank is charged. The charging power of the battery bank is determined by:

$$P_{battery}(t) = P_{battery}(t-1) * (1 - \sigma) + [\sum P_i(t) - \frac{P_{load}(t)}{\eta_{inveter}}] * \eta_{batt,ch} \quad (83)$$

Conversely, when load demand surpasses the available generated energy or when the SOC(t) is greater than maximum $SOC_{max}(t)$, the battery bank discharges. The available capacity of the battery bank during discharge is determined as follows:

$$P_{battery}(t) = P_{battery}(t-1) * (1-\sigma) - [-\sum P_i(t) + \frac{P_{load\ (t)}}{\eta_{inveter}}] * \eta_{batt,disch} \quad (84)$$

where $P_{battery}(t)$ is the available battery bank power during charging and discharging at time t, $P_{battery}(t-1)$ is the available battery bank power at time (t-1), σ is the self-discharge rate of the battery bank, $P_i(t)$ is the total power generated by the PVs , VAWTs, Gensets (kW), $\eta_{inveter}$ is the AC-DC inverter efficiency, $\eta_{batt,ch}$ is battery efficiency during charging process, and $\eta_{batt,disch}$ is battery efficiency during discharging process. In addition, using the battery model known as internal resistance model or Rint model is shown in Figure 30, and the battery SOC and battery current (I_{batt}) can be expressed as follows:

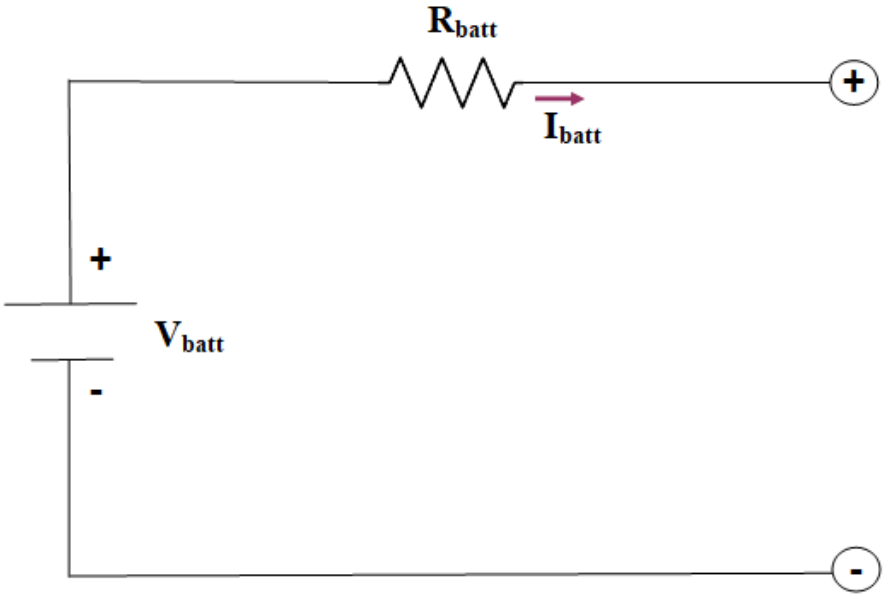

Figure 30: Simplified equivalent circuit battery model

$$\frac{d\,SOC}{dt} = \frac{I_{batt} * \eta_{colm}}{3600\,Q} \tag{85}$$

$$I_{batt} = \frac{V_{batt} - \sqrt{V_{batt} - 4P_{battery}R_{batt}}}{2R_{batt}}$$

where Q denotes the battery capacity (Ah), η_{colm} is the coulombic efficiency (%), V_{batt} is the battery open-circuit voltage (V), and R_{batt} is the battery resistance (ohms).

5.2.7.6. Environmental Assessment

Tugboats are known to produce high emissions due to their speed and diverse operational modes. Specifically, the mass emission rate (MER) measures the pollutants emitted from the combustion of fuel in the main engines and Gensets. Thus, the key pollutants include carbon monoxide (CO), carbon dioxide (CO_2), sulfur oxides (SO_x), nitrogen oxides (NO_x), nitrous oxide (N_2O), particulate matter (PM), and unburned hydrocarbons (UHC) or methane (CH_4). The MER is expressed as follows [47] :

$$\begin{aligned} MER_{total}(t) &= MER_{engine}(t) + MER_{genset}(t) \\ &= \sum_{n=1}^{n=N} EF_j * \left[\dot{m}_{engine}(t) + \dot{m}_{genset}(t)\right] \\ &= \sum_{n=1}^{n=N} EF_j * \left[\,\dot{m}_{total}(t)\right] \end{aligned} \tag{86}$$

where $\mathrm{MER_{total}(t)}$ is the total mass emission rate (kg/h), $\dot{m}_{total}(t)$ denotes the total mass flow rate of fuel consumption from both the diesel engines and Genset (kg/hr), EF_j denotes the emission factor for each pollutant (g/kg-fuel), and j is the type of pollutant for marine fuel (unitless). Furthermore, for new vessels, including fully autonomous tugboats, the IMO requires the implementation of energy efficiency measures, represented by the energy efficiency operational indicator (EEOI) [288], to ensure regulatory compliance. However, the application of EEOI in tugboats may differ due to their unique operational patterns, such as frequent short trips and fluctuating loads. Consequently, reducing fuel consumption throughout the voyage is an effective approach to lowering the EEOI (kg/ton-nm), is expressed as follows:

$$EEOI = \frac{\sum_j EF_{CO_2,j} * [m_{total}(t)]}{m_{cargo} * D} \quad (87)$$

where $EF_{CO_2,j}$ denotes the emission factor for the CO_2 for the fuel type j, $m_{total}(t)$ is the total fuel consumption (kg), m_{cargo} signifies the weight of the cargo in metric tons (or number of passengers), and D is the distance in nautical miles corresponding to the cargo carried or work done.

Furthermore, the emission cost or penalty (EC), which considered a cost factor in the HRES assessment, reflects the environmental cost of using non-renewable energy sources compared to renewable alternatives. Its purpose is to create an economic incentive for reducing emissions [289], [290]. The EP is expressed as follows [47]:

$$EC = \sum_{n=1}^{n=N} C_j * \left[\dot{m}_{engine}(t) + \dot{m}_{genset}(t)\right] \quad (88)$$

where C_j denotes the environmental cost of emission (USD/kg).

5.2.8. Estimation of Propeller Load

Understanding propeller load disturbances is essential for maintaining system equilibrium and solving the optimal HRES management problem. The effect of random waves on propeller torque is validated through extended Kalman filtering (EKF). Propeller torque can be estimated using an extended state observer (ESO) with engine speed and torque measurement [250]. Therefore, the accurate estimation of this influence is crucial for optimal HRES management and torque data. Additionally, based on propeller strip theory, propeller rotation power (P_{prop}) is proportional to the cube of engine speed n_{eng} ($P_{prop} = Q_{load}\omega_{prop} = Z_{load}n_{eng}^3$). Therefore, the propeller load torque can be determined as follows:

$$Q_{load} = \frac{\pi}{8} K_Q(J)\, \rho_w {D_{prop}}^3 {V_{hy}}^2 \quad (89)$$

where Z_{load} is the proportional parameter which is dependent on the tugboat's environmental and the load conditions. Thus, the Equation (89) can be written as follows:

$$Q_{load} = \frac{W_Q}{4\pi^2}\,\rho_w {D_{prop}}^5 \omega_{prop}|\omega_{prop}|$$
$$W_Q = \frac{1}{8}K_Q(J)\left[(0.7\pi)^2 + \left(\frac{V_{wp}}{n_{prop}D_{prop}}\right)^2\right] \quad (90)$$

The calculation of the propeller Q_{load} in Equation (90) uses angular velocity ω_{prop}, which is measured from the speed sensor. This enables the determination of Q_{load} without the need for additional parameters. Therefore, Equation (90) is substituted into Equation (71) to define the unknown disturbance (d), which is to be estimated using the extended state observer principle as follows:

$$\frac{d\omega_{engine}(t)}{dt} = \frac{1}{J_{total}}\left[Q_{engine}(t) + Q_{motor}(t) - {\lambda_{gear}}^{-3} d\ \omega_{prop}|\omega_{prop}|\ \right]$$
$$d = \frac{W_Q}{4\pi^2}\,\rho_w {D_{prop}}^5 \quad (91)$$

The EKF operates in two stages. In the first stage, it predicts the next state and error covariance using the system's nonlinear model and state transition. In the second stage, the state estimate is updated with the new measurement, and the error covariance matrix is revised accordingly. The EKF design for the plant model is expressed as follows:

$$\overline{x}(k+1) = f(\overline{x}(k), u(k) + w(k)), \qquad w(k) \sim (0, Q(k))$$
$$y(k) = h\left(\overline{x}(k), u(k)\right) + v(k), \qquad v(k) \sim (0, R(k)) \quad (92)$$

where $\overline{x} = \begin{bmatrix}\omega_{engine}\\ d\end{bmatrix}$ is the augmented state vector, u = $\begin{bmatrix}Q_{engine}\\ Q_{motor}\end{bmatrix}$ is the input, y = ω_{engine} is the output, k is the time steps, v is the measurement noise, w is the process noise, h is the nonlinear state transition function, and Q and R are the noise of covariances.

The estimated unknown disturbance d is used in conjunction with the above methods to get the estimate disturbance $\hat{d}$. The gathered estimated value is used to determine observed strip constant coefficient $\hat{Z}_{load}$ as follows:

$$\hat{Z}_{load} = \frac{Z_{load}}{\lambda_{gear}^3} = \frac{\widehat{K_Q}\,\rho_w {D_{prop}}^5}{\lambda_{gear}^3 60^2} = \frac{4\pi^2 \hat{d}}{\lambda_{gear}^3 60^2} = \frac{\pi^2 \hat{d}}{900\lambda_{gear}^3} \tag{93}$$

Thus, $\hat{Z}_{load}$ observed by the EKF in Equation (93) is used to determine the propeller torque as follows:

$$Q_{load} = \hat{Q}_{load} = \frac{30{n_{eng}}^2 \hat{Z}_{load}}{\pi} \tag{94}$$

5.2.9. Proposed Nonlinear Model Predictive Control (NMPC) Method for the Energy Management System (EMS) via Grey Wolf Optimization (GWO)

This section evaluates the energy management system (EMS) for a hybrid propulsion plant integrating renewable energy sources to optimize shipboard load distribution. The EMS regulates engine speed and power distribution between the energy sources and manages power allocation across main engines, Gensets, PVs, VAWTs, and battery banks for shipboard loads and propulsion loads. The proposed EMS method utilizes a hybrid approach combining NMPC with GWO strategy to optimize the power split between power sources. The rule-based system ensures robustness and fail-safes, NMPC enables real-time optimization, and GWO tunes parameters or optimizes long-term strategies, with GWO-derived parameters feeding into NMPC for efficient real-time control. This combination allows for a more adaptive, flexible, and optimized energy management solution.

5.2.9.1. Grey Wolf Optimisation (GWO)

The grey wolf optimization (GWO) algorithm is a nature-inspired metaheuristic based on the hunting and social behavior of grey wolves. Similar to other nature-based methods, such as the genetic algorithm, GWO begins by generating a set of random candidate solutions. Two primary components define the algorithm's behavior: the social hierarchy and the hunting strategy. The social hierarchy, illustrated in Figure 31(a), ranks wolves based on strength, with alphas (α), betas (β), deltas (δ), and omegas (ω) representing the top to lowest ranks, respectively. The alpha wolf is considered the fittest solution, followed by beta and delta, while omega represents the remaining candidates. During the optimization process, the top three wolves namely α, β, and δ guide others toward promising search regions.

In addition to the social structure, the hunting strategy involves wolves working collectively to hunt prey. They coordinate to separate the prey from the herd, with one or two wolves attacking while the others handle stragglers. In the optimization context, wolves, operating as a team, explore and track potential solutions, encircle them, and apply pressure until the prey (optimal solution) is captured. When the prey moves, the wolves adjust their strategy to maintain the encirclement, ensuring continued progress toward the optimal solution.

In the mathematical model of GWO, let $\overrightarrow{X_P}(t)$ and $\vec{X}(t)$ represent the positions of the prey and wolf, respectively, at iteration. The encircling behavior of the wolves is mathematically modeled as follows:

$$\vec{D} = \left|\vec{C}.\overrightarrow{X_P}(t) - \vec{X}(t)\right|$$

$$\vec{X}(t+1) = \overrightarrow{X_P}(t) - \vec{A}.\vec{D}$$

$$\vec{A} = 2\vec{a}\,.\overrightarrow{r_1} - \vec{a} \tag{95}$$

$$\vec{C} = 2\overrightarrow{r_2}$$

where t denotes the current or number of iterations, $\vec{D}$ is distance between grey wolf and prey, $\vec{C}$ is coefficient vector, $\vec{A}$ is coefficient vector, $\vec{a}$ is the linearly decreased from 2 to 0 over the course of iterations, $\overrightarrow{r_1}$ and $\overrightarrow{r_2}$ are random vectors in the interval of [0, 1].

During the optimization (hunting phase), the ω wolves update their positions around the prey or encircling α, β, and δ wolves based on Equation (96). In addition, in Figure 31(b) illustrates how the ω wolf adjusts position based on the locations of the α, β, and δ wolves in the search space.

$$\overrightarrow{D_\alpha} = \left|\overrightarrow{C_1}.\overrightarrow{X_\alpha} - \vec{X}\right| \ , \ \overrightarrow{D_\beta} = \left|\overrightarrow{C_2}.\overrightarrow{X_\beta} - \vec{X}\right| \ , \ \overrightarrow{D_\delta} = \left|\overrightarrow{C_3}.\overrightarrow{X_\delta} - \vec{X}\right|$$

$$\overrightarrow{X_1} = \overrightarrow{X_\alpha} - \overrightarrow{A_1}.\overrightarrow{D_\alpha} \ , \ \overrightarrow{X_2} = \overrightarrow{X_\beta} - \overrightarrow{A_2}.\overrightarrow{D_\beta} \ , \ \overrightarrow{X_3} = \overrightarrow{X_\delta} - \overrightarrow{A_3}.\overrightarrow{D_\delta} \quad (96)$$

$$\vec{X}(t+1) = \frac{\overrightarrow{X_1} + \overrightarrow{X_2} + \overrightarrow{X_3}}{3}$$

where $\overrightarrow{D_\alpha}$, $\overrightarrow{D_\beta}$, $\overrightarrow{D_\delta}$ are the three position vectors of the α, β, and δ respectively, $\overrightarrow{C_1}$, $\overrightarrow{C_2}$, $\overrightarrow{C_3}$ are coefficient vectors, $\overrightarrow{A_1}$, $\overrightarrow{A_2}$, $\overrightarrow{A_3}$ are the adaptive vectors, $\overrightarrow{X_\alpha}$, $\overrightarrow{X_\beta}$, $\overrightarrow{X_\delta}$ are the position vectors of the α, β, and δ respectively, $\overrightarrow{X_1}$, $\overrightarrow{X_2}$, $\overrightarrow{X_3}$ are current positions of the α, β, and δ, respectively, $\vec{X}(t+1)$ denotes the position update for ω wolf.

The vectors $\vec{A}$ and $\vec{C}$ govern the exploration and exploitation phases of the GWO algorithm. In addition, the exploration is emphasized when $|\vec{A}| \geq 1$, while exploitation is emphasized when $|\vec{A}| < 1$. Furthermore, as the algorithm progresses, $\vec{A}$ gradually decreases, with the first half of the iterations focusing on exploration and the latter half on exploitation. Also, the random nature of $\vec{C}$ further enhances the balance between exploration and exploitation, preventing the algorithm from converging to local optima.

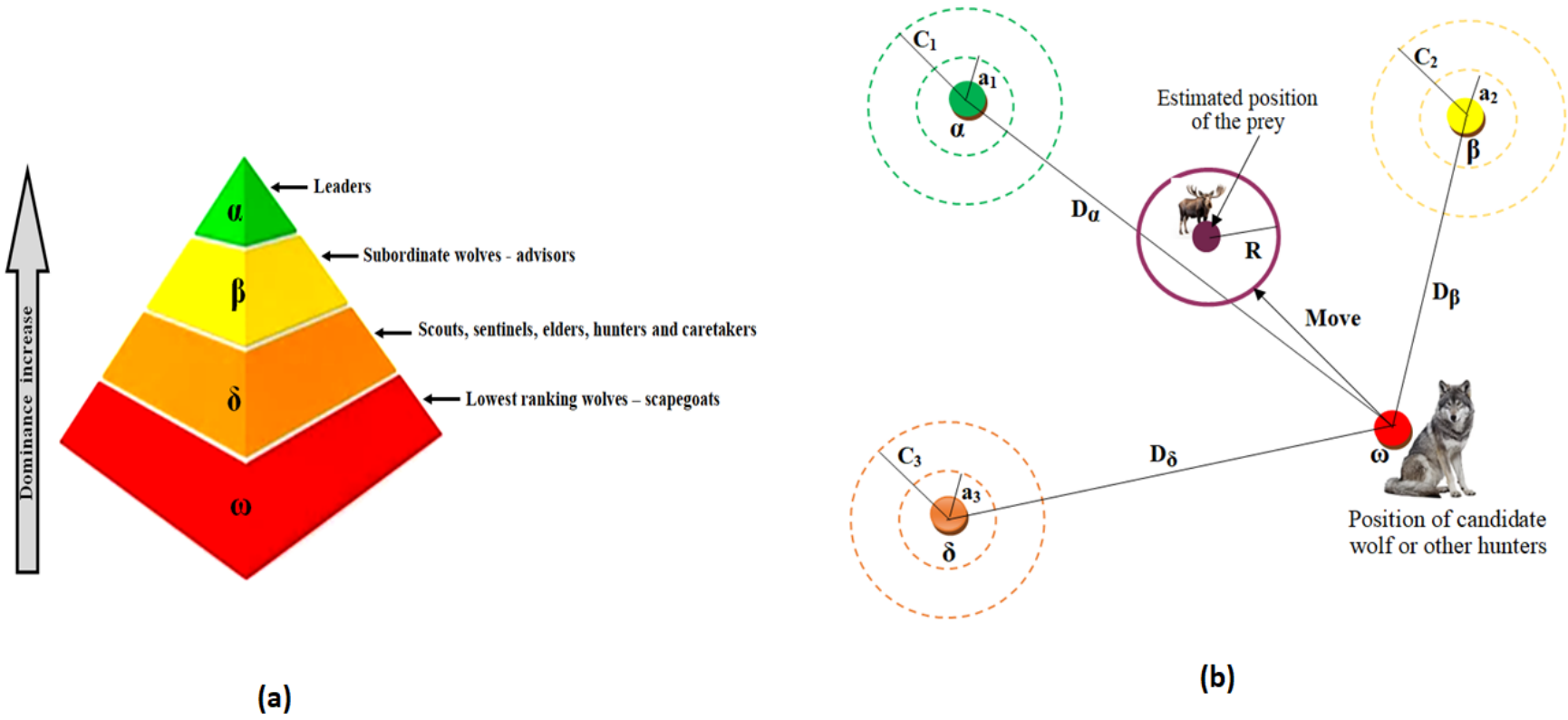

Figure 31: Principle of social structure and hunting strategy of GWO: (a) social hierarchy in wolf pack, (b) updating of wolf position after the prey is encircled.

5.2.9.2. Nonlinear Model Predictive Control (NMPC)

The nonlinear model predictive control (NMPC) algorithm is ideal for dynamic systems with intricate, nonlinear interactions among subsystems such as propulsion, energy sources, and environmental factors. The NMPC can optimize power distribution across energy sources by using GWO to adjust parameters or refine control inputs (**U**(k)) while considering the system's dynamics and constraints to ensure optimal performance over time.

The HRES is governed by a set of nonlinear dynamics that describe how the state of the system evolves over time. Thus, after discretization, the nonlinear system model can be represented as follows:

$$x\,(k+1) = f\big(\boldsymbol{x}(k), \boldsymbol{u}(k)\big) \qquad \text{k} = 0, \ldots., N_p - 1 \tag{97}$$

where $x\,(k+1)$ is the prediction model, f is the nonlinear system dynamics function; for this HRES the NMPC has the following system state parameters:

$\boldsymbol{x}(k) = \left[\,\text{RPM}_{\text{engine}}, SOC, C_{motor},\ C_{engine}, P_{genset}, \dot{\text{m}}_{\text{total}}\right]^T$, control inputs or variables are used as controller at each time step to optimize system behavior at time step k, $\boldsymbol{U}(k) = \left[\,\dot{C_{motor}}, \dot{C_{engine}}, \varphi,\right]^T$ are the control inputs and φ denotes the slack parameter which introduced as an additional control input to enforce soft constraints, significantly penalizing limit violations within the prediction horizon in the cost function. Similarly, the $\boldsymbol{d}(k)$ is fed to the NMPC controller as a disturbance whiles the system's outputs is determine as $\boldsymbol{y}(k)$**.**

The cost function J, which must be minimized to solve the optimal control HRES problem, is as follows:

$$J\left(\mathrm{RPM}_{\mathrm{engine}}, SOC, C_{motor}, \dot{C_{motor}}, \dot{C_{engine}}, P_{genset}, \dot{\mathrm{m}}_{\mathrm{total}}, \varphi\right) =$$

$$\sum_{k=0}^{N_p-1} W_i \begin{bmatrix} (RPM_{engine,i} - RPM_{engine,ref})^2 \\ (SOC_i - SOC_{ref})^2 \\ \left(C_{motor,i}\right)^2 \\ \left(\dot{C_{motor,i}}\right)^2 \\ (\mathrm{P}_{\mathrm{genset}} - P_{genset,ref})^2 \\ \left(\dot{C_{engine,i}}\right)^2 \\ \varphi^2 \end{bmatrix}^T + W_N \begin{bmatrix} (RPM_{engine,N} - RPM_{engine,ref})^2 \\ (SOC_N - SOC_{ref})^2 \\ (\mathrm{P}_{\mathrm{genset}} - P_{genset,ref})^2 \\ \left(\dot{\mathrm{m}}_{\mathrm{total,N}}\right)^2 \end{bmatrix}^T \quad (98)$$

where W_i is the stage cost matrix and W_N is the final cost matrix, N_p is the prediction time. The optimization problem is expressed as:

$$\min J(\mathrm{RPM}_{\mathrm{engine}}, SOC, C_{motor}, \dot{C_{motor}}, \dot{C_{engine}}, P_{genset}, \dot{\mathrm{m}}_{\mathrm{total}}, \varphi)$$

Subjected to:

Eq. (1) – (35)

$$SOC_{min,soft} - \varphi \leq SOC \leq SOC_{max,soft} + \varphi$$

$$SOC_{min,hard} \leq SOC \leq SOC_{max,hard}$$

$$RPM_{engine,min,soft} - \varphi \leq RPM_{engine,soft} \leq RPM_{engine,max,soft} + \varphi$$

$$RPM_{engine,min,hard} \leq RPM_{engine,hard} \leq RPM_{engine,max,hard}$$

$$0 \leq C_{engine} \leq C_{engine,max}(RPM_{engine})$$

$$\dot{C_{engine}}_{min} \leq \dot{C_{engine}} \leq \dot{C_{engine}}_{max}$$

$$C_{motor}{}_{min} \leq C_{motor} \leq C_{motor}{}_{max} \quad (99)$$

$$\dot{C_{motor}}_{min} \leq \dot{C_{motor}} \leq \dot{C_{motor}}_{max}$$

$$\varphi \geq 0$$

$$P_{genset,min}(t) \leq P_{genset}(t) \leq P_{genset,max}(t)$$

$$P_{PV,min}(t) \leq P_{PV}(t) \leq P_{PV,max}(t)$$

$$P_{VAWT,min}(t) \leq P_{VAWT}(t) \leq P_{VAWT,max}(t)$$

$$\mathrm{P_{engine}(t)} + P_{genset}(t) + P_{PV,total}(t) + P_{VAWT}(t) + P_{battery}(t) \geq P_{\mathrm{total,load}}(\mathrm{t})$$

$$P_{\mathrm{total,load}}(\mathrm{t}) = P_{ship,load}(t) + P_{prop,Load}(t)$$

5.2.9.3. Simulation procedure for the proposed NMPC-GWO algorithm

The flowchart of the NMPC-GWO algorithm for the fully autonomous HRES model is presented in Figure 32. Initially, the data are collected and prepared, and the energy source constraints are defined. This is followed by the initialization of the GWO vector constraints, the weight factors, and the bounds for the objective functions of all energy sources within the control loop. Since the GWO is employed as the dynamic optimizer for the NMPC, the NMPC cost function serves as the input for determining the fitness of the GWO, as indicated by the letter "A" in Figure 32(a). The GWO algorithm then explores the parameter space to identify the optimal values for the NMPC control loop, thereby enhancing its ability to minimize fuel consumption and emissions. Additionally, during each iteration, if the optimizer's criteria are not met, these values are introduced into the NMPC cost function as weight metrics Q and R, as denoted by the letter "B" in Figure 32(b).

All simulations were conducted in a Python 3.11.6 environment on a Windows 11 system, utilizing key libraries such as CasADi for nonlinear model predictive control and custom implementations of the GWO. Data processing and numerical computations employed NumPy and Pandas, while visualization was performed with Matplotlib 3.7.0. Additional tools such as SciPy, Scikit-learn, and FilterPy support statistical analysis and state estimation. The NMPC was implemented over a prediction horizon of 10-time steps with a control horizon of 5, and a sampling time of 0.5 minute.

The GWO algorithm used a population size of 30 search agents and a maximum of 100 iterations per control loop. The cost function integrated fuel consumption, emission cost, battery SOC, and power flow penalties to ensure optimal energy management under physical and operational constraints. The operating profile used for the simulation represents a typical daily round-trip of a harbor tugboat, covering sailing, towing, idling, and return segments. This mission profile was extracted from a preprocessed subset of a year-long operational dataset. It reflects realistic energy demands encountered during routine operations under moderate sea states, which influence the vessel's resistance and load characteristics.

Furthermore, the EKF is used to filter out the random disturbances caused by waves. The EKF estimates the true state of the propulsion system (such as torque and load) by removing noise and accounting for non-linearities in the system dynamics. As a result, the optimal solution sequence $\mathbf{U}(k)$ is obtained by solving the function in Equation (97), with the first element of $\mathbf{U_0}(k)$ being fed into the closed loop to adjust control actions in response to wave-induced disturbances in the proposed plant model.

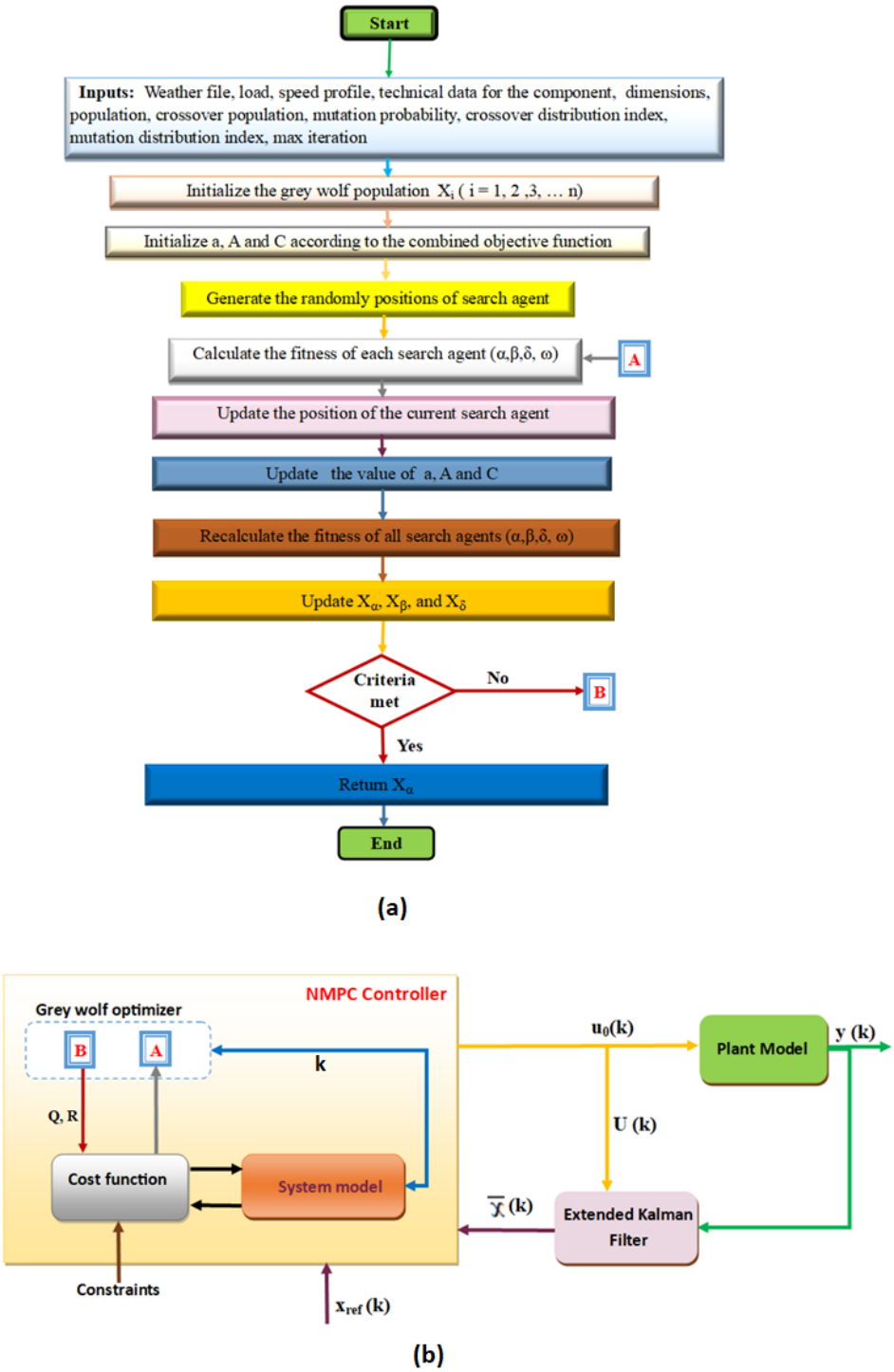

Figure 32: Simplified architecture and implementation of the NMPC -GWO algorithm: (a) GWO and (b) NMPC algorithm

5.2.10. Data acquisition

This study employs the ship particulars, the ship's logbook, and AIS data of a conventional tugboat to model a fully autonomous tugboat. A modified hybrid configuration is proposed, featuring four-stroke marine diesel engines, four-stroke Gensets, renewable energy sources, and a battery bank. The AIS data, including vessel heading, course, speed, positional coordinates (latitude and longitude), and dynamic parameters, were sourced from ship log book and MarineTraffic [146] , with details provided in the appendix. In addition, the shipload, which is generally minimal compared to the propulsion load, is detailed in the authors' previous work [48]. The estimation of propulsion load power for the autonomous tugboat is presumed to be analogous to that of the conventional tugboat, utilizing historical operational data from the vessel's log. Figure 33 depicts an extract of the actual operating profile of the tugboat, which includes periods of intense pulling operations sustained over an extended duration in the Port of Los Angeles (USA). This dynamic profile was created by integrating ship log data, engine performance records, and input collected from discussions and interviews with tug operators and experts in the marine sector. The typical operational sequence involves the tugboat sailing out, awaiting further instructions, performing a series of pushing and pulling tasks, and ultimately completing the assignment before sailing back to port.

Similarly, meteorological data, such as ambient radiation intensity, wind speed, and temperature along the navigational route, were obtained from the NASA Prediction of Worldwide Energy Resources (POWER) database, and these are detailed in the authors' previous work [48]. Also, the environmental data, including sea state conditions, wind direction, wave height, and current, were extracted from the ship logbook and external sources [291]. The daily profiles of sea conditions along the navigational routes are presented in Figure 34.

Although tugboat operations are typically confined to sheltered port waters, the dataset also includes segments near the breakwaters of the Ports of Los Angeles and its environs. These semi-exposed areas may experience low to moderate wave activity, with significant wave heights ranging from 0.5 to 1.2 meters, according to National Oceanic and Atmospheric Administration (NOAA) buoy data (Station 46222).

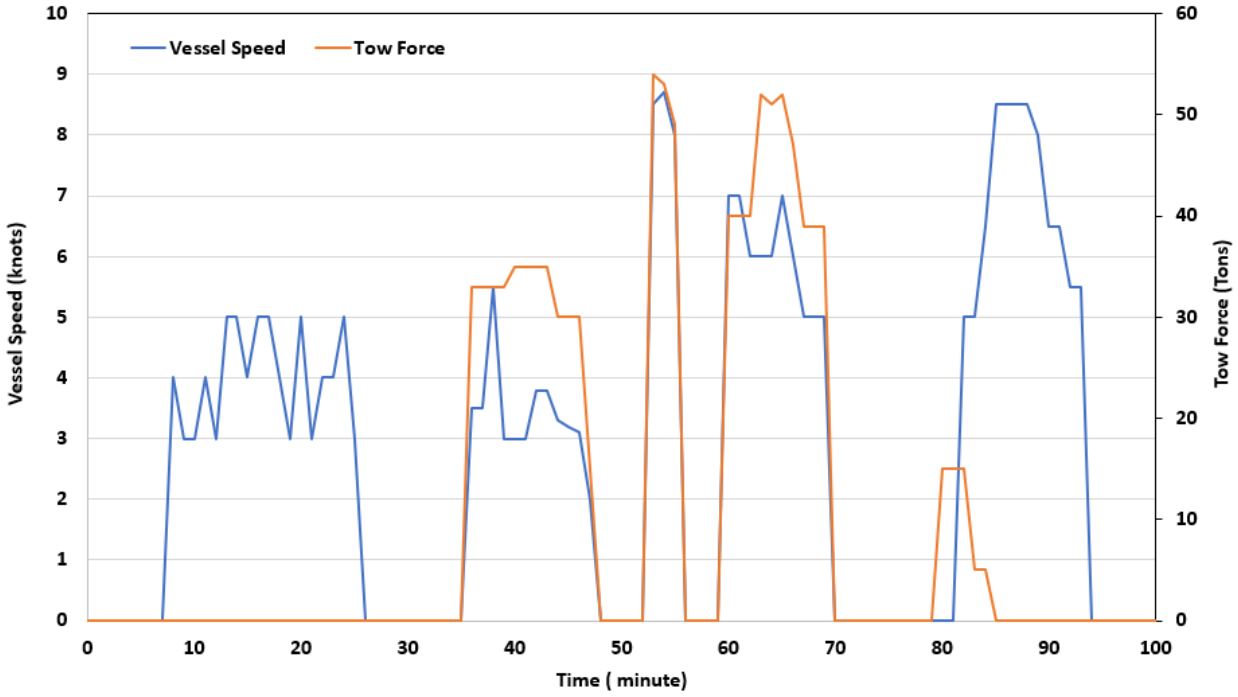

Figure 33: Dynamic operating profile for tugboat with timescale.

Under adverse weather conditions, particularly when navigating in head seas and rough sea states, the ship's resistance can increase by up to 100% compared to calm sea conditions [281]. Also, the definition of adverse sea conditions varies depending on ship length, with the World Meteorological Organization (WMO) classifying adverse conditions for tugboats under 200 meters as sea state 5.

To account for these effects, a simplified stochastic wave model was implemented. Though wave influence is generally secondary to thrust and load dynamics in tug operations, this model introduces low-frequency disturbances to simulate their indirect impact on propulsion load and energy demand. This approach ensures realistic estimation of fuel consumption and emissions, particularly during dynamic positioning, towing, and escorting in nearshore environments.

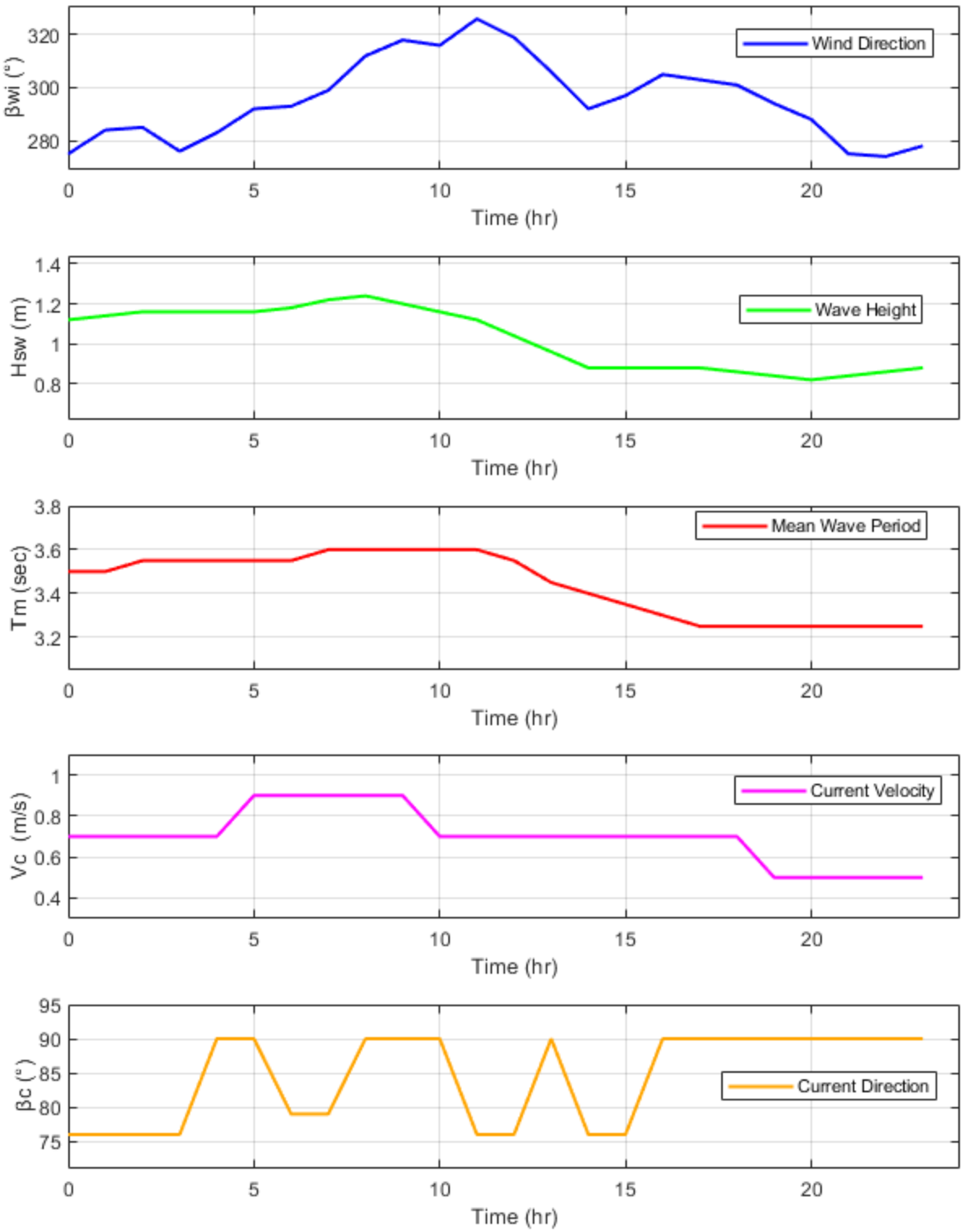

Figure 34: Graph of sea conditions along the navigational routes

5.3. Results and Discussion

Figure 35 illustrates the relationship between engine torque and RPM under the three proposed control algorithms. The NMPC-GWO algorithm demonstrates superior performance for the HRES integrated into the tugboat. It achieves the most favorable torque-RPM balance, contributing to reduced fuel consumption and lower emissions. The NMPC-GA algorithm performs moderately well but is hindered by slower convergence and less effective torque distribution. Conversely, the Rule-Based (RB) method yields the worst results due to its non-adaptive framework, which fails to accommodate dynamic disturbances such as wave-induced torque variations, resulting in inefficient fuel usage and higher emissions.

Similarly, Figures 36 - 38 present the comparative simulation results of power generation from photovoltaic (PV) modules, vertical-axis wind turbines (VAWTs), and diesel generator sets (Gensets), along with fuel consumption and battery state of charge (SOC) across the three algorithms. In Figure 36(a), the solar power output remained constant across all cases, indicating negligible environmental variability. In contrast, in Figure 36(b) the wind power exhibited notable fluctuations. Both NMPC-GWO and NMPC-GA algorithms adapted effectively to these variations, outperforming the RB method in wind energy utilization.

Regarding Genset usage in Figure 37(a), NMPC-GWO and NMPC-GA demonstrated more efficient load-sharing strategies, thereby minimizing reliance on diesel power. The RB method, which utilizes the same hybrid renewable energy system (HRES) platform but employs a static, non-adaptive control strategy, by contrast exhibited over-dependence on Gensets during suboptimal intervals, resulting in elevated fuel consumption, as shown in Figure 37(b). This trend is reflected in the cumulative fuel consumption graph, where the RB approach, though initially efficient, incurred higher total fuel usage due to its static fuel management. In addition, Battery performance in Figure 38 further distinguishes the algorithms. NMPC-GWO and NMPC-GA maintained SOC within an optimal operational range of 50–70%, with NMPC-GWO exhibiting tighter control and better charge balance. The RB method, however, revealed large SOC deviations, indicative of inefficient energy storage control.

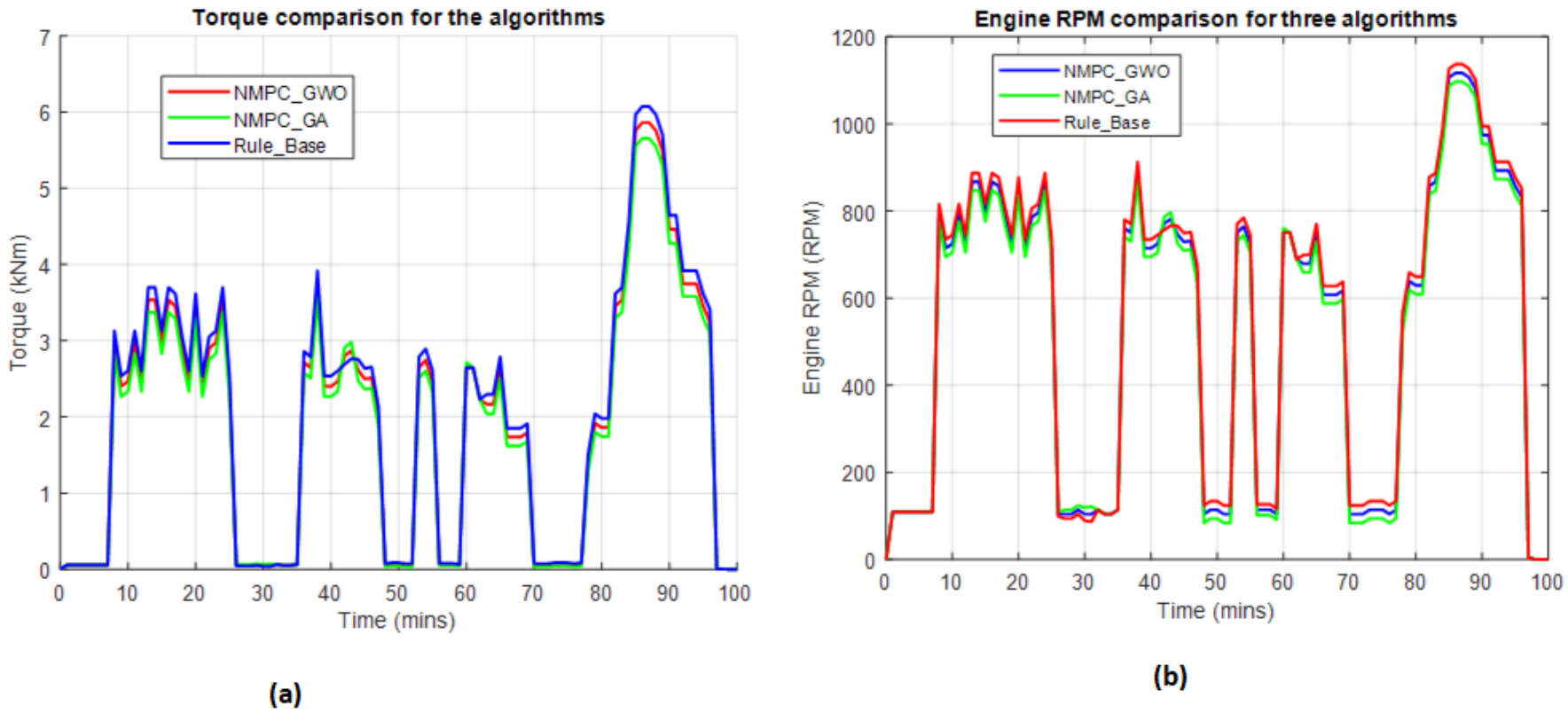

Figure 35: Comparison of the engine RPM and torque for the algorithms.

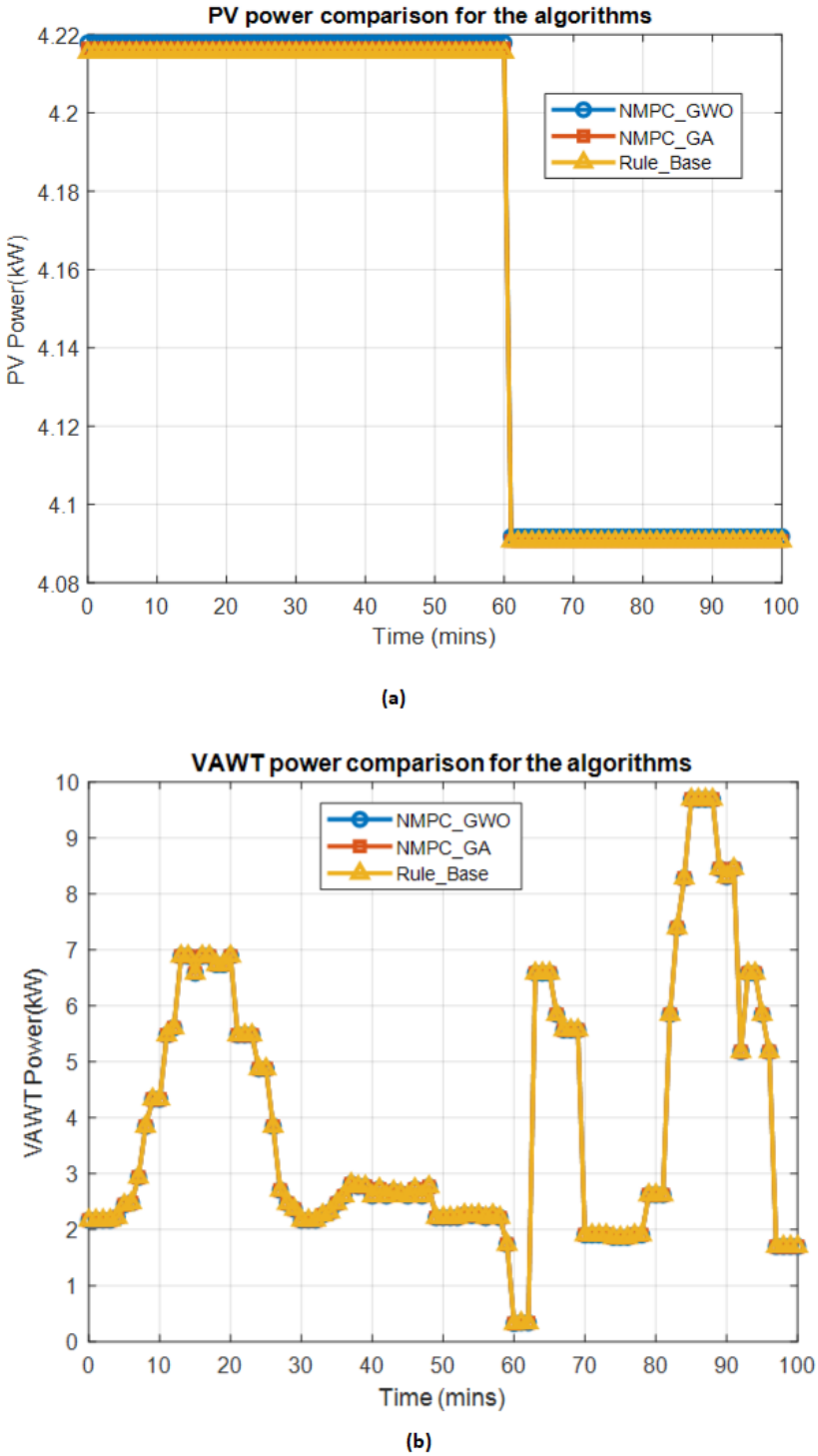

Figure 36: Renewable power generation under different control algorithms: (a) PV power, (b) VAWT power.

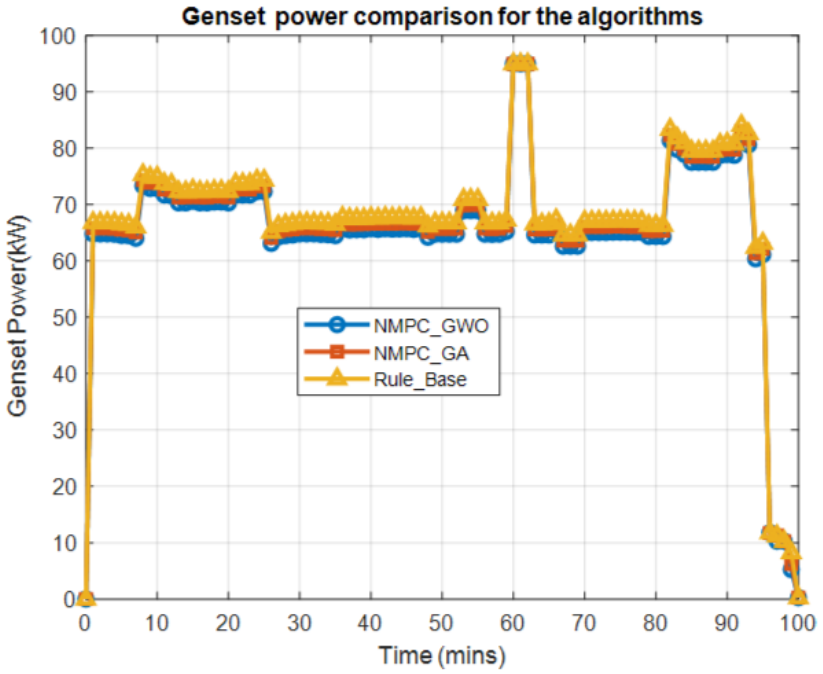

(a)

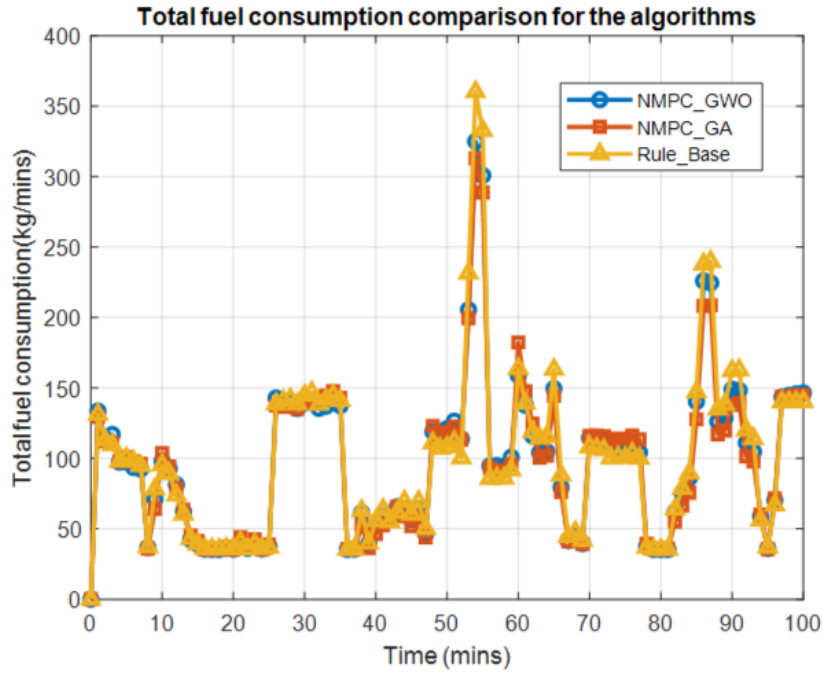

(b)

Figure 37: Power management and fuel usage under different control algorithms: (a) Gensets power (b) total fuel consumption.

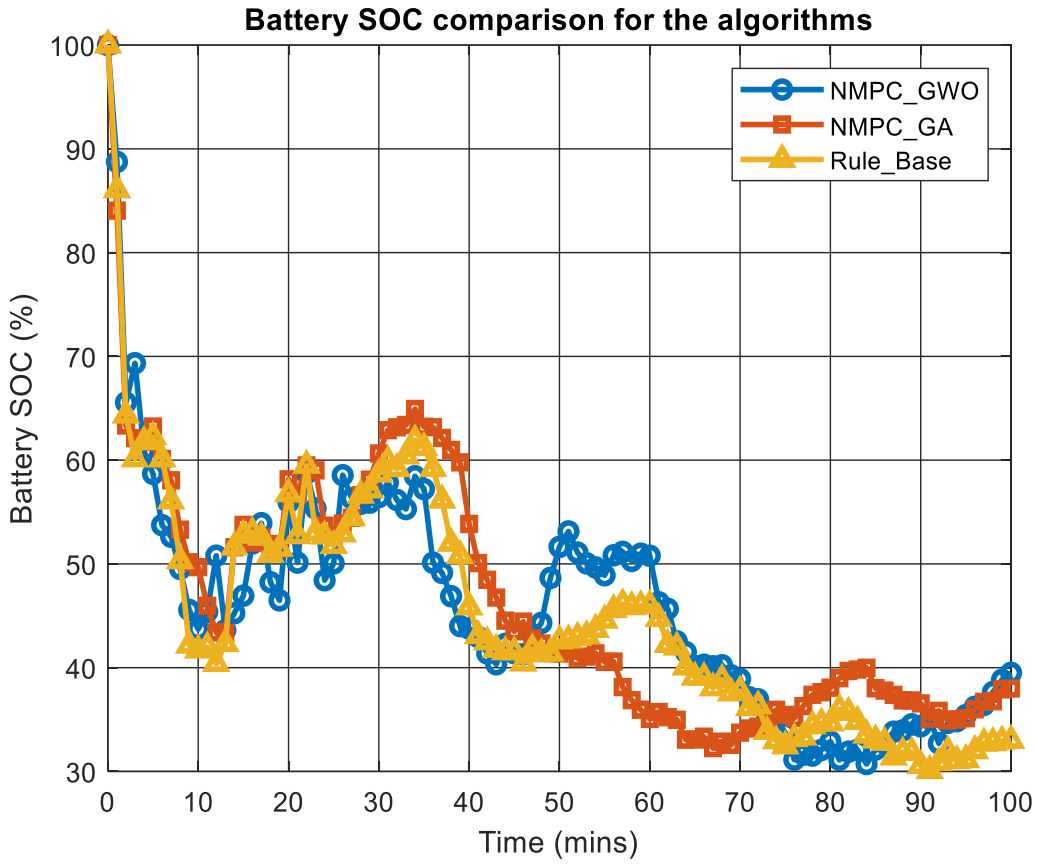

Figure 38: Battery State of Charge (SOC) comparison under different control algorithms.

Table 23, quantitatively reinforces these findings. The NMPC-GWO algorithm achieved the lowest fuel consumption (161.517 kg), mass emission rate (518.967 kg/hr), emission cost (9,973.84 USD), and Energy Efficiency Operational Indicator (EEOI) of 3.609 kg/ton-nm, while also attaining the fastest computational time (31.601 s). The RB method performed the worst across all key performance indicators due to its lack of adaptiveness. NMPC-GA provided intermediate results, constrained by its genetic algorithm's slower convergence and suboptimal energy allocation.

Table 23: Results of the proposed algorithms for the HRES fitted on the fully autonomous tugboat.

Algorithms	Total fuel consumption (kg)	Total mass emission rate (kg/hr.)	Emission cost (EC) (USD/kg)	EEOI (kg/ton-nm)	Total computational time (s)
RB	165.661	532.281	10,229.72	3.796	353.153
NMPC - GWO	161.517	518.967	9,973.84	3.609	31.601
NMPC - GA	163.476	525.263	10,094.84	3.697	3113.783

To quantitatively evaluate the predictive performance of the proposed hybrid Energy Management System (EMS) algorithms, standard statistical regression metrics—Root Mean Squared Error (RMSE), Mean Absolute Error (MAE), and the coefficient of determination (R^2)—were computed using a conventional tugboat without HRES integration as the baseline. This baseline reflects a traditional marine propulsion configuration devoid of hybridization or autonomous control, and it serves as a reference point for assessing the gains achieved through predictive control and energy optimization.

Table 24 presents the comparative results for four primary performance indicators: fuel consumption, emission rate, emission cost, and the Energy Efficiency Operational Indicator (EEOI). These metrics were used to quantify the predictive accuracy and control effectiveness of the NMPC-GWO and NMPC-GA algorithms. In the case of fuel consumption, the NMPC-GA algorithm yielded the lowest RMSE and MAE values, indicating a marginally higher prediction accuracy compared to NMPC-GWO, although both models substantially outperformed the baseline. For emission rate and emission cost predictions, NMPC-GA again demonstrated slightly lower error values and stronger correlation coefficients, affirming its statistical robustness in modeling environmental impact. However, NMPC-GWO exhibited a higher R^2 value in predicting EEOI, suggesting better alignment with operational efficiency under hybrid-electric propulsion.

It should be noted that the rule-based (RB) method, although implemented on the same hybrid renewable energy platform, lacks the predictive estimation framework required for regression analysis and therefore is excluded from Table 24. Instead, its performance is evaluated through aggregate metrics, as presented earlier in Table 23.

Table 24: Performance metrics of NMPC-GWO and NMPC-GA algorithms compared to baseline

Metric	Algorithm	RMSE	MAE	R^2
Fuel Consumption (kg)	NMPC-GWO	11.10	10.74	0.948
	NMPC-GA	9.82	9.58	0.969
Emission Rate (kg/h)	NMPC-GWO	35.26	32.77	0.964
	NMPC-GA	30.44	29.42	0.972
Emission Cost (USD)	NMPC-GWO	692.45	648.96	0.965
	NMPC-GA	607.6	574.31	0.973
EEOI (kg/ton-nm)	NMPC-GWO	0.281	0.259	0.96
	NMPC-GA	0.276	0.265	0.945

These findings confirm that both predictive algorithms offer statistically significant improvements in modeling accuracy, energy efficiency, and environmental performance when compared to conventional marine propulsion systems. While NMPC-GA showed slightly superior accuracy across most regression metrics, NMPC-GWO remains preferable in real-time maritime applications due to its faster computational speed, robust adaptability to environmental disturbances, and superior control convergence, as demonstrated in the subsequent sensitivity analysis. This underscores the practical suitability of NMPC-GWO for integration into autonomous energy management frameworks in the maritime domain. These promising results motivate the subsequent sensitivity analysis of NMPC-GWO under variable operating parameters.

5.3.1. Sensitivity Analysis

A sensitivity analysis was conducted to evaluate the robustness and performance adaptability of the proposed HRES governed by the NMPC-GWO algorithm under varying operational conditions in a fully autonomous tugboat. Key system input parameters were varied by ±15% —a range reflecting realistic operational fluctuations—and their effects on total fuel consumption, mass emission rate, emission cost, and EEOI are summarized in Table 25.

Firstly, a 15% reduction in vessel speed led to marginal improvements in energy efficiency, reflected by lower fuel consumption, emissions, and EEOI. This outcome is attributed to reduced propulsion power demand at lower speeds. Conversely, a 15% increase in speed resulted in higher fuel consumption and emissions due to elevated engine loading and reduced propulsion system efficiency.

Secondly, wind speed variations also had a notable impact. A 15% decrease in wind speed diminished the power output from the VAWTs, increasing reliance on the diesel Gensets and battery storage, thereby raising fuel use and emissions. In contrast, a 15% increase in wind speed enhanced wind energy harvesting, improving system efficiency by reducing Genset operation and associated emissions.

Thirdly, ambient temperature and solar radiation exhibited negligible influence on system performance. While minor fluctuations may slightly affect PV output and battery charge–discharge behavior, the overall impact on fuel consumption and emissions was statistically insignificant.

Fourthly, the towing force exhibited a strong correlation with energy demand. A 15% reduction in towing resistance significantly improved fuel efficiency by lowering shaft torque requirements and reducing engine workload. In contrast, an equivalent increase in towing force imposed higher torque demands, thereby escalating fuel usage, emissions, and EEOI.

Lastly, variations in vessel deadweight (load) also influenced system behavior. Reduced load conditions improved fuel economy by enabling greater utilization of renewable energy sources. However, increased load intensified propulsion and auxiliary power demand, thereby increasing dependence on Gensets and resulting in elevated fuel consumption and emissions. These findings highlight the critical importance of adaptive energy management in maintaining operational

efficiency under dynamic maritime conditions, validating the NMPC-GWO's suitability for real-time control of hybrid propulsion systems in autonomous vessels.

Table 25: Sensitivity analysis of HRES for a fully autonomous tugboat using NMPC-GWO algorithm with impact of operational parameters on fuel consumption, emission rate, emission cost, and EEOI.

Parameters	Percentage variation	Total fuel consumption (kg)	Total mass emission rate (kg/hr.)	Emission cost (EC) or penalty (USD/kg)	EEOI (kg/ton-nm)
Ship speed (knots)	-15%	161.8208	516.6979	9,930.23	2.0310
	+15%	163.9685	526.8439	10,125.22	1.7099
Wind speed (knots)	-15%	162.8371	519.9431	9,992.60	3.6225
	+15%	161.5115	518.9493	9,973.50	3.6086
Ambient temperature (°C)	-15%	161.5217	518.9820	9,974.12	3.6091
	+15%	161.5136	518.9561	9,973.63	3.6087
Ambient radiation intensity (kW/m2)	-15%	161.5237	518.9885	9,974.25	3.6092
	+15%	161.4644	518.7980	9,970.59	3.6065
Towing force (tons)	-15%	143.4226	461.7921	8,875.01	2.8575
	+15%	459.0715	1,475.03	28,348.12	29.15
Ship load (kW)	-15%	161.5049	518.9281	9,973.09	3.6083
	+15%	162.6464	522.5959	10,043.58	3.6595

5.3.2. Discussion

This study presents a novel multi-objective predictive Energy Management Strategy (EMS) tailored for Hybrid Renewable Energy Systems (HRES) onboard autonomous marine vessels, representing a significant advancement beyond existing methodologies. Unlike prior research that primarily emphasizes minimizing fuel consumption, the proposed approach concurrently optimizes fuel usage, renewable energy integration, and pure-electric sailing duration, achieving a balanced operational performance.

Previous studies, such as those by Roslan et al. [248] and Chan et al. [255] employed Rule-Based (RB) and Equivalent Consumption Minimization Strategy (ECMS) algorithms for hybrid propulsion. However, these conventional methods often neglect the influence of dynamic environmental conditions and system uncertainties. In contrast, the proposed Nonlinear Model Predictive Control integrated with Grey Wolf Optimization (NMPC-GWO) explicitly incorporates such variabilities, resulting in improved system adaptability and efficiency.

Compared to the RB method, which demonstrated suboptimal energy distribution and higher emissions, the NMPC-GWO algorithm consistently outperformed in terms of fuel efficiency, emissions reduction, and effective load balancing, particularly under fluctuating wind conditions. This highlights the critical advantage of adaptive and predictive control strategies over static frameworks in marine hybrid energy management.

Furthermore, the NMPC-GWO results align with findings by Chen et al. [250], on NMPC applications in tugboats but offer enhanced computational efficiency and dynamic responsiveness. The sensitivity analysis reinforced the algorithm's robustness by demonstrating stable performance across a range of operational scenarios, validating its reliability for real-time implementation in autonomous maritime propulsion systems.

5.4. Conclusion

In this research presents an innovative multi-objective predictive Energy Management System (EMS) for optimizing Hybrid Renewable Energy Systems (HRES) in autonomous ships. By integrating advanced predictive-metaheuristic algorithms—namely NMPC-GWO, NMPC-GA, and Rule-Based (RB) methods—the study addresses fuel consumption, emissions, renewable energy integration, and pure-electric sailing duration within a unified framework. A realistic modeling approach incorporates random wave effects on propeller load torque, with state estimation supported by an Extended Kalman Filter to improve prediction accuracy.

The NMPC-GWO algorithm demonstrated superior performance in fuel efficiency, emission reduction, and computational speed, outperforming NMPC-GA and RB methods. This superiority was quantitatively confirmed through standard regression metrics—Root Mean Squared Error (RMSE), Mean Absolute Error (MAE), and coefficient of determination (R^2)—which highlighted NMPC-GWO's accuracy and reliability in predicting fuel consumption and emissions compared to a conventional diesel-only baseline. Sensitivity analyses further verified the robustness and adaptability of the NMPC-GWO under varying operational parameters such as vessel speed, wind conditions, and towing forces, confirming its suitability for real-time energy management in dynamic maritime environments.

Ultimately, this study offers a comprehensive and adaptable energy management framework that advances the integration of renewable energy sources in autonomous vessel propulsion and power systems.

For future work, real-world validation through experimental testing or sea trials on autonomous vessels is recommended to assess the practical performance of the proposed system. Additionally, the EMS framework can be extended to other vessel types, such as ferries and cargo ships, to evaluate its scalability. Further enhancement may include integrating alternative renewable energy sources like fuel cells or wave energy converters into the HRES model for broader applicability and improved sustainability. Moreover, efforts will focus on optimizing the computational efficiency of the NMPC-GWO algorithm to enable real-time implementation in dynamic maritime environments.

CHAPTER 6. CONCLUSION AND FUTURE WORKS

The maritime industry remains a significant contributor to global GHG emissions, notably sulfur oxides (SO_x), nitrogen oxides (NO_x), and carbon dioxide (CO_2), primarily due to the incomplete combustion of conventional marine fuels. Recent studies have shown that maritime operations account for over 13% of global SO_x emissions, prompting the enforcement of stringent regulatory frameworks such as the IMO 2020 sulfur cap, which mandates a maximum sulfur content of 0.50% m/m in marine fuels. In parallel, the IMO has set ambitious long-term decarbonization targets, including a 50% reduction in CO_2-equivalent emissions from international shipping by 2050 relative to 2008 levels. These regulatory measures underscore the urgent need for the development and integration of cleaner, more sustainable marine propulsion technologies and energy management systems to ensure environmental compliance and support the global transition toward low-emission maritime transport.

This thesis has addressed these challenges by developing a comprehensive framework for the energy management of both conventional and fully autonomous short-sea vessels. It presents a multi-faceted investigation into sustainable energy solutions, focusing on three core areas: hybrid renewable energy integration, alternative marine fuel evaluation, and predictive energy management under dynamic operating conditions.

Firstly, this research addresses a critical gap in marine energy systems research by proposing and optimizing standalone hybrid renewable energy systems (HRES) for both conventional and fully autonomous tugboats, a topic largely overlooked in existing literature. Unlike prior studies that either focused on partial operational periods or lacked robustness and statistical validation, this research introduces a comprehensive techno-economic and environmental assessment framework integrating PV, VAWT, battery storage, and diesel Gensets. Five HRES configurations were evaluated using advanced metaheuristic algorithms —specifically the ABC, PSO, GA—alongside HOMER Pro software, the study identifies the Genset/PV/VAWT/Battery configuration (Case 1) as the optimal power architecture. Results show that the ABC algorithm consistently delivers superior performance across all configurations, achieving the lowest annualized cost of system (ACS), total net present cost (TNPC), levelized cost of energy (LCOE), and CO_2 emissions, owing to its enhanced convergence rate and optimization efficiency. The fully autonomous tugboat,

benefiting from reduced operational load and higher renewable energy integration, demonstrated significantly lower emissions and energy costs compared to its conventional counterpart. Robustness tests further confirmed the model's resilience under varying operational and environmental conditions, while one-way ANOVA and Tukey post-hoc analyses validated the statistical significance of the optimization results, identifying the ABC algorithm as the most effective among the tested methods. These findings underscore the viability and economic advantage of integrating renewable energy into autonomous marine propulsion systems and contribute to the strategic design of low-emission, high-efficiency hybrid marine power systems in compliance with IMO decarbonization goals. Ultimately, this research offers a novel decision-support framework for shipboard HRES integration, applicable to diverse vessel types and operational profiles.

Secondly, in response to the ongoing challenge of identifying the most viable alternative fuel for short-sea shipping vessels, this study addresses key gaps in the literature by integrating dynamic, geospatially-informed bottom-up methodologies to assess fuel consumption, emissions, and cost implications across various vessel types and operational profiles. Despite a robust body of research on alternative marine fuels, few studies simultaneously evaluate the environmental and economic performance of these fuels in the context of high-speed, short-sea, and autonomous operations. This study contributes to the marine engineering field by developing a comprehensive Python-based mathematical model that utilizes AIS data, vessel specifications, and port information to simulate operational conditions and evaluate multiple marine fuels against key performance indicators (TMER, TGWP, TEI, TEDC, NPV). Our analysis reveals that LNG emerges as the optimal marine fuel, offering the highest economic returns and lowest environmental impact across both conventional and fully autonomous high-speed passenger ferries and tugboats. Furthermore, the incorporation of sensitivity and stochastic analyses distinguishes this research by capturing the influence of operational variability and economic uncertainty—factors often omitted in prior studies. These findings align with existing literature on the benefits of cleaner fuels and fuel cell technologies but advance the discourse by demonstrating how autonomy enhances fuel efficiency and profitability. Our work not only provides a decision-support framework for stakeholders seeking compliance with IMO regulations but also underscores the feasibility of integrating alternative fuels within next-generation vessel designs, thereby contributing a practical, scalable tool for sustainable marine engineering.

Lastly, the problem addressed in this study centers on the lack of robust, comprehensive EMS frameworks for optimizing HRES in fully autonomous vessels, particularly under dynamic marine environmental conditions. Existing literature primarily focuses on limited emission types, omits key ship dynamic influences, and lacks sensitivity analyses and comprehensive emission metrics like EEOI, resulting in suboptimal power distribution strategies. In response, this study introduces a multi-objective predictive EMS for a fully autonomous tugboat integrating PV arrays, VAWTs, battery banks, and diesel-based power sources. Using a nonlinear model predictive control (NMPC) scheme enhanced with metaheuristic algorithms—GWO and GA—the proposed system dynamically allocates power while incorporating wave-induced disturbances filtered via an Extended Kalman Filter. Our contributions lie in modeling realistic ship dynamics (including wind/current resistance), optimizing fuel use and emission costs, and accounting for all key pollutants (CO_2, NO_x, SO_x, PM, CH_4, CO, N_2O). The model is benchmarked against a traditional rule-based (RB) method, with NMPC-GWO outperforming all others in minimizing fuel consumption, emissions, and EEOI. Sensitivity analysis further validates the robustness of the proposed system to environmental and operational variations. These findings align with and extend existing marine energy research by integrating predictive EMS with adaptive optimization and regulatory compliance, thereby advancing the operational viability of low-emission autonomous marine propulsion systems. This study offers a scalable, regulation-aware approach to enhancing sustainability and efficiency in next-generation shipboard power systems, in line with IMO decarbonization objectives.

Future works should focus on the real-world implementation and validation of the proposed systems to bridge the gap between simulation and operational deployment. For the HRES configuration aboard tugboats, sea trials on both conventional and fully autonomous platforms are essential to assess system resilience across varying navigational routes, shiploads, and climatic conditions. The modeling framework should also be extended to other vessel types, such as ferries or offshore supply vessels, to test scalability and adaptability.

In the context of marine alternative fuels, future studies should consider the long-term economic impacts of fluctuating fuel prices, regulatory developments, and infrastructure readiness. Expanding the fuel assessment to include emerging alternatives such as biofuels, hydrogen, and ammonia will enhance strategic foresight for sustainable shipping. Furthermore, comprehensive

life cycle assessments (LCAs) of these fuels—from cradle to grave—should be conducted to capture their full environmental impact, including feedstock extraction, production, transportation, on-board usage, and end-of-life emissions. This will ensure a holistic evaluation of each fuel's sustainability profile beyond tailpipe emissions alone.

Regarding the energy management system (EMS) architecture, the next phase should involve hardware-in-the-loop simulations and field trials to evaluate controller responsiveness under real-time marine dynamics. Integrating additional renewable technologies—such as wave energy converters or marine fuel cells—could further enhance energy diversity and operational sustainability. Across all systems, improving access to high-fidelity sensor data from autonomous vessels will enable more accurate modeling, ultimately strengthening the reliability and decision-making capabilities of sustainable marine energy systems.

Moreover, this study has already demonstrated the value of predictive control through the application of nonlinear model predictive control (NMPC), which leverages system dynamics to optimize performance over a finite prediction horizon. Building on this foundation, the integration of Artificial Intelligence (AI) techniques presents a promising direction for future research. AI-driven approaches—such as reinforcement learning, deep learning, and data-driven predictive analytics—could enhance the adaptability and robustness of energy management systems by enabling real-time, self-learning control strategies tailored to complex and dynamic marine environments.

These techniques could also support multi-objective optimization in evaluating marine alternative fuels, balancing environmental performance, cost efficiency, and regulatory constraints under uncertain operating conditions. In hybrid power configurations, AI can be leveraged to process high-fidelity sensor data from autonomous vessels, improving forecasting accuracy, anomaly detection, and decision-making. Incorporating AI into future system architectures would complement the current NMPC-based framework, aligning with the broader vision of intelligent, autonomous, and sustainable maritime operations.

REFERENCES

[1] UN Trade and Development (UNCTAD), "Ports in the global liner shipping network: Understanding their position, connectivity, and changes over time." Accessed: Apr. 04, 2023. [Online]. Available: https://unctad.org/news/ports-global-liner-shipping-network-understanding-their-position-connectivity-and-changes-over?

[2] "Marine Fuels: What is Heavy Fuel Oil?," Clear Seas. Accessed: Apr. 07, 2022. [Online]. Available: https://clearseas.org/en/blog/marine-fuels-what-is-heavy-fuel-oil/

[3] IMO, MARINE ENVIRONMENTAL PROTECTION, "IMO 2020 – cutting sulphur oxide emissions." Accessed: Apr. 07, 2022. [Online]. Available: https://www.imo.org/en/MediaCentre/HotTopics/Pages/Sulphur-2020.aspx

[4] H. M. Stein, "How to achieve energy efficiency excellence," Maritime. Accessed: Feb. 02, 2022. [Online]. Available: https://www.dnv.com/article/how-to-achieve-energy-efficiency-excellence-102139

[5] K. Chopra, "What is Ship Energy Efficiency Management Plan?" Accessed: Feb. 02, 2022. [Online]. Available: https://www.marineinsight.com/maritime-law/what-is-ship-energy-efficiency-management-plan/

[6] S. Parker, C. Raucci, T. Smith, and L. Laffineur, "Understanding the Energy Efficiency Operational Indicator: An empirical analysis of ships from the Royal Belgian Shipowners' Association."

[7] A. Haseltalab and R. R. Negenborn, "Model predictive maneuvering control and energy management for all-electric autonomous ships," *Appl. Energy*, vol. 251, no. 113308, pp. 1–27, May 2018, doi: 10.1016/j.apenergy.2019.113308.

[8] M. Höyhtyä, J. Huusko, M. Kiviranta, K. Solberg, and J. Rokka, "Connectivity for Autonomous Ships: Architecture, Use Cases, and Research Challenges," in *ViRePAS - Virtual Research Platform for Autonomous Ships*, Jeju Island, Korea: Research Gate, Oct. 2017, pp. 1–7. doi: 10.1109/ICTC.2017.8191000.

[9] Z. Pietrzykowski, J. Pietrzykowski, and J. Hajduk, “Operations of Maritime Autonomous Surface Ships,” *TRANSNAV Int. J. Mar. Navig. Saf. Sea Transp.*, vol. 13, no. 4, pp. 725–733, Dec. 2019.

[10] IMO, “MEPC 74/7/2. Reduction of GHG emissions from ships. Energy efficiency improvement measure for existing ships.,” Japan, Mar. 2019. Accessed: Nov. 10, 2023. [Online]. Available: https://www.intercargo.org/wp-content/uploads/2019/09/Paper-GHG%E2%80%93-Short-term-EEXI-past-verion.pdf

[11] International Maritime Organization (IMO), “2023 IMO Strategy on Reduction of GHG Emissions from Ships.” Accessed: Sep. 18, 2024. [Online]. Available: https://www.imo.org/en/OurWork/Environment/Pages/2023-IMO-Strategy-on-Reduction-of-GHG-Emissions-from-Ships.aspx

[12] Marine Environment Protection Committee (MEPC), “MEPC.328(76) - 2021 AMENDMENTS TO THE ANNEX OF THE PROTOCOL OF 1997 TO AMEND THE INTERNATIONAL CONVENTION FOR THE PREVENTION OF POLLUTION FROM SHIPS, 1973, AS MODIFIED BY THE PROTOCOL OF 1978 RELATING THERETO.” Accessed: Jan. 03, 2023. [Online]. Available: https://wwwcdn.imo.org/localresources/en/OurWork/Environment/Documents/Air%20pollution/MEPC.328(76).pdf

[13] G. Dobie, J. Whitehead, D. Didt, H. Kidston, and D.-M. Ciobanu, “Global Claims Review Liability In Focus - Loss trends and emerging risks for businesses,” Top causes of liability loss per line of business (by value of claims). Accessed: Feb. 01, 2022. [Online]. Available: https://www.agcs.allianz.com/content/dam/onemarketing/agcs/agcs/reports/AGCS-Global-Claims-Review-2017.pdf

[14] A. Amro, V. Gkioulos, and S. Katsikas, “Connect and Protect: Requirements for Maritime Autonomous Surface Ship in Urban Passenger Transportation,” in *Computer Security*, Springer Link, Feb. 2020, pp. 69–85. doi: 10.1007/2F978-3-030-42048-2_5.

[15] Geo Garage, “Rolls-Royce demonstrates fully autonomous passenger ferry in Finland,” Plain sailing. Accessed: Feb. 01, 2022. [Online]. Available: https://blog.geogarage.com/2018/12/rolls-royce-demonstrates-fully.html

[16] S. Li and K. S. Fung, “Maritime autonomous surface ships (MASS): implementation and legal issues,” *Emerald Publ. Ltd.*, vol. 4, no. 2397–3757, pp. 330–339, Nov. 2019, doi: 10.1108/MABR-01-2019-0006.

[17] Kevin Daffey, “Technology Progression of Maritime Autonomous Surface Ships,” presented at the MSC 100 - One hundred sessions enhancing safety and security of international shipping, London, Dec. 03, 2018. Accessed: Jan. 23, 2022. [Online]. Available: https://wwwcdn.imo.org/localresources/en/MediaCentre/IMOMediaAccreditation/Documents/MSC%20100%20special%20session%20presentations/20181203_Technology_Progression_In_MASS_IMO_Final_For_PDF.pdf

[18] M. Belabyad, C. Kontovas, R. Pyne, and C.-H. Chang, “Skills and competencies for operating maritime autonomous surface ships (MASS): a systematic review and bibliometric analysis,” *Marit. Policy Manag.*, Mar. 2025, Accessed: Apr. 05, 2025. [Online]. Available: https://www.tandfonline.com/doi/abs/10.1080/03088839.2025.2475177

[19] Rolls-Royce, “Autonomous ships The next step,” *Rolls-Royce plc 2016*, vol. 06, no. 2016, pp. 1–8, 2016.

[20] Wright, Glenn R., *Unmanned and Autonomous Ships: An Overview of Mass*, First. New York: CRC Press, 2020. Accessed: Feb. 02, 2022. [Online]. Available: https://books.google.ca/books?id=fxPWDwAAQBAJ&printsec=frontcover&source=gbs_ViewAPI&redir_esc=y#v=onepage&q&f=false

[21] A. Farnsworth, “Auto-docking - a giant leap for passenger vessels,” Wartsila.com. Accessed: Apr. 08, 2022. [Online]. Available: https://www.wartsila.com/insights/article/auto-docking---a-giant-leap-for-passenger-vessels

[22] Finferries, “Finferries’ Falco world’s first fully autonomous ferry,” Finferries. Accessed: Apr. 08, 2022. [Online]. Available: https://www.finferries.fi/en/news/press-releases/finferries-falco-worlds-first-fully-autonomous-ferry.html

[23] ABB, “Suomenlinna II,” ABB took a groundbreaking next step in autonomous shipping with a remote control trial of passenger ferry Suomenlinna II. Accessed: Feb. 01, 2022. [Online]. Available: https://new.abb.com/marine/marine-references/suomenlinna-ii

[24] P. Dean, T. Walters, J. Goulding, and H. Clack, “Autonomous ships: MASS for the MASSes,” HFW. Accessed: Apr. 08, 2023. [Online]. Available: https://www.hfw.com/insights/autonomous-ships-mass-for-the-masses/

[25] Adams. Simon, “ReVolt – next generation short sea shipping,” DNV. Accessed: Apr. 08, 2022. [Online]. Available: https://www.dnv.com/news/revolt-next-generation-short-sea-shipping-7279/

[26] Norwegian University of Science and Technology, “Autoferry - NTNU.” Accessed: Apr. 08, 2023. [Online]. Available: https://www.ntnu.edu/autoferry

[27] Science Business Publishing Ltd., “NTNU trials world’s first urban autonomous passenger ferry.” Accessed: Apr. 08, 2022. [Online]. Available: https://sciencebusiness.net/network-updates/ntnu-trials-worlds-first-urban-autonomous-passenger-ferry

[28] H. Yukinori, “Japanese Consortium Ticks Off Autonomous Shipping Milestone,” nippon.com. Accessed: Apr. 08, 2023. [Online]. Available: https://www.nippon.com/en/japan-topics/g02047/

[29] Sym Naval, “First autonomous vessels already sailing in Japan.” Accessed: Apr. 08, 2023. [Online]. Available: https://sym-naval.com/blog/autonomous-vessels-japan/

[30] Yara International ASA, “Yara Birkeland, two years on,” Yara None. Accessed: Apr. 08, 2023. [Online]. Available: https://www.yara.com/knowledge-grows/yara-birkeland-two-years-on/

[31] S. Papageorgiou, “Ongoing MASS projects in Norway.” Accessed: Nov. 11, 2024. [Online]. Available: https://wwwcdn.imo.org/localresources/en/About/Events/Documents/2024%20IMO-ROK%20MASS%20Symposium%20presentations/1-1.%20Ongoing%20MASS%20projects%20in%20Norway%20-%20Sifis%20Papageorgiou%20(Norway%20Maritime%20Authority).pdf

[32] X. Tu, B. Yan, Z. Tu, and S. H. Chan, “A novel development of an unmanned surface vehicle directly powered by an air-cooled proton exchange membrane fuel cell stack,” *Appl. Energy*, vol. 374, p. 124002, Nov. 2024, doi: 10.1016/j.apenergy.2024.124002.

[33] J. Renau *et al.*, “Design, development, integration and evaluation of hybrid fuel cell power systems for an unmanned water surface vehicle,” *Int. J. Hydrog. Energy*, vol. 54, pp. 1273–1285, Feb. 2024, doi: 10.1016/j.ijhydene.2023.12.043.

[34] Y. Li, Y. Guo, and Y. Zhang, “Equivalent Consumption Minimization Energy Management Strategy Based on Frequency Decoupling for Unmanned Surface Vehicle,” in *2023 3rd International Conference on Energy, Power and Electrical Engineering (EPEE)*, Sep. 2023, pp. 1261–1267. doi: 10.1109/EPEE59859.2023.10351889.

[35] J. Fu, H. You, J. wei Zhao, X. Li, Y. Xu, and X. Wu, “An Energy control strategy of fuel cell hybrid Unmanned Surface Vehicle based on PMP algorithm,” in *2020 Chinese Automation Congress (CAC)*, Nov. 2020, pp. 6260–6264. doi: 10.1109/CAC51589.2020.9326546.

[36] T. Zaman *et al.*, “Endurance Driven Energy Management System for All-Electric Marine Autonomous Surface Vehicle,” in *IECON 2022 – 48th Annual Conference of the IEEE Industrial Electronics Society*, Oct. 2022, pp. 1–6. doi: 10.1109/IECON49645.2022.9968947.

[37] P. F. Rynne and K. D. von Ellenrieder, “Development and Preliminary Experimental Validation of a Wind- and Solar-Powered Autonomous Surface Vehicle,” *IEEE J. Ocean. Eng.*, vol. 35, no. 4, pp. 971–983, Oct. 2010, doi: 10.1109/JOE.2010.2078311.

[38] S. D. Kristensen, Dallolio ,A., and I. B. and Utne, “A systems approach to hazard identification for solar-powered and wave-propelled unmanned surface vehicle,” *J. Mar. Eng. Technol.*, vol. 23, no. 2, pp. 122–134, Mar. 2024, doi: 10.1080/20464177.2024.2315646.

[39] E. Eide *et al.*, “The Autonomous Urban Passenger Ferry milliAmpere2: Design and Testing,” *J. Offshore Mech. Arct. Eng.*, vol. 147, no. 031409, Jan. 2025, doi: 10.1115/1.4067370.

[40] J. S. Wolfe *et al.*, “Evaluation of the Energy Budget of a Solar Powered Autonomous Surface Vehicle,” in *OCEANS 2023 - Limerick*, Jun. 2023, pp. 1–6. doi: 10.1109/OCEANSLimerick52467.2023.10244732.

[41] A. Riccobono *et al.*, “A comparison of multi-source power supply systems for autonomous marine vehicles: The SWAMP case study,” *Int. J. Hydrog. Energy*, vol. 80, pp. 1124–1136, Aug. 2024, doi: 10.1016/j.ijhydene.2024.07.206.

[42] G. Zhang, J. Li, T. Chang, W. Zhang, and L. Song, “Autonomous navigation and control for a sustainable vessel: A wind-assisted strategy,” *Sustain. Horiz.*, vol. 13, p. 100117, Mar. 2025, doi: 10.1016/j.horiz.2024.100117.

[43] L. Chen, A. Haseltalab, V. Garofano, and R. R. Negenborn, “Eco-VTF: Fuel-Efficient Vessel Train Formations for All-Electric Autonomous Ships,” in *2019 18th European Control Conference (ECC)*, Jun. 2019, pp. 2543–2550. doi: 10.23919/ECC.2019.8796033.

[44] A. Makhsoos *et al.*, “Design, simulation and experimental evaluation of energy system for an unmanned surface vehicle,” *Energy*, vol. 148, pp. 362–372, Apr. 2018, doi: 10.1016/j.energy.2018.01.158.

[45] K. Sornek *et al.*, “Development of a solar-powered small autonomous surface vehicle for environmental measurements,” *Energy Convers. Manag.*, vol. 267, p. 115953, Sep. 2022, doi: 10.1016/j.enconman.2022.115953.

[46] A. Ait Allal, K. Mansouri, M. Youssfi, and M. Qbadou, “Toward energy saving and environmental protection by implementation of autonomous ship,” in *Mediterranean Electrotechnical Conference (MELECON)*, Marrakech, Morocco: IEEE Xplore, May 2018, pp. 177–180. doi: 10.1109/MELCON.2018.8379089.

[47] H. Laryea and A. Schiffauerova, “Environmental and Cost Assessments of Marine Alternative Fuels for Fully Autonomous Short-Sea Shipping Vessels Based on the Global Warming Potential Approach,” *J. Mar. Sci. Eng.*, vol. 12, no. 11, Art. no. 11, Nov. 2024, doi: 10.3390/jmse12112026.

[48] H. Laryea and A. Schiffauerova, “A novel standalone hybrid renewable energy systems onboard conventional and autonomous tugboats,” *Energy*, vol. 303, p. 131948, Sep. 2024, doi: 10.1016/j.energy.2024.131948.

[49] J. L. D. Dantas and G. Theotokatos, “A framework for the economic-environmental feasibility assessment of short-sea shipping autonomous vessels,” *Ocean Eng.*, vol. 279, p. 114420, Jul. 2023, doi: 10.1016/j.oceaneng.2023.114420.

[50] J.-P. Rodrigue and T. Notteboom, "5.4 – Maritime Transportation | The Geography of Transport Systems." Accessed: Feb. 27, 2023. [Online]. Available: https://transportgeography.org/contents/chapter5/maritime-transportation/

[51] "Visualization for World merchant fleet data (2016 -2021)," infomaritime.eu. Accessed: Dec. 01, 2021. [Online]. Available: http://infomaritime.eu/index.php/2021/08/22/top-15-shipowning-countries/

[52] "10 Largest Ports in the world," Shipa Freight. Accessed: Dec. 01, 2021. [Online]. Available: https://www.shipafreight.com/knowledge-series/largest-ports-in-the-world/

[53] L. Mofor, P. Nuttall, and A. Newell, "Renewable Energy Options for Shipping - Technology Brief," Jan. 2015, Accessed: Feb. 10, 2023. [Online]. Available: https://www.irena.org/-/media/Files/IRENA/Agency/Publication/2015/IRENA_Tech_Brief_RE_for-Shipping_2015.pdf

[54] MARPOL, "Annex VI of MARPOL." Accessed: Jun. 27, 2022. [Online]. Available: https://www.imo.org/About/Conventions/ListOfConventions/%20Pages/International-Convention-for-the-Prevention-of-Pollution-from-Ships-(MARPOL).aspx

[55] International Renewable Energy Agency (IRENA), "Renewable Energy Options for Shipping - Technology Brief", Accessed: Jan. 01, 2022. [Online]. Available: https://www.irena.org/-/media/Files/IRENA/Agency/Publication/2015/IRENA_Tech_Brief_RE_for-Shipping_2015.pdf

[56] M. Baldauf, T. Fonseca, R. Mehdi, and M. Kitada, "Conventional Vessels and Marine Autonomous Surface Ships – A Love Marriage?," presented at the Autonomous Shipping in inland navigation 2018, Geneva, Switzerland, Feb. 14, 2018. Accessed: Jan. 24, 2022. [Online]. Available: https://unece.org/fileadmin/DAM/trans/doc/2018/sc3wp3/10._WMU.pdf

[57] U. Marine, "Autonomous Ships! Is It the End Game for Seafarers?," UNITEAM MARINE. Accessed: Jun. 27, 2022. [Online]. Available: https://www.uniteammarine.com/autonomous-ships-is-it-the-end-game-for-seafarers/

[58] International Renewable Energy Agenc (IRENA), “Renewable Power Generation Costs in 2021.” Accessed: Nov. 21, 2022. [Online]. Available: https://www.irena.org/publications/2022/Jul/Renewable-Power-Generation-Costs-in-2021

[59] T. Ma, H. Yang, and L. Lu, “A feasibility study of a stand-alone hybrid solar–wind–battery system for a remote island,” *Appl. Energy*, vol. 121, pp. 149–158, May 2014, doi: 10.1016/j.apenergy.2014.01.090.

[60] A. S. O. Ogunjuyigbe, T. R. Ayodele, and O. A. Akinola, “Optimal allocation and sizing of PV/Wind/Split-diesel/Battery hybrid energy system for minimizing life cycle cost, carbon emission and dump energy of remote residential building,” *Appl. Energy*, vol. 171, pp. 153–171, Jun. 2016, doi: 10.1016/j.apenergy.2016.03.051.

[61] M. Z. Farahmand, M. E. Nazari, and S. Shamlou, “Optimal sizing of an autonomous hybrid PV-wind system considering battery and diesel generator,” in *2017 Iranian Conference on Electrical Engineering (ICEE)*, May 2017, pp. 1048–1053. doi: 10.1109/IranianCEE.2017.7985194.

[62] B. Zhao, X. Zhang, P. Li, K. Wang, M. Xue, and C. Wang, “Optimal sizing, operating strategy and operational experience of a stand-alone microgrid on Dongfushan Island,” *Appl. Energy*, vol. 113, pp. 1656–1666, Jan. 2014, doi: 10.1016/j.apenergy.2013.09.015.

[63] A. Vicenzutti, R. Menis, and G. Sulligoi, “All-Electric Ship-Integrated Power Systems: Dependable Design Based on Fault Tree Analysis and Dynamic Modeling,” *IEEE Trans. Transp. Electrification*, vol. 5, no. 3, pp. 812–827, Sep. 2019, doi: doi: 10.1109/TTE.2019.2920334.

[64] X. Sun, C. Yao, E. Song, Q. Yang, and X. Yang, “Optimal control of transient processes in marine hybrid propulsion systems: Modeling, optimization and performance enhancement,” *Appl. Energy*, vol. 321, p. 119404, Sep. 2022, doi: https://doi.org/10.1016/j.apenergy.2022.119404.

[65] Z. Wang *et al.*, “Optimizing Energy Management and Case Study of Multi-Energy Coupled Supply for Green Ships,” *J. Mar. Sci. Eng.*, vol. 11, no. 7, Art. no. 7, Jul. 2023, doi: https://doi.org/10.3390/jmse11071286.

[66] Y. Ren, L. Zhang, P. Shi, and Z. Zhang, "Research on Multi-Energy Integrated Ship Energy Management System Based on Hierarchical Control Collaborative Optimization Strategy," *J. Mar. Sci. Eng.*, vol. 10, no. 10, Art. no. 10, Oct. 2022, doi: https://doi.org/10.3390/jmse10101556.

[67] Y. Yuan, J. Wang, X. Yan, B. Shen, and T. Long, "A review of multi-energy hybrid power system for ships," *Elsevier*, vol. 132, no. 110081, pp. 1–15, Jun. 2020, doi: 10.1016.

[68] M. U. Mutarraf, Y. Terriche, K. A. K. Niazi, J. C. Vasquez, and J. M. Guerrero, "Energy Storage Systems for Shipboard Microgrids—A Review," *Energies*, vol. 11, no. 12, Art. no. 12, Dec. 2018, doi: 10.3390/en11123492.

[69] S. Antonopoulos, K. Visser, M. Kalikatzarakis, and V. Reppa, "MPC Framework for the Energy Management of Hybrid Ships with an Energy Storage System," *J. Mar. Sci. Eng.*, vol. 9, no. 9, Art. no. 9, Sep. 2021, doi: https://doi.org/10.3390/jmse9090993.

[70] O. B. Inal, J.-F. Charpentier, and C. Deniz, "Hybrid power and propulsion systems for ships: Current status and future challenges," *Renew. Sustain. Energy Rev.*, vol. 156, p. 111965, Mar. 2022, doi: 10.1016/j.rser.2021.111965.

[71] F. Mylonopoulos, H. Polinder, and A. Coraddu, "A Comprehensive Review of Modeling and Optimization Methods for Ship Energy Systems," *IEEE Access*, vol. 11, pp. 32697–32707, 2023, doi: 10.1109/ACCESS.2023.3263719.

[72] A. M. Aboelezz, B. E. Sedhom, M. M. El-Saadawi, A. A. Eladl, and P. Siano, "State-of-the-Art Review on Shipboard Microgrids: Architecture, Control, Management, Protection, and Future Perspectives," *Smart Cities*, vol. 6, no. 3, Art. no. 3, Jun. 2023, doi: https://doi.org/10.3390/smartcities6030069.

[73] S. Wen *et al.*, "Optimal sizing of hybrid energy storage sub-systems in PV/diesel ship power system using frequency analysis," *Energy*, vol. 140, pp. 198–208, Dec. 2017, doi: 10.1016/j.energy.2017.08.065.

[74] R. Yang, Y. Yuan, R. Ying, B. Shen, and T. Long, "A Novel Energy Management Strategy for a Ship's Hybrid Solar Energy Generation System Using a Particle Swarm Optimization Algorithm," *Energies*, vol. 13, no. 6, Art. no. 6, Jan. 2020, doi: 10.3390/en13061380.

[75] A. Bouhouta, S. Moulahoum, and N. Kabache, “Hybrid backup energy based on PV/Wind system for marine tugboat: A case study of ASD tug of Arzew port in Algeria,” *Wind Eng.*, vol. 46, no. 5, pp. 1343–1358, Oct. 2022, doi: 10.1177/0309524X221077455.

[76] S. Wen, H. Lan, J. Dai, Y.-Y. Hong, D. C. Yu, and L. Yu, “Economic Analysis of Hybrid Wind/PV/Diesel/ESS System on a Large Oil Tanker,” *Electr. Power Compon. Syst.*, vol. 45, no. 7, pp. 705–714, Apr. 2017, doi: 10.1080/15325008.2017.1292569.

[77] Y. Si, R. Wang, S. Zhang, W. Zhou, A. Lin, and G. Zeng, “Configuration optimization and energy management of hybrid energy system for marine using quantum computing,” *Energy*, vol. 253, p. 124131, Aug. 2022, doi: 10.1016/j.energy.2022.124131.

[78] K. Kusakana and H. J. Vermaak, “Hybrid diesel generator/renewable energy system performance modeling,” *Renew. Energy*, vol. 67, pp. 97–102, Jul. 2014, doi: 10.1016/j.renene.2013.11.025.

[79] Unacademy, “Brake Thermal Efficiency,” Unacademy. Accessed: Nov. 12, 2022. [Online]. Available: https://unacademy.com/content/gate/study-material/mechanical-engineering/brake-thermal-efficiency/

[80] F. K. Abo-Elyousr and A. Elnozahy, “Bi-objective economic feasibility of hybrid micro-grid systems with multiple fuel options for islanded areas in Egypt,” *Renew. Energy*, vol. 128, pp. 37–56, Dec. 2018, doi: 10.1016/j.renene.2018.05.066.

[81] A. Maleki and F. Pourfayaz, “Sizing of stand-alone photovoltaic/wind/diesel system with battery and fuel cell storage devices by harmony search algorithm,” *J. Energy Storage*, vol. 2, pp. 30–42, Aug. 2015, doi: 10.1016/j.est.2015.05.006.

[82] “Greenhouse-Gas-Calculations.” Accessed: Apr. 13, 2023. [Online]. Available: https://plan.sa.gov.au/__data/assets/pdf_file/0007/574531/Appendix-O-Greenhouse-Gas-Calculations.pdf

[83] F. S. Mahmoud, A. M. Abdelhamid, A. Al Sumaiti, A.-H. M. El-Sayed, and A. A. Z. Diab, “Sizing and Design of a PV-Wind-Fuel Cell Storage System Integrated into a Grid Considering the Uncertainty of Load Demand Using the Marine Predators Algorithm,” *Mathematics*, vol. 10, no. 19, Art. no. 19, Nov. 2022, doi: 10.3390/math10193708.

[84] A. A. Z. Diab, H. M. Sultan, and O. N. Kuznetsov, “Optimal sizing of hybrid solar/wind/hydroelectric pumped storage energy system in Egypt based on different meta-heuristic techniques,” *Environ. Sci. Pollut. Res.*, vol. 27, no. 26, pp. 32318–32340, Sep. 2020, doi: 10.1007/s11356-019-06566-0.

[85] A. H. Fathima and K. Palanisamy, “Optimization in microgrids with hybrid energy systems – A review,” *Renew. Sustain. Energy Rev.*, vol. 45, pp. 431–446, May 2015, doi: 10.1016/j.rser.2015.01.059.

[86] A. M. Jasim, B. H. Jasim, and V. Bureš, “A novel grid-connected microgrid energy management system with optimal sizing using hybrid grey wolf and cuckoo search optimization algorithm,” *Front. Energy Res.*, vol. 10, 2022, doi: https://doi.org/10.3389/fenrg.2022.960141.

[87] M. Mahmoud, M. Ramadan, M. A. Abdelkareem, and A. G. Olabi, “Chapter 3.1 - Introduction and definition of wind energy,” in *Renewable Energy - Volume 1 : Solar, Wind, and Hydropower*, A. G. Olabi, Ed., Academic Press, 2023, pp. 299–314. doi: 10.1016/B978-0-323-99568-9.00016-9.

[88] Luvside, “7 Advantages of Vertical Axis Wind Turbines (VAWT) | The Windy Blog,” https://www.luvside.de/en/. Accessed: Oct. 27, 2023. [Online]. Available: https://www.luvside.de/en/vawt-advantages/

[89] S. Singh, M. Singh, and S. C. Kaushik, “Feasibility study of an islanded microgrid in rural area consisting of PV, wind, biomass and battery energy storage system,” *Energy Convers. Manag.*, vol. 128, pp. 178–190, Nov. 2016, doi: 10.1016/j.enconman.2016.09.046.

[90] A. Maleki and F. Pourfayaz, “Optimal sizing of autonomous hybrid photovoltaic/wind/battery power system with LPSP technology by using evolutionary algorithms,” *Sol. Energy*, vol. 115, pp. 471–483, May 2015, doi: https://doi.org/10.1016/j.solener.2015.03.004.

[91] Lithium Hub, “What Are The Different Types Of Marine Batteries?,” https://lithiumhub.com/. Accessed: Dec. 30, 2023. [Online]. Available: https://lithiumhub.com/what-are-the-different-types-of-marine-batteries/

[92] EVLithium Limited, “Reliable and Efficient Power for Your Marine Vessel with LiFePO4 Batteries,” Evlithium. Accessed: Dec. 30, 2023. [Online]. Available: https://www.evlithium.com/Blog/lifepo4-batteries-for-your-marine-using.html

[93] J. Verma and D. Kumar, “Recent developments in energy storage systems for marine environment,” *Mater. Adv.*, vol. 2, no. 21, pp. 6800–6815, 2021, doi: 10.1039/D1MA00746G.

[94] T. Hussain *et al.*, “Standard Research -Alternative Fuels and Energy Systems for the Marine Sector,” Jul. 2020, Accessed: Dec. 08, 2023. [Online]. Available: https://www.csagroup.org/wp-content/uploads/CSA-Group-Research-Alternative-Marine-Fuels-and-Energy.pdf

[95] “Batteries on board ocean-going vessels - MAN Energy Solutions Future in the making.” Accessed: Dec. 30, 2023. [Online]. Available: https://www.man-es.com/docs/default-source/marine/tools/batteries-on-board-ocean-going-vessels.pdf?sfvrsn=deaa76b8_14

[96] M. Irandoostshahrestani and D. R. Rousse, “Photovoltaic Electrification and Water Pumping Using the Concepts of Water Shortage Probability and Loss of Power Supply Probability: A Case Study,” *Energies*, vol. 16, no. 1, Art. no. 1, Jan. 2023, doi: https://doi.org/10.3390/en16010001.

[97] M. Sufyan, N. A. Rahim, C. Tan, M. A. Muhammad, and S. R. S. Raihan, “Optimal sizing and energy scheduling of isolated microgrid considering the battery lifetime degradation,” *PLOS ONE*, vol. 14, no. 2, p. e0211642, Feb. 2019, doi: https://doi.org/10.1371/journal.pone.0211642.

[98] HOMER Pro 3.16, “Renewable Fraction - HOMER Pro 3.16.” Accessed: Mar. 23, 2024. [Online]. Available: https://support.ul-renewables.com/homer-manual-pro/_renewable_fraction.html

[99] P. Cheng, T. Pan, R. Li, and N. Liang, “Research on optimal matching of renewable energy power generation system and ship power system,” *IET Renew. Power Gener.*, vol. 16, no. 8, pp. 1649–1660, 2022, doi: https://doi.org/10.1049/rpg2.12470.

[100] D. Karaboğa, “AN IDEA BASED ON HONEY BEE SWARM FOR NUMERICAL OPTIMIZATION,” 2005. Accessed: Oct. 13, 2022. [Online]. Available:

https://www.semanticscholar.org/paper/AN-IDEA-BASED-ON-HONEY-BEE-SWARM-FOR-NUMERICAL-Karabo%C4%9Fa/cf20e34a1402a115523910d2a4243929f6704db1

[101] C. Gusain, M. Mohan Tripathi, and U. Nangia, "Study of Meta-heuristic Optimization Methodologies for Design of Hybrid Renewable Energy Systems," *Therm. Sci. Eng. Prog.*, vol. 39, p. 101711, Mar. 2023, doi: 10.1016/j.tsep.2023.101711.

[102] Z. Zheng, S. Yang, Y. Guo, X. Jin, and R. Wang, "Meta-heuristic Techniques in Microgrid Management: A Survey," *Swarm Evol. Comput.*, vol. 78, p. 101256, Apr. 2023, doi: 10.1016/j.swevo.2023.101256.

[103] A. Bouaouda and Y. Sayouti, "Hybrid Meta-Heuristic Algorithms for Optimal Sizing of Hybrid Renewable Energy System: A Review of the State-of-the-Art," *Arch. Comput. Methods Eng.*, vol. 29, no. 6, pp. 4049–4083, 2022, doi: 10.1007/s11831-022-09730-x.

[104] K. Ullah, Q. Jiang, G. Geng, S. Rahim, and R. A. Khan, "Optimal Power Sharing in Microgrids Using the Artificial Bee Colony Algorithm," *Energies*, vol. 15, no. 3, Art. no. 3, Jan. 2022, doi: 10.3390/en15031067.

[105] C. Altin, "Artificial Bee Colony Algorithm Based Very Fast Renewable Energy System Optimization Tool Design," in *2023 27th International Conference Electronics*, Jun. 2023, pp. 1–6. doi: 10.1109/IEEECONF58372.2023.10177657.

[106] D. K. Geleta, M. S. Manshahia, D. K. Geleta, and M. S. Manshahia, "Artificial Bee Colony-Based Optimization of Hybrid Wind and Solar Renewable Energy System," https://services.igi-global.com/resolvedoi/resolve.aspx?doi=10.4018/978-1-5225-9420-8.ch017. Accessed: Dec. 06, 2023. [Online]. Available: https://www.igi-global.com/gateway/chapter/www.igi-global.com/gateway/chapter/232103

[107] D. Karaboga and B. Basturk, "A powerful and efficient algorithm for numerical function optimization: artificial bee colony (ABC) algorithm," *J. Glob. Optim.*, vol. 39, no. 3, pp. 459–471, Nov. 2007, doi: https://doi.org/10.1007/s10898-007-9149-x.

[108] Marine Traffic, "MarineTraffic: Global Ship Tracking Intelligence | AIS Marine Traffic." Accessed: Aug. 16, 2022. [Online]. Available: https://www.marinetraffic.com/en/ais/home/centerx:-118.2/centery:33.7/zoom:11

[109] A. Ait Allal, K. Mansouri, M. Youssfi, and M. Qbadou, "Toward a Study of Environmental Impact of Shipping Industry and Proposal of Alternative Solutions," in *Advanced Intelligent Systems for Sustainable Development (AI2SD'2018)*, M. Ezziyyani, Ed., in Advances in Intelligent Systems and Computing. Cham: Springer International Publishing, 2019, pp. 245–256. doi: https://doi.org/10.1007/978-3-030-11881-5_21.

[110] J. Faber *et al.*, "Fourth IMO GHG Study 2020 - Full report and annexes," 2020. Accessed: Dec. 29, 2023. [Online]. Available: https://wwwcdn.imo.org/localresources/en/OurWork/Environment/Documents/Fourth%20IMO%20GHG%20Study%202020%20-%20Full%20report%20and%20annexes.pdf

[111] I. D. Dawangi and M. A. Budiyanto, "Ship Energy Efficiency Management Plan Development Using Machine Learning: Case Study of CO2 Emissions of Ship Activities at Container Port," Dec. 2021, doi: https://doi.org/10.14716/ijtech.v12i5.5183.

[112] P. Agand, A. Kennedy, T. Harris, C. Bae, M. Chen, and E. J. Park, "Fuel Consumption Prediction for a Passenger Ferry using Machine Learning and In-service Data: A Comparative Study," *Ocean Eng.*, vol. 284, p. 115271, Sep. 2023, doi: 10.1016/j.oceaneng.2023.115271.

[113] IMO, "IMO's work to cut GHG emissions from ships." Accessed: Jun. 14, 2024. [Online]. Available: https://www.imo.org/en/MediaCentre/HotTopics/Pages/Cutting-GHG-emissions.aspx

[114] P. Balcombe *et al.*, "How to decarbonise international shipping: Options for fuels, technologies and policies," *Energy Convers. Manag.*, vol. 182, pp. 72–88, Feb. 2019, doi: 10.1016/j.enconman.2018.12.080.

[115] A. Orthmann, S. Fitzgerald, J. Gerlach, A. McKee, and K. Reynolds, "ENERGY EFFICIENCY AND DECARBONIZATION TECHNICAL GUIDE." Nov. 01, 2022. Accessed: Oct. 10, 2023. [Online]. Available: https://www.maritime.dot.gov/sites/marad.dot.gov/files/2022-11/Energy%20Efficiency%20%26%20Decarbonization%20Technical%20Guide%20%2810-2022%29.pdf

[116] M. Campbell *et al.*, "REDUCTION OF GHG EMISSIONS FROM SHIPS Report on the study on the readiness and availability of low- and zero-carbon ship technology and marine fuels," Apr. 2023. Accessed: Sep. 09, 2023. [Online]. Available:

https://wwwcdn.imo.org/localresources/en/OurWork/Environment/Documents/FFT%20Project/MEPC80-INF.10%20-%20Summary%20report%20on%20the%20study%20.PDF

[117] RINA Italian Decarbonization Committee, "From Today to 2050: Challenges and Opportunities for the Maritime Industry." Oct. 15, 2023. Accessed: Jan. 25, 2024. [Online]. Available: https://scresources.rina.org/media/From-Today-to-2050-Challenges-and-Opportunities-for-the-Maritime-Industry.pdf

[118] Crown Oil Ltd, "Guide to Bunker Fuel," Crown Oil. Accessed: Jun. 14, 2024. [Online]. Available: https://www.crownoil.co.uk/guides/bunker-fuel-guide/

[119] M. Palmén, A. Lotrič, A. Laakso, V. Bolbot, M. Elg, and O. A. Valdez Banda, "Selecting Appropriate Energy Source Options for an Arctic Research Ship," *J. Mar. Sci. Eng.*, vol. 11, no. 12, Art. no. 12, Dec. 2023, doi: 10.3390/jmse11122337.

[120] Lubmarine, "Short Sea Shipping." Accessed: Jun. 14, 2023. [Online]. Available: https://lubmarine.totalenergies.com/maritime-industries/short-sea

[121] Port of Vancouver, "Short sea shipping | Port of Vancouver." Accessed: Jun. 14, 2024. [Online]. Available: https://www.portvancouver.com/marine-operations/short-sea-shipping/

[122] The Cooperative Logistics Network and J. M. B.-F. F. N. SOLUTIONS, "Advantages of short sea shipping for the container shipping industry," The Cooperative blog. Accessed: Jun. 14, 2024. [Online]. Available: https://www.thecooperativelogisticsnetwork.com/blog/2022/06/08/advantages-of-short-sea-shipping-in-the-container-shipping-industry/

[123] Clear Seas, "Think globally, ship locally: Short-sea shipping moves goods efficiently and reduces emissions." Accessed: Jun. 14, 2024. [Online]. Available: https://clearseas.org/insights/think-globally-ship-locally-short-sea-shipping-moves-goods-efficiently-and-reduces-emissions/

[124] Containerlift Services Ltd, "7 Benefits of Short Sea Shipping -." Accessed: Jun. 14, 2024. [Online]. Available: http://www.containerlift.co.uk/stories/7-benefits-of-short-sea-shipping/

[125] International Waterway E70, “BENEFITS OF INLAND TRANSPORT.” Accessed: Jun. 14, 2024. [Online]. Available: https://mdwe70.pl/en/inland-water-transport/benefits-of-inland-transport/

[126] “A Guide to Inland Logistics: Road, Rail and Barge.” Accessed: Jun. 14, 2024. [Online]. Available: https://www.cogoport.com/en-IN/blogs/complete-guide-to-road-rail-barge-transport-what-exporters-importers-need-to-know

[127] S. International, “Sea vs Air vs Land Freight - What’s Best for your needs?” Accessed: Jun. 14, 2024. [Online]. Available: https://www.seaspace-int.com/sea-vs-air-vs-land-freight-what-is-the-best-method-of-transport-for-you/

[128] C. Whitt *et al.*, “Future Vision for Autonomous Ocean Observations,” *Front. Mar. Sci.*, vol. 7, Sep. 2020, doi: 10.3389/fmars.2020.00697.

[129] E. Ziajka-Poznańska and J. Montewka, “Costs and Benefits of Autonomous Shipping—A Literature Review,” *Appl. Sci.*, vol. 11, no. 10, Art. no. 10, Jan. 2021, doi: 10.3390/app11104553.

[130] H. Laryea and A. Schiffauerova, “A novel standalone hybrid renewable energy systems onboard conventional and autonomous tugboats,” *Energy*, vol. 303, p. 131948, Sep. 2024, doi: 10.1016/j.energy.2024.131948.

[131] N. P. Reddy *et al.*, “Zero-Emission Autonomous Ferries for Urban Water Transport: Cheaper, Cleaner Alternative to Bridges and Manned Vessels,” *IEEE Electrification Mag.*, vol. 7, no. 4, pp. 32–45, Dec. 2019, doi: 10.1109/MELE.2019.2943954.

[132] A. Miola and B. Ciuffo, “Estimating air emissions from ships: Meta-analysis of modelling approaches and available data sources,” *Atmos. Environ.*, vol. 45, no. 13, pp. 2242–2251, Apr. 2011, doi: 10.1016/j.atmosenv.2011.01.046.

[133] L. T. Le, G. Lee, H. Kim, and S.-H. Woo, “Voyage-based statistical fuel consumption models of ocean-going container ships in Korea,” *Marit. Policy Manag.*, vol. 47, no. 3, pp. 304–331, Apr. 2020, doi: 10.1080/03088839.2019.1684591.

[134] O. Endresen, J. Bakke, E. Sorgård, T. F. Berglen, and P. Holmvang, “Improved modelling of ship SO2 emissions -: a fuel-based approach,” *Atmos. Environ.*, vol. 39, no. 20, pp. 3621–3628, Jun. 2005, doi: 10.1016/j.atmosenv.2005.02.041.

[135] K. Cullinane, P.-H. Tseng, and G. Wilmsmeier, “Estimation of container ship emissions at berth in Taiwan,” *Int. J. Sustain. Transp.*, vol. 10, no. 5, pp. 466–474, May 2016, doi: 10.1080/15568318.2014.975303.

[136] Q. Chen, Y. Lau, M. Kanrak, X. Sun, P. Zhang, and Y.-M. Tang, “Using a bottom-up method to assess cruise ship activity impacts on emissions during 2019–2020 in China,” *Heliyon*, vol. 10, no. 5, p. e27101, Mar. 2024, doi: 10.1016/j.heliyon.2024.e27101.

[137] X. Chen and J. Yang, “Analysis of the uncertainty of the AIS-based bottom-up approach for estimating ship emissions,” *Mar. Pollut. Bull.*, vol. 199, p. 115968, Feb. 2024, doi: 10.1016/j.marpolbul.2023.115968.

[138] F. G. Aarskog, J. Danebergs, T. Strømgren, and Ø. Ulleberg, “Energy and cost analysis of a hydrogen driven high speed passenger ferry,” *Int. Shipbuild. Prog.*, vol. 67, no. 1, pp. 97–123, Jan. 2020, doi: 10.3233/ISP-190273.

[139] S. Jafarzadeh and I. Schjølberg, “Operational profiles of ships in Norwegian waters: An activity-based approach to assess the benefits of hybrid and electric propulsion,” *Transp. Res. Part Transp. Environ.*, vol. 65, pp. 500–523, Dec. 2018, doi: 10.1016/j.trd.2018.09.021.

[140] K. Kouzelis, K. Frouws, and E. van Hassel, “Maritime fuels of the future: what is the impact of alternative fuels on the optimal economic speed of large container vessels,” *J. Shipp. Trade*, vol. 7, no. 1, p. 23, Oct. 2022, doi: 10.1186/s41072-022-00124-7.

[141] V. Kosmas and M. Acciaro, “Bunker levy schemes for greenhouse gas (GHG) emission reduction in international shipping,” *Transp. Res. Part Transp. Environ.*, vol. 57, pp. 195–206, Dec. 2017, doi: 10.1016/j.trd.2017.09.010.

[142] N. R. Ammar and I. S. Seddiek, “Eco-environmental analysis of ship emission control methods: Case study RO-RO cargo vessel,” *Ocean Eng.*, vol. 137, pp. 166–173, Jun. 2017, doi: 10.1016/j.oceaneng.2017.03.052.

[143] R. Helgason, D. Cook, and B. Davíðsdóttir, “An evaluation of the cost-competitiveness of maritime fuels – a comparison of heavy fuel oil and methanol (renewable and natural gas) in Iceland,” *Sustain. Prod. Consum.*, vol. 23, pp. 236–248, Jul. 2020, doi: 10.1016/j.spc.2020.06.007.

[144] I. Jovanović, N. Vladimir, M. Perčić, and M. Koričan, "The feasibility of autonomous low-emission ro-ro passenger shipping in the Adriatic Sea," *Ocean Eng.*, vol. 247, p. 110712, Mar. 2022, doi: 10.1016/j.oceaneng.2022.110712.

[145] L. Kretschmann, H.-C. Burmeister, and C. Jahn, "Analyzing the economic benefit of unmanned autonomous ships: An exploratory cost-comparison between an autonomous and a conventional bulk carrier," *Res. Transp. Bus. Manag.*, vol. 25, pp. 76–86, Dec. 2017, doi: 10.1016/j.rtbm.2017.06.002.

[146] MarineTraffic, "MarineTraffic Data | Vessel details, Current position, Voyage information, and AIS Marine Traffic." Dec. 30, 2023. Accessed: Dec. 30, 2023. [Online]. Available: https://www.marinetraffic.com/en/data/?asset_type=vessels&columns=flag%2Cshipname%2Cphoto%2Crecognized_next_port%2Creported_eta%2Creported_destination%2Ccurrent_port%2Cimo%2Cship_type%2Cshow_on_live_map%2Ctime_of_latest_position%2Clat_of_latest_position%2Clon_of_latest_position%2Cnotes

[147] Google, "Google Maps," Google Maps. Accessed: Oct. 12, 2024. [Online]. Available: https://www.google.com/maps/place/Port+of+Los+Angeles/@33.7396613,-118.342372,12z/data=!3m1!4b1!4m6!3m5!1s0x80dd37ae652ef523:0xd88f6472b07283a5!8m2!3d33.7365401!4d-118.264982!16zL20vMDI2emhk?entry=ttu&g_ep=EgoyMDI0MTAwOS4wIKXMDSoASAFQAw%3D%3D

[148] The Port of Los Angeles, "2024 Port of Los Angeles Mariners Guide," Dec. 2023. Accessed: Feb. 02, 2024. [Online]. Available: https://kentico.portoflosangeles.org/getmedia/71c5fa80-cb50-4df4-aa98-d7ea880dcc5e/2024-pola-mariners-guide

[149] Valero, "VALERO Wilmington Refinery Marine Terminal Manual for Vessels Calling at Berth LA-164," Jan. 2020. Accessed: Dec. 21, 2023. [Online]. Available: http://lgb.ports.moranshipping.com/Lists/Documents/VALERO%20Terminal%20Manual%20for%20Vessels%20Calling%20at%20Berth%20LA-164%202020-01.pdf

[150] L. Browning and K. Bailey, “Current Methodologies and Best Practices for Preparing Port Emission Inventories”, Accessed: Sep. 11, 2023. [Online]. Available: https://www3.epa.gov/ttn/chief/conference/ei15/session1/browning.pdf

[151] United States Environmental Protection Agency (EPA), “Regulatory Impact Analysis: Control of Emissions of Air Pollution from Category 3 Marine Diesel Engines,” Dec. 2009. Accessed: Apr. 05, 2024. [Online]. Available: https://archive.epa.gov/region9/mediacenter/web/pdf/420r09019.pdf

[152] “Regulatory Impact Analysis: Control of Emissions of Air Pollution from Category 3 Marine Diesel Engines.” Accessed: Apr. 05, 2024. [Online]. Available: https://archive.epa.gov/region9/mediacenter/web/pdf/420r09019.pdf

[153] Ship Business, “Load management for main engine, auxiliary engine & electrical loads - shipboard energy efficiency measures.” Accessed: Sep. 12, 2022. [Online]. Available: http://shipsbusiness.com/engine-load-management.html

[154] G. Nicewicz and D. Tarnapowicz, “ASSESSMENT OF MARINE AUXILIARY ENGINES LOAD FACTOR IN PORTS,” Jan. 2012, Accessed: Dec. 01, 2023. [Online]. Available: https://web.archive.org/web/20171215031730id_/http://wydawnictwo.panova.pl:80/pliki/07_2012/2012_7_03.pdf

[155] J. L. D. Dantas and G. Theotokatos, “A framework for the economic-environmental feasibility assessment of short-sea shipping autonomous vessels,” *Ocean Eng.*, vol. 279, p. 114420, Jul. 2023.

[156] The Maritime Executive, “NTNU Trials World’s First Urban Autonomous Passenger Ferry,” The Maritime Executive. Accessed: Oct. 24, 2023. [Online]. Available: https://maritime-executive.com/editorials/ntnu-trials-world-s-first-urban-autonomous-passenger-ferry

[157] G. P. IMO, “About the Low Carbon GIA: GreenVoyage2050.” Accessed: Dec. 12, 2023. [Online]. Available: https://greenvoyage2050.imo.org/about-the-gia/

[158] IMO, “Alternative fuel use - regulatory status mapped.” Accessed: Dec. 12, 2023. [Online]. Available: https://www.imo.org/en/MediaCentre/Pages/WhatsNew-1841.aspx

[159] G. P. IMO, “Alternative marine fuels: Regulatory mapping: GreenVoyage2050.” Accessed: Dec. 12, 2023. [Online]. Available: https://greenvoyage2050.imo.org/alternative-marine-fuels-regulatory-mapping/

[160] K. Andersson, S. Brynolf, J. Hansson, and M. Grahn, “Criteria and Decision Support for A Sustainable Choice of Alternative Marine Fuels,” *Sustainability*, vol. 12, no. 9, Art. no. 9, Jan. 2020, doi: 10.3390/su12093623.

[161] American Bureau of Shipping (ABS), “Marine Fuel Oil Advisory,” Mar. 2023, Accessed: Nov. 11, 2023. [Online]. Available: https://ww2.eagle.org/content/dam/eagle/advisories-and-debriefs/marine-fuel-oil-advisory.pdf

[162] Caribbean Fuels, “Marine Gas Oil - Find a quality MGO Fuel Supplier Near You Anywhere in the Caribbean with Caribbean Fuels!,” caribbeanfuels. Accessed: Apr. 06, 2023. [Online]. Available: https://www.caribbeanfuels.com/mgo

[163] Spectra Fuels, “Live bunkers -What is the difference between MDO and MGO ?” Accessed: Apr. 06, 2023. [Online]. Available: https://livebunkers.com/what-difference-between-mdo-and-mgo

[164] Sustainable Ships, “Specific Fuel Consumption [g/kWh] for Marine Engines,” Sustainable Ships. Accessed: Oct. 25, 2022. [Online]. Available: https://www.sustainable-ships.org/stories/2022/sfc

[165] T. C. Bond *et al.*, “Bounding the role of black carbon in the climate system: A scientific assessment,” *J. Geophys. Res. Atmospheres*, vol. 118, no. 11, pp. 5380–5552, Jun. 2013, doi: 10.1002/jgrd.50171.

[166] Y. Wang and L. A. Wright, “A Comparative Review of Alternative Fuels for the Maritime Sector: Economic, Technology, and Policy Challenges for Clean Energy Implementation,” *World*, vol. 2, no. 4, Art. no. 4, Dec. 2021, doi: 10.3390/world2040029.

[167] U.S. Energy Information Administration, “EIA expects U.S. gasoline and diesel retail prices to decline in 2023 and 2024.” Accessed: Jan. 01, 2024. [Online]. Available: https://www.eia.gov/todayinenergy/detail.php?id=55179

[168] J. Zou and B. Yang, “Evaluation of alternative marine fuels from dual perspectives considering multiple vessel sizes,” *Transp. Res. Part Transp. Environ.*, vol. 115, p. 103583, Feb. 2023, doi: 10.1016/j.trd.2022.103583.

[169] Ship & Bunker, “LA / Long Beach Bunker Prices -MGO,” Ship & Bunker. Accessed: Nov. 06, 2023. [Online]. Available: https://shipandbunker.com/prices/am/nampac/us-lax-la-long-beach

[170] A. Elkafas, M. Rivarolo, and A. F. Massardo, “Assessment Of Alternative Marine Fuels from Environmental, Technical, and Economic Perspectives Onboard Ultra Large Container Ship,” *Int. J. Marit. Eng.*, vol. 164, no. A2, Art. no. A2, Nov. 2022, doi: 10.5750/ijme.v164iA2.768.

[171] X. Wang, J. Zhu, and M. Han, “Industrial Development Status and Prospects of the Marine Fuel Cell: A Review,” *J. Mar. Sci. Eng.*, vol. 11, no. 2, Art. no. 2, Feb. 2023, doi: 10.3390/jmse11020238.

[172] P. Nikolaidis and A. Poullikkas, “A comparative overview of hydrogen production processes,” *Renew. Sustain. Energy Rev.*, vol. 67, pp. 597–611, Jan. 2017, doi: 10.1016/j.rser.2016.09.044.

[173] I. Ocko and S. Hamburg, “For hydrogen to be a climate solution, leaks must be tackled.” Accessed: Feb. 28, 2024. [Online]. Available: https://www.edf.org/blog/2022/03/07/hydrogen-climate-solution-leaks-must-be-tackled

[174] Marine Service Noord, “How much hydrogen do I need?” Accessed: Dec. 29, 2023. [Online]. Available: https://marine-service-noord.com/en/products/alternative-fuels-and-technologies/hydrogen/how-much-hydrogen-do-i-need/

[175] Eastern Research Group, Inc and Energy & Environmental Research Associates, LLC, “Shore Power Technology Assessment at U.S. Ports 2022 Update - EPA-420-R-22-037,” Dec. 2022. Accessed: Dec. 30, 2023. [Online]. Available: https://aapapowers.com/wp-content/uploads/2023/04/Shore-Power-Technology-Assessment-2022-Update

[176] G. Kleen, W. Gibbons, and J. Fornaciari, “DOE Hydrogen Program Record,” May 2023. Accessed: Feb. 28, 2024. [Online]. Available:

https://www.hydrogen.energy.gov/docs/hydrogenprogramlibraries/pdfs/23002-hd-fuel-cell-system-cost-2022.pdf?Status=Master

[177] Battelle Memorial Institute, “Manufacturing Cost Analysis of PEM Fuel Cell Systems for 5- and 10-kW Backup Power Applications,” 2016, Accessed: Dec. 30, 2023. [Online]. Available: https://www.energy.gov/eere/fuelcells/articles/manufacturing-cost-analysis-pem-fuel-cell-systems-5-and-10-kw-backup-power

[178] BloombergNEF, “Green Hydrogen to Undercut Gray Sibling by End of Decade,” BloombergNEF. Accessed: Jan. 01, 2024. [Online]. Available: https://about.bnef.com/blog/green-hydrogen-to-undercut-gray-sibling-by-end-of-decade/

[179] MAN Energy Solutions, “Batteries on board ocean-going vessels - MAN Energy Solutions Future in the making,” Sep. 2019. Accessed: Dec. 30, 2023. [Online]. Available: https://www.man-es.com/docs/default-source/marine/tools/batteries-on-board-ocean-going-vessels.pdf

[180] PowerTech Systems, “Lithium-ion Battery Charging & Advantages – PowerTech Systems.” Accessed: Dec. 30, 2023. [Online]. Available: https://www.powertechsystems.eu/home/tech-corner/lithium-ion-battery-advantages/

[181] Tyto Robotics, “AC vs DC vs BLDC Motor Efficiency Comparison.” Accessed: Dec. 30, 2023. [Online]. Available: https://www.tytorobotics.com/blogs/articles/ac-vs-dc-motor-efficiency#:~:text=DC%20motors%20are%20known%20for,the%20motor's%20windings%20and%20brushes.

[182] Independent Power, “Battery Storage 101: Depth of Discharge,” Independent Power: Solar, Storage and Electrification. Accessed: Feb. 26, 2023. [Online]. Available: https://www.solarips.com/battery-storage-101-what-is-depth-of-discharge

[183] Nereus Subsea - Admin, “How Biodiesel Is Revolutionizing The Marine Industry?” Accessed: Feb. 28, 2024. [Online]. Available: https://www.nereussubsea.com/blog/biodiesel-technology/

[184] US Department of Energy, “Alternative Fuels Data Center: Biodiesel Blends.” Sep. 2022. Accessed: Oct. 25, 2022. [Online]. Available: https://afdc.energy.gov/fuels/biodiesel_blends.html

[185] B. Karpanai Selvan *et al.*, "Utilization of biodiesel blended fuel in a diesel engine – Combustion engine performance and emission characteristics study," *Fuel*, vol. 311, p. 122621, Mar. 2022, doi: 10.1016/j.fuel.2021.122621.

[186] R. Gautam and S. Kumar, "Performance and combustion analysis of diesel and tallow biodiesel in CI engine," *Energy Rep.*, vol. 6, pp. 2785–2793, Nov. 2020, doi: 10.1016/j.egyr.2020.09.039.

[187] N. Sönnichsen, "U.S. B20 and B100 retail fuel prices 2023." May 21, 2024. Accessed: Jan. 02, 2024. [Online]. Available: https://www.statista.com/statistics/1200903/us-b20-retail-fuel-price/

[188] S. A. Mohseni, E. van Hassel, C. Sys, and T. Vanelslander, "Economic evaluation of alternative technologies to mitigate Sulphur emissions in maritime container transport from both the vessel owner and shipper perspective," *J. Shipp. Trade*, vol. 4, no. 1, p. 15, Dec. 2019, doi: 10.1186/s41072-019-0051-8.

[189] R. Aronietis, C. Sys, E. van Hassel, and T. Vanelslander, "Investigating the bunkering choice determinants: the case of the port of Antwerp," *J. Shipp. Trade*, vol. 2, no. 1, p. 8, Dec. 2017, doi: 10.1186/s41072-017-0025-7.

[190] Winterhur Gas & Diesel, "Technical Information Note 008-1: Regulatory requirements towards liquid fuels to be used on dual-fuel (DF) engines, including pilot fuels," Jan. 2019. Accessed: Mar. 01, 2024. [Online]. Available: https://www.wingd.com/en/documents/technical-information-notes/wingd_tin008-1_regulatory-requirements-liquid-fuels-for-df-engines/

[191] European Inland Barging Innovation Platform(EIBIP) Secretariat, "Liquefied Natural Gas (LNG)- alternative fuel, CNG, LNG," EIBIP. Accessed: Mar. 01, 2024. [Online]. Available: https://eibip.eu/publication/liquefied-natural-gas-lng/

[192] M. M. El-Gohary, "The future of natural gas as a fuel in marine gas turbine for LNG carriers," *Proc. Inst. Mech. Eng. Part M J. Eng. Marit. Environ.*, vol. 226, no. 4, pp. 371–377, Nov. 2012, doi: 10.1177/1475090212441444.

[193] B. Zincir and C. Deniz, "Methanol as a Fuel for Marine Diesel Engines," in *Alcohol as an Alternative Fuel for Internal Combustion Engines*, P. C. Shukla, G. Belgiorno, G. Di Blasio, and

A. K. Agarwal, Eds., in Energy, Environment, and Sustainability. , Singapore: Springer, 2021, pp. 45–85. doi: 10.1007/978-981-16-0931-2_4.

[194] K. Andersson and C. M. Salazar, "Methanol as a marine fuel report," 2015. Accessed: Mar. 01, 2024. [Online]. Available: https://www.methanol.org/wp-content/uploads/2018/03/FCBI-Methanol-Marine-Fuel-Report-Final-English.pdf

[195] C. Moroianu and F. Postolache, "Marine Propulsion Engine Behaviour using Fossil Fuel and Methanol," *J. Phys. Conf. Ser.*, vol. 1122, p. 012018, Nov. 2018, doi: 10.1088/1742-6596/1122/1/012018.

[196] Scramento State, Office of Water Programs, "Mass emission rate." Accessed: Dec. 14, 2023. [Online]. Available: https://www.owp.csus.edu/glossary/mass-emission-rate.php

[197] P. Timm, "A Guide to Understanding Emission Factors," Ecometrica. Accessed: Dec. 21, 2023. [Online]. Available: https://ecometrica.com/knowledge-bank/guides/understanding-emission-factors/

[198] O. US EPA, "Basic Information of Air Emissions Factors and Quantification." Accessed: Dec. 21, 2023. [Online]. Available: https://www.epa.gov/air-emissions-factors-and-quantification/basic-information-air-emissions-factors-and-quantification

[199] D. Roten *et al.*, "Chapter 2 - CO2 emissions from energy systems and industrial processes: Inventories from data- and proxy-driven approaches," in *Balancing Greenhouse Gas Budgets*, B. Poulter, J. G. Canadell, D. J. Hayes, and R. L. Thompson, Eds., Elsevier, 2022, pp. 31–57. doi: 10.1016/B978-0-12-814952-2.00002-2.

[200] Wartsila, "EXHAUST GAS EMISSIONS FROM SHIPS," Wartsila.com. Accessed: Oct. 25, 2022. [Online]. Available: https://www.wartsila.com/encyclopedia/term/exhaust-gas-emissions-from-ships

[201] J. Faber, S. Hanayama, S. Zhang, P. Pereda, B. Comer, and E. Hauerhof, "Fourth IMO GHG Study 2020 Full report and annexes compressed," Jul. 2021. Accessed: Dec. 22, 2023. [Online]. Available: https://greenvoyage2050.imo.org/wp-content/uploads/2021/07/Fourth-IMO-GHG-Study-2020-Full-report-and-annexes_compressed.pdf

[202] M. Perčić, N. Vladimir, M. Koričan, I. Jovanović, and T. Haramina, “Alternative Fuels for the Marine Sector and Their Applicability for Purse Seiners in a Life-Cycle Framework,” *Appl. Sci.*, vol. 13, no. 24, Art. no. 24, Jan. 2023, doi: 10.3390/app132413068.

[203] M. Perčić, N. Vladimir, and A. Fan, “Life-cycle cost assessment of alternative marine fuels to reduce the carbon footprint in short-sea shipping: A case study of Croatia,” *Appl. Energy*, vol. 279, p. 115848, Dec. 2020, doi: 10.1016/j.apenergy.2020.115848.

[204] E. Altarriba, S. Rahiala, and T. Tanhuanpää, “Comparative study of LNG/MGO emission levels on a ROPAX ship,” *J. Marit. Res.*, vol. 21, no. 1, Art. no. 1, Apr. 2024.

[205] United States Environmental Protection Agency, “Understanding Global Warming Potentials.” Accessed: Dec. 21, 2023. [Online]. Available: https://www.epa.gov/ghgemissions/understanding-global-warming-potentials

[206] California Air Resources Board, “High-GWP Refrigerants | California Air Resources Board.” Accessed: Dec. 21, 2023. [Online]. Available: https://ww2.arb.ca.gov/resources/documents/high-gwp-refrigerants

[207] European Environment Agency, “Glossary:Global-warming potential (GWP).” Accessed: Dec. 21, 2023. [Online]. Available: https://ec.europa.eu/eurostat/statistics-explained/index.php?title=Glossary:Global-warming_potential_(GWP)

[208] O. Balli and H. Caliskan, “Environmental impact assessments of different auxiliary power units used for commercial aircraft by using global warming potential approach,” *Environ. Sci. Pollut. Res.*, vol. 29, no. 58, pp. 87334–87346, Dec. 2022, doi: 10.1007/s11356-022-21876-6.

[209] G. N. Lee *et al.*, “Environmental Life-Cycle Assessment of Eco-Friendly Alternative Ship Fuels (MGO, LNG, and Hydrogen) for 170 GT Nearshore Ferry,” *J. Mar. Sci. Eng.*, vol. 10, no. 6, Art. no. 6, Jun. 2022, doi: 10.3390/jmse10060755.

[210] O. Balli, U. Kale, D. Rohács, and T. H. Karakoc, “Exergoenvironmental, environmental impact and damage cost analyses of a micro turbojet engine (m-TJE),” *Energy Rep.*, vol. 8, pp. 9828–9845, Nov. 2022, doi: 10.1016/j.egyr.2022.07.157.

[211] U.S. Environmental Protection Agency, “EPA Report on the Social Cost of Greenhouse Gases: Estimates Incorporating Recent Scientific Advances,” Nov. 2023, Accessed: Dec. 15, 2023.

[Online]. Available: https://www.epa.gov/system/files/documents/2023-12/epa_scghg_2023_report_final.pdf

[212] P. Jun, M. Gillenwater, W. Barbour, and K. Rypdal, "CO2 , CH4 , AND N2O EMISSIONS FROM TRANSPORTATION-WATER-BORNE NAVIGATION," Jun. 2024. Accessed: Jul. 30, 2024. [Online]. Available: https://www.ipcc-nggip.iges.or.jp/public/gp/bgp/2_4_Water-borne_Navigation.pdf

[213] E. J. C. Cavalcanti, T. J. S. Ribeiro, and M. Carvalho, "Exergoenvironmental analysis of a combined cycle power plant fueled by natural gas from an offshore platform," *Sustain. Energy Technol. Assess.*, vol. 46, p. 101245, Aug. 2021, doi: 10.1016/j.seta.2021.101245.

[214] World Health Organization (WHO), "Climate impacts of air pollution." Accessed: Nov. 15, 2023. [Online]. Available: https://www.who.int/teams/environment-climate-change-and-health/air-quality-energy-and-health/health-impacts/climate-impacts-of-air-pollution

[215] O. Balli, "Exergetic, sustainability and environmental assessments of a turboshaft engine used on helicopter," *Energy*, vol. 276, p. 127593, Aug. 2023, doi: 10.1016/j.energy.2023.127593.

[216] Sustainability Impact Metrics, "The way eco-costs of emissions are determined," Sustainability Impact Metrics. Accessed: Feb. 15, 2024. [Online]. Available: https://www.ecocostsvalue.com/ecocosts/eco-costs-emissions/

[217] United States Environmental Protection Agency (EPA), "Greenhouse Gas Emissions - Overview of Greenhouse Gases," Overviews and Factsheets, Apr. 2024. Accessed: May 20, 2024. [Online]. Available: https://www.epa.gov/ghgemissions/overview-greenhouse-gases

[218] T. Abdallah, "Chapter 4 - Environmental Impacts," in *Sustainable Mass Transit*, T. Abdallah, Ed., Elsevier, 2017, pp. 45–59. doi: 10.1016/B978-0-12-811299-1.00004-6.

[219] M. A. Rosen, "Exergy Analysis of Waste Emissions," in *Encyclopedia of Energy*, C. J. Cleveland, Ed., New York: Elsevier, 2004, pp. 623–632. doi: 10.1016/B0-12-176480-X/00127-3.

[220] J. Tickner, M. M. Jacobs, and N. B. Mack, "Alternatives assessment and informed substitution: A global landscape assessment of drivers, methods, policies and needs," *Sustain. Chem. Pharm.*, vol. 13, p. 100161, Sep. 2019, doi: 10.1016/j.scp.2019.100161.

[221] Port of Los Angeles, “PORT OF LOS ANGELES – TARIFF NO. 4.” Accessed: Jan. 03, 2024. [Online]. Available: https://kentico.portoflosangeles.org/getmedia/1d2840b6-c814-4907-abfc-6039ce1957f6/sec04

[222] Discover Boating, “The Life Expectancy of the Marine Engine.” Accessed: Dec. 07, 2023. [Online]. Available: https://www.discoverboating.com/resources/the-life-expectancy-of-the-marine-engine

[223] YCharts, “US Discount Rate.” Accessed: Jan. 04, 2024. [Online]. Available: https://ycharts.com/indicators/us_discount_rate

[224] REN21, “Renewables 2023 Global Status Report Collection, Renewables in Energy Demand.” Accessed: Jun. 20, 2025. [Online]. Available: https://www.ren21.net/gsr-2023/

[225] J. van Leeuwen and J. Monios, “Decarbonisation of the shipping sector – Time to ban fossil fuels?,” *Mar. Policy*, vol. 146, p. 105310, Dec. 2022, doi: 10.1016/j.marpol.2022.105310.

[226] U.S. DEPARTMENT OF TRANSPORTATION, “Techno-Economic Analysis and Life Cycle Assessment of Greenhouse Gas and Criteria Air Pollutant Emissions for Biobased Marine Fuels.” Accessed: Sep. 18, 2023. [Online]. Available: https://www.maritime.dot.gov/innovation/meta/techno-economic-analysis-and-life-cycle-assessment-greenhouse-gas-and-criteria-air

[227] SINAY Maritime Data Solution, “How Much Does the Shipping Industry Contribute to Global CO2 Emissions?,” https://sinay.ai/. Accessed: Sep. 18, 2023. [Online]. Available: https://sinay.ai/en/how-much-does-the-shipping-industry-contribute-to-global-co2-emissions/

[228] H. Naghash, D. Schott, and J. Pruyn, “Shifting waves of shipping: a review on global shipping projections and methodologies,” *J. Shipp. Trade*, vol. 9, no. 1, p. 29, Dec. 2024, doi: 10.1186/s41072-024-00187-8.

[229] P. Xie *et al.*, “Optimization-Based Power and Energy Management System in Shipboard Microgrid: A Review,” *IEEE Syst. J.*, vol. 16, no. 1, pp. 578–590, Mar. 2022, doi: 10.1109/JSYST.2020.3047673.

[230] K. Lim and secretariat, “Autonomous shipping,” International Maritime Organization. Accessed: Jan. 20, 2022. [Online]. Available: https://www.imo.org/en/MediaCentre/HotTopics/Pages/Autonomous-shipping.aspx

[231] K. Lim and secretariat, “IMO takes first steps to address autonomous ships,” International Maritime Organization. Accessed: Jan. 27, 2022. [Online]. Available: https://www.imo.org/en/MediaCentre/PressBriefings/Pages/08-MSC-99-MASS-scoping.aspx

[232] K. Sornek *et al.*, “Development of a solar-powered small autonomous surface vehicle for environmental measurements,” *Energy Convers. Manag.*, vol. 267, p. 115953, Sep. 2022, doi: 10.1016/j.enconman.2022.115953.

[233] IMO, “Symposium on Maritime Autonomous Surface Ships (MASS) 2025 and IMO MASS Code.” Accessed: Jun. 20, 2025. [Online]. Available: https://www.imo.org/en/About/Events/Pages/MASS-Symposium-2025.aspx

[234] MarineLink, “MSC 108 Revises Autonomous Ship Roadmap,” MarineLink. Accessed: Jun. 20, 2025. [Online]. Available: https://www.marinelink.com/news/msc-revises-autonomous-ship-roadmap-514062

[235] MarineLink, “MSC 109 Advances Autonomous Ship Code,” MarineLink. Accessed: Jun. 20, 2025. [Online]. Available: https://www.marinelink.com/news/msc-advances-autonomous-ship-code-520397

[236] MarineLink, “IMO’s Facilitation Committee Revised MASS Roadmap,” MarineLink. Accessed: Jun. 20, 2025. [Online]. Available: https://www.marinelink.com/news/imos-facilitation-committee-revised-mass-512983

[237] Ship Technology, “Mayflower Autonomous Research Ship (MARS),” Ship Technology. Accessed: Jun. 21, 2025. [Online]. Available: https://www.ship-technology.com/projects/mayflower-autonomous-research-ship-mars/

[238] R. High, “The Mayflower Autonomous Ship Has Reached North America,” IBM Newsroom. Accessed: Jun. 21, 2025. [Online]. Available: https://newsroom.ibm.com/The-Mayflower-Autonomous-Ship-Has-Reached-North-America

[239] A. Haseltalab, F. Wani, and R. R. Negenborn, “Multi-level model predictive control for all-electric ships with hybrid power generation,” *Int. J. Electr. Power Energy Syst.*, vol. 135, p. 107484, Feb. 2022, doi: 10.1016/j.ijepes.2021.107484.

[240] S. B. Roslan, D. Konovessis, and Z. Y. Tay, “Sustainable Hybrid Marine Power Systems for Power Management Optimisation: A Review,” *Energies*, vol. 15, no. 24, Art. no. 24, Jan. 2022, doi: 10.3390/en15249622.

[241] P. Nema, R. K. Nema, and S. Rangnekar, “A current and future state of art development of hybrid energy system using wind and PV-solar: A review,” *Renew. Sustain. Energy Rev.*, vol. 13, no. 8, pp. 2096–2103, Oct. 2009, doi: 10.1016/j.rser.2008.10.006.

[242] S. Hajiaghasi, A. Salemnia, and M. Hamzeh, “Hybrid energy storage system for microgrids applications: A review,” *J. Energy Storage*, vol. 21, pp. 543–570, Feb. 2019, doi: 10.1016/j.est.2018.12.017.

[243] P. Zhang, F. Yan, and C. Du, “A comprehensive analysis of energy management strategies for hybrid electric vehicles based on bibliometrics,” *Renew. Sustain. Energy Rev.*, vol. 48, pp. 88–104, Aug. 2015, doi: 10.1016/j.rser.2015.03.093.

[244] Y. Cao, M. Yao, and X. Sun, “An Overview of Modelling and Energy Management Strategies for Hybrid Electric Vehicles,” *Appl. Sci.*, vol. 13, no. 10, Art. no. 10, Jan. 2023, doi: 10.3390/app13105947.

[245] X. Peng, H. Chen, and C. Guan, “Energy Management Optimization of Fuel Cell Hybrid Ship Based on Particle Swarm Optimization Algorithm,” *Energies*, vol. 16, no. 3, Art. no. 3, Jan. 2023, doi: 10.3390/en16031373.

[246] M. D. A. Al-Falahi, K. S. Nimma, S. D. G. Jayasinghe, H. Enshaei, and J. M. Guerrero, “Power management optimization of hybrid power systems in electric ferries,” *Energy Convers. Manag.*, vol. 172, pp. 50–66, Sep. 2018, doi: 10.1016/j.enconman.2018.07.012.

[247] S. Kim, H. Jeon, and K. Yoon, “Simplified rule-based strategy control for electric propulsion system,” *J. Adv. Mar. Eng. Technol.*, vol. 45, no. 6, pp. 380–385, Dec. 2021, doi: 10.5916/jamet.2021.45.6.380.

[248] S. B. Roslan, Z. Y. Tay, D. Konovessis, J. H. Ang, and N. V. Menon, "Rule-Based Control Studies of LNG–Battery Hybrid Tugboat," *J. Mar. Sci. Eng.*, vol. 11, no. 7, Art. no. 7, Jul. 2023, doi: 10.3390/jmse11071307.

[249] J. Hou, J. Sun, and H. Hofmann, "Adaptive model predictive control with propulsion load estimation and prediction for all-electric ship energy management," *Energy*, vol. 150, pp. 877–889, May 2018, doi: 10.1016/j.energy.2018.03.019.

[250] L. Chen, D. Gao, and Q. Xue, "Energy management strategy for hybrid power ships based on nonlinear model predictive control," *Int. J. Electr. Power Energy Syst.*, vol. 153, p. 109319, Nov. 2023, doi: 10.1016/j.ijepes.2023.109319.

[251] L. Chen, D. Gao, and Q. Xue, "Energy Management Strategy of Hybrid Ships Using Nonlinear Model Predictive Control via a Chaotic Grey Wolf Optimization Algorithm," *J. Mar. Sci. Eng.*, vol. 11, no. 9, Art. no. 9, Sep. 2023, doi: 10.3390/jmse11091834.

[252] S. Paran, T. V. Vu, T. E. Mezyani, and C. S. Edrington, "MPC-based power management in the shipboard power system," in *2015 IEEE Electric Ship Technologies Symposium (ESTS)*, Jun. 2015, pp. 14–18. doi: 10.1109/ESTS.2015.7157855.

[253] E. K. Dedes, D. A. Hudson, and S. R. Turnock, "Investigation of Diesel Hybrid systems for fuel oil reduction in slow speed ocean going ships," *Energy*, vol. 114, pp. 444–456, Nov. 2016, doi: 10.1016/j.energy.2016.07.121.

[254] M. Kalikatzarakis, R. D. Geertsma, E. J. Boonen, K. Visser, and R. R. Negenborn, "Ship energy management for hybrid propulsion and power supply with shore charging," *Control Eng. Pract.*, vol. 76, pp. 133–154, Jul. 2018, doi: 10.1016/j.conengprac.2018.04.009.

[255] R. R. Chan, L. Chua, and T. Tjahjowidodo, "Enabling technologies for sustainable all — Electric hybrid vessels (Invited paper)," in *2016 IEEE International Conference on Sustainable Energy Technologies (ICSET)*, Nov. 2016, pp. 401–406. doi: 10.1109/ICSET.2016.7811818.

[256] F. D. Kanellos, G. J. Tsekouras, and N. D. Hatziargyriou, "Optimal Demand-Side Management and Power Generation Scheduling in an All-Electric Ship," *IEEE Trans. Sustain. Energy*, vol. 5, no. 4, pp. 1166–1175, Oct. 2014, doi: 10.1109/TSTE.2014.2336973.

[257] W. Chen *et al.*, "Robust Real-Time Shipboard Energy Management System With Improved Adaptive Model Predictive Control," *IEEE Access*, vol. 11, pp. 110342–110360, 2023, doi: 10.1109/ACCESS.2023.3321692.

[258] F. Baldi, F. Ahlgren, F. Melino, C. Gabrielii, and K. Andersson, "Optimal load allocation of complex ship power plants," *Energy Convers. Manag.*, vol. 124, pp. 344–356, Sep. 2016, doi: 10.1016/j.enconman.2016.07.009.

[259] W. Tarelko and K. Rudzki, "Applying artificial neural networks for modelling ship speed and fuel consumption," *Neural Comput. Appl.*, vol. 32, no. 23, pp. 17379–17395, Dec. 2020, doi: 10.1007/s00521-020-05111-2.

[260] W. Chen *et al.*, "Data-Driven Propulsion Load Profile Prediction for All-Electric Ships," in *2022 International Conference on Electrical, Computer, Communications and Mechatronics Engineering (ICECCME)*, Nov. 2022, pp. 1–9. doi: 10.1109/ICECCME55909.2022.9988368.

[261] N. Planakis, G. Papalambrou, and N. Kyrtatos, "Ship energy management system development and experimental evaluation utilizing marine loading cycles based on machine learning techniques," *Appl. Energy*, vol. 307, p. 118085, Feb. 2022, doi: 10.1016/j.apenergy.2021.118085.

[262] A. Haseltalab, M. A. Botto, and R. R. Negenborn, "Model Predictive DC Voltage Control for all-electric ships," *Control Eng. Pract.*, vol. 90, pp. 133–147, Sep. 2019, doi: 10.1016/j.conengprac.2019.06.018.

[263] K. Wang, X. Yan, Y. Yuan, X. Jiang, X. Lin, and R. R. Negenborn, "Dynamic optimization of ship energy efficiency considering time-varying environmental factors," *Transp. Res. Part Transp. Environ.*, vol. 62, pp. 685–698, Jul. 2018, doi: 10.1016/j.trd.2018.04.005.

[264] P. Xie, S. Tan, J. M. Guerrero, and J. C. Vasquez, "MPC-informed ECMS based real-time power management strategy for hybrid electric ship," *Energy Rep.*, vol. 7, pp. 126–133, Apr. 2021, doi: 10.1016/j.egyr.2021.02.013.

[265] J. Hou, J. Sun, and H. Hofmann, "Adaptive model predictive control with propulsion load estimation and prediction for all-electric ship energy management," *Energy*, vol. 150, pp. 877–889, May 2018, doi: 10.1016/j.energy.2018.03.019.

[266] J. Hou, Z. Song, H. Hofmann, and J. Sun, “Adaptive model predictive control for hybrid energy storage energy management in all-electric ship microgrids,” *Energy Convers. Manag.*, vol. 198, p. 111929, Oct. 2019, doi: 10.1016/j.enconman.2019.111929.

[267] L. Chen, D. Gao, and Q. Xue, “Energy Management Strategy of Hybrid Ships Using Nonlinear Model Predictive Control via a Chaotic Grey Wolf Optimization Algorithm,” *J. Mar. Sci. Eng.*, vol. 11, no. 9, Art. no. 9, Sep. 2023, doi: 10.3390/jmse11091834.

[268] A. Haseltalab, F. Wani, and R. R. Negenborn, “Multi-level model predictive control for all-electric ships with hybrid power generation,” *Int. J. Electr. Power Energy Syst.*, vol. 135, p. 107484, Feb. 2022, doi: 10.1016/j.ijepes.2021.107484.

[269] N. Planakis, G. Papalambrou, and N. Kyrtatos, “Ship energy management system development and experimental evaluation utilizing marine loading cycles based on machine learning techniques,” *Appl. Energy*, vol. 307, p. 118085, Feb. 2022, doi: 10.1016/j.apenergy.2021.118085.

[270] Astute Analytica India Pvt Ltd, “Global Tugboat Charter Services Market Valuations to Sail Past US$ 31.69 Billion By 2032,” GlobeNewswire News Room. Accessed: Jun. 22, 2025. [Online]. Available: https://www.globenewswire.com/news-release/2024/11/13/2980375/0/en/Global-Tugboat-Charter-Services-Market-Valuations-to-Sail-Past-US-31-69-Billion-By-2032-Astute-Analytica.html

[271] T. I. Fossen, *Handbook of Marine Craft Hydrodynamics and Motion Control*. John Wiley & Sons, 2011.

[272] United State Naval Academy, “Chapter 7 Resistance and Powering of Ships.” Accessed: Jul. 03, 2023. [Online]. Available: https://www.usna.edu/NAOE/_files/documents/Courses/EN400/02.07%20Chapter%207.pdf

[273] B. Smoker and B. Eng, “Escort Tug Performance Prediction: A CFD Method,” University of Victoria. Accessed: Jul. 03, 2023. [Online]. Available: https://www.uvic.ca/research/centres/iesvic/assets/docs/dissertations/Dissertation-Smoker.pdf

[274] Mermaid- Consultants, “SHIP RESISTANCE CALCULATION,” SHIP DESIGN | NAVAL ARCHITECTS | MARINE CONSULTANTS | OFFSHORE ENGINEERING | INDIA.

Accessed: Jul. 13, 2023. [Online]. Available: https://www.mermaid-consultants.com/ship-resistance-calculation.html

[275] H. Captain Hensen, *Tug Use in Port - A Practical Guide*, 2nd ed. The Nautical Institute, 2003. Accessed: Jul. 19, 2024. [Online]. Available: https://www.scribd.com/document/352814340/Tug-Use-in-Port-A-Practical-Guide

[276] E. C. Tupper, *Introduction to Naval Architecture*. 2004. Accessed: Jul. 18, 2024. [Online]. Available: https://shop.elsevier.com/books/introduction-to-naval-architecture/tupper/978-0-7506-6554-4

[277] A. F. Molland and S. R. Turnock, "10 - Propulsion," in *Marine Rudders and Control Surfaces*, A. F. Molland and S. R. Turnock, Eds., Oxford: Butterworth-Heinemann, 2007, pp. 359–360. doi: 10.1016/B978-075066944-3/50013-5.

[278] "PROPELLERS AND PROPULSION." Accessed: Jul. 16, 2024. [Online]. Available: https://ocw.mit.edu/courses/2-154-maneuvering-and-control-of-surface-and-underwater-vehicles-13-49-fall-2004/3eb3728a69a0e5c3a809e4111f7e036d_lec12.pdf

[279] M. B. Flikkema, J. Holtrop, and T. van Terwisga, "A parametric power prediction model for tractor pods: T-POD Conference," *2nd Int. Conf. Technol. Adv. Podded Propuls. T-POD*, pp. 1–16, 2006.

[280] K. J. Rawson and E. C. Tupper, "15 - Ship design," in *Basic Ship Theory (Fifth Edition)*, K. J. Rawson and E. C. Tupper, Eds., Oxford: Butterworth-Heinemann, 2001, pp. 617–654. doi: 10.1016/B978-075065398-5/50018-2.

[281] MAN Diesel & Turbo, "Basic Principles of Ship Propulsion." 2012. Accessed: Nov. 23, 2024. [Online]. Available: https://www.dieselduck.info/machine/02%20propulsion/2012%20MAN%20Basic%20Ship%20Propulsion.pdf

[282] Wärtsilä, "Wake fraction coefficient," Wartsila.com. Accessed: Oct. 05, 2024. [Online]. Available: https://www.wartsila.com/encyclopedia/term/wake-fraction-coefficient

[283] K. Kim, K. Park, G. Roh, and K. Chun, "DC-grid system for ships: a study of benefits and technical considerations," *J. Int. Marit. Saf. Environ. Aff. Shipp.*, vol. 2, no. 1, pp. 1–12, Nov. 2018, doi: 10.1080/25725084.2018.1490239.

[284] P. Johannesen and U. Heine, "DC or not DC, that is the question," Wartsila.com. Accessed: Aug. 15, 2022. [Online]. Available: https://www.wartsila.com/insights/article/dc-or-not-dc-that-is-the-question

[285] "2022 - Requirements for Direct Current (DC) Power Distrib.pdf." Accessed: Aug. 15, 2024. [Online]. Available: https://ww2.eagle.org/content/dam/eagle/rules-and-guides/current/other/293-requirements-for-direct-current-(dc)-power-distribution-systems-for-marine-and-offshore-applications/293-dc-power-reqts-july22.pdf

[286] C. Jung and D. Schindler, "The role of the power law exponent in wind energy assessment: A global analysis", doi: 10.1002/er.6382.

[287] K. Raiambal and C. Chellamuthu, "Modeling and simulation of grid connected wind electric generating system," in *2002 IEEE Region 10 Conference on Computers, Communications, Control and Power Engineering. TENCOM '02. Proceedings.*, Oct. 2002, pp. 1847–1852 vol.3. doi: 10.1109/TENCON.2002.1182696.

[288] IMO, "GUIDELINES FOR VOLUNTARY USE OF THE SHIP ENERGY EFFICIENCY OPERATIONAL INDICATOR (EEOI)-MEPC.1/Circ.684." Aug. 17, 2009. Accessed: Oct. 11, 2024. [Online]. Available: https://wwwcdn.imo.org/localresources/en/OurWork/Environment/Documents/Circ-684.pdf

[289] The port of Los Angeles, "Environmental Ship Index Program - Port of Los Angeles Voluntary Environmental Ship Index Program." Accessed: Dec. 26, 2024. [Online]. Available: https://www.portoflosangeles.org/environment/air-quality/environmental-ship-index

[290] International association of ports and harbors (IAPH), "Environmental Ship Index (ESI)-ESI Portal." Accessed: Jan. 01, 2011. [Online]. Available: https://www.environmentalshipindex.org/

[291] Windy.com, "Professional weather forecast," Windy.com/. Accessed: Jun. 22, 2024. [Online]. Available: https://www.windy.com/33.738/-118.262?waves,33.218,-118.262,8

[292] S. Capt(N) Richard, G. PM 1 Doutre, M. PM 1 Quillan, Y. Lt(N) Hwang, B. McCullough, and T. Douglas, “Revue du Génie maritime - La Tribune du Génie maritime au Canada,” no. 94, 2020, Accessed: Apr. 05, 2023. [Online]. Available: https://www.canada.ca/content/dam/dnd-mdn/documents/mej/40-033-revue-du-genie-maritime-94.pdf

[293] E. and C. C. Canada, “Beaufort wind scale table.” Accessed: Aug. 30, 2023. [Online]. Available: https://www.canada.ca/en/environment-climate-change/services/general-marine-weather-information/understanding-forecasts/beaufort-wind-scale-table.html

[294] Royal Meterological Society (RMets), “The Beaufort Wind Scale,” RMetS. Accessed: Aug. 30, 2023. [Online]. Available: https://www.rmets.org/metmatters/beaufort-wind-scale

APPENDICES

Appendix A – Supplementary Material for Journal 3

Table A.1: Main particulars for the study vessels

Parameters	Vessel	Parameters	Vessel
Overall length (m)	25	Engine torque coefficient, C3 (N.m/rpm)	-0.0043
Breadth (m)	10	Engine torque coefficient, C4 (N.m/rpm)	2.3932
Draft (m)	5	Motor torque command, Cmotor (N.m/%)	5.8
Gross tonnage (ton)	298	Number of motors	2
Design speed (knots)	12.5	Diesel Genset (kW)	125
Vessel displacement (m^3)	1250	Number of Genset	2
Wetted surface area (m^2)	375	Nominal RPM for Genset	1800
Cross-sectional or frontal area (m^2)	50	Brake thermal efficiency for Genset (%)	37.5
Main Engine power(kW)	1,920.18	Generator efficiency (%)	33.7
Number of engines	2	Diameter of propeller (m)	2.4
Engine RPM	1600	Number of propellers	2
Engine torque coefficient, C1 (N.m/%)	90.51	Shaft efficiency (%)	95
Engine torque coefficient, C2 (N.m/rpm2)	0.0047	Gearbox reduction ratio	3.05:1

Table A.2: Technical specifications for the PV modules

Parameters	Value
Nominal Power (kW)	0.37
Temp Coefficient (% / °C)	-0.29
Efficiency (%)	22.7
NOCT (°C)	41.5
Maximum power voltage at STC (V)	59.1
Maximum power current at STC (A)	6.26

Table A.3: Technical specifications for the lithium-ion battery bank.

Parameters	Value
Battery voltage (V)	48
Nominal Capacity (Ah)	135
Maximum State of charge (%)	100
Minimum State of Charge (%)	20
Charging Efficiency (%)	80
Discharge Efficiency (%)	100

Table A.4: Technical specifications for the vertical axis wind turbine (VAWT)

Parameters	Value
Nominal Power (kW)	5
Hub Height (m)	4.8
Number of Turbines	2
Number of blades per turbine	3
Swept area of the wind turbine (m^2)	15.9
Rotor diameter (m)	4.5
Overall Efficiency (%)	29.8
Rate Wind Speed (m/s)	11
Survival Wind Speed (m/s)	52.2
Cut-in Wind Speed (m/s)	1.5
Cut-out Wind Speed (m/s)	15

Table A.5: Simulation parameters

Parameters	Value
Sample time	0.5
Prediction Horizon (steps)	10
Control Horizon (steps)	5
Cost matrix (Wi)	diag [1,100,5,0.5,10, 0.5]
Final Cost matrix (Wn)	diag [15,1000,50.0.5]
SOC soft constraints (%)	[25, 75]
SOC hard constraints (%)	[20, 80]
Engine RPM soft constraints (RPM)	[600, 1600]
Engine RPM hard constraints (RPM)	[500, 1700]
Engine command rate (%/min)	[-20,10]
Motor command (%)	[-95,95]
Motor command rate (%/min)	[-50, 50]
State noise covariance matrix (Q [k])	0.0005
Input noise covariance matrix (R[k])	4
Population size (number of wolves)	30
Maximum number of iterations	100

Table A.6 : Emission factors (EF) for marine alternative fuels (g/kg fuel) [47].

Alternative Fuels	CO_2	CO	N_2O	NOx	SOx	PM	CH4
B20 (Biofuel)	-	2.52	0.15	61.21	2.64	1.02	0.06
HFO	3114	2.87	0.18	78.61	50.83	7.53	0.05
Hydrogen	-	-	-	-	-	-	-
LNG	2753	3.57		10.95	0.03	0.11	11.22
Methanol	1375	-		8	-	-	-
MGO	3161	3.6	0.08	46.2	1.50	0.31	0.39
MDO	3206	2.54	0.10	56.72	2.74	0.97	0.05

Table A.7: Environmental costs of emissions for marine alternative fuels [47].

Pollutants	CO_2	CO	N_2O	NOx	SOx	PM	CH4
Cost of emission, C_j (USD/kg)	0.128	0.201	2.66	5.912	9.670	40.40	2.78

Table A.8: NATO sea state numeral table for the open ocean North Atlantic [292].

Sea State	Significant Wave Height (m)		Sustained Wind Speed (knots) [1]		Percentage Probability of Sea State	Modal wave period (sec)	
	Range	Mean	Range	Mean		Range[2]	Most Probable[3]
0-1	0 - 0.1	0.05	0 -6	3	0.7	-	-
2	0.1 - 0.5	0.3	7 - 10	8.5	8.5	3.3 - 12.8	7.5
3	0.5 - 1.25	0.88	11-16	13.5	13.5	5 - 14.8	7.5
4	1.25 -2.5	1.88	17 - 21	19	19	6.1 - 15.2	8.8
5	2.5 - 4	3.25	22 - 27	24.5	24.5	8.3 - 15.5	9.7
6	4 -6	5	28 - 47	37.5	37.5	9.8 - 16.2	12.4
7	6 - 9	7.5	48 - 55	51.5	51.5	11.8 - 18.5	15
8	9 - 14	11.5	56 - 63	59.5	59.5	14.2 - 18.6	16.4
> 8	> 14	> 14	> 63	> 63	> 63	18 -3.7	20

1. Ambient wind sustained at 19.5m above surface to generate full-developed seas. To convert to another altitude, H_2 apply $V_2 = V_1(H_2/19.5)^{1/7}$
2. Minimum is the 5th percentile and maximum is the 95th percentile for periods given wave height range.
3. Based on periods associated with central frequencies included in Hindcast Climatology.

Table A.9: The Beaufort wind scale table [293], [294].

Wind Forces	Description	Wind Speed		Probable Wave Height		Sea State
		km/h	knots	Min	Max	
0	Calm	< 1	< 1	-	-	0
1	Light air	1 - 5	1 - 3	0.1	0.1	1
2	Light breeze	6 - 11	4 -7	0.2	0.3	2
3	Gentle breeze	12 -19	8 - 12	0.6	1.0	3
4	Moderate breeze	20 - 28	13 -18	1.0	1.5	3 - 4
5	Fresh breeze	29 - 38	17 - 21	2.0	2.5	4
6	Strong breeze	39 - 49	22 - 27	3.0	4	5
7	Near gale	50 - 61	28 - 33	4.0	5.5	5 - 6
8	Gale	62 - 74	34 - 40	5.5	7.5	6 - 7
9	Strong gale	75 - 88	41 - 47	7.0	10.0	7
10	Storm	89 - 102	48 - 55	9.0	12.5	8
11	Violent Storm	103 - 117	56 - 63	11.5	16.0	8
12	Hurricane	118 - 133	64 - 71	14 +	-	9